THE GEOLOGY AND TECTONIC EVOLUTION OF THE OBI REGION, EASTERN INDONESIA

BY

DWI ATMO AGUSTIYANTO

A thesis submitted for the degree of Master of Philosophy at the University of London

Department of Geological Sciences

University College London

1995

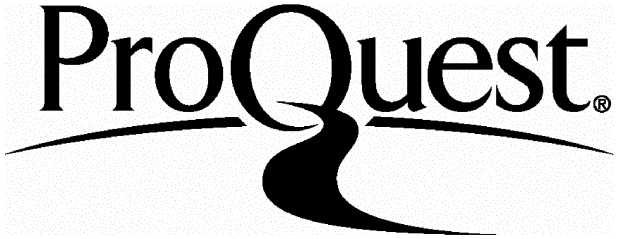

ABSTRACT

Obi is located in eastern Indonesia in the zone of convergence between the Australian, Philippine Sea and Eurasian plates, and is situated within strands of the Sorong Fault system at the Australian-Philippine Sea plate boundary. A new stratigraphy and geological map of Obi have been constructed using new data collected during fieldwork, supplemented by information acquired from aerial photographic studies, biostratigraphic dating, K-Ar dating, petrography, mineral and whole rock geochemistry.

The oldest rocks in Obi belong to the Tapas Metamorphic Complex which is probably of Palaeozoic or greater age. The Tapas metamorphic rocks include phyllites, schists and gneisses with mineral assemblages typical of regional metamorphism at greenschist to amphibolite facies. Triassic and Jurassic sedimentary rocks of the Soligi Formation and the Gomumu Formation, which comprise micaceous sandstones and black shales, are interpreted to rest unconformably on the Tapas metamorphic rocks. These rocks are considered to be derived from the Australian continental margin and formed part of its Mesozoic passive margin.

Ophiolitic rocks, of supposed Jurassic age, form the basement of most of the Obi region. These rocks are unconformably overlain by Cretaceous volcaniclastic rocks, limestones and mudstones of the Leleobasso Formation. Similarities between the stratigraphies of Obi, east Halmahera, Waigeo and other islands of the North Moluccas, are consistent with a common origin as part of a single plate, the Philippine Sea plate. Subduction of the Indo-Australian plate beneath the Philippine Sea plate in the early Tertiary led to arc volcanic activity which resulted in diorite intrusions and the deposition of the volcaniclastic Oligocene Anggai Formation above the ophiolitic rocks. Early Neogene collision between the Australian continent and the Philippine Sea plate arc caused uplift which was followed by deposition of limestones of the Fluk Formation. In the Late Miocene the region underwent uplift and erosion, associated with renewed arc volcanic activity which produced the Woi and the Guyuti Formations. When arc activity ceased, limestones of the Anggai Formation were deposited.

Juxtaposition of the ophiolitic and continental rocks in south Obi probably occurred in the Late Neogene. Pliocene thrusting on Obi, as on Halmahera, has dramatically contracted the late Neogene arc, and on Obi carried the Woi Formation arc over the Guyuti Formation forearc. This juxtaposition was accompanied and followed by uplift, tilting, erosion forming conglomerates and sandstones of the Plio-Pleistocene South Obi Formation.

A brief summary of the geological history is synthesised with regional tectonic events and the large scale tectonic development of eastern Indonesia to provide a model of the tectonic evolution of the Obi region.

ACKNOWLEDGEMENTS

I would like to take this opportunity to express my deep sense of gratitude and sincere thanks to my supervisor Prof. Robert Hall, for all valuable guidance, encouragement, useful discussions, practical suggestions and his patience with me throughout the course of my research. I am deeply indebted.

My sincere gratitude to Drs. Gary Nichols, Tim Charlton, Jason Ali, Jeffrey Malaihollo, Emily Forde, Giz Mariner, Hillary Downes, Diane Cameron, Simon Baker and Andy Beard for all assistance and encouragement.

I thank Drs. Irwan Bahar and Rab. Sukamto who have give me the support an opportunity to improve my knowledge and to finish my study.

I also thank my Indonesian colleagues Sardjono, Agus Guntoro and Alit Ngakan who give me support, encouragement, discussion and comment which useful in arranging this thesis.

I wish to thank my mother Mrs. Sugiarti Moerhardjo and my mother in law Mrs. Tum Silowati Hani Sarono and all my family for their supporting and sincere praying.

My very special sincere thanks to my wife Dwi Harini for encouraging, understanding, assistance and all the hard time she has been through. Special thanks to my children Ivan Yudha Nugraha Putra and Ayu Puspaningrum for their understanding, prayers and encouragement.

CONTENTS

1. INTRODUCTION 1

1.1 PREAMBLE 1

1.2 AIM OF THIS STUDY 1

1.3 GEOGRAPHIC SETTING 4

1.3.1 Location 4

1.3.2 Morphology and Relief 4

1.3.3 Settlement and Culture 6

1.3.4 Climate, Flora and Fauna 6

1.3.5 Accessibility and Logistics 7

1.4 REVIEW OF PREVIOUS WORK 8

1.4.1 Investigations Prior to the Second World War 8

1.4.2 Post-War Studies of Obi 10

1.4.3 Regional Tectonic Investigations 11

1.4.4 London University-GRDC Investigations 18

1.5 PRESENT TECTONIC FRAMEWORK OF THE AREA SURROUNDING OBI 22

1.5.1 Halmahera Arc 22

1.5.2 Molucca Sea Plate 23

1.5.3 Philippine Sea Plate 23

1.5.4 Sorong Fault Zone 23

1.5.5 Obi 24

1.6 METHODS 24

1.6.1 Sampling Methods 24

1.6.2 Petrographic Methods 24

1.6.3 Photogeological Interpretation 24

1.6.4 Microprobe Methods 26

1.6.5 X-ray Fluorescence (XRF) Methods 26

1.6.6 K-Ar Methods 26

1.7 PLAN OF THE THESIS 26

2. OVERVIEW OF THE GEOLOGY OF OBI 28

2.1 INTRODUCTION TO THE STRATIGRAPHY 28

2.2 THE NEW GEOLOGICAL MAP OF OBI 28

2.2.1 SW Obi: Australian Continental Rocks 32

2.2.2 NW, NE and SE Obi: Philippine Sea Plate Rocks 32

2.2.3 STRUCTURE 34

3. METAMORPHIC BASEMENT AND JURASSIC SEDIMENTARY ROCKS: CONTINENTAL CRUST AND COVER 36

3.1 INTRODUCTION 36

3.2 TAPAS METAMORPHIC COMPLEX 36

3.2.1 Synonymy 36
3.2.2 Aerial Photographic and Topographic Interpretation 38
3.2.3 Type Section 38
3.2.4 Age 38
3.2.5 Thickness 40
3.2.6 Distribution 40
3.2.7 Lower and Upper Contacts 40
3.2.8 Petrology of the Metamorphic Rocks 41
3.2.9 Whole Rock Chemistry 45
3.3 SOLIGI FORMATION 47
3.3.1 Synonymy 47
3.3.2 Aerial Photography and Topographic Interpretation 47
3.3.3 Type section 47
3.3.4 Age 49
3.3.5 Thickness 49
3.3.6 Distribution 49
3.3.7 Lower and Upper Contacts 49
3.3.8 Description 49
3.3.9 Depositional Environment 49
3.4 GOMUMU FORMATION 49
3.4.1 Synonymy 49
3.4.2 Aerial Photography and Topographic Interpretation 51
3.4.3 Type Locality 51
3.4.4 Age 51
3.4.5 Thickness 51
3.4.6 Distribution 51
3.4.7 Lower and Upper Contacts 51
3.4.8 Description 51
3.4.9 Depositional Environment 51

4. THE OPHIOLITIC BASEMENT COMPLEX 52

4.1 INTRODUCTION 52
4.2 LITHOLOGIES 52
4.3 AERIAL PHOTOGRAPHIC AND TOPOGRAPHIC INTERPRETATION 55
4.4 AGE 55
4.5 THICKNESS 59
4.6 DISTRIBUTION 59
4.7 PETROGRAPHY AND MINERAL CHEMISTRY 59
4.7.1 Peridotites 59
4.7.2 Plutonic Rocks 59
4.7.3 Dolerites 62

4.7.4 Diorites 62
4.7.5 Basaltic Rocks 62
4.7.6 Mineralogy and Mineral Chemistry 64
4.8 GEOCHEMISTRY 66
4.8.1 Major Elements 66
4.8.2 Trace Elements 67
4.8.3 Discussion 75

5. CRETACEOUS AND TERTIARY SEDIMENTARY AND VOLCANIC ROCKS 76

5.1 INTRODUCTION 76
5.2 LELEOBASSO FORMATION 76
5.2.1 Synonymy 76
5.2.2 Aerial Photography and Topographic Interpretation 76
5.2.3 Type Section 78
5.2.4 Age 78
5.2.5 Thickness 78
5.2.6 Distribution 78
5.2.7 Lower and Upper Contacts 81
5.2.8 Description 81
5.2.9 Depositional Environment 83
5.3 ANGGAI RIVER FORMATION 83
5.3.1 Synonymy 83
5.3.2 Aerial Photography and Topographic Interpretation 83
5.3.3 Type section 83
5.3.4 Age 83
5.3.5 Thickness 85
5.3.6 Distribution 85
5.3.7 Lower and Upper Contacts 85
5.3.8 Description 85
5.3.9 Whole Rock Chemistry 90
5.3.10 Depositional Environment 90
5.4 FLUK FORMATION 95
5.4.1 Synonymy 95
5.4.2 Aerial Photography and Topographic Interpretation 95
5.4.3 Type Locality 95
5.4.4 Age 95
5.4.5 Thickness 95
5.4.6 Distribution 95
5.4.7 Lower and Upper Contacts 95
5.4.8 Description 97
5.4.9 Depositional Environment 97

5.5 WOI FORMATION 97
5.5.1 Synonymy 97
5.5.2 Aerial Photography and Topographic Interpretation 99
5.5.3 Type Section 99
5.5.4 Age 99
5.5.5 Thickness 100
5.5.6 Distribution 100
5.5.7 Lower and Upper Contacts 100
5.5.8 Description 100
5.5.9 Whole Rock Chemistry 110
5.5.10 Depositional Environment 110
5.6 GUYUTI FORMATION 115
5.6.1 Synonymy 115
5.6.2 Aerial Photography and Topographic Interpretation 115
5.6.3 Type Section 115
5.6.4 Age 115
5.6.5 Thickness 115
5.6.6 Distribution 117
5.6.7 Lower and Upper Contacts 117
5.6.8 Description 117
5.6.9 Whole Rock Chemistry 121
5.6.10 Depositional Environment 121
5.7 ANGGAI FORMATION 127
5.7.1 Synonymy 127
5.7.2 Aerial Photography and Topographic Interpretation 127
5.7.3 Type Section 127
5.7.4 Age 127
5.7.5 Thickness 127
5.7.6 Distribution 129
5.7.7 Lower and Upper Contacts 129
5.7.8 Description 129
5.7.9 Depositional Environment 129
5.8 SOUTH OBI FORMATION 129
5.8.1 Synonymy 132
5.8.2 Aerial Photography and Topographic Interpretation 132
5.8.3 Type Section 132
5.8.4 Age 132
5.8.5 Thickness 132
5.8.6 Distribution 132
5.8.7 Lower and Upper Contacts 132
5.8.8 Description 132

5.8.9 Depositional Environment 133
5.9 QUATERNARY LIMESTONE 133
5.10 QUATERNARY ALLUVIUM 134
6. STRUCTURE AND REGIONAL TECTONICS 135
6.1 INTRODUCTION 135
6.2 STRUCTURE 135
6.2.1 CROSS SECTIONS 139
6.2.2 Stratigraphic Considerations 141
6.3 Palaeomagnetic Rotations 141
6.4 TECTONIC EVOLUTION 143
6.4.1 Continental Crust 143
6.4.2 Ophiolitic Basement Complex 144
6.4.3 Cretaceous and Tertiary Sedimentary and Volcanic Rocks 144
6.5 CORRELATION WITH REGIONAL EVENTS 146
6.5.1 Early Mesozoic 146
6.5.2 Mid Cretaceous to Late Cretaceous 100 - 70 Ma 147
6.5.3 Eocene - Oligocene 56 - 23 Ma 147
6.5.4 Oligocene - Early Miocene ~22-15 Ma 147
6.5.5 Middle Miocene 15 Ma 150
6.5.6 Late Miocene - Early Pliocene 11 - 3 Ma 150
6.5.7 Late Pliocene to Present 3 - 0 Ma 150
6.6 CONCLUSIONS 153
REFERENCES 154
APPENDIX A Isotopic Dating Methods 158
APPENDIX B Microprobe Analyses 160
APPENDIX C Bulk Rock Chemical Analyses 206
APPENDIX D Key to diagrams of logged sections 220

LIST OF FIGURES

1. INTRODUCTION

1.1. Location of the Obi Islands.

1.2. Tectonic setting of the Obi Islands.

1.3. Principal physiographic features and morphological areas of the Obi Islands.

1.4. Aerial photographic coverage of the Obi Islands.

1.5. Tectonic map of the region around Obi, modified from Hamilton (1979).

1.6. Geological provinces of the Halmahera region, after Sukamto *et al.* (1981).

1.7. Tectonic map of the Halmahera region, from Letouzey *et al.* (1983).

1.8. Structural map and position of sedimentary basins (after Letouzey *et al.*, 1983).

1.9. Principal tectonic features of the Halmahera region, from Hall & Nichols (1990). Solid circles are active volcanoes of the Halmahera and Sangihe arcs.

1.10. Simplified block diagram showing the present-day tectonics of the southern Philippine Sea Plate and the Sorong Fault Zone, from Hall *et al.* (1995b).

1.11. Location of samples collected during this study.

2. OVERVIEW OF THE GEOLOGY OF OBI

2.1. Geological map of the Obi Islands based on this study.

2.2. Stratigraphy of the Obi Islands based on this study.

2.3. Comparisons of previous and present stratigraphic schemes for the Obi Islands.

2.4. Cross-sections of Obi Island. The locations of the profiles are shown on Fig. 2.1.

3. METAMORPHIC BASEMENT AND JURASSIC SEDIMENTARY ROCKS: CONTINENTAL CRUST AND COVER

3.1. Distribution of the Tapas Metamorphic Complex.

3.2. Well foliated quartzose mica schists, dipping southwest on the south coast of Tapas.

3.3. Folded foliation in float sample of quartzose mica schist, south Tapas.

3.4. A. (above) Photomicrograph of rotated porphyroblast of plagioclase containing inclusions of epidote in an epidote amphibolite (OR251). Plane polarised light. Width of photograph is 1.6 mm. B. (below) crossed polars.

3.5. MORB-normalised trace element spidergram for Tapas metabasic hornblendites. Normalising factors from Pearce et al. (1984).

3.6. MORB-normalised trace element spidergram for Tapas ultrabasic hornblendites. Normalising factors from Pearce et al. (1984).

3.7. Distribution of the Soligi Formation.

3.8. Distribution of the Gomumu Formation.

4. THE OPHIOLITIC BASEMENT COMPLEX

4.1. Distribution of basic and ultrabasic rocks of the Ophiolitic Basement Complex of Obi.

4.2. View of hills underlain by serpentinite and covered by thick lateritic soils in NW Obi.

4.3. Gabbro pegmatites intruding microgabbros in Airpati River, SW Obi.

4.4. Dolerite dykes exposed in central Obi on logging road north of Ocimaloleo.

4.5. Dolerite dykes exposed on the Ricang logging road about 28 km from the coast in west Obi.

4.6. Pillow lavas exposed on the coast of Wobo Island, south of Obi Latu.

4.7. A. (above) Photomicrograph of partly serpentinised harzburgite (OR53). Orthopyroxene forms large crystals, whereas olivines are fractured and crossed by numerous narrow veins of serpentine. Plane polarised light. Width of photograph is 1.6 mm. B. (below) crossed polars.

4.8. A. (above) Photomicrograph of fresh olivine gabbro (OJ108), possibly a cumulate. Plane polarised light. Width of photograph is 1.6 mm. B. (below) crossed polars.

4.9. A. (above) Photomicrograph of hornblende diorite (OS6), containing granophyric intergrowths of quartz and K feldspar. Plane polarised light. Width of photograph is 1.6 mm. B. (below) crossed polars.

4.10. Plot of K_2O versus SiO_2 for basalts and dolerites of the ophiolite. Compositional fields from Taylor *et al.* (1981).

4.11. Plot of Na_2O+K_2O versus SiO_2 for basalts and dolerites of the ophiolite. Compositional fields from Le Bas & Streckeisen (1991).

4.12. MORB-normalised trace element spidergrams for basalts and dolerites of the ophiolite. Normalising factors from Pearce et al. (1984).

4.13. Ti-Zr-Y discriminant diagram for basalts and dolerites of the ophiolite (after Pearce & Cann, 1973).

4.14. Mn-Ti-P discriminant diagram for basalts and dolerites of the ophiolite (after Mullen, 1983).

4.15. Trace element covariation diagrams for basalts and dolerites of the ophiolite used to decipher their tectonic setting of formation. A, B, D and E after Pearce (1982). C after Pearce & Norry, 1979.

4.16. Plot of Na_2O+K_2O versus SiO_2 for diorites intruding the ophiolite. Compositional fields from Cox *et al.* (1979).

4.17. MORB-normalised trace element spidergram for diorites intruding the ophiolite. Normalising factors from Pearce et al. (1984).

4.18. Ti-Zr-Y discriminant diagram for diorites intruding the ophiolite (after Pearce & Cann, 1973).

4.19. Mn-Ti-P discriminant diagram for diorites intruding the ophiolite (after Mullen, 1983).

4.20. Trace element covariation diagrams for diorites intruding the ophiolite. A, B, D and E after Pearce (1982). C after Pearce & Norry, 1979.

5. CRETACEOUS AND TERTIARY SEDIMENTARY AND VOLCANIC ROCKS

5.1. Distribution of the Leleobasso Formation.

5.2. Bedded volcaniclastic conglomerates and sandstones of the Leleobasso Formation at Tanjung Leleobasso, NW Obi Major. Bedding dips gently away from the observer and the trace of the bedding can be seen running from left to right across the photo from the foot of Spencer Roberts (right hand side of photo).

5.3. Fractured foraminifera-bearing calcareous mudstones of the Leleobasso Formation at Tanjung Leleobasso, NW Obi Major.

5.4. Section of the Leleobasso Formation measured on the coast south of Alam Kenangan village, Obi Latu.

5.5. Distribution of the Anggai River Formation.

5.6. Bedded, steeply dipping, coarse and fine volcaniclastic sandstones of the Anggai River Formation in the Anggai River, north Obi Major.

5.7. Gently dipping, volcaniclastic sandstones of the Anggai River Formation in the Anggai River, north Obi Major.
5.8. Section of the Anggai River Formation measured in the type area of the Anggai River.
5.9. Section of the Anggai River Formation measured in the type area of the Anggai River.
5.10. Plot of K_2O versus SiO_2 for volcanic and volcaniclastic sedimentary rocks of the Anggai River Formation. Compositional fields from Taylor *et al.* (1981).
5.11. Plot of Na_2O+K_2O versus SiO_2 for volcanic and volcaniclastic sedimentary rocks of the Anggai River Formation. Compositional fields from Le Bas & Streckeisen (1991).
5.12. MORB-normalised trace element spidergrams for volcanic rocks (above) and volcaniclastic sedimentary rocks (below) rocks of the Anggai River Formation. Normalising factors from Pearce et al. (1984).
5.13. Ti-Zr-Y discriminant diagram for volcanic and volcaniclastic sedimentary rocks of the Anggai River Formation (after Pearce & Cann, 1973).
5.14. Mn-Ti-P discriminant diagram for volcanic and volcaniclastic sedimentary rocks of the Anggai River Formation (after Mullen, 1983).
5.15. Trace element covariation diagrams for volcanic and volcaniclastic sedimentary rocks of the Anggai River Formation. A, B, D and E after Pearce (1982). C after Pearce & Norry, 1979.
5.16. Distribution of the Fluk Formation.
5.17. Distribution of the Woi Formation.
5.18. Bedded basaltic andesitic lavas of the Woi Formation in the lower Sesepe River, northeast Obi Major.
5.19. Flow-banded andesitic lavas of the Woi Formation in the upper Sesepe River, northeast Obi Major.
5.20. A. (above) Photomicrograph of biotite andesite (OD14), containing brown biotite, clinopyroxene and plagioclase phenocrysts in a finer matrix. Plane polarised light. Width of photograph is 1.6 mm. B. (below) crossed polars.
5.21. Section of part of the Woi Formation measured in the Guyuti River in south Obi. Location shown on inset map.
5.22. Section of part of the Woi Formation measured below the waterfall near the former logging camp north of Bobo in south Obi. Location shown on inset map.
5.23. Section of part of the Woi Formation measured in a tributary of the Woi River, south Obi. Location shown on inset map.
5.24. Plot of K_2O versus SiO_2 for volcanic rocks of the Woi Formation. Compositional fields from Taylor *et al.* (1981). Areas identified are those in which the high-K rocks were collected.
5.25. Plot of Na_2O+K_2O versus SiO_2 for volcanic rocks of the Woi Formation. Compositional fields from Le Bas & Streckeisen (1991).
5.26. MORB-normalised trace element spidergrams for volcanic rocks of the Woi Formation. Normalising factors from Pearce et al. (1984).
5.27. Ti-Zr-Y discriminant diagram for volcanic rocks of the Woi Formation (after Pearce & Cann, 1973).
5.28. Mn-Ti-P discriminant diagram for volcanic rocks of the Woi Formation (after Mullen, 1983).

5.29. Trace element covariation diagrams for volcanic rocks of the Woi Formation. A, B, D and E after Pearce (1982). C after Pearce & Norry, 1979.
5.30. Distribution of the Guyuti Formation.
5.31. Andesitic conglomerates of the Guyuti Formation in the Woi River include large compact limestone blocks containing shallow water debris including corals.
5.32. Section of part of the Guyuti Formation measured in the Guyuti River in south Obi. Location shown on inset map.
5.33. A. (above) Photomicrograph of basalt (OD199) from the Guyuti Formation, containing clinopyroxene and plagioclase phenocrysts in a finer matrix. Plane polarised light. Width of photograph is 1.6 mm. B. (below) crossed polars.
5.34. Plot of K_2O versus SiO_2 for volcanic rocks of the Guyuti Formation. Compositional fields from Taylor *et al.* (1981).
5.35. Plot of Na_2O+K_2O versus SiO_2 for volcanic rocks of the Guyuti Formation. Compositional fields from Le Bas & Streckeisen (1991).
5.36. MORB-normalised trace element spidergram for volcanic rocks of the Guyuti Formation. Normalising factors from Pearce et al. (1984).
5.37. Ti-Zr-Y discriminant diagram for volcanic rocks of the Guyuti Formation (after Pearce & Cann, 1973).
5.38. Mn-Ti-P discriminant diagram for volcanic rocks of the Guyuti Formation (after Mullen, 1983).
5.39. Trace element covariation diagrams for volcanic rocks of the Guyuti Formation. A, B, D and E after Pearce (1982). C after Pearce & Norry, 1979.
5.40. Distribution of the Anggai Formation.
5.41. Limestone from the Anggai Formation (OD124) from the Kelo logging road containing shallow water debris including corals.
5.42. Distribution of the South Obi Formation.

6. STRUCTURE AND TECTONICS

6.1. Principal structures of the Obi islands based on this study.
6.2. Cross-sections of Obi Island. The location of the profiles are shown on Fig. 6.1.
6.3. Cross-section of Obi Island. The location of the profile is shown on Fig. 6.1.
6.4. Palaeomagnetic rotations in the Sorong Fault Zone, from Ali & Hall (1995).
6.5. Simplified tectonic setting of the Obi region during the Middle to Late Cretaceous.
6.6. Simplified tectonic setting of the Obi region during the Late Oligocene to Early Miocene.
6.7. Simplified tectonic setting of the Obi region during the Early to Middle Miocene.
6.8. Simplified tectonic setting of the Obi region during the Late Miocene.
6.9. Simplified tectonic setting of the Obi region during the Early Pliocene.
6.10. Simplified tectonic setting of the Obi region during the Late Pliocene to Pleistocene.
6.11. Neogene tectonic development of the Obi region at the boundary of the Philippine Sea and Australian plates, modified from Hall (1996).

CHAPTER 1

INTRODUCTION

1. INTRODUCTION

1.1 Preamble

Indonesia consists of about 13,750 islands and includes those of the Obi group in northeastern Indonesia (Fig. 1.1). The Obi region is tectonically very complex, because it lies at the junction between the Eurasian, the Philippine Sea and the Australian Plates, and it is located within the Sorong Fault Zone, which is a major strike-slip system forming the present boundary between the Australian and Philippine Sea plates (Fig. 1.2). As a result, the geology of this region is complicated, both stratigraphically and structurally. Particularly interesting is the juxtaposition of rocks which originated from the Australian continent (Hamilton, 1979, Morris *et al.*, 1983; Hall *et al.*, 1988a,b) and ophiolitic/arc rocks derived from the Philippine Sea Plate (Hall *et al.*, 1991), a feature which has attracted geologists to study the area. Parts of Obi and the nearby Bacan islands have been interpreted as micro-continents (Hartono & Tjokrosapoetro, 1984) originating from part of Papua New Guinea and moved towards the west by the left-lateral Sorong Fault (Pigram & Panggabean, 1984; Hall *et al.*, 1992; Hamilton, 1979). Sukamto *et al.* (1981) considered that Obi was part of the Neogene western Halmahera volcanic arc. Thus, the association of continental metamorphic rocks, ophiolitic rocks and volcanic rocks gives an indication that Obi and surrounding islands may provide some important clues in unravelling the tectonic development of the region.

1.2 Aim of this study

Despite their situation there has been little previous work, as discussed in greater detail below, on the Obi islands. Early reports by Dutch geologists date from the first decades of the twentieth century and only recently did the Geological Research and Development Centre (GRDC) of Indonesia publish the first 1:250,000 geological map and stratigraphy of the area (Sudana & Yasin, 1983). Since this mapping the Gondwana Company (1985) conducted a programme of geological mapping and gravity measurements in Obi related to oil surveying. Hall (1989, 1992) and Hall *et al.* (1992) undertook geological mapping and palaeomagnetic measurements on the North Molucca islands, as a part of the Sorong Fault Project, and Emily Forde has been studying the geochemistry of the Neogene volcanic rocks in Obi, Bacan and Halmahera islands as part of a Ph.D. project.

The primary aim of this study was to synthesise the published and unpublished information of earlier studies, together with the large amount of new data acquired during the University of London-GRDC cooperative investigation of the Sorong Fault Zone, and integrate all this data to produce a new stratigraphy and a new geological map of the Obi islands. The author was a

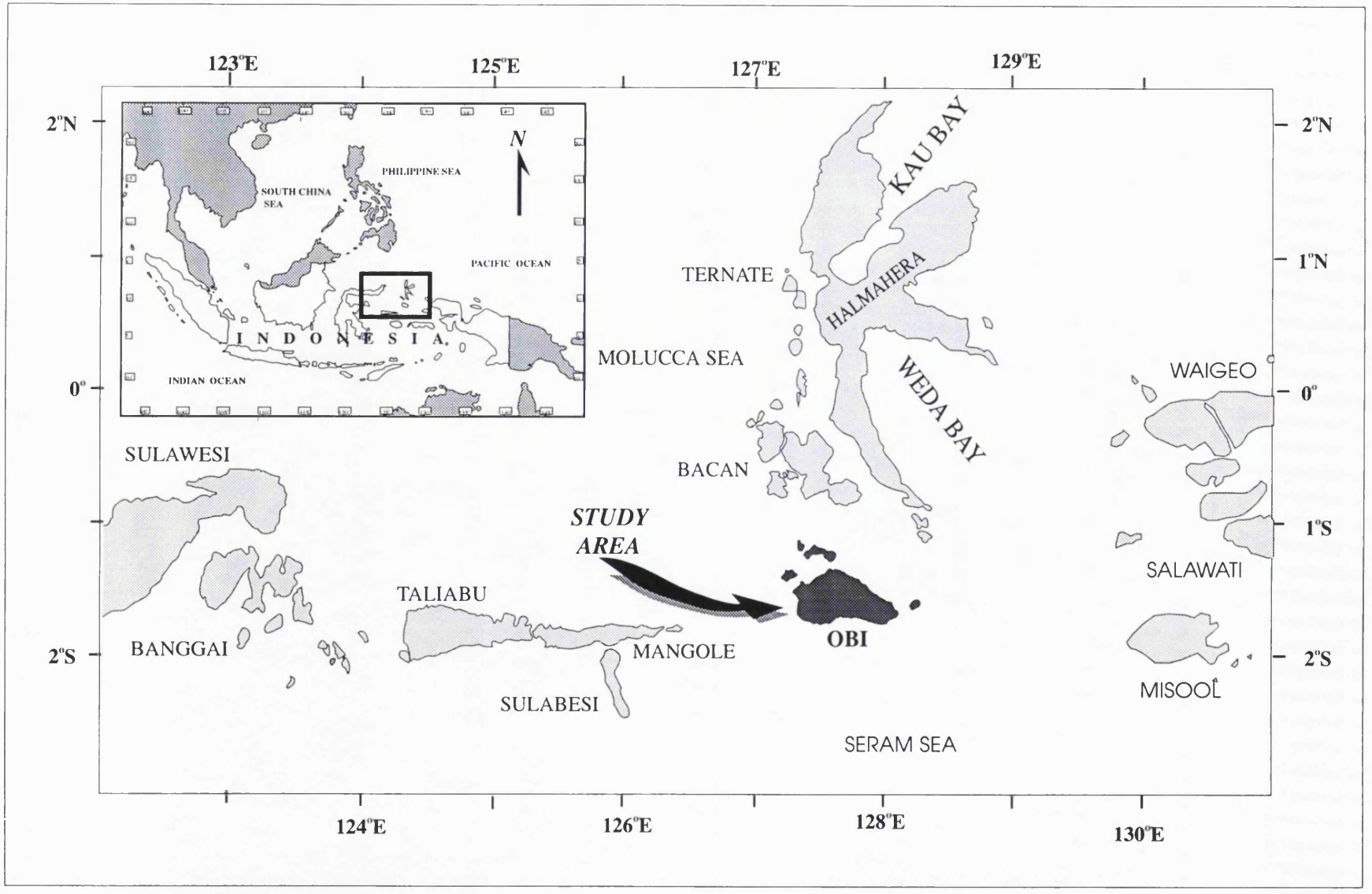

Fig. 1.1. Location of the Obi Islands.

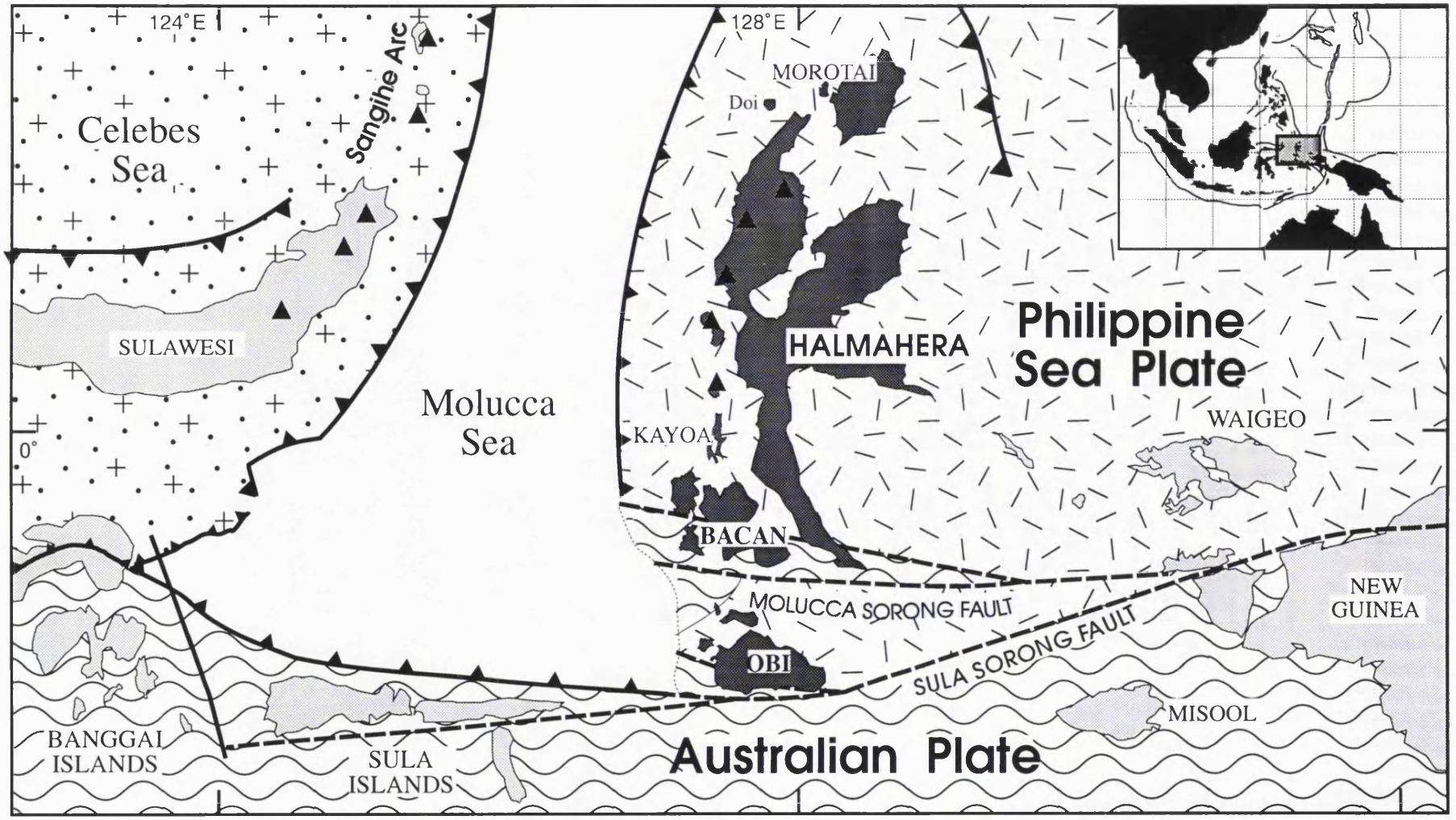

Fig. 1.2 Tectonic setting of the Obi Islands.

member of three expeditions to the islands in 1989, 1990 and 1992 which were part of the Sorong Fault Project, and has subsequently been working principally on petrological investigations of the material collected by these expeditions.

A second aim was to understand the tectonic and the geological evolution of the region, particularly that related to the petrology, geochemistry and mineralogy of rocks from several formations, including volcanic, plutonic and metamorphic rocks. New ages based on potassium-argon dating were obtained by the author and by Simon Baker who is conducting a regional K-Ar dating study as part of a Ph.D. project. Many new dates were based on palaeontology during the project. Thus, this study has involved describing and analysing the rocks in the field and laboratory; determining major, trace and rare earth element compositions of igneous and metamorphic rocks to identify their character and their history of alteration and metamorphism; and classifying the rocks to determine the tectonic history and evolution of the islands. The result this study were intended to improve the geological map and our understanding of the stratigraphy of the region; interpret sedimentologically and chemically the depositional environment of the units; decide the timing of depositional processes and relate them to the regional tectonic context; and finally reconstruct the tectonic evolution including identification of tectonostratigraphic units and the timing of their amalgamation.

1.3 Geographic setting

1.3.1 Location

The Obi islands are situated in the North Molucca islands, bordered to the north by the Bacan islands, to the east by Misool island, to the south by Seram island and to the west by Sulabesi and Mangole islands of the Sula group. They are located between 127°15' and 128°15' longitude, and between 1°21' and 1°45'N latitude (Fig. 1.1). The main island is Obi Major which is surrounded by Bisa, Tapas, Obi Latu, and Gomumu islands, covering an area of about 3,500 km^2. Administratively, Obi and the surrounding islands belong to the Laiwui District (Kecamatan), which is part of the North Molucca Regency (Kebupaten), in the province of Molucca.

1.3.2 Morphology and Relief

Based on morphology and relief Obi can be subdivided broadly into four parts: NE Obi, central Obi , SW-NW Obi and SE Obi (Fig. 1.3). NE Obi is dominated by Quaternary to Recent limestones resting upon Neogene limestones, sedimentary and volcanic rocks. This area extends from Kelo to the Anggai River, Belang-belang, and the islands of Bisa and Tapas (northern Obi). The island of Gomumu, south Obi has a similar morphology. The morphology is characteristic of karst topography with rough surfaces and conical hill shapes formed by older limestones,

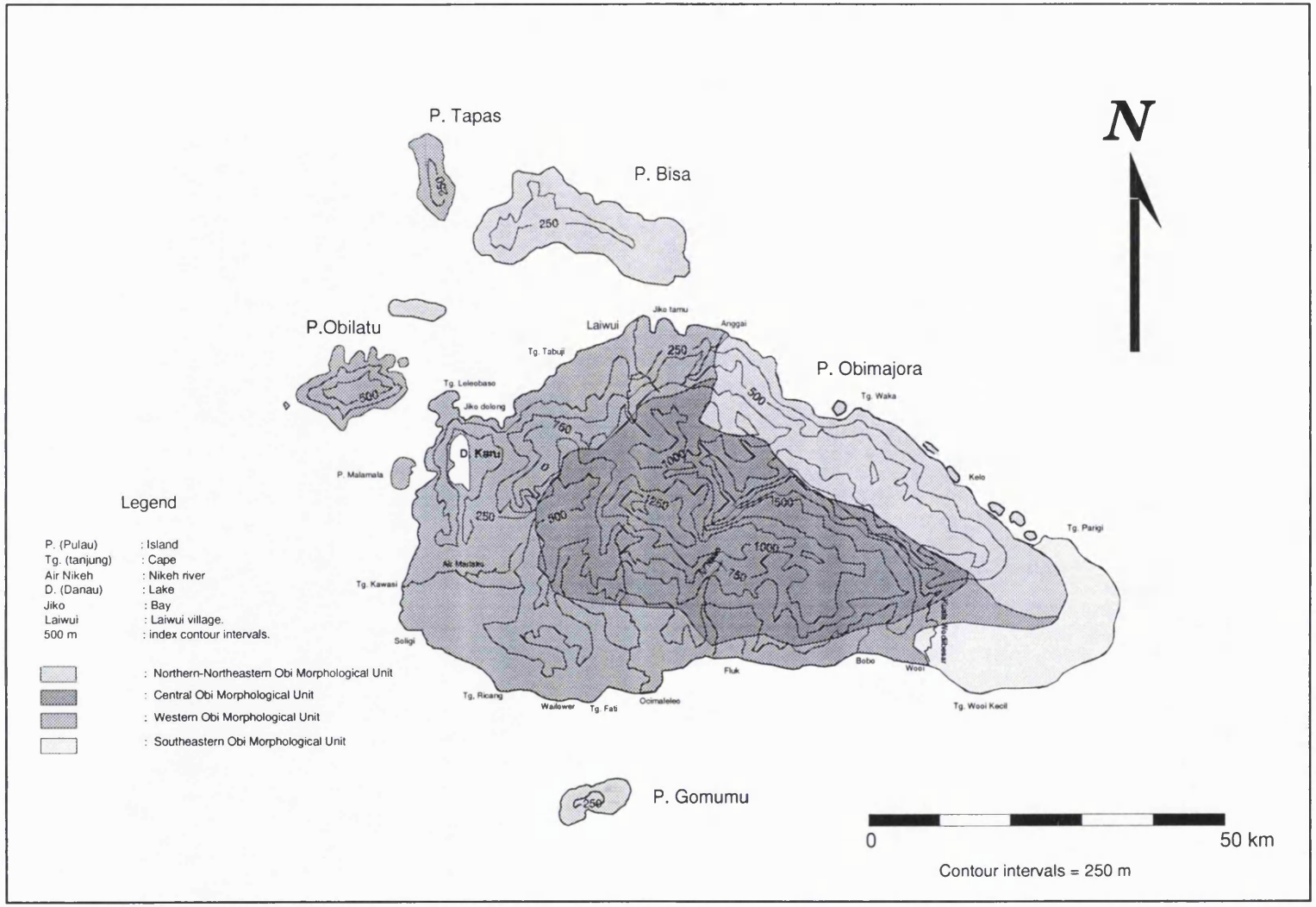

Fig. 1.3 Principal physiographic features and morphological areas of the Obi Islands.

whereas the younger limestones have a smoother morphology and in some places form terraces indicating rapid uplift or a fall in sea level. Both older and younger limestone areas have few rivers or subsurface running water. The highest point is about 1,500 m above sea level to the south of Anggai village. Typically, this unit is not densely covered by vegetation.

Central Obi is predominantly formed by the Neogene volcanics with very rough, high hills (up to 1,318 m above sea level), very deeply incised valleys, irregular topography and a coarse drainage pattern; locally it shows dissected streams, waterfalls and V-shaped valleys which indicate juvenile rivers.

SW Obi and NW Obi are formed by pre-Tertiary and Quaternary rocks. This area extends from the villages of Ocimaleleo, Tanjung Ricang and Jikodolong, and includes the island of Obi Latu and surrounding areas. It is characterised by undulating or rolling uplands, irregular streams and a dendritic drainage pattern. Some places show a smooth surface and light shading on aerial photographs which indicate serpentinites (pre-Tertiary rocks). Areas with rough surfaces and dendritic drainage pattern indicate that they are underlain by Quaternary rocks. The highest point is about 500 metres above sea level.

SE Obi is dominated by Quaternary to Recent rocks. The highest point in this unit is about 500 m above sea level and is underlain by alluvium and Quaternary limestones. Some parts are swamps or marshes and may be intermittently invaded by tidal seawater.

1.3.3 Settlement and Culture

The population lives on the coast, and inland areas are normally covered by primary forest. The people live in big groups in the villages which are led by a village chiefs (Kepala Desa). Most came from Halmahera and the surrounding islands, but some of them came from the other islands, particularly business men, such as logging camp managers. Their daily life depends on a slash-burn agriculture, fishing, collecting resin (damar) or working for timber companies. Islam is the dominant religion in the region, but there are Christians often living together with Moslems in a village.

1.3.4 Climate, Flora and Fauna

Since Obi is situated close to the equator, the climate in Obi is hot and humid. Temperatures vary between 26°C and 35°C. There are only two seasons in Obi, dry and wet, the former between September and March, while the latter is usually between April and August. The areas of tropical forest include very thick wild vegetation that extends up to the ridges of the mountains, except in the limestone areas which are sometimes covered by plantation. Coconut trees usually grow on the coast along with cocoa, nutmeg, and clove trees. The big trees such as meranti merah and meranti putih, which are used to produce building materials, grow in inland

areas, along with the damar (resin), rattan and gaharu trees. The fauna present in the area includes cockatoos, parrots, kingfishers, eagles, snakes, crocodiles, lizards, and many kinds of butterflies.

1.3.5 Accessibility and Logistics

Several documents (security clearances and work permits) are needed from several government departments as letters of permission to enter and to research a survey area. These documents are arranged by the Geological Research and Development Centre (GRDC) and are then brought to the Home Office Social Political Division in Jakarta. After that letters from the Home Office and the security clearances are used to obtain additional letters of permission from the provincial Governor and the Police Department in Ambon. Then other letters of permissions are obtained from the local Regency (Bupati), the District Administrator (Camat), and finally the head of the village (Kepala Desa) who we always visit. Porters can be hired through the Kepala Desa to help carry equipment, normally for 3 to 5 day survey traverses.

The survey area is accessible by plane from Jakarta (Merpati airline) or from Bandung (Bouraq airline) followed by boat. The route of Merpati (MNA) is Jakarta-Ambon-Ternate or Jakarta-Menado-Ternate, whereas the route of Bouraq is Bandung-Surabaya-Ujung Pandang-Ambon-Ternate. From Ternate, the survey area can be reached by boat that sails from Ternate-Labuha (Bacan Island)-Jikotamu or Laiwui (Obi Island). This journey from Ternate to Laiwui takes approximately 2 days. The expeditions for this survey hired a boat with capacity of 30 tonnes in Ternate for 60 days, which was used as a base and was used to travel between islands along the coasts. To reach the beach or to traverse along the lower parts of the rivers, a small speed-boat or long-boat with a 25 horsepower engine was used.

Small boats cannot reach the interior of Obi because the rivers are very shallow and they often have steep gradients and waterfalls. There are now several logging roads by which it is possible to travel inland up to about 26 km from the coast. Several of them were built by timber companies that exist in Kelo, Bobo and Ocimaleleo villages, whereas from Ricang, the logging road has gone through to Jikodolong. Although the timber companies are very helpful, often lending their vehicles for research, most of the traverses could only be made on foot. Traverses on foot in the wet season are not recommended, as we must follow tortuous slippery paths. Even in dry season the rivers sometimes flood suddenly without significant rainfall in the area of the traverse due to heavy local rain upstream in the interior. Survey equipment must be brought from England or Bandung, whereas food, fly camp equipment and fuel are available in Ternate or Bacan, but are unavailable in Obi.

The topographic maps that were used in fieldwork were topographic map series 1501, sheet SA 52-6 with a scale of 1:250,000, made by the United States Army in the Second World War. Aerial photographs, which have approximately 1:100,000 scale, made by cooperation between Australia and Indonesia, are available. Topographic maps are sometimes unreliable, especially

for location purposes. The best way is to interpret from aerial photographs, which cover the entire area (Fig. 1.4), although it is impossible to have stereo coverage during a traverse. Mapping was therefore mainly carried out on enlargements of aerial photographs, using compass and river features (bends and details of rivers are very easy to use for accurate location). In addition, during many traverses we were able to locate positions using a Magellan Navpro 1000 GPS receiver.

1.4 Review of Previous work

Little attention was paid to the geology of Obi until recently. Perhaps due to its inaccessible location and lack of many provisions, especially fuel, studies of the Obi region are scarce. However, there are many published and unpublished geological reports on the surrounding areas, particularly Halmahera which has a similar geological history. Some geological investigations of Obi and surrounding areas were undertaken by the Dutch between 1900 and the Second World War. After the Second World War, there have been regional investigations of geophysics, geochemistry and tectonic evolution of the region, which have been undertaken by the Geological Research and Development Centre (Indonesia), University of London, and other Indonesian and foreign institutions. In the past ten years there has been renewed interest in the geology of Obi.

1.4.1 Investigations Prior to the Second World War

Early geological investigations were undertaken by Martin (1903), Wanner (1913), Brouwer (1924) and Kuenen (1935). Although these studies were based on reconnaissance traverses, their reports have been very useful in the present investigation. Martin (1903) reported the presence of the Tertiary limestones containing foraminifera from Obi and Bacan. Wanner (1913) reported Jurassic ammonites as float in rivers of SW Obi. Brouwer (1924) in his reconnaissance report suggested that the Jurassic sediments in Gomumu and SW Obi Major are similar in character to the Jurassic sediments of the Sula islands. Although the sedimentary rocks (tuff, marly tuff and marl) in NW Obi Major were reported to be of uncertain age, they were considered similar to Jurassic sedimentary rocks of Buru and Misool islands, whereas Jurassic marly limestones of Obi Major were said to be similar to the rocks from Buru (Miting Limestone), East Seram (Nief Limestone), Misool and Timor. Based on this report, Brouwer (1924) concluded that the Jurassic beds in the Sula, Obi and Misool islands have many similarities to the Spiti Shales in the Himalayas. The presence of *Phylloceras* and *Stephanoceras humphriesi* in black shales with ferruginous concretions and quartzitic sandstone indicated that they were probably Upper Bajocian (Jurassic). Mesozoic and Tertiary sedimentary rocks in the southern part of the Obi Major islands, which are locally folded intensely, slightly or not all, were considered geologically similar to rocks of the islands of Timor and Seram. On the other hand the northern part of the islands of the Obi Major and the adjacent islands were said to show a close resemblance to the North Molucca islands. Pliocene volcanic rocks (augite andesite, containing amphibole and/or

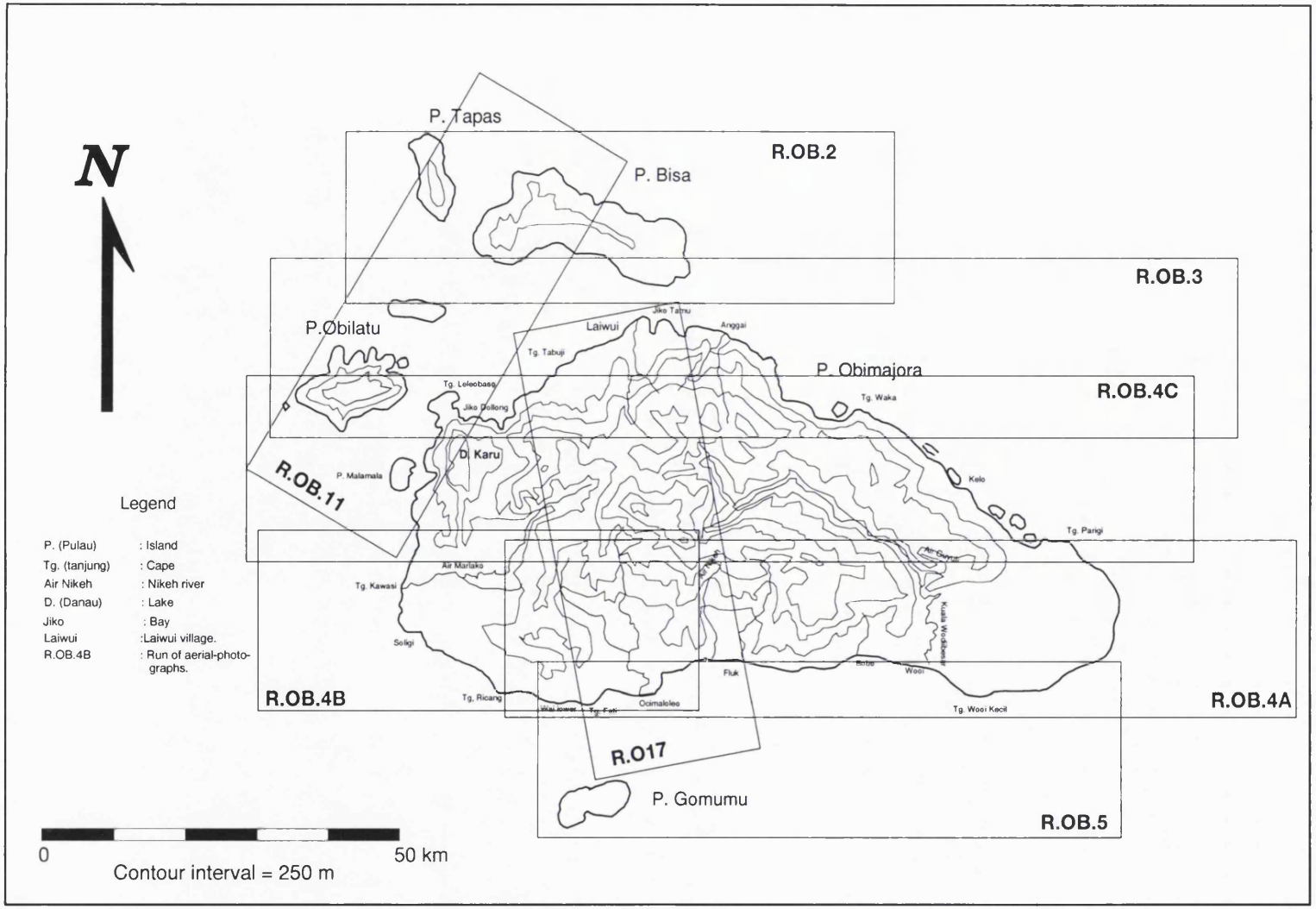

Fig. 1.4 Aerial photographic coverage of the Obi Islands.

biotite) in the eastern part of Obi Major were observed to be similar to Halmahera and Bacan volcanic rocks.

Kuenen (1935) accompanied the Snellius Expedition and described volcanic rocks of Tidore in the Halmahera arc. On the basis of silica contents the lavas were reported to include a fairly wide range of basalts and andesites with a glassy matrix. He proposed that the melts may have been derived from basic and ultrabasic rocks, which are widespread in the Halmahera and Obi area.

1.4.2 Post-War Studies of Obi

The major report from the early part of this period was written by Van Bemmelen (1949) who summarised previous, mainly Dutch, investigations. After that there were many studies of geology and geophysics of the surrounding region undertaken by Indonesian and foreign institutions in cooperation.

In his summary Van Bemmelen suggested that the oldest rocks of Obi are crystalline schists cropping out on Tapas island which may be metamorphosed Palaeozoic rocks corresponding to those of the Sula islands and Bacan. The crystalline basement complex of the Sibela Mountains of Bacan (Brouwer, 1924) consists of varieties of gneisses, schists, quartzites, amphibolites and acid intermediate igneous intrusions (granites, granite porphyries, diorites and diorite porphyries). This basement complex is unconformably overlain by the Jurassic-Cretaceous sedimentary rocks which are associated with basic and ultrabasic rocks. The oldest members of the basic-ultrabasic suite are probably peridotites which are largely serpentinized. They are succeeded by gabbroic and gabbro-dioritic rocks. The contact of basaltic rocks with dunite and gabbro-diorite is undoubtedly intrusive according to Kuenen (1935). The upper Mesozoic and lower Tertiary successions of sedimentary rocks are unconformably overlain by Pliocene sedimentary rocks. A considerable subsidence must have occurred in comparatively recent time (Kuenen, 1935), as on the west coast of Bacan an old fortress has been submerged one metre below low tide level (Van Bemmelen, 1949).

In his report on the tectonics of the Indonesian region, Hamilton (1979) based his geological information on the island of Obi from reports by Wanner (1913) and Brouwer (1924). He assumed that the presence of gabbro, diabase, basaltic rocks, quartzite, slates, jasper, schist, Jurassic black shale and Cretaceous globigerinid marl were part of a Tertiary melange. Ultramafic (serpentinite, harzburgite, lherzolite and wehrlite) rocks, were presumed to represent subduction melange, and Brouwer (1924) reported these were thrust over Tertiary andesites. The Tertiary melange is unconformably overlain by gently folded Neogene sedimentary rocks and Quaternary reefs. Hamilton suggested that some of the rock types, particularly the quartz monzonite, were derived from a continental fragment of north-western New Guinea which is

being carried westward (Fig. 1.5). He considered that Obi consists of Tertiary melange and Tertiary magmatic-arc volcanic rocks.

Sudana & Yasin (1983) published a stratigraphy and a 1:250,000 geological map of Obi, based on GRDC mapping. Gondwana Company (1985) undertook a geological survey for oil investigations and agreed with Hamilton (1979) in reporting the presence of melange in SW Obi.

1.4.3 Regional Tectonic Investigations

Marine geophysical and seismological interpretations have resulted from investigations undertaken in the Molucca Sea between Halmahera, Sulawesi and the Philippines. Hatherton & Dickinson (1969) published the first contoured map of earthquake hypocentres in Indonesia, which shows the foci beneath the Molucca Sea define two Benioff zones: Sangihe in the west and Halmahera in the east. Fitch (1972) made the first detailed studies of the relationship between earthquake focal mechanisms and the regional tectonics of eastern Indonesia. Cardwell *et al.* (1980) reviewed the principal results of previous seismological studies by Cardwell & Isacks (1978) and. Hatherton & Dickinson (1969). Using the spatial distribution of earthquakes in the region and earthquake focal mechanism solutions, they tried to envisage the geometry of lithosphere subducted beneath the eastern Indonesia and Philippine islands. They concluded that the Molucca Sea plate had been subducted to a depth of more than 200 km beneath the Halmahera arc, whereas at the time when the Talaud-East Mindanao Arc collided with the Sangihe-West Mindanao arc, the Molucca Sea Plate had been subducted almost 700 km beneath the western Mindanao arc and Celebes Basin.

Sukamto *et al.* (1981) divided the Halmahera group of islands into three provinces, which are based on physiography, rock assemblages, stratigraphy, structure and tectonic development (Fig. 1.6). According to Sukamto, the first province is the East Halmahera-Waigeo non-volcanic arc (east arm of Halmahera, Gebe, Gag, and Waigeo), characterised by ophiolite rocks, imbricated with deep water Mesozoic sediments containing fragments of ophiolite rocks and Tertiary clastic and carbonate sedimentary rocks. The structures of this area are dominated by compressional tectonics. The second province is the West Halmahera-Obi volcanic arc (Morotai, west arm of Halmahera, Ternate, Tidore, Makian, Bacan and Obi), which is characterised by volcanic activity since the Oligocene. These volcanic rocks unconformably overlie the basement rocks which consist of ophiolitic rocks in Obi Major and regional metamorphic rocks in Tapas and Bacan. The volcanoes were active in the Oligocene-Middle Miocene and were associated with marine clastic, and carbonate deposits. They were active again in the Late Miocene-Pliocene on Bacan. The structure of this province reflects tensional tectonics which caused the development of block faulting. The third province is the Talaud-Tifore non-volcanic arc of the central Molucca Sea, characterised by ophiolitic rocks associated with melange. These rocks are

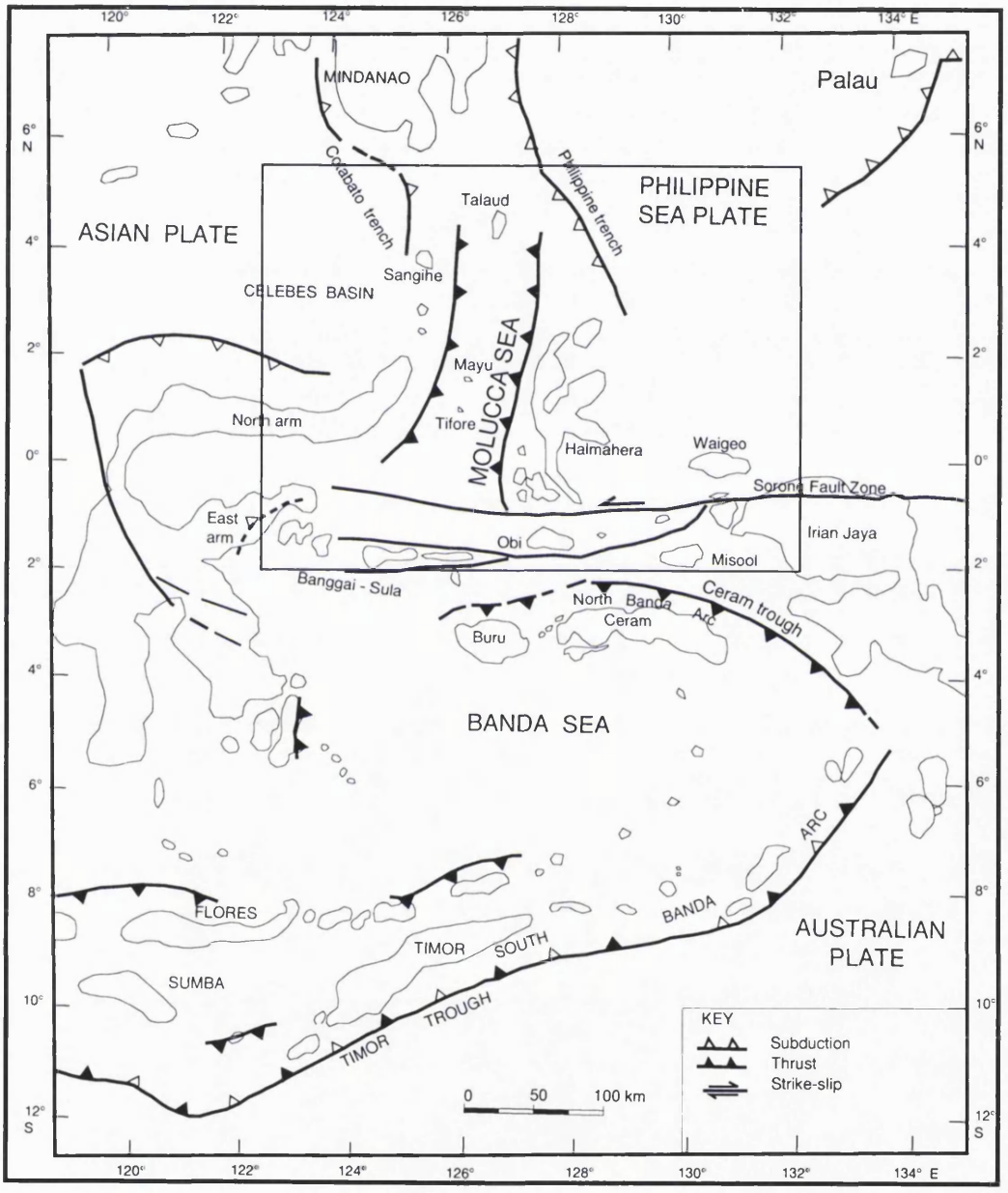

Fig. 1.5 Tectonic map of the region around Obi, modified from Hamilton (1978).

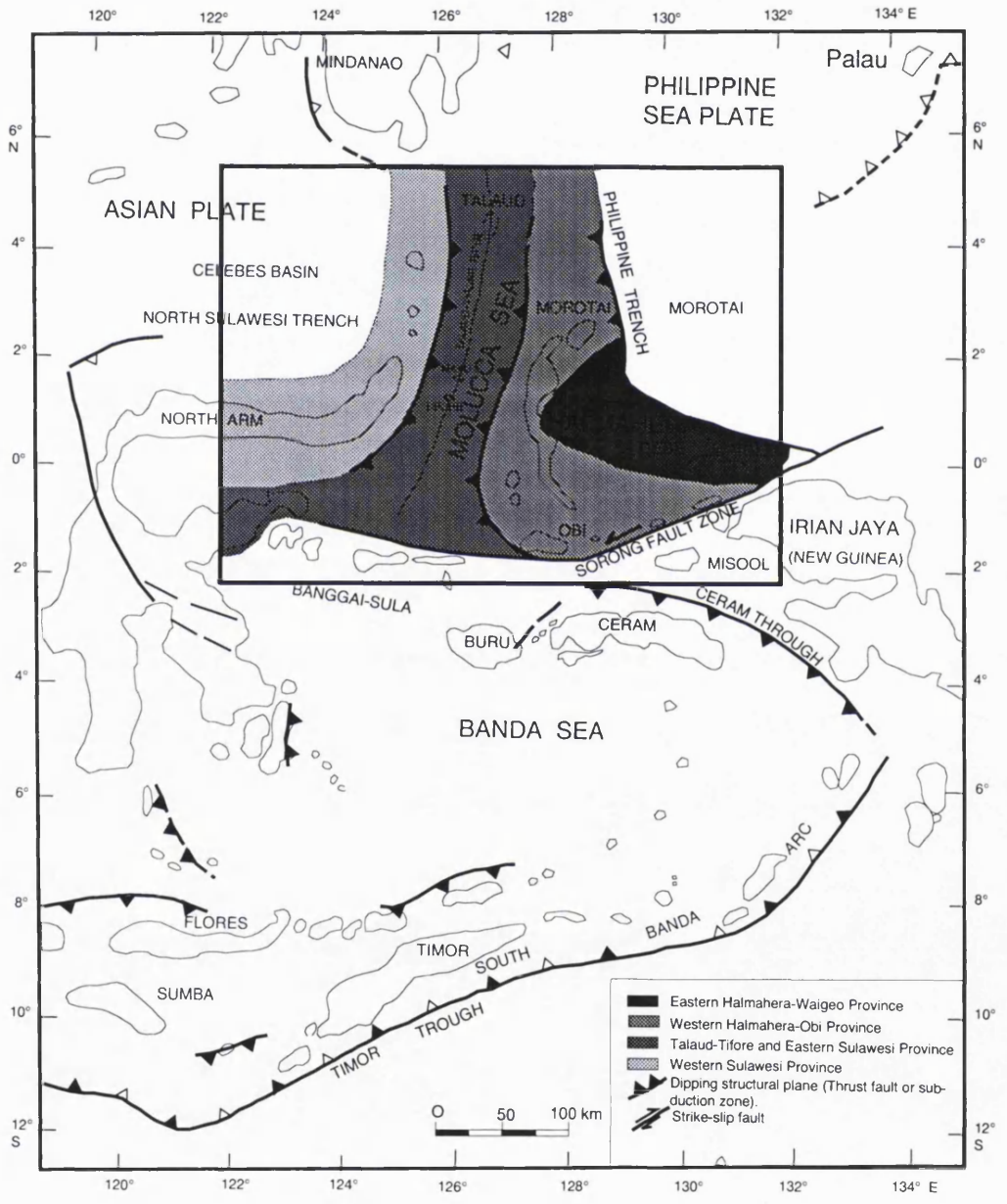

Fig. 1.6. Geological Provences of the Halmahera Region after Sukamto et al. (1981).

overlain by a sequence of Middle Miocene to Pliocene sedimentary rocks. Thrust faulting, associated with melange, indicates compressional tectonics to be dominant.

Soeria-Atmadja (1981) believed that Halmahera represents a paired metamorphic belt which is composed of a high pressure metamorphic belt on the ocean side (eastern arc) and a low pressure metamorphic belt on the western side. However, he did not describe any evidence for the presence of high pressure metamorphic rocks in eastern Halmahera. Based on the variation of SiO_2, FeO*, MgO and TiO_2, he also concluded that the Oligocene-Miocene volcanic rocks of the western Halmahera-Obi province (Sukamto *et al.*, 1981) have calc-alkaline affinities indicated by decreasing FeO* and TiO_2 contents with increasing FeO*/MgO. On the other hand the ophiolitic rocks in the Eastern Halmahera-Waigeo province were said to have a tholeiitic affinity shown by increasing TiO_2 and FeO* contents with increasing FeO*/MgO. He also believed that the ophiolite of Obi belonged to an island arc setting.

Morris *et al.* (1983) studied the geochemistry of the volcanic rocks in the Halmahera region using major, trace element and isotopic analyses. They divided the arc region into three provinces which are characterised by a distinct chemistry and tectonic setting. The first province is the active arc from Kayoa northwards to NW Halmahera. It consists of basaltic andesite and andesite, characterised by high Al_2O_3 and less than 1% TiO_2. The concentrations of alkali elements, Ba and Sr are typical of oceanic island arcs. The second province is the southern part of Bacan which consists of dacitic rocks. These have a high $^{87}Sr/^{86}Sr$ ratio and high concentrations of Rb and Cs, indicating interaction with continental crust. The third province includes inactive volcanic islands along the Sorong Fault Zone dominated by andesites with high Al_2O_3 contents, low TiO_2, and no FeO* enrichment trend with fractionation. Alkali contents are higher than lavas from the oceanic arm. Ba and Sr show large enrichments.

Silver & Smith (1983) considered that the tectonic setting of the east Indonesian-New Guinea region is an analogue of the tectonic setting in the Mesozoic Western Cordillera of the USA. This analogy is reflected by terranes which are considered to have travelled hundreds to thousands of kilometres and which appear to include as relics of island arcs, oceanic plateaus and islands, continental margin fragments and complex accretionary terranes including melange belts, ophiolite fragments and thrust faulted forearc provinces. They suggested that the movement of terranes has been driven by the motion of the Pacific, Caroline, Australian and SE Asian plates.

Pigram & Panggabean (1984) suggested that the rifting (start of break-up) of the upper Palaeozoic-Mesozoic sequence of the northern part of the Australian continent began at about 230 Ma. The post-break-up unconformity related to the initiation of sea floor spreading is dated as about 185 Ma in Papua New Guinea and 170 Ma in Irian Jaya. Based on resemblances of the continental basement complex of Obi-Bacan to the basement in the central Papua New Guinea,

they suggested that the Obi-Bacan microcontinent was derived from Papua New Guinea and not from the northern edge of the Bird's Head where there are no Jurassic sedimentary rocks.

Hartono & Tjokrosapoetro (1984) subdivided the Indonesian archipelago into 13 terranes based on palaeontology, palaeomagnetics and stratigraphy. The terranes are Proto-Kalimantan, Sumatra basement, SW Sulawesi, Australia, northern Irian Jaya arc, Sulawesi ophiolite, Sumba, Seram, Timor, Buton, Banggai-Sula, Buru and Bacan. The slicing of northernmost portion of Irian Jaya and movement of the slices westward by Sorong Fault Zone have formed the Banggai-Sula, Bacan and Buru terranes. The ultrabasic rocks in Bacan are interpreted to belong to the Tertiary island arc terrane of Irian Jaya-Halmahera, whereas the metamorphic rocks in Bacan were derived from New Guinea.

In studying the structure of the North Banda-Molucca area from multi-channel seismic reflection data, Letouzey *et al.* (1983) concluded that NW-SW late Neogene thrusts and anticlines are present in the NE part of the south Halmahera basin. In addition, several sinistral, transcurrent and reverse faults appear along the Sorong Fault Zone (Fig. 1.7). The remnants of the Molucca Sea plate were interpreted to be exposed in Obi and east Sulawesi, due to collision of the Philippine Sea and the Australian plates. They also suggested that thick Neogene sediments in the north and east Obi basins were forearc sequences of a volcanic-plutonic complex, uplifted during the collision. Intrusion related to the present Halmahera volcanic arc disturbed the sediments in these basins (Fig. 1.8).

In a paper concerning Cenozoic plate tectonics and basin evolution in Indonesia, Daly *et al.* (1991) suggested that in the Late Eocene (40 Ma) the Philippine Sea plate migrated NW, whereas the western boundary moved clockwise on a collisional course with Australian plate. In the Early Miocene (20 Ma) the island arcs between Australia and the Pacific collided with the northern margin of Australia. The effect of this collision was to move parts of the northern passive margin of Australia westward. In the Middle Miocene (10 Ma) a strike-slip fault displaced Banggai-Sula to the NW to collide with the east arm of Sulawesi. At this time the Halmahera region was possibly an oceanic plateau or another shallow marine feature and belonging to the Philippine Sea plate. In the Early Pliocene (5 Ma) the dip direction of the Philippine trench had flipped to be east-facing, resulting in Halmahera moving westward to the present position and forming the Molucca Sea.

Struckmeyer *et al.* (1993) interpreted the Triassic to late Cenozoic evolution of the New Guinea-east Indonesian region and attempted to restore allochthonous components to their original locations, placing the reconstructions in a global latitudinal framework. On the basis of palaeomagnetic data and the kinematic constraints of plate motion, they produced computer-generated plate tectonic reconstructions and depositional environment maps of the Australian margin. There are six palaeogeographic maps for the New Guinea region capturing

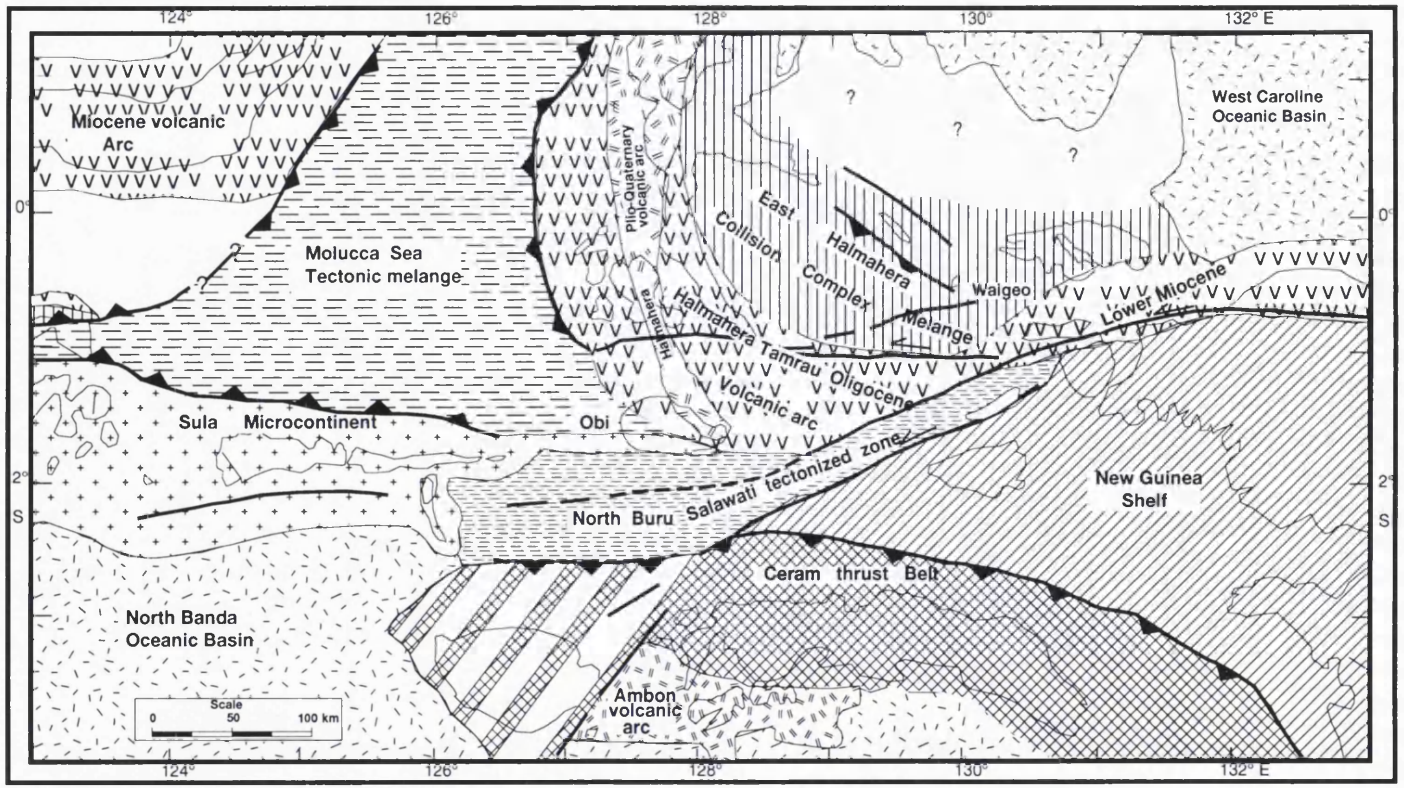

Fig. 1.7 Tectonic map of the Halmahera region, from Letouzey et al.,(1983)

- Pre-Jurassic continental basement
- Australian continental basement
- Oceanic crust
- Plio-Quaternary volcanic arc
- Paleogene-Miocene volcanic and plutonic arc
- Ultramafic and collision complex melange
- Ceram thrust belt
- Molucca Sea tectonic melange
- North Buru-Salawati tectonic zone
- Main fault
- Front of sedimentary prism

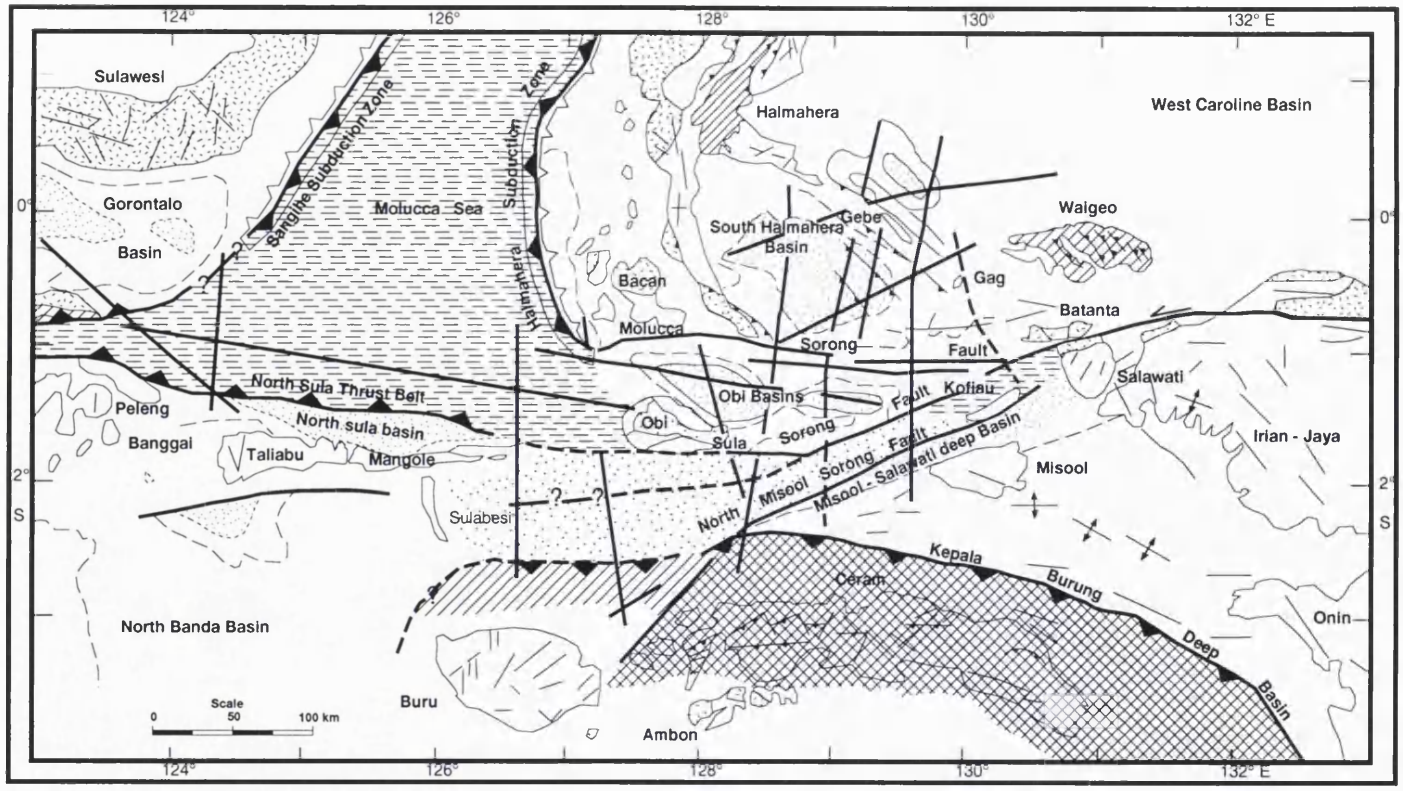

Fig. 1.8 Structural map and position of sedimentary basin (after Letouzey et al., 1983)

- Ultramafic and collision complex melange
- Volcanic and plutonic rocks
- Isopach 1 TWT
- Isopach 2 TWT
- Isopach > 2TWT
- Molucca Sea Tectonic melange
- North Buru-Salawati tectonized zone
- Ceram thrust belt
- Main Faults
- Wrench Faults
- Front of sediment wedge
- Dip of Benioff Zone

interpretations of major plate tectonic events and processes during the Mesozoic to Cenozoic development of the New Guinea Orogen.

Hall *et al.* (1995a,b,c) reviewed the tectonic development of eastern Indonesia and the Philippine Sea plate based on new geological and palaeomagnetic data collected during the Sorong Fault Project. They proposed that continental fragments from the northern margin of Australia have moved west in the Sorong Fault Zone after collision between a Philippine Sea plate arc and Australia in the early Miocene. Fragments of the Philippine Sea plate arc are suggested to be represented in Obi. Palaeomagnetic rotations recorded from Obi (Ali & Hall, 1995) are suggested to reflect strike-slip movements in the Sorong Fault system which was initiated in the early Neogene. Hall (1995a,b) has integrated the Philippine Sea plate history and geological development of the Halmahera-Obi region into a plate tectonic model for the whole of SE Asia. This model suggests that Obi formed part of the Philippine Sea plate before the Neogene and subsequently was situated in a complex strike-slip plate boundary zone which resulted in the juxtaposition of Australian continental and Philippine Sea fragments in east Indonesia.

1.4.4 London University-GRDC Investigations

The most recent work in the Halmahera and the surrounding area has been carried out by collaboration between the University of London and GRDC, Bandung. The work was undertaken by field expeditions in 1984, 1987, 1988, 1989, 1990 and 1992 and has produced unpublished reports and several publications concerning the stratigraphy, geological history and the tectonic evolution of the region.

In the first publication, Hall (1987) suggested that the Upper Cretaceous-Lower Tertiary basement complex of Halmahera and east Mindanao has formed part of a single plate, the Philippine Sea plate, since the Late Eocene-Early Oligocene. Volcanic activity began in the Pliocene in Halmahera, due to eastward subduction of the Molucca Sea plate beneath Halmahera. He reported that in the area of investigation in the NE arm and central Halmahera there was no evidence for an Oligo-Miocene volcanic arc. The movement of the Philippine Sea plate was impeded by diachronous collision at the western edge of the Philippine Sea Plate which began in Mindanao in the Late Miocene, causing further motion to be taken up by a combination of strike-slip motion along the Philippine Fault, subduction of the Philippine Sea at the Philippine trench and subduction of the Molucca Sea lithosphere beneath Halmahera (Figs. 1.9 and 1.10).

Hall *et al.* (1988a) suggested that the ophiolitic basement of eastern Halmahera is overlain unconformably by middle Oligocene and younger sedimentary and volcanic rocks. The basement includes a dismembered ophiolite with slices of Mesozoic and Eocene sedimentary rocks. Stratigraphical and petrological similarities with the Mariana forearc caused them to interpret the eastern Halmahera Basement Complex as a pre-Oligocene forearc lacking an accretionary

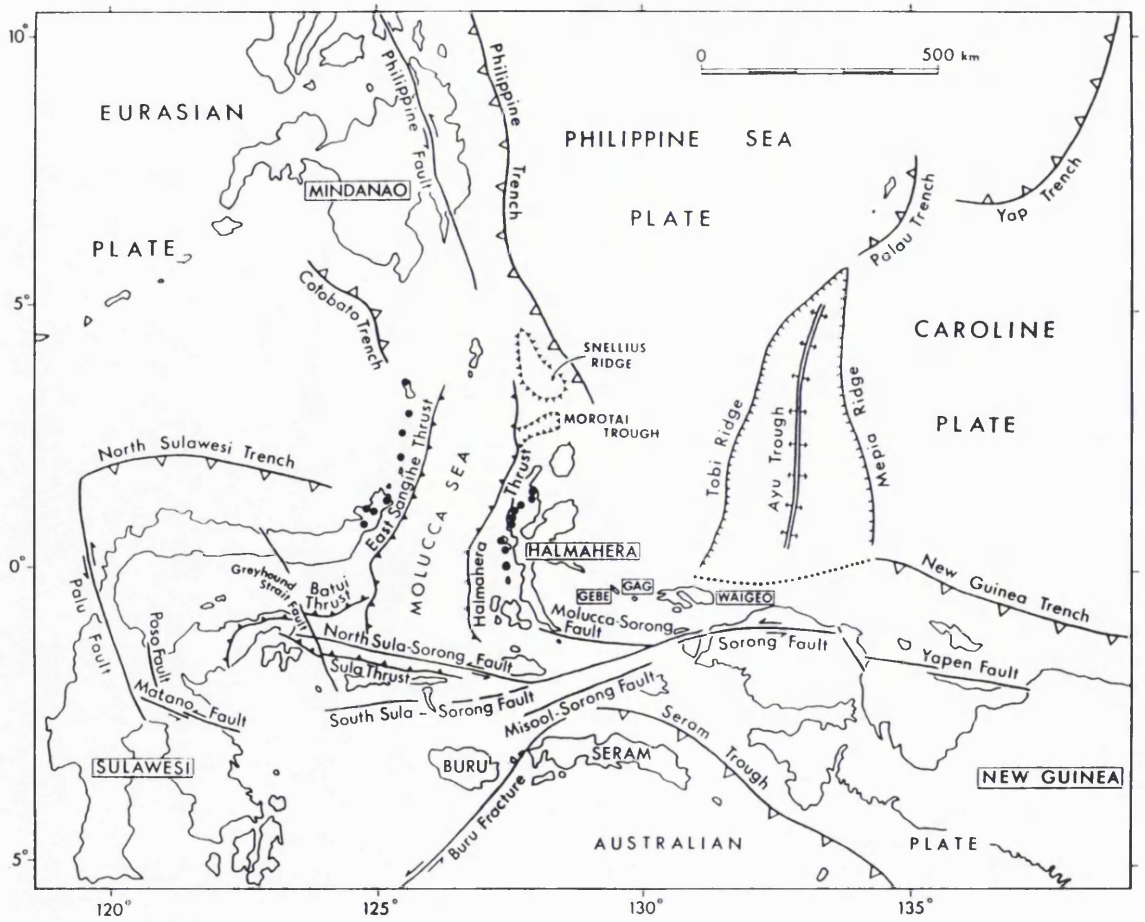

Fig. 1.9 Principal tectonic features of the Halmahera region, from Hall (1987), after Hamilton (1979) and Silver (1981). Solid triangles are active volcanoes of the Halmahera and Sangihe arcs. Slip rates along the Philippine Trench from Ranken et al. (1984).

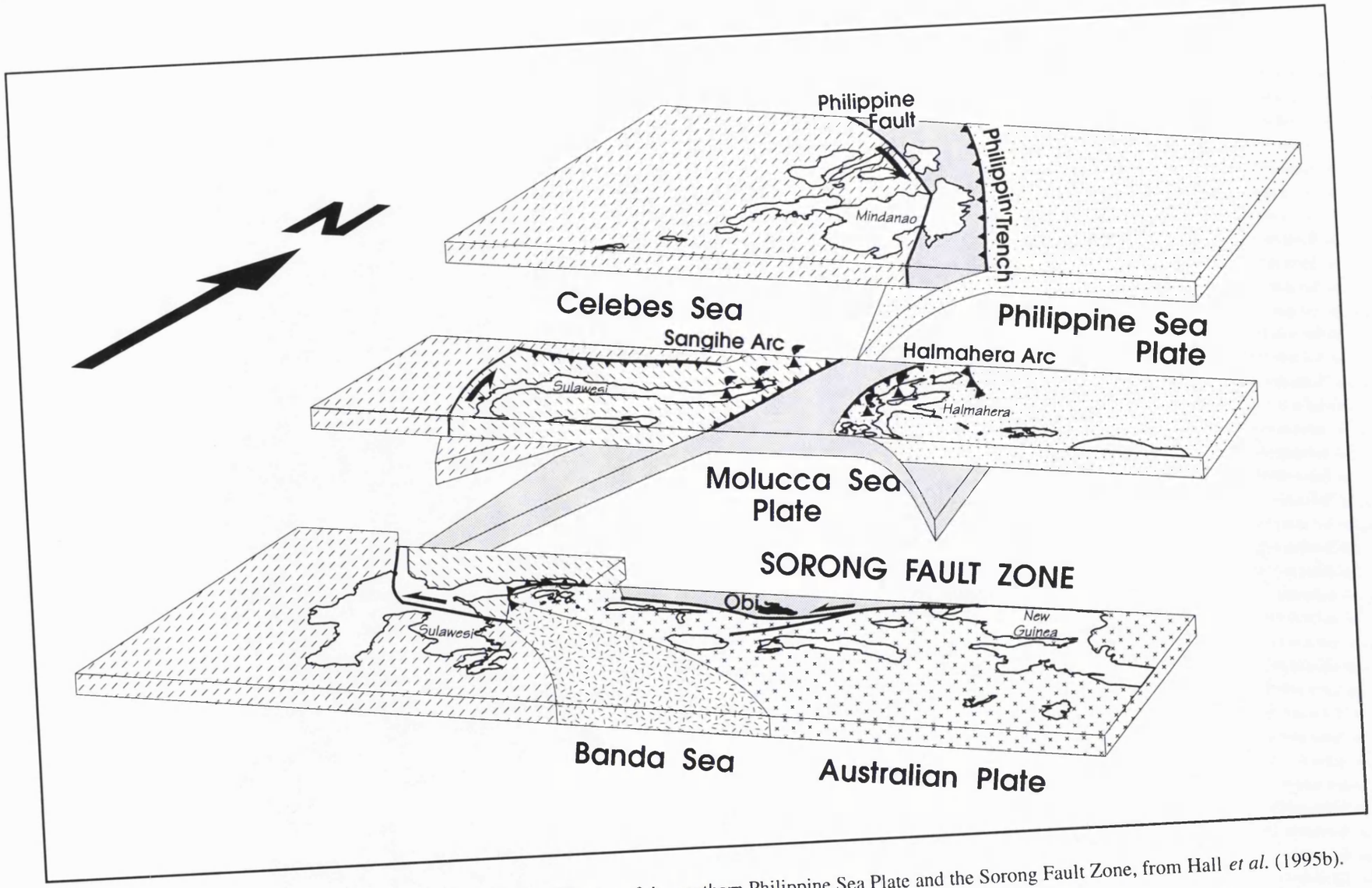

Fig. 1.10. Simplified block diagram showing the present-day tectonics of the southern Philippine Sea Plate and the Sorong Fault Zone, from Hall *et al.* (1995b).

complex. There is some evidence that the pre-Oligocene volcanic arc, behind this forearc, formed part of the basement of western Halmahera. The deeper parts of forearc are represented by imbricated igneous, metamorphic, and Mesozoic and Tertiary sedimentary rocks. The eastern Halmahera Basement Complex can be traced into eastern Mindanao, and may be related to similar terranes within and around the present Philippine Sea plate. The basement of continental metamorphic rocks in Bacan was interpreted to be part of the north Australian continental margin basement which is separated from Halmahera Basement Complex by a splay of the Sorong Fault System and the deformed Ophiolite Complex of Bacan was suggested to represent magmatism in the fault zone.

Hall *et al.* (1988b) described a new stratigraphy and the Neogene history of Halmahera and the development of the present island arc. According to them, part of a Cretaceous-Early Tertiary forearc, which is formed by the Ophiolitic Basement Complex, is unconformably overlain by Upper Paleogene and younger rocks. After volcanic arc activity ceased in the Eocene, the former forearc of eastern Halmahera was uplifted and eroded in the Late Paleogene. Shallow water carbonate deposition began between the mid-late Oligocene and the end of Miocene and there is no evidence for arc volcanism in central Halmahera. The subduction of the Molucca Sea Plate eastwards beneath Halmahera caused subsidence in the backarc region, and as a result a sedimentary basin formed which was filled by turbidite sediments and Pliocene volcanic debris derived from the western arm of Halmahera. A Plio-Pleistocene deformation event caused folding and local thrusting in central Halmahera. The activity of the Quaternary volcanic arc began within the last 1 Ma and unconformably covered the Pliocene volcanic arc.

Hakim (1989) and Hakim & Hall (1991) described the petrology, geochemistry, and low temperature alteration of volcanic rocks in Halmahera. They compared the pre-Neogene (Upper Cretaceous?) Oha volcanic rocks and the Neogene Weda Group volcanics. The Oha volcanics are mainly basalts (with minor andesites) typical of island arc tholeiites with olivine, plagioclase and clinopyroxene which are chemically similar to Upper Cretaceous rocks from east Halmahera. In contrast, Weda Group volcanics are andesites with minor basalts and dacites reflecting plagioclase, pyroxene, hornblende and magnetite fractionation and including some medium-K to high-K calc-alkaline rocks. The Weda Group volcanics are fresh, although some rocks are affected by local low-grade alteration which indicate typical geothermal alteration, whereas the Oha volcanics have suffered zeolite and local sub-greenschist facies alteration. The Weda Group volcanics were considered similar to rocks from the Marianas, New Hebrides and other island arcs of the west Pacific.

Hall *et al.* (1991) reported that there were three distinctly different groups of pre-Neogene basement rock types in the islands around the southern Molucca Sea: ophiolitic complexes overlain by Upper Cretaceous and Eocene forearc sedimentary rocks on east Halmahera, Waigeo,

Gebe, Gag and Obi; arc volcanic and volcaniclastic rocks from Morotai, NW Halmahera, SW Halmahera, and north and south Bacan; continental metamorphic complexes from central Bacan and Obi. They reported that high-grade metamorphic rocks on the island of Tapas, NW of Obi, resemble those of the Sibela Mountains of Bacan. They include highly foliated epidote, chlorite and hornblende schists and coarse, locally pegmatitic amphibolites and hornblendites. These rocks are in fault contact with basic and ultrabasic rocks of the ophiolite complex of Obi. In SW Obi the metamorphic rocks are not exposed but there are (?)Triassic-Jurassic micaceous sandstones containing *Pentacrinus*. Hall *et al.* (1991) interpreted Obi as the contact between the Australian continental margin and an ophiolite complex of a `Pacific' terrane. The continental margin basement was interpreted to be the high-grade metamorphic rocks exposed on the west coast of Tapas and the contact between the ophiolite complex and the continental basement with its Mesozoic cover may be a thrust or a strike-slip fault.

Malaihollo (1993) studied the geology, mineral chemistry and geochemistry of the continental, volcanic and ophiolite rocks in Bacan and produced a new geological map and stratigraphy, and proposed an interpretation of the tectonic evolution of this region. Principally he agreed with Hamilton's (1979) opinion that the Sibela Mountain continental rocks were derived from the Australian Craton. This unit was juxtaposed against the unmetamorphosed Sibela Ophiolite which was probably derived from the Philippine Sea Plate. He interpreted the arrival of the Australian continental fragment in Bacan to have occurred before the Late Miocene, due to either : a) collision, b) strike-slip translation and subsequent thrusting, or c) both collision followed by strike-slip translation and subsequent thrusting.

1.5 Present Tectonic Framework of the Area Surrounding Obi

As a result of the investigations in eastern Indonesia, particularly those of the last 15 years, the principal features of the tectonic framework of the region around Obi can now be identified. These are outlined below on the basis of the studies reviewed above.

1.5.1 Halmahera Arc

Halmahera is bounded by the Molucca Sea to the west, the Philippine Sea to the east, the Sorong Fault Zone to the south and a NE-SW strike slip fault to the north. All of Halmahera currently forms part of the Philippine Sea plate. The Halmahera arc formed above an east-dipping Benioff zone which is present to a depth of ~230 km. Molucca Sea plate subduction eastward beneath Halmahera began in the late Middle Miocene (Baker & Malaihollo, 1995) and led to the formation of a Neogene volcanic arc (Weda Group) which is built unconformably upon the volcanic sequence of the Oha Formation in west Halmahera (Hakim & Hall, 1991), now thought to be Eocene-Oligocene in age (R. Hall, pers. comm., 1995). Eastern Halmahera has a basement of ophiolitic rocks with slices of the Mesozoic and Eocene sedimentary rocks interpreted formed

in a Late Cretaceous-Early Tertiary forearc. Eocene-Oligocene arc rocks are now known from the whole of the Halmahera groups of islands (Hall *et al.*, 1992).

1.5.2 Molucca Sea Plate

The Molucca Sea plate lies between the Eurasian Plate (represented by the Sangihe arc and the area to the west) and the Philippine Sea plate. It is bounded by Sorong Fault Zone to the south and Philippine archipelago to the north. This plate is being subducted beneath Halmahera to the east and beneath Sangihe to the west (Hatherton & Dickinson, 1969; Hamilton, 1979) and has been almost completely eliminated by subduction and now has an inverted U-shaped configuration (Cardwell *et al.*, 1980). Collision on both side creates a high central ridge exposing the islands of Talaud, Mayu and Tifore interpreted as the Molucca Sea 'melange' wedge or collision complex (Silver & Moore, 1978: Hamilton, 1979; Moore *et al.*, 1981; Sukamto *et al.*, 1981). This complex has been thrusted eastward, westward and southward (Silver & Moore, 1978) as a result of the convergence between the Halmahera and Sangihe arcs.

1.5.3 Philippine Sea Plate

Philippine Sea plate, which separates the Eurasian and Pacific Plates, is formed of oceanic crust bordered by strands of arc systems. It is bounded by the Ryukyu trough to the north, the Mariana and Bonin trenches to the east, the Sorong Fault Zone to the south and the Philippine trench and the Halmahera trough to the west. This plate has been subducted westward under the Philippine archipelago as the plate rotated clockwise with respect to Eurasia (Haston & Fuller, 1991). The total rotation since the early Eocene is ~ 90° (Hall *et al.* 1995c). The Philippine trench northeast of Halmahera is very young and there is less than 150 km of subducted lithosphere (Cardwell *et al.*, 1980). It does not extend south of about 2° N, but seismicity suggests that the Philippine trench ceases south at about 2°50'N with a NE-SW dextral strike-slip zone linking the Philippine trench to the Molucca Sea collision zone (Nichols *et al.*, 1990). Halmahera is in the process of amalgamation from the Philippine Sea Plate to the Eurasian Plate (Hall & Nichols, 1990).

1.5.4 Sorong Fault Zone

The Sorong Fault Zone is a major sinistral strike-slip fault system which runs approximately east-west from the Bird's Head of the northern part of Irian Jaya to eastern Sulawesi. This fault is divided into two strands in the area of Obi: the Molucca Sorong Fault Zone and the Sula Sorong Fault Zone (Hamilton, 1979). The Molucca Sorong Fault Zone forms the southern boundary of the Molucca Sea plate and the Philippine Sea Plate, whereas the Sula Sorong Fault Zone forms a boundary with the Australian continental fragments of Irian Jaya, Buru and Seram to the south (Hamilton, 1979; Letouzey *et al.*, 1983; Pigram & Panggabean, 1984; Dow & Sukamto, 1984).

There are several other splays of the Sorong Fault system in the region (Letouzey *et al.*, 1983) and the amount of displacement on each is uncertain.

1.5.5 Obi

Obi lies between the Sula Sorong and the Molucca Sorong faults (Hamilton, 1979; Letouzey *et al.*, 1983) and the geology of the island is summarised in Chapter 2 and discussed in detail in subsequent chapters. Parts of NW and SW Obi are built on high-grade metamorphic rocks, only exposed in Tapas island. These rocks are thought to be unconformably overlain by Triassic and Jurassic sediments which are exposed in the SW Obi. These parts of Obi are considered to represent fragments of Australian continental origin which originated from New Guinea and were moved by the Sorong Fault Zone to the west (Hamilton, 1979). Quaternary sediments unconformably overlie the older rocks.

The remaining parts of Obi, principally in the north, NE and SE of the island are underlain by ophiolitic rocks which constitute the basement. The age of these rocks is uncertain but they are not younger than Cretaceous. They include ultramafic rocks, plutonic rocks and volcanic rocks unconformably overlain by the Cretaceous sediments which consist of volcaniclastic sediments and pelagic limestones. The ophiolite rocks resemble the rocks of the Philippine Sea plate known from Halmahera. These rocks are covered by Tertiary volcanic and sedimentary rocks. An inferred unconformity separates the Mesozoic rocks from the volcanic and volcaniclastic rocks of Oligocene age. These arc rocks are folded and deformed and overlain by Neogene limestones, followed by volcanic and volcaniclastic rocks considered to represent the earliest activity of the Halmahera arc following eastward subduction of the Molucca Sea plate. Plio-Pleistocene limestones and clastic sediments overlie all the older rocks. Volcanic activity ceased in the Pliocene and currently there is no volcanic activity on the island.

1.6 Methods

1.6.1 Sampling Methods

Geological mapping was carried out during October-November 1989, July-August 1990, and September-October 1992, as part of the University of London Sorong Fault Zone Project in collaboration with GRDC. Nearly 1000 samples were collected during traverses, both from outcrop and as float; sample localities are shown on Fig. 1.11.

1.6.2 Petrographic Methods

Thin sections were examined using a binocular polarising microscope to describe texture and mineralogy, used to identify and classify the formations based on their character. Limestones have been classified according to the scheme of Dunham (1962).

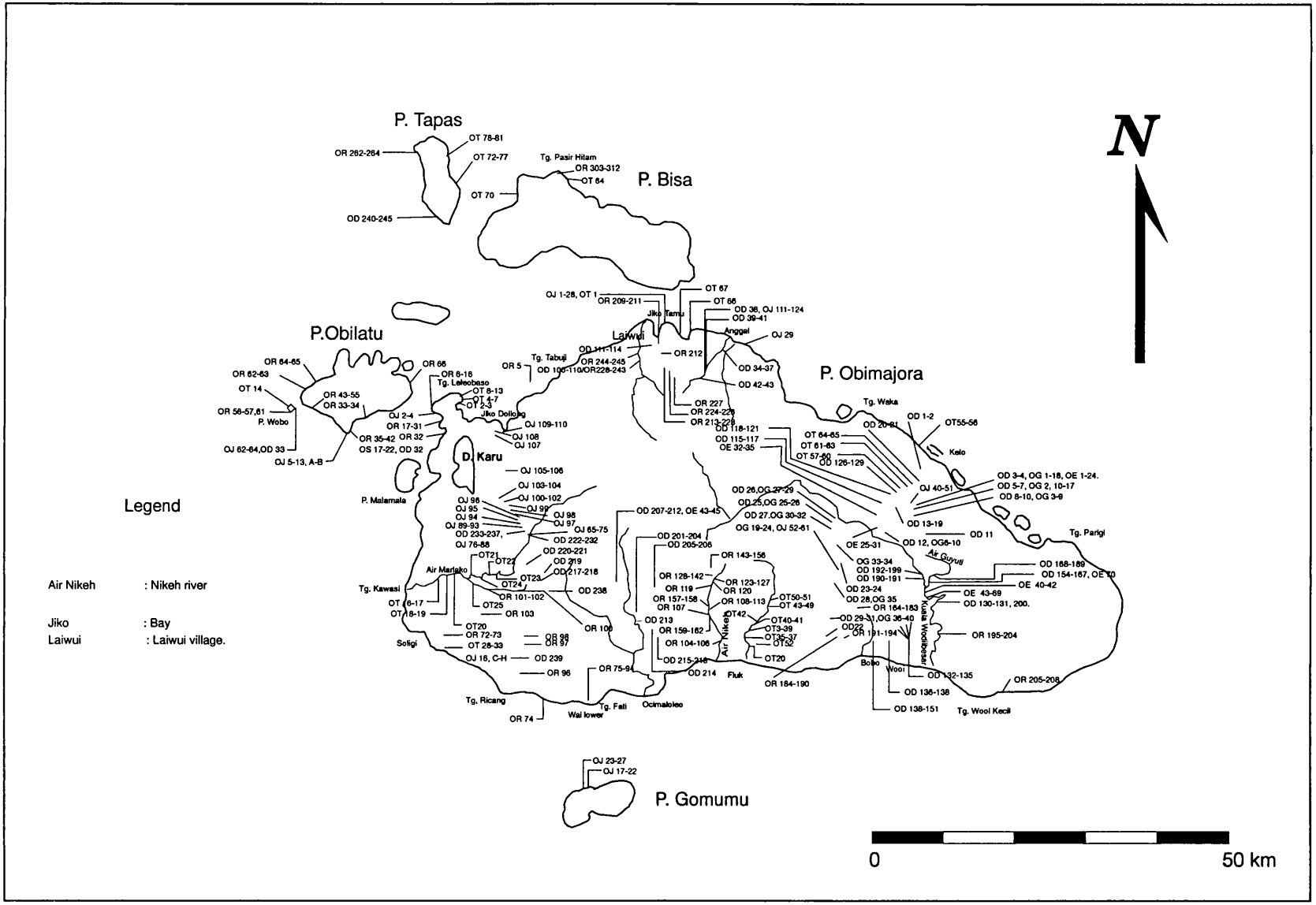

Fig. 1.11. Location of samples collected during this study.

1.6.3 Photogeological Interpretation

Aerial photographs of 1:100,000 scale were used to interpret the morphology, lithology, geological boundary, structure, positions of unit and characteristics of units.

1.6.4 Microprobe Methods

Selected samples were prepared as a polished thin sections coated by carbon. Mineral analyses were made on a JEOL 733 Superprobe electron microprobe with a Link System energy dispersive analyser AN 10000/555 and LEMAS stage control. An accelerating beam potential of 15 kV and a probe current of 10 Na were used, with a minimum beam spot of 1 mm. Elements routinely analysed were Si, Ti, Al, Fe, Mn, Mg, Ca, Na, K and Cr. Natural silicates and pure metals were used as standards, and during analyses cobalt was used as a primary reference standard. Correction procedures were carried out using the ZAF correction programme supplied by Link (iterative spectrum stripping technique). Stoichiometric calculations were achieved using Pascal programs developed by R. Hall.

1.6.5 X-ray Fluorescence (XRF) Methods

XRF methods were used to chemically analyse selected samples for major and trace elements. Samples were chosen on the basis of their freshness and any altered samples were avoided as far as possible. Samples were crushed using a hardened steel jaw crusher and subsequently by a WC Tema mill. Major element analyses were determined on fused glass discs made from powder samples diluted with lithium metaborate. Trace elements were analysed on pressed powder pellets made from powdered samples mixed with Mowiol (~ 2 % polyvinyl alcohol), and compressed under a hydraulic press (~ 10 tons). A Philips PW 1400 X-ray spectrometer was used to analyse the elements. A tungsten anode tube was used to determine major elements, Sc, La, Ba, V, Nd, Ce, Cr, Ni, Cu, and Zn, whereas a rhodium tube was used to determine Pb, Th, Rb, Sr, Y, Zr, Nb, Cl, and Ga. Details of instrument conditions are given in Thirlwall & Marriner (1986), from which the 2σ errors were calculated to be: ±1 ppm for most elements, ±0.2 ppm for Rb, ±0.3 ppm for Nb, ±0.6 ppm for Y, ±1.3 ppm for La and Ce, ±2.0 ppm for Cu, V, and Zn, ±3.0 ppm for Ba, ±6.0 ppm for Cr, ±12.0 ppm for Cl. Data was processed using the VAX-VMS computer system.

1.6.6 K-Ar Methods

K-Ar dating of selected samples was carried out at the NERC Isotope Laboratories, Keyworth. Details of the methods, analytical details and results are presented in Appendix A.

1.7 Plan of the Thesis

Chapter 2 presents the new geological map made during this study and outlines the stratigraphy and structure of the islands. Chapter 3 to 5 deal systematically with the stratigraphy of all the formations defined and redefined during this project, and include new whole rock chemical data from some of the igneous rocks. Chapter 6 discusses the structure of the Obi region based on cross sections constructed across the area and observed field relations, and attempts to interpret these results in a regional context. Chapter 6 also provides a summary of the conclusions of this study.

CHAPTER 2
OVERVIEW OF THE GEOLOGY OF OBI

2. OVERVIEW OF THE GEOLOGY OF OBI

2.1 Introduction to the Stratigraphy

As outlined in Chapter 1, previous work has suggested that Obi includes rocks from two different plates, the Australian and Philippine Sea plates, which are juxtaposed in western Obi (see Chapters 4 and 5). Therefore the stratigraphy of the region is divided into two parts: SW Obi, and NW-SE and NE Obi. The basement rocks of SW Obi are probably the medium grade metamorphic rocks of possible Palaeozoic age which are exposed on the island of Tapas. These Australian continental basement rocks are overlain by Middle Mesozoic and Cenozoic rocks. In contrast, the remainder of Obi has a basement of ophiolitic rocks of probable age which originally formed part of the Philippine Sea Plate. These are overlain by Upper Mesozoic and Cenozoic rocks. Both areas are overlain by Quaternary sedimentary rocks.

The new geological map (Fig. 2.1) and the new stratigraphy of Obi (Figs. 2.2 and 2.3) are very different from the previous map and stratigraphy of earlier investigators (Fig. 2.2). This in part reflects the very large amount of new data acquired during the Sorong Fault project, in particular the very large number of new biostratigraphic and isotopic dates. As far as possible previous stratigraphic nomenclature has been adapted but because some terms have been over-extended throughout the region (e.g. the term Bacan Formation was not clearly defined in its type area; Malaihollo, 1993) and other terms were founded on mis-correlations based on assumed ages (e.g. Leleobasso Formation), disproved as new ages were acquired, it has been necessary to introduce a number of new formation names. Obi is significantly lacking in named geographical localities and this has required the use of some similar terms (e.g. Anggai Formation and Anggai River Formation). In this chapter only an introduction to the stratigraphy, geological map and structure of the Obi region is provided; the stratigraphy will be discussed in detail in Chapters 3-5 and the structure in Chapter 6.

2.2 The New Geological Map of Obi

Schematic geological maps of Obi have been produced by several previous workers although only one map by the Geological Research and Development Centre (Sudana & Yasin, 1983) has been published. In 1989, 1990 and 1992 the University of London has conducted research in the North Moluccas in collaboration with GRDC. This research has produced several geological maps of which the new map of Obi is one. The geological map of Obi is based on field data collection, air photo interpretation and stratigraphic information from microfossils, nannofossils and K-Ar dating.

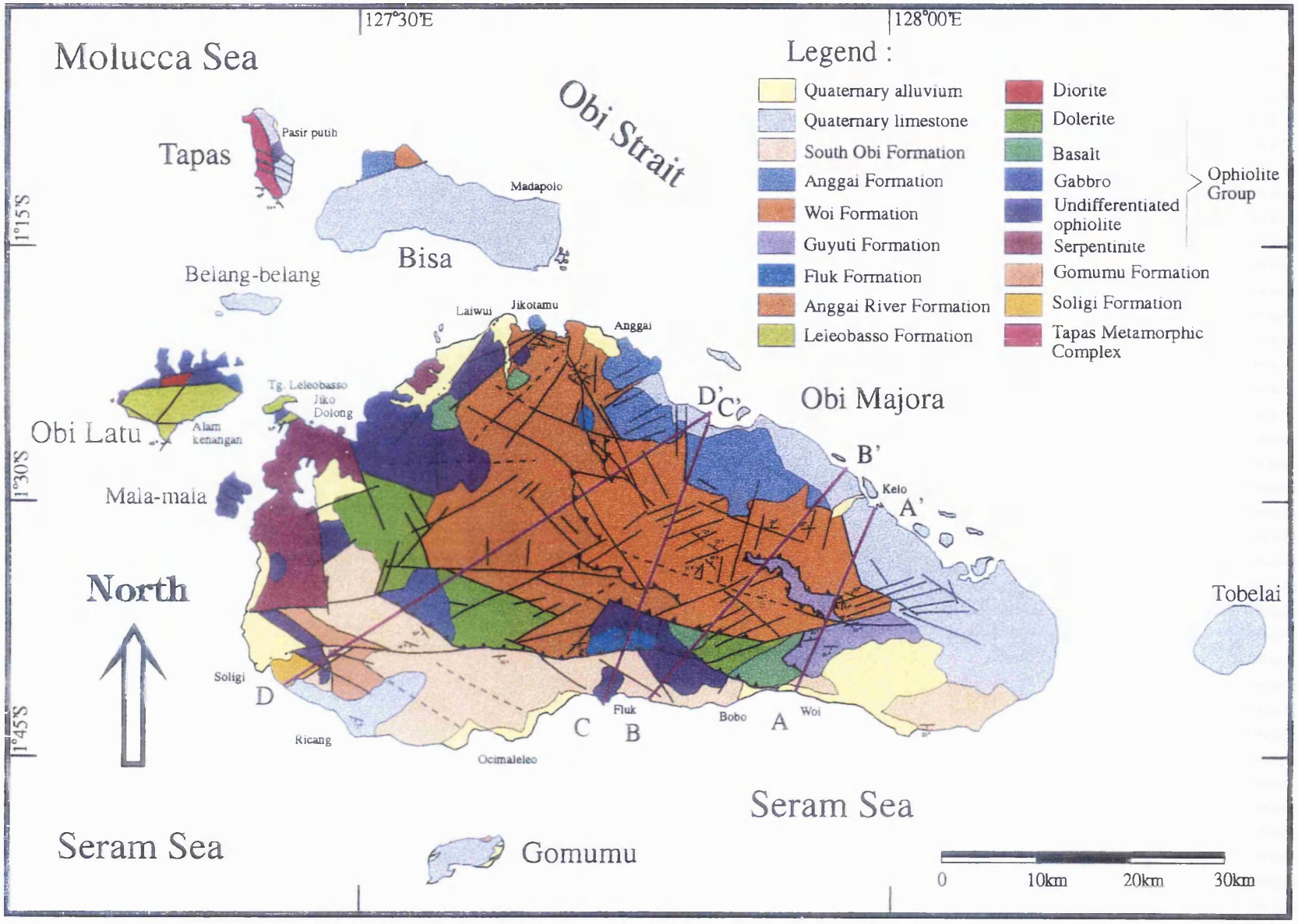

Fig. 2.1 Geological map of the Obi Islands based on this study.

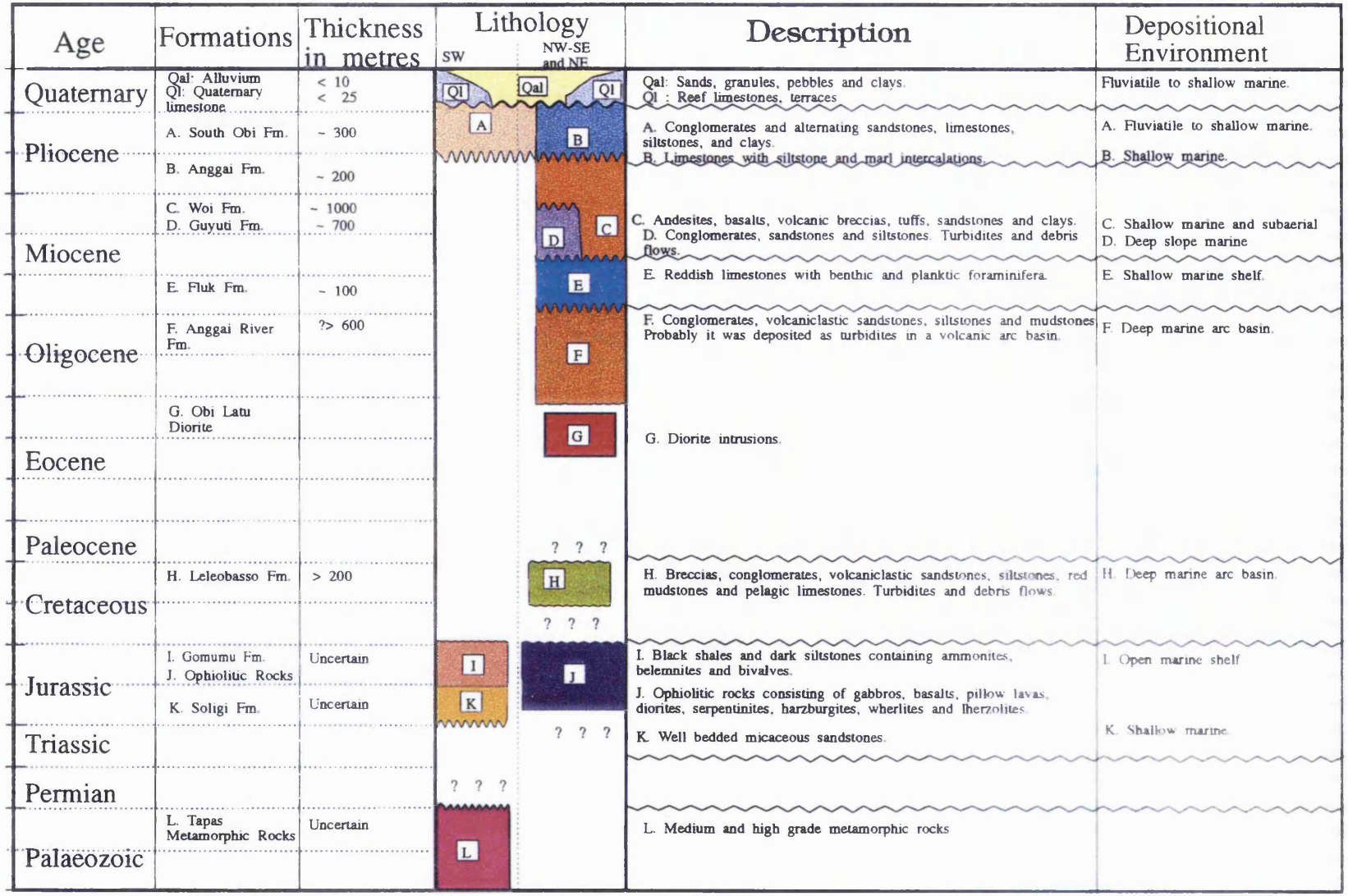

Fig.2.2 Stratigraphy of the Obi Islands based on this study

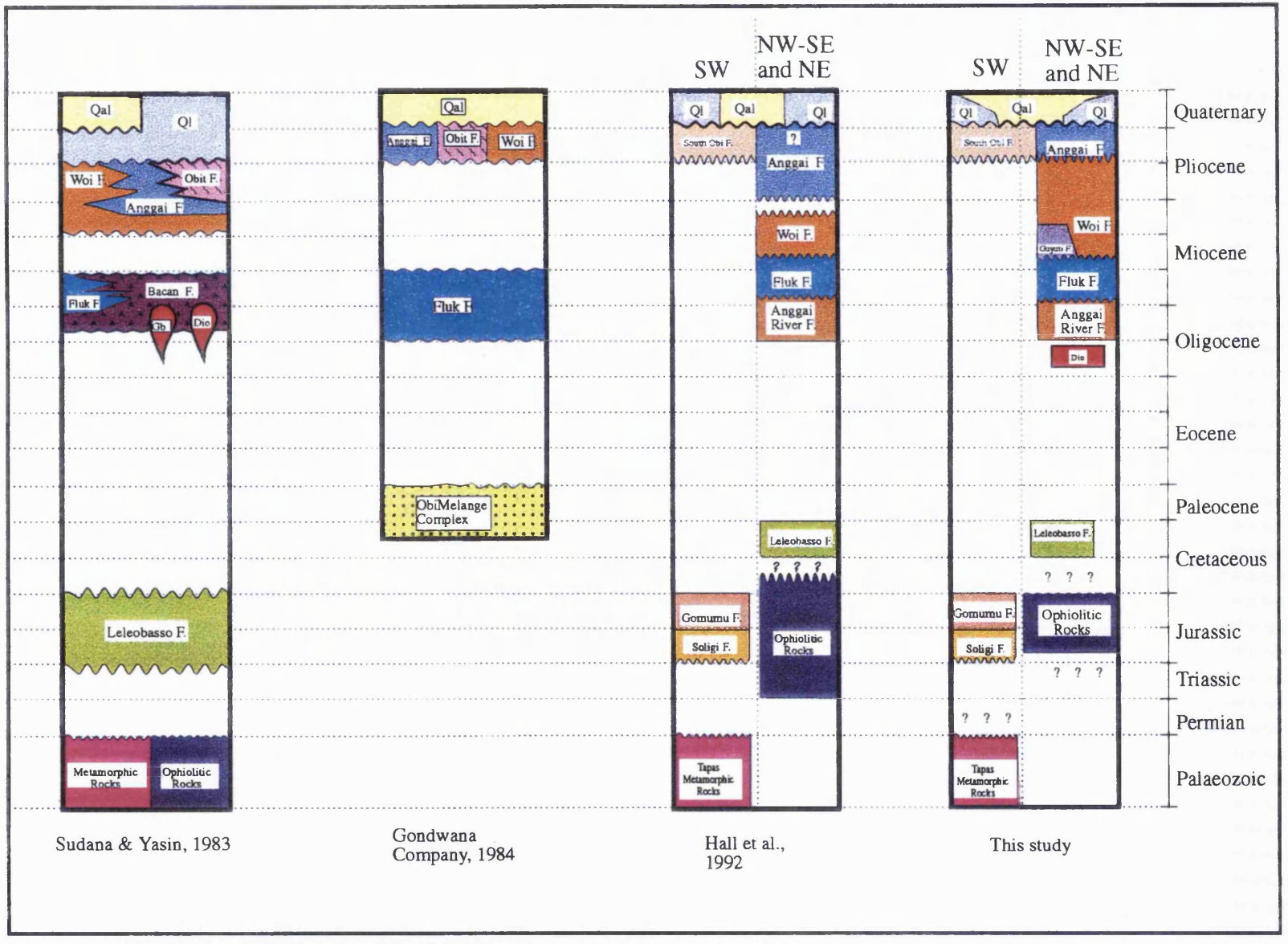

Fig. 2.3 Comparison of previous and present stratigraphic schemes for the Obi Islands.

2.2.1 SW Obi: Australian Continental Rocks

The oldest rocks in the Obi islands are metamorphic rocks assigned to the TAPAS METAMORPHIC COMPLEX (Chapter 3), exposed on the island of Tapas (Fig. 2.1) immediately NW of Obi, similar to those exposed on Bacan 50 km to the north. On Tapas there are both continental lithologies (Chapter 3) and metabasic rocks (Chapter 4). Continental metamorphic rocks, including micaceous schists and gneisses, are presumed to be Palaeozoic or older. Isotopic ages from these rocks on Obi and Bacan have so far yielded very young ages which are reset by Neogene volcanic and hydrothermal activity (Malaihollo, 1993; Baker & Malaihollo, 1995). Metabasic rocks in this complex yield radiometric ages >100 Ma and are interpreted as metamorphosed Philippine Sea plate ophiolitic rocks (S. J. Baker, pers. comm. 1992) by analogy with Bacan (Malaihollo, 1993). The continental metamorphic rocks probably form the basement in SW Obi where they are found as float samples in rivers and there is a series of Mesozoic sediments unlike any of the Philippine Sea Plate rocks. The SOLIGI FORMATION (Chapter 3) is a series of decalcified sandstones and siltstones which contain fragments of *Pentacrinus*, indicating a Lower Jurassic age. These rocks are notable in containing detrital quartz which is absent in all Philippine Sea plate rocks. Wanner (1913) reported Jurassic ammonites as float in SW Obi. In SW Obi and on the small island of Gomumu to the south there are siltstones and shales of the GOMUMU FORMATION (Chapter 3). This formation locally contains a rich fauna including ammonite fragments, aptychi, belemnites and bivalves. Palynomorphs and belemnites indicate Middle-Upper Jurassic ages. The Soligi and Gomumu Formations are very similar to Jurassic rocks of the Australian margin known throughout eastern Indonesia. A thrust fault separates the metamorphic and ophiolitic rocks on Tapas, and is assumed to be a thrust, based on interpretation of Bacan (Malaihollo, 1993) although mapping suggests a high angle feature. In SW Obi the older rocks are overlain by Plio-Pleistocene sub-aerial clastic sediments of the SOUTH OBI FORMATION (Chapter 5) and by Quaternary limestones and alluvium.

2.2.2 NW, NE and SE Obi: Philippine Sea Plate Rocks

Throughout most of western Obi, and parts of south Obi, ophiolitic rocks of presumed Philippine Sea plate origin are exposed. Limited field evidence and geochemical evidence from younger volcanic rocks (E. Forde, pers. comm., 1994) indicates that similar rocks underlie the whole of north and east Obi. These rocks are assigned to the OPHIOLITIC BASEMENT COMPLEX (Chapter 4) which consists of peridotites, gabbros, dolerites and basalts, extending from Bobo to Obi Latu Island. Mostly peridotites crop out along the western coast and inland from the coast of Obi Major, from Jikodolong southward to Soligi village. Peridotite remnants are also found distributed to the north of Bobo, and south of Lawui. Gabbros are exposed to the north of Ricang village, and south of Jikodolong, along the logging road. Close the centre of Obi dolerites occupy

a vast area which extends from north of Ocimaleleo to the south of Jikodolong. To the north of Bobo dolerites are also found along the logging road next to pillow basalts. The age of the ophiolites is uncertain. They are in fault contact with Upper Cretaceous rocks and overlain in some areas by Neogene rocks. Radiometric ages from metabasic rocks on Tapas are >100 Ma and indicate post-formation metamorphism (S. J. Baker, pers. comm. 1992). Evidence from elsewhere in the Halmahera-Waigeo region suggests the ophiolites are Early Mesozoic in age, possibly Jurassic.

The oldest sedimentary rocks associated with the ophiolitic rocks of Obi are Upper Cretaceous rocks of the LELEOBASSO FORMATION (Chapter 5) which consists of deep water volcaniclastic sediments and pelagic limestones. These are well exposed on the NW tip of Obi Major and along the south coast of Obi Latu. The formation is interpreted as a sequence of rocks deposited in a forearc basin. In places the Leleobasso Formation is intruded by diorite with resultant contact metamorphism and minor mineralisation.

The centre of Obi is occupied by the Oligocene-Lower Miocene ANGGAI RIVER FORMATION (Chapter 5) from the north coast to the southward to the north of Fluk Village. The Anggai River Formation consists of subordinate volcanic rocks and coarse to fine volcaniclastic sedimentary rocks probably deposited as turbidites in a volcanic arc basin. Almost all boundaries of Anggai River Formation with other formations are fault contacts which have predominantly NE-SW, NW-SE and east-west orientations.

Early-Middle Miocene shallow water limestones are present in small areas of south Obi near Fluk village and in central north Obi south of Anggai and are assigned to the FLUK FORMATION (Chapter 5).

Bordering the Anggai River Formation is the WOI FORMATION (Chapter 5) occupying western part of Obi, from north of Fluk toward south of Anggai. The Woi Formation includes volcanic rocks and volcaniclastic sediments deposited subaerially and in shallow water during the Middle Miocene to Early Pliocene. This formation is well exposed in a large area of east Obi surrounding the Woi River. In the Woi River itself, and structurally beneath the Woi Formation is the GUYUTI FORMATION (Chapter 5) which is also composed of volcanic and volcaniclastic rocks, of the same age as the Woi Formation, but deposited in a much deeper water environment, interpreted to have been a offshore marine forearc slope.

Overlying the Woi Formation and Anggai River Formation are Upper Pliocene to Pleistocene limestones of the ANGGAI FORMATION (Chapter 5) which are exposed in the northeast of Obi stratigraphically below Quaternary limestones, but occupying topographically higher areas due to the dip of the strata. A small area of the same formation is exposed in the northern part of Bisa island. This formation appears to dip, and becomes younger, northward.

Quaternary limestones and alluvium are found on the coasts of Obi Major, Bisa island, Gomumu island, Tapas island and near Ricang village, and in some large areas inland, principally around the lower part of the Woi River in SE Obi and in west Obi near to Karu Lake.

2.3 Structure

Four cross sections are shown on Fig. 2.4 which cut the geological map from the south to the north coast. These have been included here for the purpose of introducing the most important features of the structure of the island and are discussed in greater detail in Chapter 6.

Geological structures present are predominantly fault structures, lineaments, and a number of small folds. The major faults commonly have east-west and NW-SE orientations, whereas less important lineaments have NE-SW directions. A major thrust separates the Woi Formation from the underlying Guyuti Formation and the Anggai River Formation (all cross sections). A second major thrust brings the Anggai River Formation and the ophiolite onto the South Obi Formation (all cross sections), which is itself cut by the thrust (cross sections DD'). The age of the formations involved in the thrusting demonstrate its age to be latest Miocene or younger. As discussed in Chapter 6 the age of the thrusting is considered to be Middle to Late Pliocene. There are few identifiable folds in the Obi region. Small ramp anticlines are associated with thrusting of the Guyuti Formation and Anggai River Formation (cross sections AA' and CC') and these folds have approximately east-west axial traces.

CHAPTER 3

METAMORPHIC BASEMENT AND JURASSIC SEDIMENTARY ROCKS: CONTINENTAL CRUST AND COVER

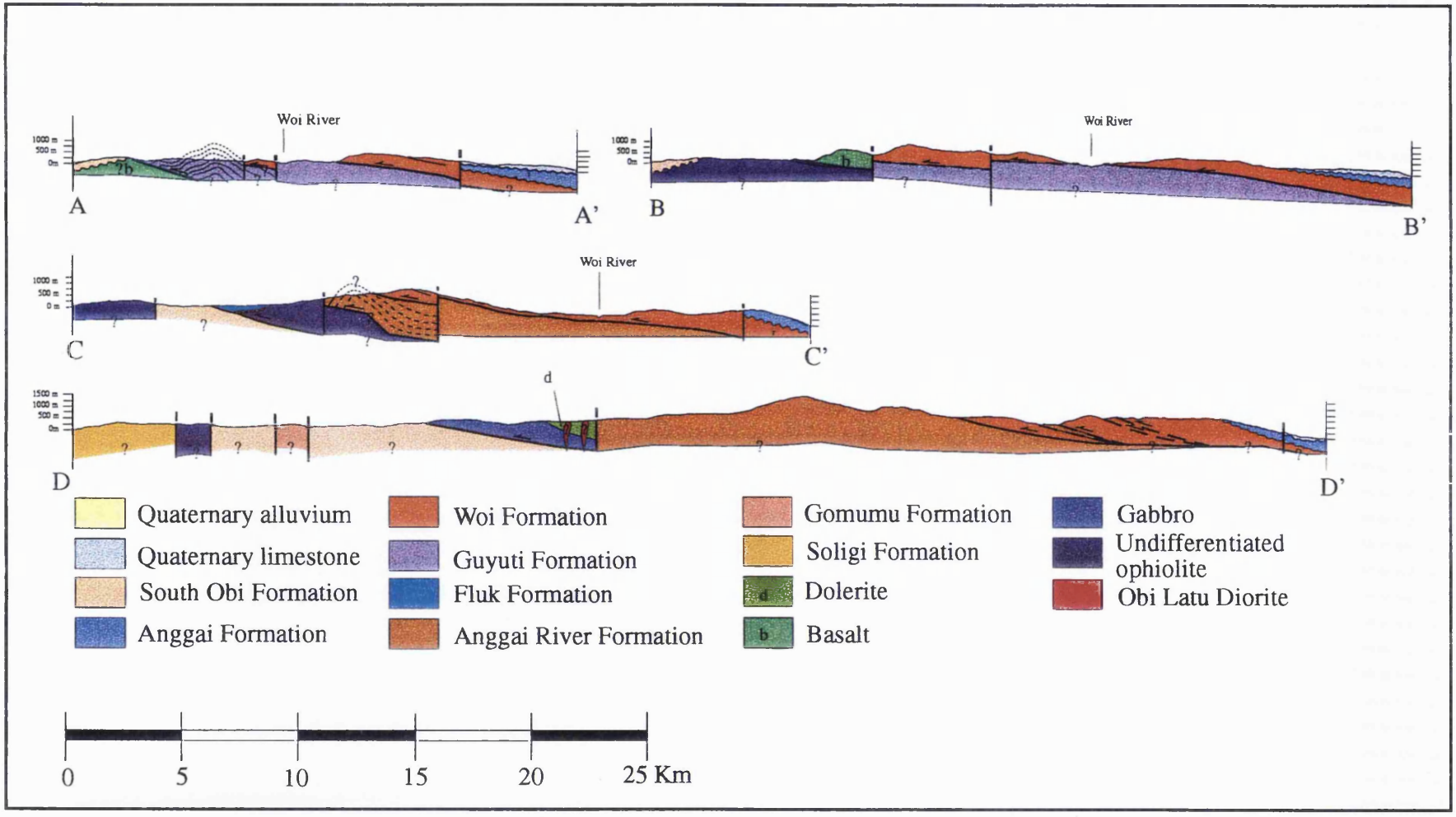

Fig.2.4 Cross-sections of the Obi Island. The location of the profiles are shown on Fig. 2.1

3. METAMORPHIC BASEMENT AND JURASSIC SEDIMENTARY ROCKS: CONTINENTAL CRUST AND COVER

3.1 Introduction

The continental crust which is exposed in Obi consists of metamorphic rocks and Mesozoic sedimentary rocks. These rocks probably originated from somewhere along the Mesozoic north Australian passive margin in Papua New Guinea or Irian Jaya (Hamilton, 1979; Struckmeyer *et al.*, 1993) although exactly where, and when they separated, are very uncertain. The contacts between the metamorphic rocks and sedimentary rocks are not seen, and are interpreted to be unconformable. The metamorphic rocks consist largely of medium grade rocks, here assigned to the Tapas Metamorphic Complex, and the sedimentary rocks consist of clastic rocks deposited in a marine environment.

3.2 Tapas Metamorphic Complex

Metamorphic rocks are exposed only on Tapas Island (Fig. 3.1) but are found in river float in SW Obi. They include quartz-mica schists and similar lithologies of sedimentary origin, as well as metabasic rocks, and all these rocks resemble medium to high-grade metamorphic rocks on Bacan described by Malaihollo (1993) who subdivided the Sibela Metamorphic Complex there into two groups, based on lithologies and isotopic age data: a continental and an ophiolitic suite. From outcrop and thin section examination it is clear that two similar suites can be recognised on Tapas. However, the area of metamorphic rocks on Tapas is much smaller than that on Bacan, and exposure is also rather limited except on parts of the coast. The two groups of rocks could not be distinguished on aerial photographs, and it seems that the extent of the ophiolitic rocks is very narrow. The contact between the continental and ophiolitic rocks appears to be a steep fault which may originally have been a thrust. Because of the limited time for the survey and the difficulties of the terrain, the two suites of rocks were not separated on Tapas, nor was structural analysis of the Tapas Complex conducted.

3.2.1 Synonymy

The first mention of metamorphic rocks in Tapas Island, to the NW of Obi Major, is by Brouwer (1923) who carried out a short survey in Obi. He reported the occurrence of crystalline schist. Sudana & Yasin (1983) referred to chlorite schist and muscovite schist as metamorphic rocks but he did not assign them to any stratigraphic unit. The Tapas Metamorphic Complex is first mentioned by Hall *et al.* (1992) who reported high grade gneiss and schist in Obi.

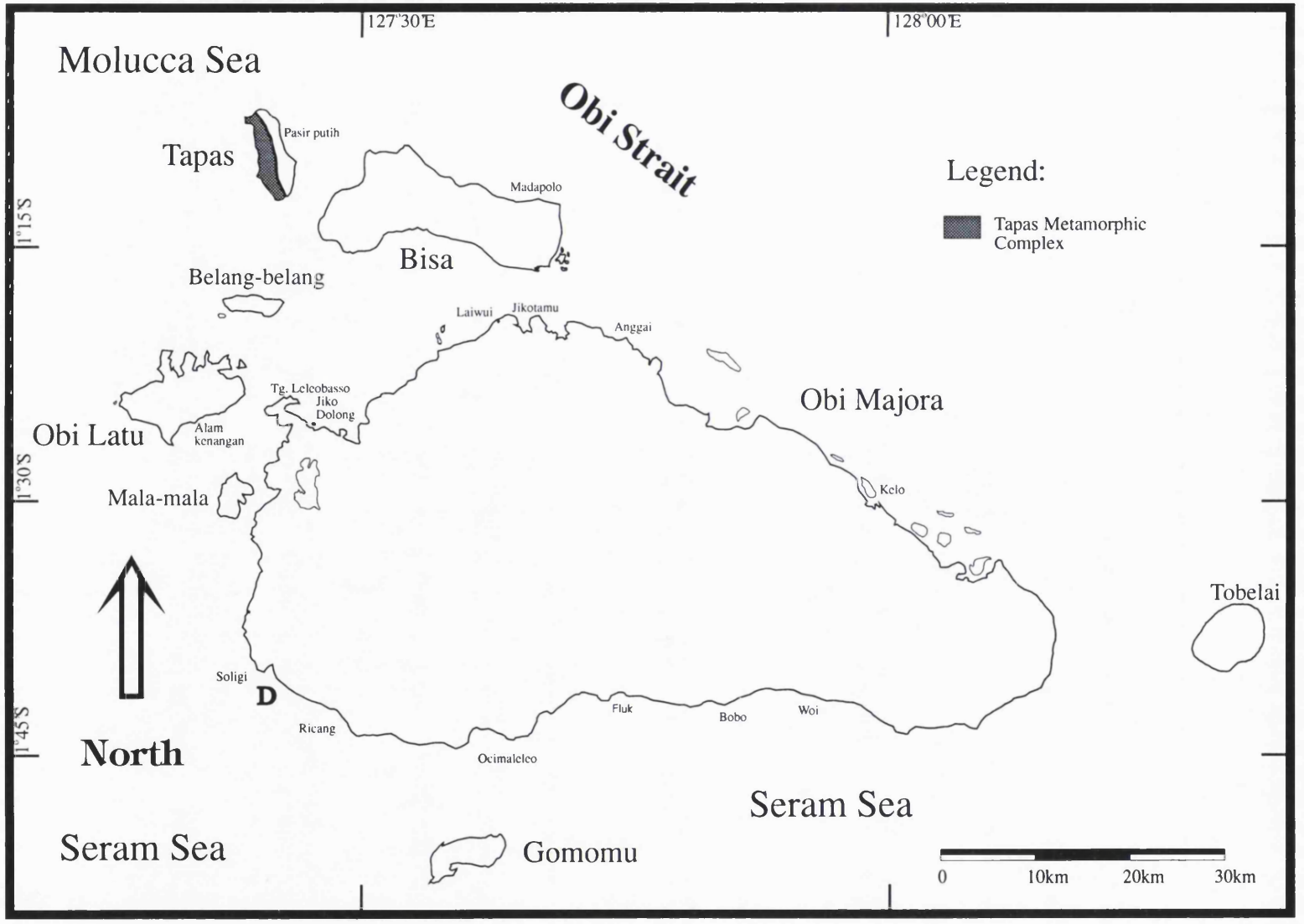

Fig. 3.1 Distrbution of the Tapas Metamophic Complex

3.2.2 Aerial Photographic and Topographic Interpretation

The area of metamorphic rocks on Tapas has a dark grey and smooth surface, and forms a narrow elongate ridge which is parallel to the elongation of the island. No subdivision of the metamorphic rocks is possible from the aerial photographs.

3.2.3 Type Section

Metamorphic rocks are well exposed along much of the coast of Tapas Island which is the type area for the metamorphic rocks (Figs. 3.2) but the exposures are often not accessible since the cliffs are in places very steep, beaches are absent or narrow, and in seas which are not calm landing is difficult or impossible. In SW Tapas the metamorphic rocks consist entirely or predominantly of mica schist, chlorite schist, quartzite and some metabasic rocks. In NW Tapas the rocks include mica schists, marble and coarse metabasic rocks. Albite porphyroblasts are up to 2 mm, and other porphyroblasts include epidote and garnet. The rocks have a good foliation which dips steeply, mainly to the south. Folds and crenulation of cleavage are seen in boulders of metamorphic rocks on the south coast (Fig. 3.3).

3.2.4 Age

Precambrian-Palaeozoic? with some Mesozoic metamorphic rocks? The association of metamorphic rocks as float and unmetamorphosed Jurassic sedimentary rocks in SW Obi suggests that metamorphic rocks form the basement to the Mesozoic sediments. Hamilton (1979), based on correlation with Australian continental material, assigned the metamorphic rocks of Obi and Bacan a Palaeozoic age. Vroon (1992) and Vroon *et al.* (1996), based on the amount of radiogenic Pb and Sr isotopes present in the Quaternary volcanic rocks in Bacan, built on the continental crust, suggested a Precambrian age for the continental basement rocks.

An attempt was made to date two samples of Tapas metamorphic rocks by the K-Ar method at the NERC Isotope Laboratories in Keyworth (Table 3.1). K-Ar analyses of duplicate samples from a mica schist (OD244) yielded ages of 7.9 ± 0.47 Ma and 10 ± 0.5 Ma. A metabasic rock (OD247) rich in amphibole gave an age of 29.4 ± 2.2 Ma. These are all interpreted to be reset ages, as for similar rocks from Bacan.

K-Ar and Ar-Ar dating was attempted by Malaihollo (1993) on rocks from Bacan. Upper amphibolite facies schists yielded ages <1 Ma interpreted as the result of interaction with hydrothermal fluids; there are many hot springs along currently active faults in the area. Malaihollo (1993) also dated amphibole-bearing rocks interpreted as cumulates from the Sibela Complex of Bacan using the Ar-Ar method. These rocks resemble coarse amphibole-rich rocks

Fig. 3.2 Well foliated quartzose mica schist, dipping southwest on the south coast of Tapas.

Fig. 3.3 Folded foliated in float sample of quartzose mica schist, south Tapas.

of NW Tapas and yielded young plateau ages of 25-37 Ma and an older plateau age of 94-97 Ma. The young plateau age was interpreted to be related to the Oligocene volcanism between ~40 and ~25 Ma, also found in Obi (Chapters 2 and 5) whereas the old plateau age was suggested to be correlated with east Halmahera (Ballantyne 1990) and the Philippine Sea plate.

Table 3.1 Summary of K-Ar results from Tapas Metamorphic rocks (wr: whole rock, musc: muscovite, amp: amphibole).

Sample	Material	Grain size (μm)	%K (1σ error)	Wt for Ar (g)	$^{40}Ar^*$ nl/g (1σ error)	$^{40}Ar_{atm}$	Age Ma (2σ error)
Continental Rocks							
OD244	musc	125-500	3.774 ± 1	0.9566	1.1619 ± 2.8%	72.03	7.9 ± 0.47
	musc	125-500	3.774 ± 1	0.6594	1.4752 ± 2.05%	63.78	10.0 ± 0.5
OD247	amp	125-500	0.2708 ± 1	1.2637	0.3127 ± 2.31%	66.64	29.4 ± 2.2
Metabasic Rocks							
OR259	wr		0.537 ± 1	2.0643	2.7186 ± 1.07%	26.17	126.0 ± 3.0
OR262	amp	250-500	0.578 ± 1.42	1.4388	2.3175 ± 1.16%	37.14	100.0 ± 4.0
OR263	amp	250-500	0.887 ± 1.57	1.2645	2.1299 ± 1.23%	41.13	60.7 ± 2.4

It is therefore probable that the metamorphic rocks of Obi include a continental suite of Precambrian age, which now yield very young isotopic ages due to interaction with young hot radiogenic waters. Lithological and isotopic data suggest some of the metabasic rocks may be related to those of Bacan which have Cretaceous ages (~95 Ma) reset during Oligocene volcanic activity.

3.2.5 Thickness

Considering the height of the Tapas Island, the thickness of the metamorphic rocks is estimated to be at least 250 m.

3.2.6 Distribution

Metamorphic rocks are exposed on Tapas Island and appear to form the whole of this unusually high, steep and narrow island. No metamorphic rocks are exposed elsewhere in the Obi islands but float samples of quartzose schist were found in rivers in SW Obi near to Ricang during the 1992 expedition. This suggests that there may be small exposures of metamorphic rocks in SW Obi although none has yet been found.

3.2.7 Lower and Upper Contacts

The lower contact of the metamorphic rocks is not seen. The upper contact is also not exposed but the association of metamorphic rocks and unmetamorphosed Mesozoic sedimentary rocks in SW Obi suggests an unconformable contact.

3.2.8 Petrology of the Metamorphic Rocks

Field and thin section examination shows that the metamorphic rocks from Tapas include pelitic and quartzo-feldspathic metamorphic rocks, metamorphic rocks derived from impure calcareous sediments, and metabasites. A number of samples were chosen to represent these different types of rocks and some of these were analysed using XRF for whole rock geochemistry and by microprobe for mineralogy. The mineralogy of the samples discussed in the text below is summarised in Table 3.2.

Table 3.2 Mineralogy of Selected Tapas Metamorphic Rocks

Pelites
OD241 muscovite-chlorite-albite-quartz-opaques
OD244 muscovite-chlorite-albite-quartz-sphene-opaques
OD251 garnet-muscovite-chlorite-albite-quartz-opaques
OD254 muscovite-chlorite-albite-quartz-opaques
Calcareous Pelites
OR252 calcite-muscovite-plagioclase-quartz-chlorite-epidote-opaques
OR253 calcite-muscovite-plagioclase-quartz-chlorite-epidote-opaques
OR258 calcite-muscovite-plagioclase-quartz-brown biotite
Metabasites
OD240 muscovite-plagioclase-quartz-chlorite-calcite-opaques
OR247 blue-green amphibole-epidote-chlorite-plagioclase-quartz-opaques
OR250 green amphibole-epidote-chlorite-albite-sphene-opaques
OR255 green amphibole-epidote-chlorite-plagioclase-brown-green biotite-sphene
Hornblende-rich Rocks
OR260 dark green hornblende-chlorite-plagioclase-green-brown biotite-quartz-opaques-(rutile?)
OR261 green hornblende-epidote-chlorite-plagioclase-opaques
OR262 dark green hornblende-chlorite-opaques
OR264 dark green hornblende-minor chlorite-plagioclase-opaques

Principal features of these rocks are the presence in some of compositional banding, and a common strong foliated fabric. It is common for rocks to show polyphase metamorphic fabrics. Many of the schistose rocks with a good foliation show a crenulation fabric deforming an earlier cleavage. Many rocks are cut by late shear planes with development of augen, and many contain rotated porphyroblasts with irregular inclusion trails. Some rocks were partially recrystallised during a retrograde metamorphic event.

The overall grade of metamorphism is an early amphibolite facies metamorphism with a later greenschist or lower metamorphic facies overprint. There are no clear indicators of grade in most rocks, reflecting the limited compositional range of samples collected. In the metabasic rocks there is garnet in a few samples, but they essentially consist otherwise of hornblende + plagioclase. The metasedimentary lithologies do not include aluminous varieties which might yield kyanite-staurolite assemblages such as those found on Bacan. No oriented samples were collected but the fabric is possibly of extensional origin.

3.2.8.1 Pelites and Quartzo-feldspathic Rocks

Pelitic metamorphic rocks derived from sediments are common along the coast of SW Tapas. They contain abundant muscovite, commonly associated with chlorite. Biotite is very rare; a few brown biotite grains are present in one or two rocks. Garnet is present in some samples but highly aluminous minerals such as kyanite and staurolite, which characterise high grade metamorphism and are present in many of the Bacan metapelites, are absent. This appears to reflect relatively aluminium-poor compositions of the Obi pelitic rocks. Several of the rocks have quartz segregations and veins. Most of the pelites have a well developed foliation, commonly crenulated, and some contain small porphyroblasts of albite. the absence of key marker minerals, such as aluminium silicates, means that the grade metamorphism is hard to determine. The mineral assemblages recorded are stable over a wide range of pressures and temperatures between the greenschist and amphibolite facies. The presence of garnet in a few samples indicates metamorphism at amphibolite facies.

Quartzo-feldspathic metamorphic rocks were probably derived from quartz-rich sedimentary rocks, but possibly from felsic igneous rocks. These rocks typically have a well-developed schistosity. They contain abundant quartz, plagioclase and subordinate mica, chlorite and opaques. They contain no key index minerals but their assemblages and close association with the pelites suggest a similar metamorphic history.

3.2.8.2 Calcareous Pelites

Metamorphic rocks deriving from calcareous sediments are present only in NW Tapas. These include rocks which are strictly impure marbles (e.g. OR258) with a minor pelitic content, to pelites with abundant calcite. They differ mineralogically from the pelites in the presence of variable amounts of calcite, and in the common presence of epidote. Biotite is again rare; a brown variety is present in one sample. Texturally they resemble the pelites in having a well developed foliation, commonly crenulated. They are also characterised by large rotated porphyroblasts of plagioclase with well developed complex inclusion trails. Inclusions which are microscopically identifiable include epidote, muscovite and opaques. No microprobe data from these rocks are available and the compositions of the plagioclases are unknown. The assemblages suggest the lower amphibolite facies.

3.2.8.3 Metabasites

Metabasic rocks are common on Tapas, and are interlayered with the metasedimentary rocks. They consist mainly of plagioclase, epidote, amphibole, quartz and chlorite. One sample contains biotite. An augen texture is commonly present and is characteristic of many of these rocks. Microprobe analysis of one sample (OD250) was undertaken. Amphibole compositions vary between hornblende and actinolite; darker grains are hornblende and lighter patches, which may be later, are actinolite. The rock contains an albite-rich plagioclase (Ab_{100-96}) as large

porphyroblasts, with inclusions of epidote, apatite and sphene (Fig. 3.4). Epidote is also present as porphyroblasts and strongly pleochroic in this and other samples. The chlorite is a bright green, moderately Mg-rich variety (pycnochlorite).

3.2.8.4 Hornblende-rich Rocks

Hornblende-rich rocks are found in two different situations in NW Tapas. At the north end of Tapas this lithology is found in a headland exposure intimately interbanded with the other metamorphic rocks described above. Here the hornblende-rich rocks appear to have an identical metamorphic history to the other metamorphic rocks. In the field they are structurally inseparable from the other rocks and have similar fabrics and foliations; in thin section also they resemble the other rocks in having polyphase metamorphic textures characterised by rotated porphyroblasts, in this case of amphibole. However, at the southern end of this coastal section where field examination was cut short by bad weather, there is a long section of coarse amphibole-rich rocks which look very different. Most of these rocks lack a strong fabric, contain very coarse amphibole, and in many cases are true hornblendites. The best exposures of these rocks were seen in very large (> 5 m across) boulders which are concentrated on the beach, and often cover the outcrop, meaning that the relationships between different lithologies are not clearly seen. There is a lack of rocks with a schistose fabric on the beach and as blocks although this may partly reflect the relatively poor resistance of such rocks to weathering and erosion.

OR260 and OR261 are examples of the first type. Both have a moderate amount of plagioclase. OR260 is mineralogically similar to the metabasites and also contains biotite which is absent in most of the hornblende-rich rocks but which is found in the other Tapas metamorphic rocks. OR261 has features in common with both the metabasites and the second group of hornblende-rich rocks. Mineralogically it is similar to the metabasites but it resembles the other hornblende-rich rocks in having a rather weakly developed foliation and in containing very coarse hornblende. The shapes of the coarse hornblende grains suggest a cumulus texture but the rock has suffered a degree of mylonitisation resulting in development of a mortar texture which means that this is very uncertain

The remaining rocks are represented by OR262 and OR264. They contain 80-90% modal hornblende, which microprobe analysis shows to be magnesio-hastingsite in OR262, with abundant opaques, and very minor chlorite and plagioclase. The opaque grains in OR262 are ilmenite and the plagioclase compositions vary between Ab_{87-93}. The two samples differ in their textures. OR262 has a coarse planar fabric defined by aligned hornblende; a second generation of paler amphibole cuts across the first. In contrast, OR264 has no planar fabric, but has coarse granular fabric similar to a high temperature metamorphic rocks in which temperature has been the dominant control on fabric development. There is a hint of a cumulus fabric, suggested by irregular opaque grains vaguely resembling an intercumulus phase but this is uncertain.

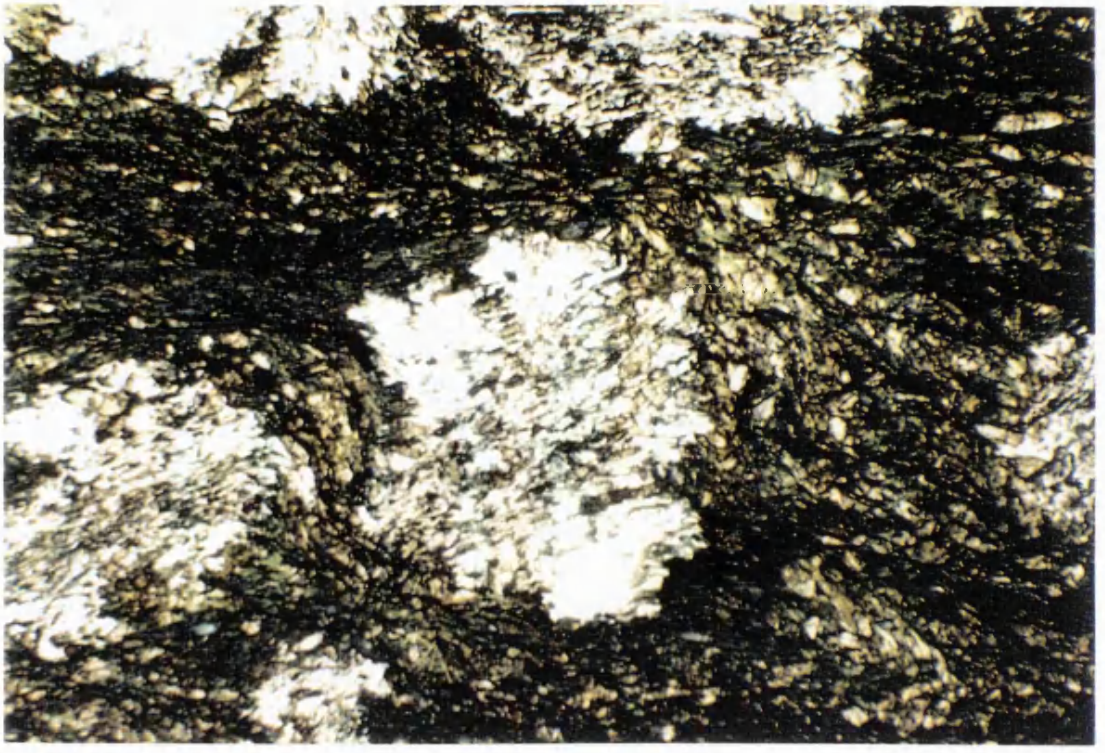

Fig. 3.4 A. (above) Photomicrograph of rotated porphyroblast of plagioclase containing inclusions of epidote in a metabasite (OR251). Plane polarised light. Width of photograph is 1.6 mm. B. (below) crossed polars.

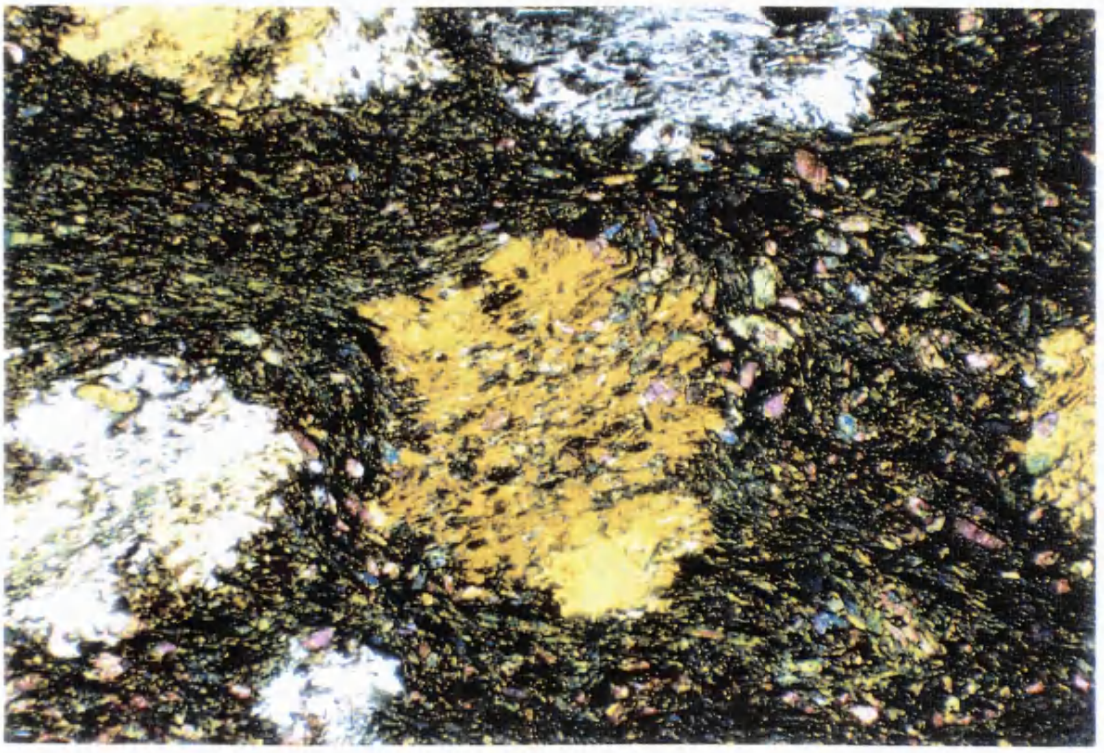

3.2.9 Whole Rock Chemistry

A number of samples of metamorphic rocks (Table 3.3), representing the principal lithologies exposed on Tapas, were analysed using XRF methods for major and trace elements in the Department of geology, Royal Holloway, University of London.

Table 3.3 Tapas Metamorphic Rocks analysed by XRF

Pelites		**Calcareous Pelites**	
OD241	mica schist	OR252	calcareous schist
OD251	garnet-mica schist	OR253	calcareous schist
Metabasites		**Hornblende-rich Rocks**	
OR240	greenschist	OR260	amphibolite
OR247	greenschist	OR261	amphibolite
OR250	greenschist	OR262	hornblendite
		OR264	hornblendite

3.2.9.1 Major Elements

The major element compositions of the metamorphic rocks are largely as expected for the types of lithologies and confirm some of the observations made above in the discussion of the rocks' petrography. The pelites and calcareous pelites have rather low Al_2O_3 (except for one mica schist OD244) which may account for the lack of index minerals such as staurolite and Al_2O_5 polymorphs, which are found in some rocks on Bacan. The metabasic rocks have compositions suggesting basaltic protoliths, which may have been igneous or volcaniclastic rocks. The two groups of hornblende-rich rocks are compositionally different. OR260 and OR261 have compositions which are more siliceous than both the metabasites or the second group of hornblende-rich rocks suggesting either andesitic igneous or volcaniclastic protoliths. The second group of hornblende-rich rocks have ultrabasic compositions and are very rich in total Fe as Fe_2O_3 and MgO. These compositions are very similar to similar hornblende rocks from Bacan (Malaihollo, 1993) which were interpreted on textural and chemical evidence to be hornblende cumulates, inferred to represent part of a metamorphosed ophiolite or arc basement sequence.

3.2.9.2 Trace Elements

With the exception of Ba, the metabasites have trace element contents which are similar to MORB, but slightly enriched for incompatible and immobile elements compared to MORB (Figs. 3.5 and 3.6). Their compositions are consistent with an origin as lavas or minor intrusions formed in a within-plate setting such as a continental margin, as suggested by their occurrence with interlayered metasedimentary rocks.

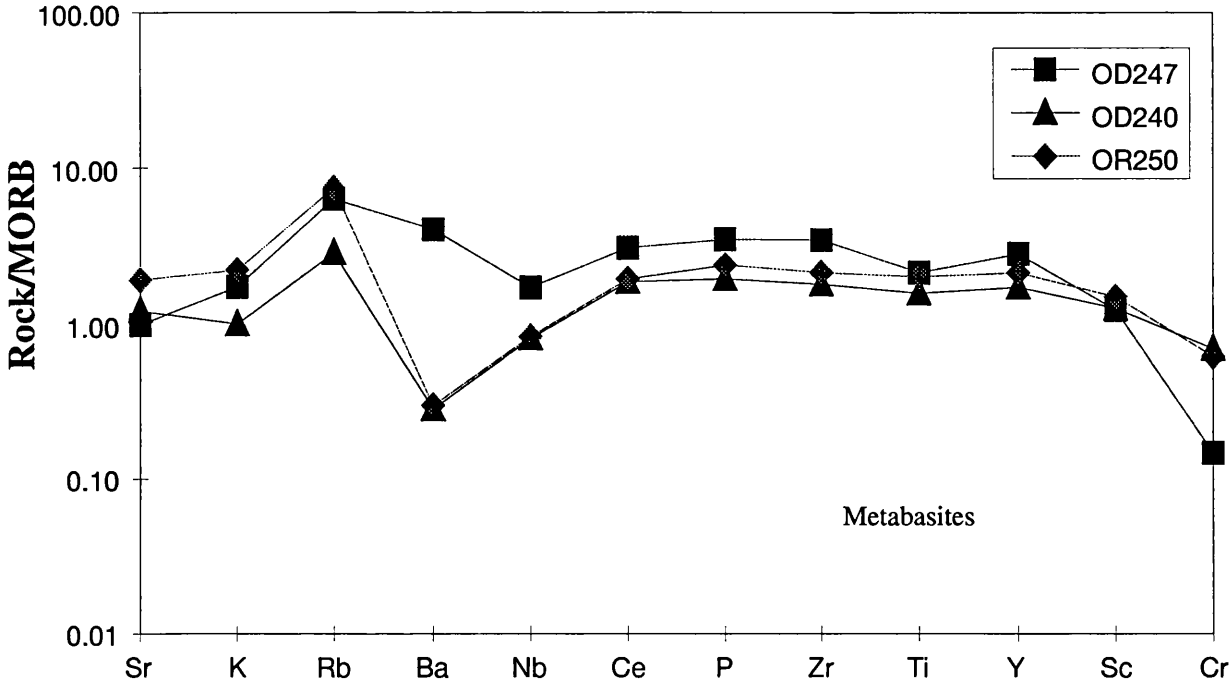

Fig. 3.5 MORB- normalised trace element spidergram for Tapas metabasic hornblendites, Normalising factors from Pearce et al. (1984)

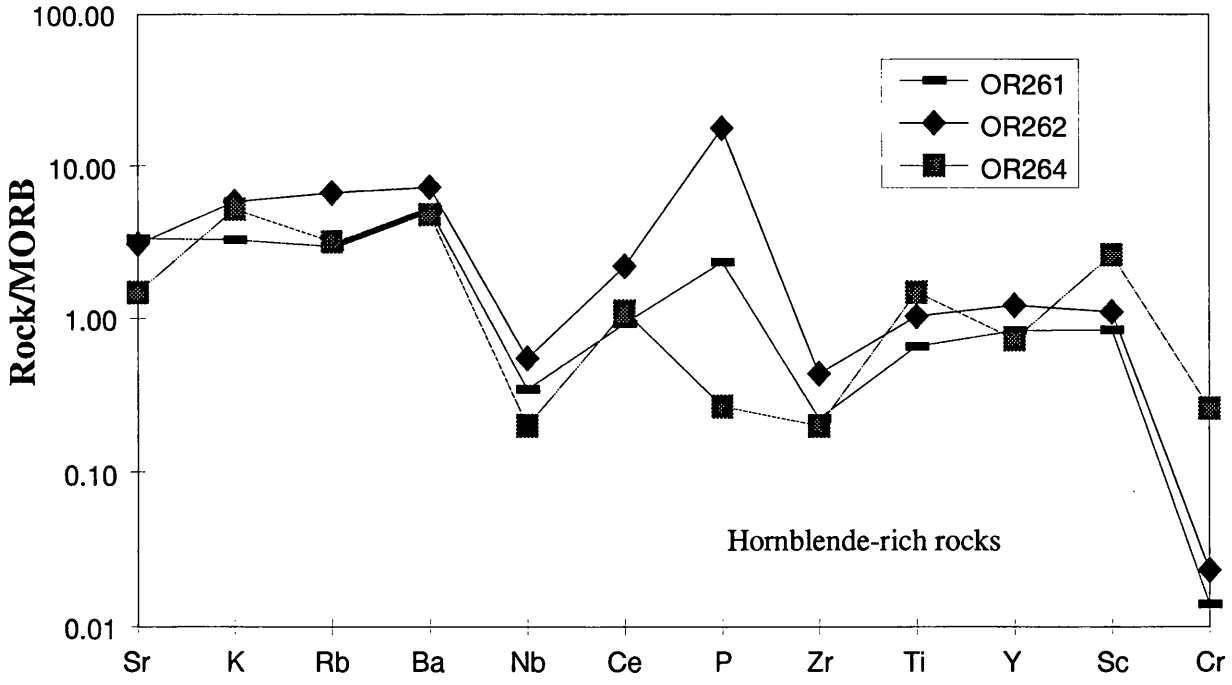

Fig. 3.6 MORB- normalised trace element spidergram for Tapas ultrabasic hornblendites, Normalising factors from Pearce et al. (1984)

The two hornblendites with high SiO2 contents, suggested above to have an andesitic or volcaniclastic protoliths have very spiky MORB-normalised trace element patterns. These irregular patterns seems most likely to be due to mixing of volcanic and sedimentary material such as in a volcaniclastic rock, rather than due to metamorphism of an igneous protolith, because the variation in incompatible elements is so irregular and unlike the smooth patterns seen in metamorphosed volcanic rocks. They tend to have mainly higher than MORB contents of most incompatible trace elements which would require the original volcanic component to be relatively enriched in these elements compared to MORB, such as might be expected in within-plate igneous rocks of basic or intermediate compositions.

In contrast, the one ultrabasic hornblende-rich rock (OR262) analysed, while also showing a spike MORB-normalised pattern, is depleted in many of the incompatible trace elements. This certainly suggests a different origin for these rocks from the other hornblende-rich rocks. It is consistent with the pattern that would be expected for a cumulate rock.

3.3 Soligi Formation

The Soligi Formation consists of micaceous sandstones of Australian continental margin affinities (Fig. 3.7).

3.3.1 Synonymy

This formation name is a new one. The first mention of micaceous sandstones is by Brouwer (1923), who found loose block of it on the northwest coast of Gomumu Island. He supposed this rock to be of Jurassic age. Sudana & Yasin (1983) did not describe rocks of this type but assigned all Jurassic rocks to the Leleobasso Formation (now redefined, see Chapter 5, since the type locality of this formation is now known to consist of Upper Cretaceous arc volcaniclastic rocks). The Gondwana Company (1984), based on their investigation in southwest Obi assigned rocks of this type to an Obi melange complex, since Hamilton (1979) had interpreted Obi as a melange based on literature descriptions. Hall *et al.* (1992) suggested the new name of Soligi Formation, after their discovery of these rocks during fieldwork in 1990, and the identification of fossils.

3.3.2 Aerial Photography and Topographic Interpretation

Aerial photographic interpretation of this formation shows it to be dark grey and soft. Actually this formation is difficult to distinguish from either its topography or its aerial photographic expression, because its outcrop is very narrow.

3.3.3 Type section

Soligi village, south Obi Major

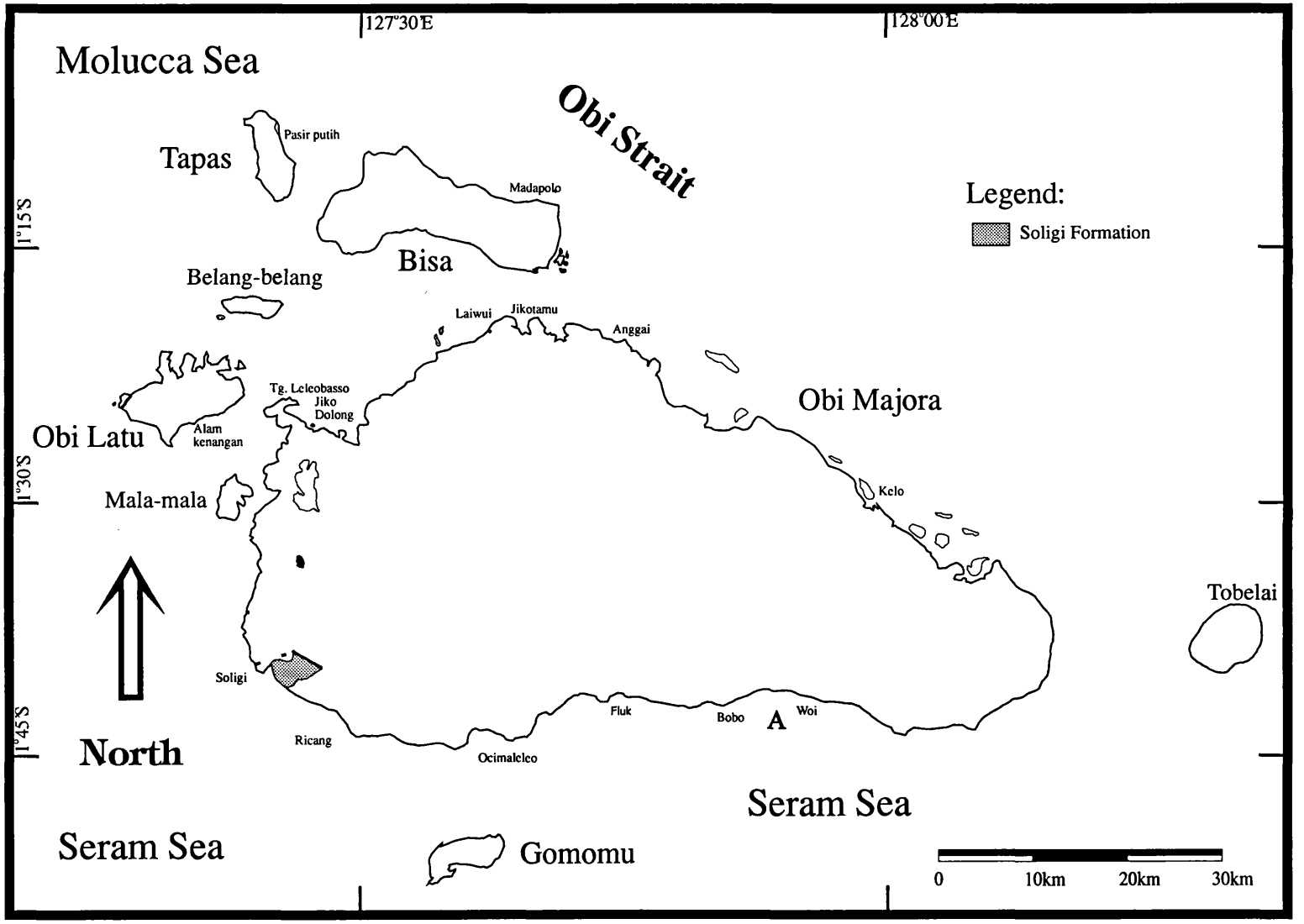

Fig. 3.7 Distribution of the Soligi Formation

3.3.4 Age

Lower Jurassic. The age is based on the discovery of *Pentacrinus* moulds at the type section.

3.3.5 Thickness

The thickness of this formation is uncertain. It is more than 50 metres.

3.3.6 Distribution

This formation is only exposed in Soligi village.

3.3.7 Lower and Upper Contacts

The contact of this formation with other formations is not seen. It is interpreted to be conformably overlain by the Gomumu Formation. The contact with other rocks is interpreted from aerial photographs to be faulted.

3.3.8 Description

On the coast at Soligi and in small outcrops immediately north of Soligi village are medium bedded micaceous sandstones with thin shale partings. The sandstones are decalcified and contain *Pentacrinus* moulds. They are notable in containing detrital quartz; they are well sorted and consist entirely of angular quartz and mica. The rocks dip at a low angle northwards and show no signs of metamorphism. North of Soligi the sandstones are poorly exposed and in contact with sheared serpentinite.

3.3.9 Depositional Environment

Marine, as indicated by the presence of *Pentacrinus*.

3.4 Gomumu Formation

The Gomumu Formation consists of the Jurassic black shales of Australian margin affinities (Fig. 3.8).

3.4.1 Synonymy

The first mention of rocks assigned here to the Gomumu Formation is by Boehm (cited by Brouwer, 1923), who found brown sandstone, marls, red limestone and dark grey marly limestone, brown-ironstone concretions, marl-shales and dark-grey clay-shale with marl-beds in the northeast part of Gomumu Island. As noted above, Sudana & Yasin (1983) considered all these rocks to be part of their Leleobasso Formation, while Gondwana Company (1984) thought them to be part of a melange complex. Based on fieldwork in 1989, the discovery of Cretaceous fossils and arc volcaniclastics at the type locality of the Leleobasso Formation, and the discovery

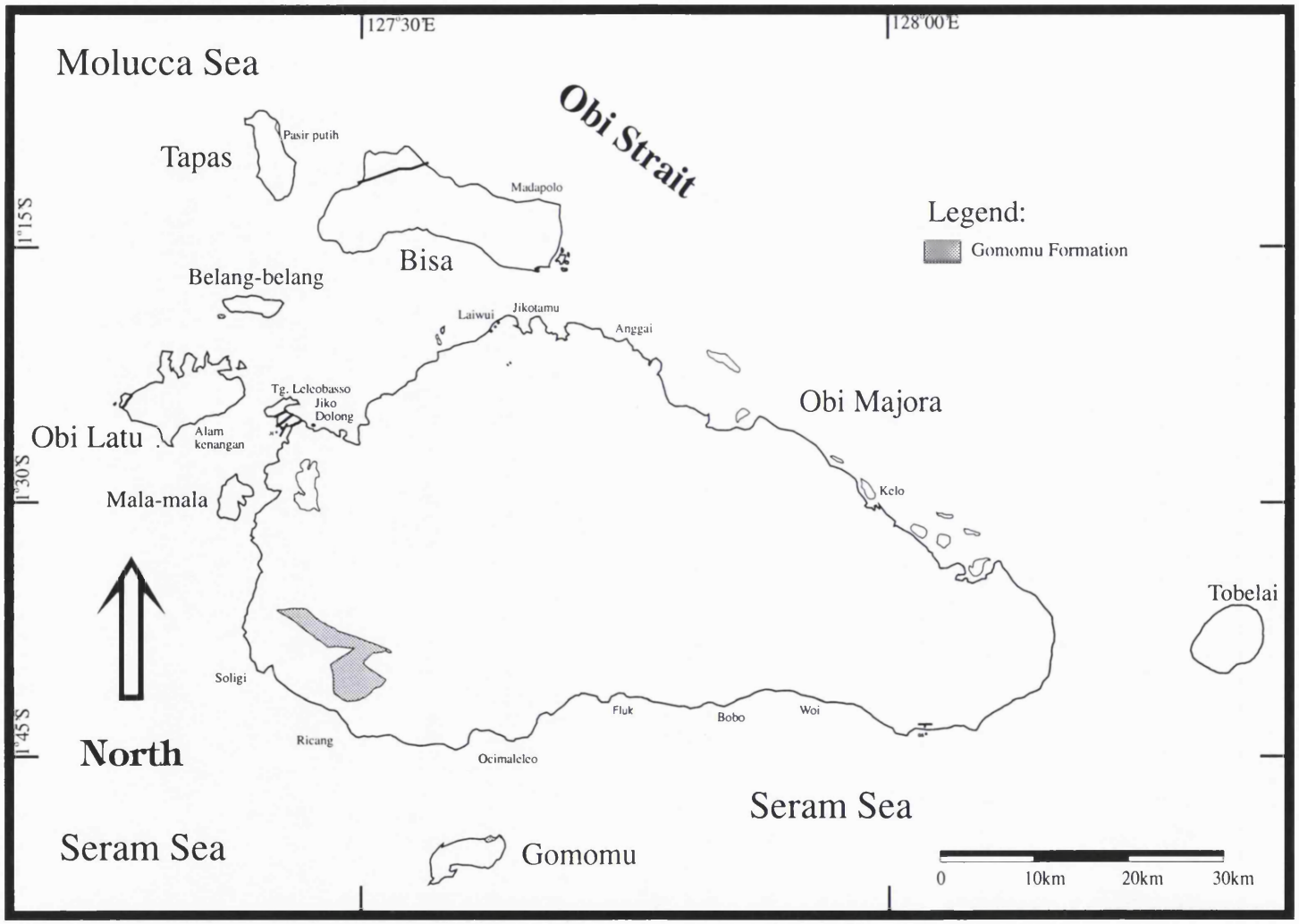

Fig. 3.8 Distribution of the Gomumu Formation

of Jurassic fossils in the dark shales, Hall *et al.* (1992) assigned the shales to a newly named Gomumu Formation.

3.4.2 Aerial Photography and Topographic Interpretation

Base on aerial photographic interpretation, this formation typically appears light grey, forming a smooth topography with minor undulations.

3.4.3 Type Locality

Logging road sections north of Soligi.

3.4.4 Age

Middle-Upper Jurassic. Palynomorphs from three samples (OR94, OR97, OT29) indicate Middle-Upper Jurassic ages and a belemnite from one sample (OR97) indicates a Middle or Upper Jurassic (probably Upper) age.

3.4.5 Thickness

The thickness of this formation is uncertain; probably more than 100 m.

3.4.6 Distribution

This formation is present in SW Obi and Gomumu Island, south of Obi.

3.4.7 Lower and Upper Contacts

The upper and lower contacts of this formation are not seen.

3.4.8 Description

North of the exposures of Soligi Formation sandstones at Soligi village serpentinites are exposed in a NW-SE trending strip several kilometres wide. To the north of the serpentinites is another strip, also trending NW-SE and several kilometres wide, which consists of black shales. These are very fissile, unmetamorphosed, and generally without a macrofauna although burrowing traces are locally present. In deeply weathered logging road cuts the shales are bleached white. Close to the serpentinites the black shales and serpentinites are sheared together; the mapped trace of the contact suggests a steeply dipping surface. On the logging road about 5.5 km north of the logging camp at Tanjung Ricang dark siltstones contain an abundant fauna including ammonite fragments, aptychi, belemnites and bivalves. This is the region from which Wanner (1913) reported Jurassic ammonites as float.

3.4.9 Depositional Environment

Open marine based on lithology and fossils.

CHAPTER 4

THE OPHIOLITIC BASEMENT COMPLEX

4. THE OPHIOLITIC BASEMENT COMPLEX

4.1 Introduction

Previous researchers have reported the existence of ultrabasic and basic igneous rocks in northern and western Obi (Fig. 4.1). which were shown as melange by Hamilton (1979) and assigned to the Bacan Formation by Sudana & Yasin (1983). Hall *et al.* (1992) concluded that these rocks were similar to ophiolitic rocks of east Halmahera and Waigeo and suggested that they formed the basement of northern and central Obi. This Ophiolitic Basement Complex has been interpreted by Hall *et al.* (1991, 1992) as the oldest rocks of the Philippine Sea plate.

4.2 Lithologies

In many parts of south Obi there are large areas of ophiolitic rocks. The ophiolite includes rocks of three principal types and although faulted appears to be in a relatively coherent state. Unlike the Halmahera and Waigeo ophiolites, where there are rapid fault-controlled changes in lithology over many short sections, on Obi there are long, continuous and thick sections of similar rocks. The three principal rock types are serpentinites, dolerites and fine grained gabbros, and pillow lavas. Coarse gabbros and cumulates are common as boulders in river and beach float in several areas but are not well exposed.

Ultramafic rocks are exposed predominantly in western Obi, and massive serpentinites occupy an extensive area of central western Obi crossed by logging roads north of Ricang. There they are overlain by lateritic soils, and they have a characteristic soft, smooth and light topography (Fig. 4.2). These rocks consist mainly of massive serpentinized dunites and harzburgites with serpentinized pyroxene-rich layers. In places they have some mineralogical banding although internal structures are not very clear. The lateritization produces a red soil, generally about 2-3 m thick, which is worked for nickel. In southeast Obi, serpentinized harzburgites are exposed on the logging road from Bobo between 15-18 km inland, although there area of exposure is not as wide as in west Obi. In some places this rock is found sheared. There are also small areas of serpentinites exposed on Tapas Island.

Cumulate gabbros are widely represented as float in boulders collected in south Obi although none have been found in situ. The most commonly represented plutonic rocks of the complex are gabbros which are exposed in the Fluk and Airpati Rivers, and on Obi Latu. Microgabbros found in Airpati River are intruded by gabbro pegmatites in some places (Fig. 4.3). Gabbros in the Fluk River show layering. In NE Obi Latu, gabbros contain large crystals of pyroxene and plagioclase, and show banding; in some places they have cumulate textures.

A variety of plutonic rocks within the area of ophiolitic rocks are exposed along the logging road between Ricang and Jikodolong. There, gabbro, diorite and plagiogranite are exposed. The

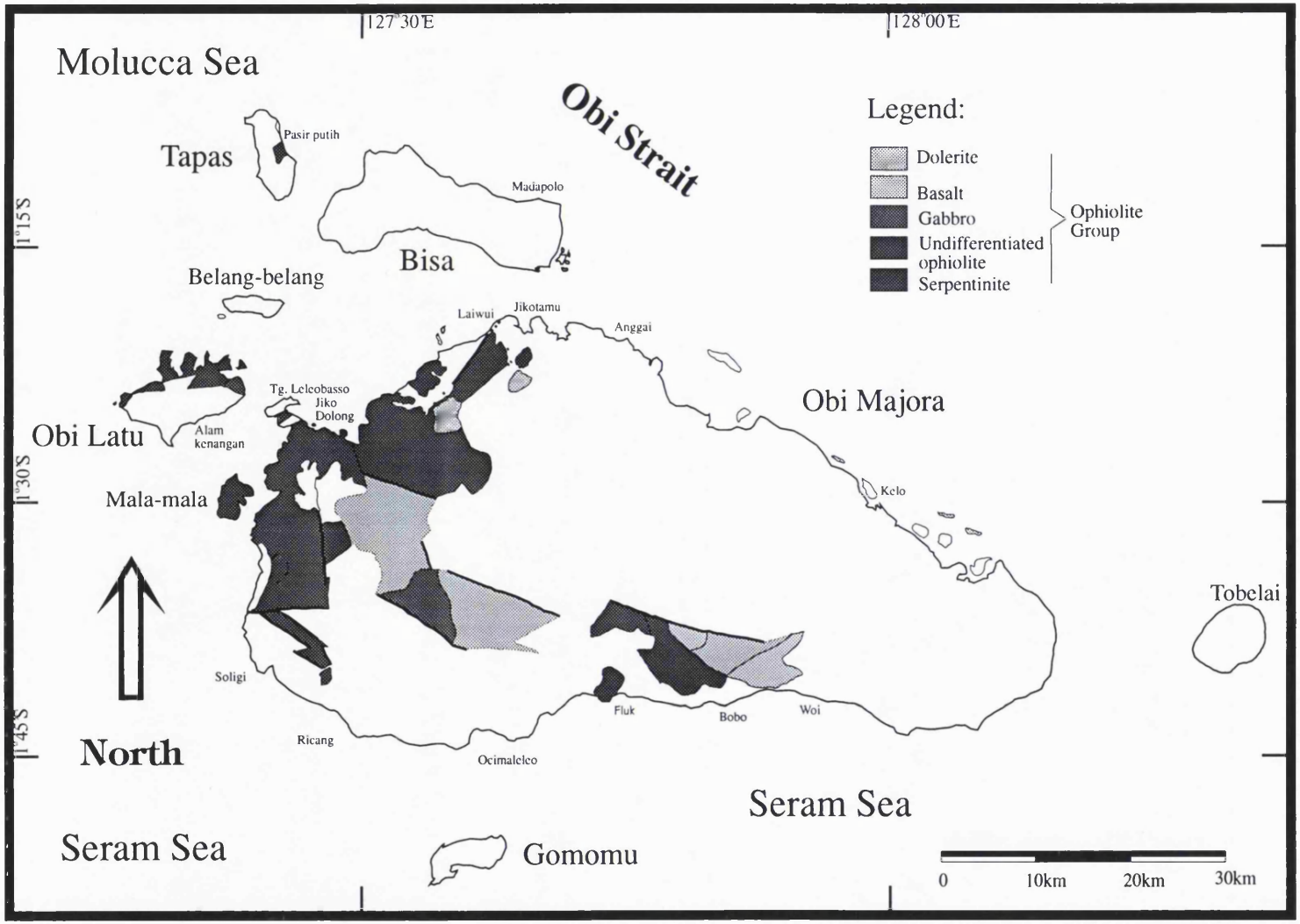

Fig. 4.1 Distribution of basic and ultrabasic rocks of the Ophiolitic Basement Complex of Obi.

Fig. 4.2 View of hills underlain by serpentinite and covered by thick laterite soils in NW Obi.

Fig. 4.3 Gabbro pegmatite intruding microgabbros in Airpati River, SW Obi.

contacts are not exposed and the diorite may intrude into the ophiolitic rocks. At Tanjung Leleobasso a diorite body which extends into Obi Latu intrudes the Upper Cretaceous Leleobasso Formation suggesting an early Tertiary age and indicating it is younger than the ophiolitic rocks. This suggestion is supported by K-Ar dates from diorites (S. Baker, pers. comm., 1995) and is consistent with similar age relationships from east Halmahera (Ballantyne, 1990).

Dolerite dykes are well exposed in central Obi on logging roads north of Ocimaloleo (Fig. 4.4) and in the Airpati and Tapaya Rivers, and in central western Obi on logging roads north of Ricang. On the roads north of Ocimaloleo the dykes seem to be in sufficient abundance to be considered a sheeted complex; although no one-way chilled sections were found there were several examples of exposures composed entirely of dykes. All were steeply dipping with an apparent regular variation of strike over the 7-8 km section crossed. In the Airpati River there are very fresh dolerite dykes intruding coarser dolerites and homogeneous fine grained gabbros. All extensional features were steeply dipping and had a consistent orientation and field relations suggest this section represents the top of the magma chamber. A similar well exposed section of dykes was found on the Ricang logging road about 28 km from the coast although they are less fresh (Fig. 4.5).

Pillow lavas are well exposed in east Obi north of Bobo on the logging road leading the Woi River, in central west Obi on the logging road north of Ricang, and on the island of Wobo at the western end of Obi Latu (fig. 4.6). In all these areas the lavas are similar. They are purple weathering amygdaloidal but otherwise aphyric basalts, mainly pillowed with some massive units. Although the lavas are broadly right-way-up there are no good structural markers to indicate their initial attitude with certainty; they lack any significant interpillow sediment. Furthermore, they are rather altered and typically deeply weathered.

4.3 Aerial Photographic and Topographic Interpretation

On aerial photographs some parts of the ophiolitic rocks are easily recognised. Areas of ultrabasic rocks have a distinctively massive, light grey and smooth appearance with a moderately undulating topography which in some places forms hills with heights up to about 850 m above sea level. Areas of pillow lavas, dolerites and microgabbros have a dark grey and rough appearance on the photos. In these areas most of the rivers dissect deeply and form V-shaped valleys.

4.4 Age

The age of the ophiolitic rocks is uncertain, but on the basis of evidence from elsewhere in the Halmahera-Waigeo region they are thought to be older than Late Cretaceous, and may be Early Mesozoic. On Gag, dolerite dykes similar to those on Obi have Late Jurassic (150-140 Ma) K-Ar ages (Pieters *et al.*1979; Hall *et al.*1995). Preliminary Nd-Sm dating of minerals from

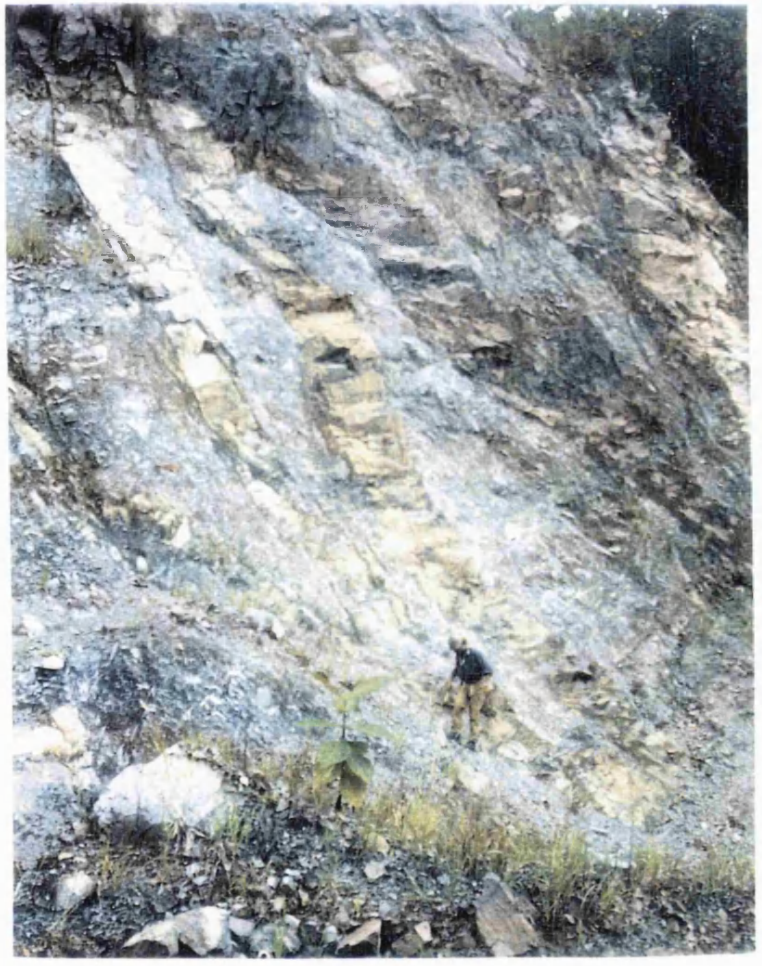

Fig. 4.4 Dolerire dykes exposed in central Obi on the logging road north of Ocimaloleo.

Fig. 4.5 Dolerite dykes exposed on the Ricang logging road about 28 km from the coast in west Obi.

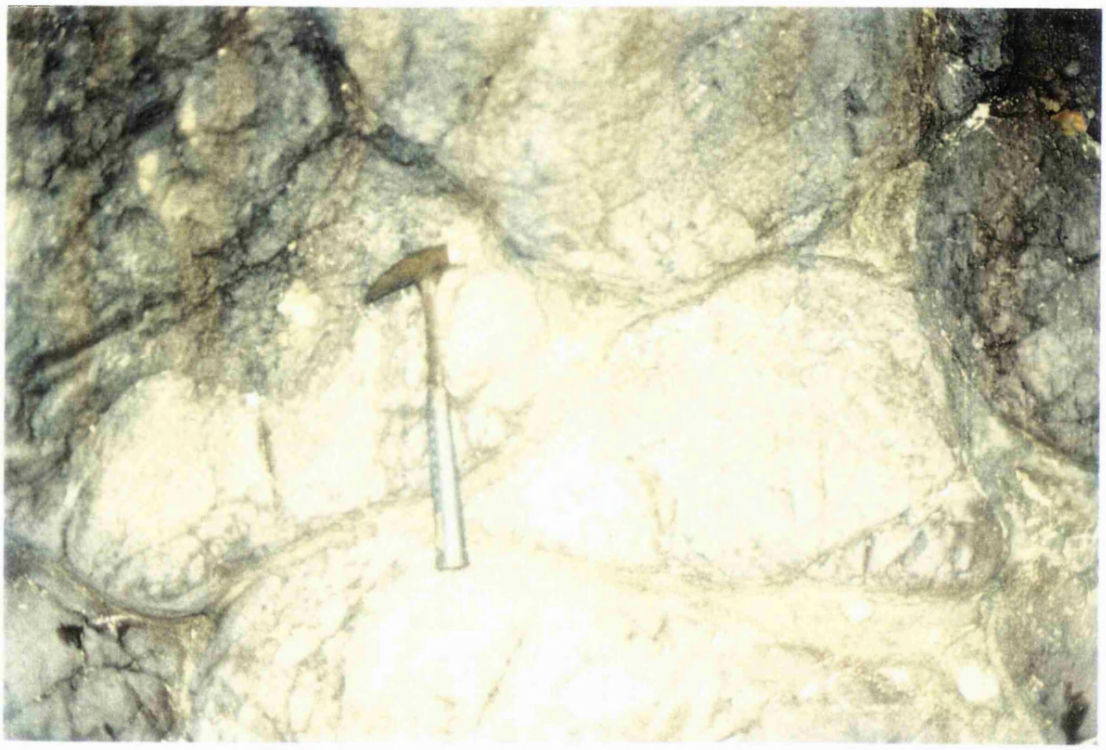

Fig. 4.6 Pillow lavas exposed on the coast of Wobo Island, south of Obi Latu.

cumulate gabbros has yielded Jurassic ages. On Waigeo, the oldest sedimentary rocks which are associated with the ophiolite are lowermost Cretaceous arc-related volcaniclastic rocks interpreted to overlie the ophiolitic basement. On Halmahera, Upper Cretaceous sedimentary rocks unconformably overlie the Ophiolite Basement Complex and are very similar to the Leleobasso Formation of Obi. Arc-related igneous rocks intruding the east Halmahera ophiolite (Ballantyne, 1990) have Ar-Ar of ages 94-72 Ma.

Table 4.1 Summary of K-Ar results from Ophiolitic rocks (wr whole rock, hb: hornblende).

Sample	Material	Grain size (μm)	%K (1σ error)	Wt for Ar (g)	$^{40}Ar^*$ nl/g (1σ error)	$^{40}Ar_{atm}$	Age Ma (2σ error)
basalts							
OD22	wr	125-300	0.4814 ± 1	2.5105	0.774 ± 1.31%	45.12	40.9 ± 1.3
OR50	wr	125-300	1.3023 ± 1	3.2893	0.7810 ± 2.74%	71.21	15.4 ± 0.9
OD235	wr	125-500	0.044 ± 1	1.0001	0.1053 ± 8.98%	89.66	60.8 ± 10.8
dolerites							
OD201	wr	125-500	0.715 ± 2.9	1.1316	1.4462 ± 1.22%	40.5	51.3 ± 3.2
OD202	wr	125-300	0.454 ± 1	1.1095	0.4921 ± 1.88%	61.07	27.7 ± 1.2
OD203	wr	125-300	1.060 ± 3	1.1744	1.8888 ± 1.05%	23.41	45.3 ± 2.8
OD207	wr	125-300	0039 ± 1	1.236	0.114 ± 9.34%	90.11	73.7 ± 13.8
OD209	wr	125-500	0.025 ± 1	1.3542	0.0673 ± 9.65%	90.35	68 ± 12.9
gabbros							
OR69	wr	125-500	0.0995 ± 1.4	1.6529	0.0802 ± 5.87%	84.97	20.6 ± 2.5
OR70	hb	125-500	0.457 ± 1	1.5379	0.2956 ± 4.26%	80.36	16.6 ± 1.4
OJ102	hb	125-300	0.113 ± 1	0.9511	0.2766 ± 1.65%	53.65	62 ± 2.4
OJ107	wr	125-300	0.048 ± 1.5	1.154	0.1602 ± 6.76%	86.81	84.4 ± 11.4

Potassium-argon dating of whole rocks and mineral separates from the ophiolitic rocks yielded a variety of ages (Table 4.1). Basalt ages range from 15-61 Ma, dolerites from 28-74 Ma, and gabbros from 17-84 Ma. Ages with large errors reflect the very low potassium contents of some samples. It is probable that all these ages are mixed ages, reflecting partial resetting of original igneous ages during an early Tertiary thermal event, and it is notable that in these samples and many other rocks there is a concentration of ages at around 40-50 Ma (S. Baker, pers. comm, 1995). It is likely that the oldest ages are minimum ages for the ophiolite, consistent with the stratigraphic evidence (Chapter 5), and that there was an episode of arc magmatism in the Paleocene-Eocene which caused partial resetting of K-Ar ages. Younger ages may also reflect reheating during the Miocene-Pliocene episode of volcanic activity (Chapter 5).

4.5 Thickness

It is not possible to determine the maximum thickness of the ophiolitic rocks as its base is never exposed. Cross sections indicate a minimum thickness of 3 km.

4.6 Distribution

The ophiolitic complex occupies a large area of west part of Obi and extends to Obi Latu island. Excellent exposures are along the logging road between Jikodolong and Ricang in the western part of the island. Smaller areas of ophiolitic rocks are found in southern Obi and good exposures are found close to Bobo and Fluk Villages, on the logging roads north of these villages, and in the Nikeh and Fluk Rivers.

4.7 Petrography and Mineral Chemistry

4.7.1 Peridotites

These rocks are typically hard, dense and dark black to green and composed of olivine and pyroxene with some cracks filled by serpentine and/or chlorite (Fig. 4.7). They are heavily serpentinized with complete alteration to serpentine, talc, carbonate, and magnetite, although relict olivine grain are often recognizable. Bastite serpentinites are composed of serpentinised olivine with well developed mesh textures, and bastites (altered orthopyroxene) are commonly veined by chlorite. Several serpentinized harzburgites contain some chrome spinel (OJ103, OR153 and OR155). Relics of olivine appear fragmental and are surrounded by fibrous serpentine. Opaque grains are found along former grain boundaries of olivine, and as stringers in chrysotile veinlets. Pyroxenites (OJ110, OJ77 and OJ78) are exposed on the logging road between Ricang and Jikodolong.

4.7.2 Plutonic Rocks

There are several varieties of gabbros found in Obi, including olivine gabbros, gabbro-norites, and hornblende gabbros (Fig. 4.8). Many of these gabbros have cumulate textures. They are very fresh and contain cumulate pyroxenes and plagioclase, with intercumulus amphibole. Several gabbros contain more than 5% olivine (OR81, OR86, OT49 and OD224), and gabbros exposed along the logging road from Ricang to Jikodolong (OJ105 and OJ108). Olivine and calcic plagioclase were the first minerals to crystallise and were followed by pyroxene and then Fe-Ti oxides. Amphibole occurs as a late-stage magmatic crystallisation product but also as a product of hydrothermal metamorphism.

Some olivines are fresh, but some of them are replaced by serpentine and iddingsite. Plagioclases are commonly altered to smectite, pumpellyite and prehnite, and in several samples plagioclases are replaced by albite (OJ88 and OJ81). Pyroxenes are replaced by actinolite, epidote, chlorite, titanomagnetite, pumpellyite and pale green amphibole. Prehnite and quartz

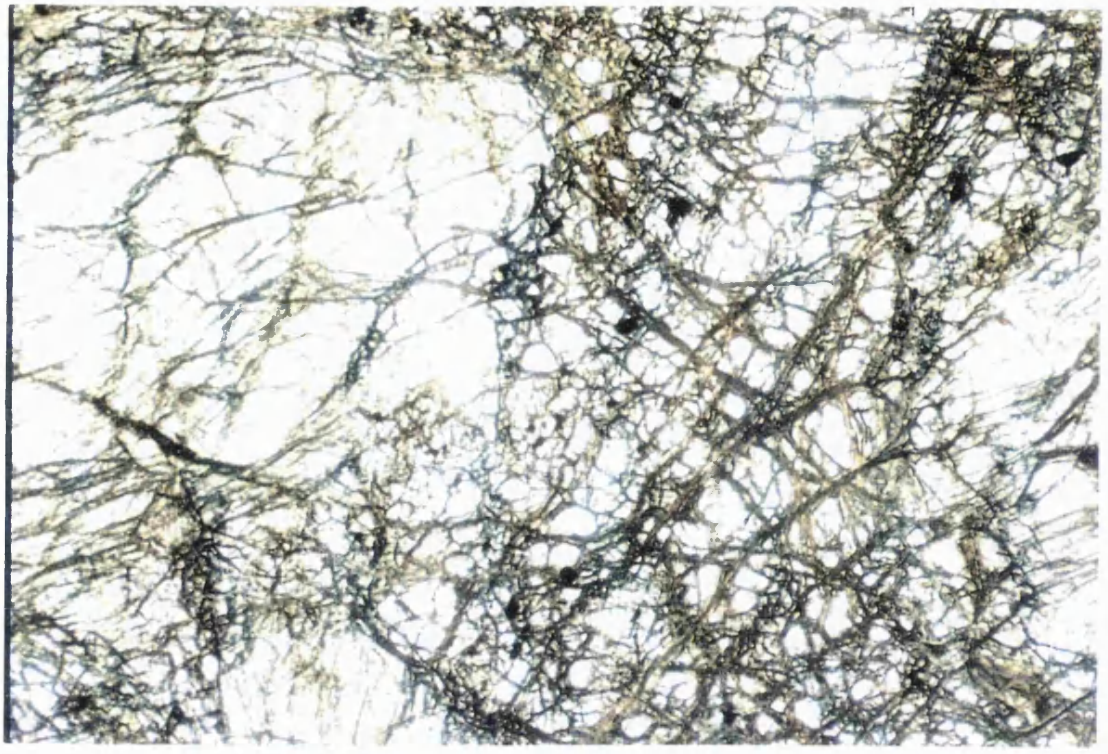

Fig. 4.7 A. (above) Photomicrograph of partly serpentinised harzburgite (OR53). Orthopyroxene forms large crystals, whereas olivine are fractured and crossed by numerous narrow veins of serpentine. Plane polarised light. Width of photograph is 1.6 mm. B. (below) crossed polars.

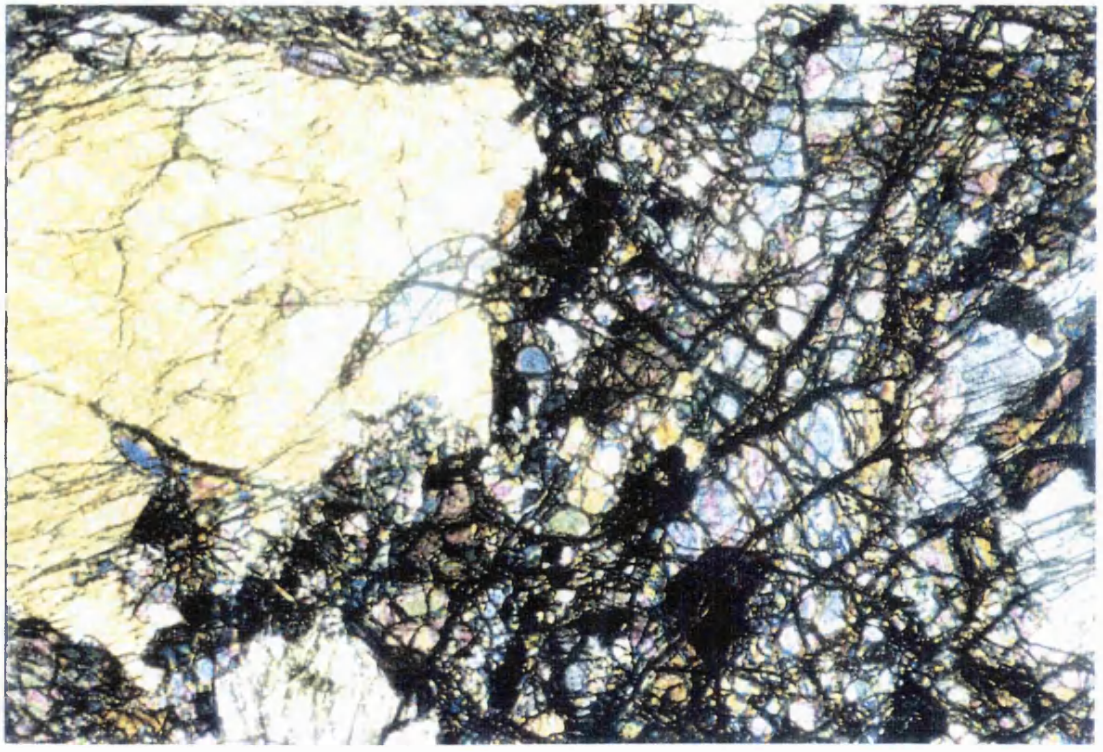

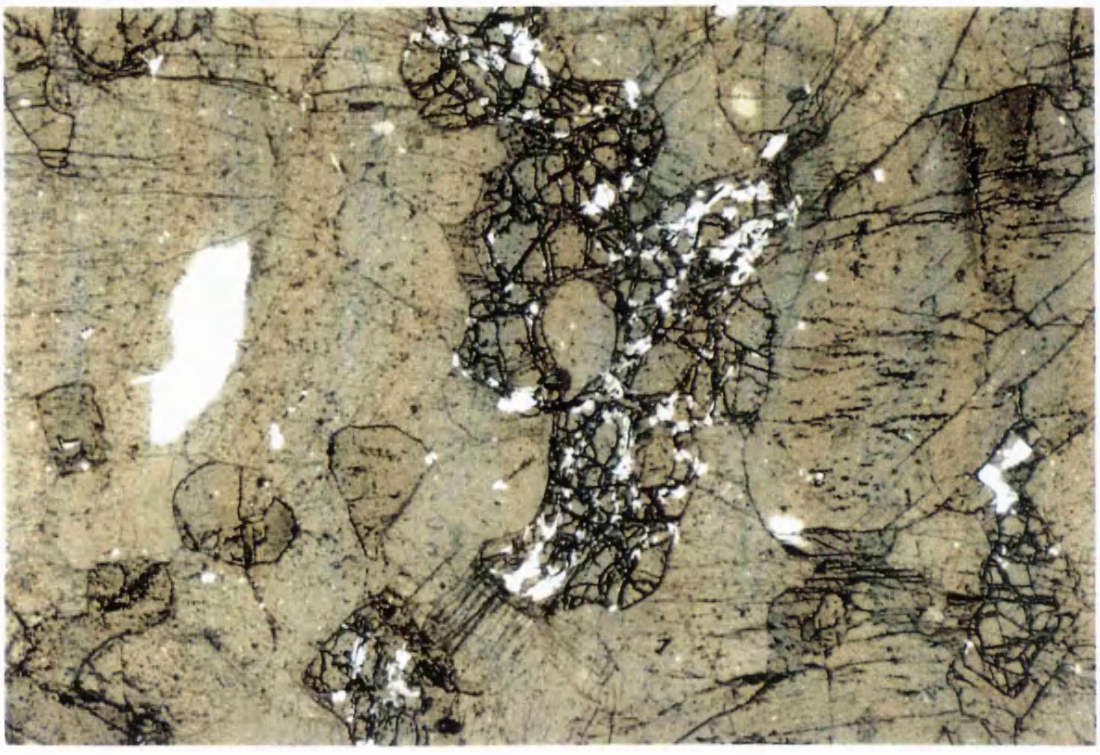

Fig. 4.8 A. (above) Photomicrograph of fresh olivine gabbro (OJ108), possible a cumulate. Plane polarised light. Width of photograph is 1.6 mm. B. (below) crossed polars.

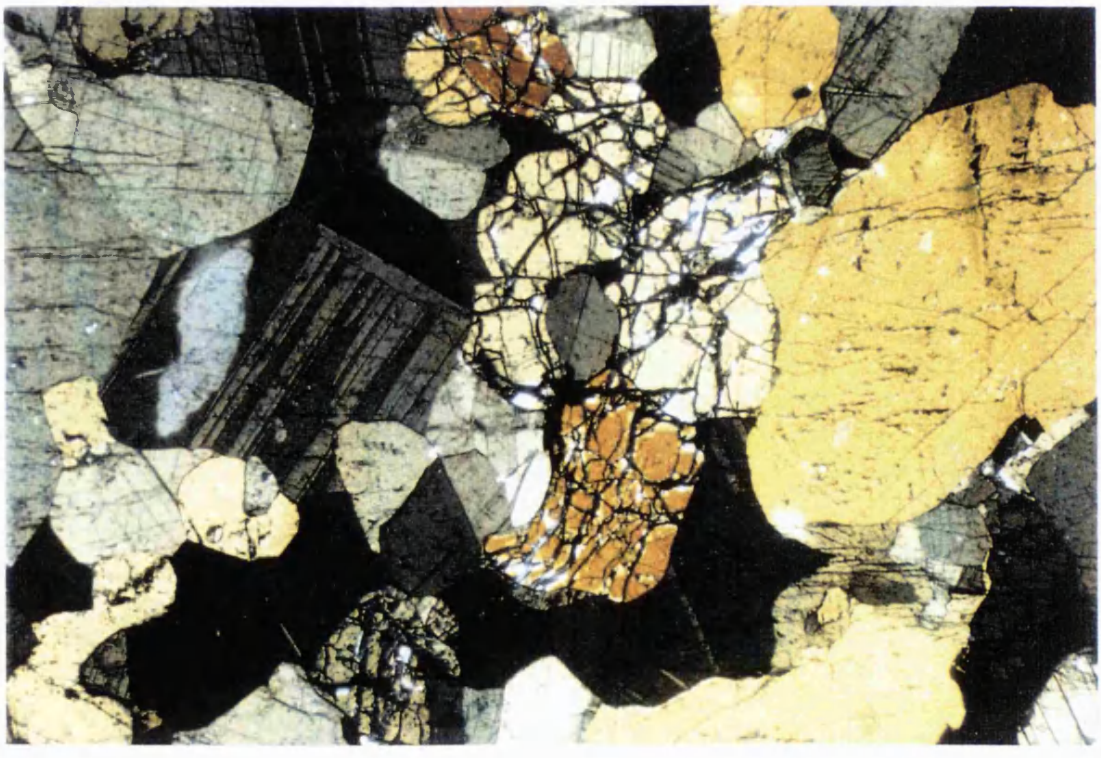

may fill cracks and veinlets of gabbros and microgabbros. In Iceland, the presence of prehnite, epidote and chlorite indicate metamorphism at temperatures above 230°C and the presence of actinolite suggests temperatures above about 300°C (Tomasson & Kristmansdottir, 1972). Their mineralogy suggests that some gabbros in Obi have been metamorphosed under low-grade metamorphic conditions to pumpellyite-actinolite (OJ88) and epidote-actinolite (OJ87) facies. This type of metamorphism is typical of metamorphism associated with submarine hydrothermal metamorphism at mid-oceanic ridges (Yardley, 1989).

4.7.3 Dolerites

On the logging road leading to Jikodolong dolerites are well exposed and have some resemblances to a sheeted dike complex. Dolerites are also exposed on the Bobo logging road and in the north Obi. Most of dolerite samples from Obi have been altered by low grade metamorphism. Typically the dolerites retain well-preserved sub-ophitic or diabasic textures although many of the original minerals have been altered to albite, actinolite, calcite, smectite, pumpellyite and chlorite (OD201, OD204, OD205 and OD208). Plagioclases are replaced by albite, carbonate, smectite, quartz and sometimes prehnite. The growth of prehnite is retarded by the carbonate content, because the present of high CO_2 activity in fluids during low grade metamorphism suppresses the development of Ca-Al silicates such as prehnite, while CO_2 reacts with Ca-Al silicates to produce calcite, epidote, quarts and chlorite (Zen, 1961). Hornblende and actinolite largely represent secondary minerals which replace pyroxenes, as relics of pyroxene are found in some rocks. Generally, epidote is present as secondary minerals which fill cracks, but sometimes is found replacing pyroxene or amphibole. As noted above, the mineralogy is typical of sub-greenschist and greenschist facies and is interpreted as hydrothermal alteration due to oceanic metamorphism.

4.7.4 Diorites

Diorite exposed near Ocimaleleo (OS6) consists of plagioclase, hornblende and apatite (Fig. 4.9). Plagiogranites are composed of plagioclase, hornblende, and quartz. Some of the original minerals are replaced by smectite and epidote. Diorites occur as small intrusions in ophiolitic rocks such as the body on Obi Latu. They comprise plagioclase, hornblende, pyroxene and a little quartz (OR92, OS65 and OJ92). Plagioclase is commonly altered to pumpellyite and smectite. Chlorite and epidote represent replacement of pyroxene and hornblende. Some cracks are filled by quartz and epidote.

4.7.5 Basaltic Rocks

Most commonly basaltic rocks are dark grey to reddish-grey pillows with interpillow sediment. They may be vesicular, amygdaloidal, and porphyritic. The phenocrysts of porphyritic basalts include plagioclase, pyroxene and opaque minerals and the groundmass contains

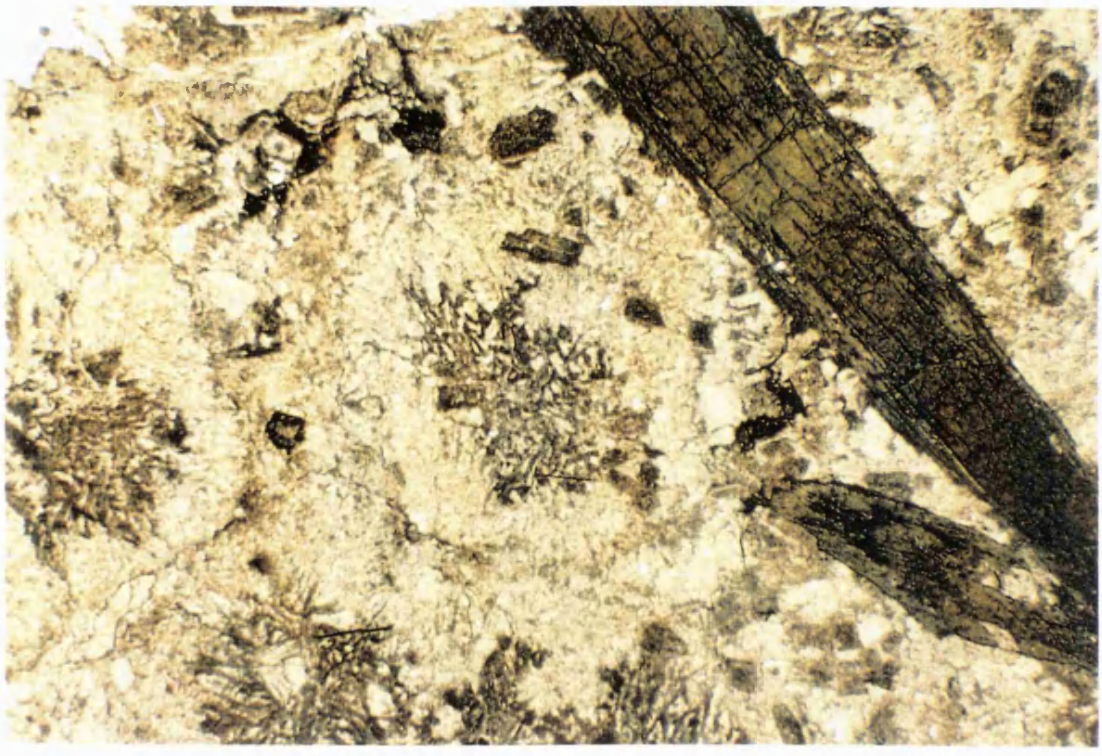

Fig. 4.9 A. (above) Photomicrograph of honblende diorite (OS6), containing granophyric intergrowths of quartz and K feldspar. Plane polarised light. Width of photograph is 1.6 mm. B. (below) crossed polars.

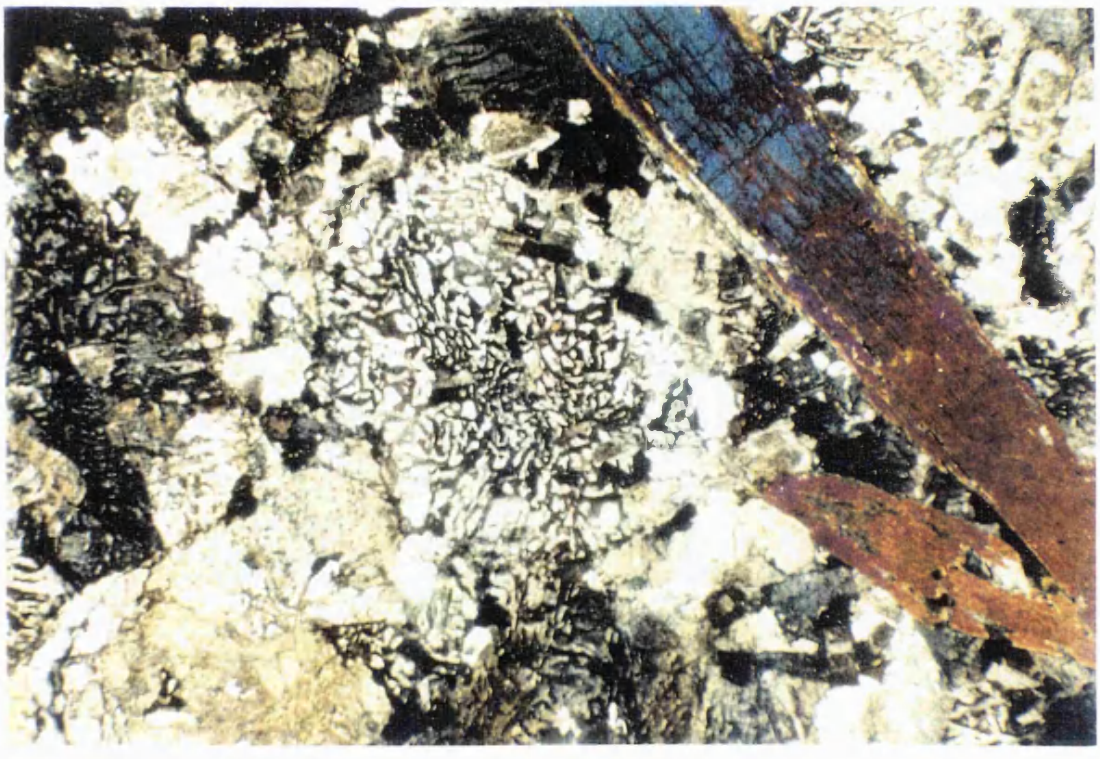

microlitic feldspars, pyroxene and volcanic glass often with a spherulitic texture. Quartz, calcite, epidote, zeolite or haematite usually infill vesicles and cracks. Reddish-grey pillow basalt are exposed in Wobo and southwest coast of Obi Latu islands (OR50 and OR57) and south of Jikodolong on the logging road. Their original mineral assemblage has been replaced by carbonate, chlorite, epidote and smectite. Volcanic glass represents about 45% to 60% of the original rock and has usually been altered to smectite. Zeolites fill amygdales in pillow lavas on Obi Latu (OR56). Fine grained sediment fills the interpillow space, but unfortunately it does not contain microfossils which could indicate the age of the lavas. The interpillow material probably represents hyaloclastic material. At some places in SW Obi Latu show there are pillow fragment breccias which contain a mixture of angular to subrounded basaltic clasts in a matrix of fine grain altered volcanic material and volcanic glass. Dark grey basalt porphyries are exposed south of Laiwui in the river, in the Fluk River (OT40) and on the logging road in Bobo (OD22). Intersertal and intergranular textures are present in several basalts. These basalts have experienced alteration of several minerals. Plagioclases are replaced by smectite and chlorite, whilst pyroxenes are replaced by epidote. The groundmass consists of volcanic glass and microlitic feldspars.

Plagioclase is the first crystallising mineral, followed by pyroxene, oxides, and then glass. The other minerals are secondary products which replaced plagioclase and pyroxene, whereas zeolite occurs as a secondary mineral which filled vesicles.The mineralogy of the alteration products suggests that some basalts have been metamorphosed under low-grade metamorphic conditions from zeolite to sub-greenschist facies.

4.7.6 Mineralogy and Mineral Chemistry

Rocks of the ophiolitic complex have been examined in thin section and a number of samples have been analysed by microprobe. The result of this work is summarised below and sample numbers cited are those from which microprobe data has been obtained. Microprobe data are given in Tables in Appendix B.

4.7.6.1 Plagioclase

Plagioclase was originally present in all rocks. In many gabbros, particularly olivine and cumulate gabbros, plagioclase is large (0.5-4 mm), shows carlsbad and albite twinning, and is in fresh condition. In some plutonic rocks plagioclase is present as inclusions in amphiboles (OJ102) and pyroxenes (OT49). In dolerites plagioclase is found intergrowth with mafic mineral to form diabasic textures. Plagioclase is replaced in many rocks, both intrusive and extrusive, by such minerals as albite, smectite, sericite, pumpellyite and prehnite. Plagioclase compositions are rather calcic (Table 4.2) but the rocks analysed include dolerites and gabbros; one gabbro is probably a cumulate (OJ107) and the other gabbros may be cumulates. Beard (1986) drew attention to the relatively high An contents of plagioclase in gabbroic rocks formed in arc

settings, related to high P_{H2O} and this has reported from elsewhere in the region (e.g Ballantyne, 1990).

Table 4.2 Plagioclase compositions in selected rocks from the ophiolite

cumulate gabbro	OJ107	An_{87-85}	
gabbro	OR70	An_{97-90}	
gabbro	OJ101	An_{90-78}	
dolerite	OD204	An_{82-78}	(and orthoclase)
dolerite	OD207	An_{65-53}	

In basalts, plagioclase is present as phenocrysts or as microlites in a glassy matrix. The proportion of plagioclase phenocrysts and microphenocrysts ranges from 20-30 modal %. The grain are commonly elongate and subrounded in outline and form subhedral to euhedral crystals with lengths from 0.1-1.5 mm. Zoning, complex and simple twinning is common in all samples. Plagioclase phenocrysts of pillow basalts (OR50 and OR 56) are replaced by albite.

4.7.6.2 Olivine

Olivine is found in peridotites (OJ103, OR153 and OR155), and some gabbros and basalts (OJ108, OT49, OR86, OJ105, OR81 and OR125). It is commonly altered although fresh and euhedral grains are preserved in some samples. Some olivines are replaced by serpentine or iddingsite, particularly at the edge of crystals, or in cracks. Alteration of olivine producing mesh structures is common in peridotites.

4.7.6.3 Pyroxene

Pyroxene is present in almost all the basic rocks and occurs as both a phenocryst and groundmass phase in basaltic rocks. Most rocks contain 15-35 modal % pyroxene. In gabbros pyroxenes range from 0.5-3 mm. In some samples they are intergrowth with plagioclase to form a diabasic or ophitic texture. Most are clinopyroxenes, and orthopyroxene is found in only a few rocks. Plagioclase inclusions in pyroxene are present in some gabbros (OR217). In the gabbros analysed clinopyroxenes are ferroan diopsides (OR70 and OJ101) and orthopyroxenes are ferroan enstatites. In a dolerite (OD204) the pyroxenes are aluminous magnesium-rich augite and aluminous ferroan diopside. In the basalts the phenocrysts are generally subhedral to euhedral grains from 0.5-1 mm across with fine grain groundmass crystals less than 0.3 mm in length.

In several dolerites and basalts, some pyroxenes are replaced by epidote, chlorite, carbonate, smectite and pumpellyite. Some are replaced by actinolite (OR217 and OT41). In one dolerite (OD201) a core of pyroxene is surrounded by a rim of fibrous amphibole which is replacing the pyroxene.

4.7.6.4 Amphibole

Amphiboles present in ophiolitic rocks are hornblende and actinolite. In most cases amphibole is a secondary mineral replacing pyroxene, but in cumulates some of the amphibole

may be an intercumulus phase. There may be up to 15 modal % hornblende in gabbros, in dolerites there is typically 15-45 modal % amphibole, whereas in basalts amphiboles are absent. Possible igneous, or early high temperature amphiboles, from gabbros have compositions which fall in the fields of magnesio-hornblende, magnesio hastingsitic-hornblende and tschermakitic hornblende (OR70, OJ101, OJ107). Amphibole is clearly present as a secondary phase in gabbros (OD237, OT43 and OJ87) and dolerites (OD201 and OD207) and compositions in one dolerite (OD207) range from actinolite to actinolitic-hornblende.

4.7.6.5 Accessory Minerals and Volcanic Glass

All opaque mineral grains analysed were ilmenite or titanomagnetite with the exception of possible chrome spinel (brown but not analysed by microprobe) in one dolerite (OD202). Volcanic glass is only found in basaltic rocks (OD22, OR50, OR184, OR186, OR60, OD202 and OD204).

4.7.6.6 Low-temperature Secondary Minerals

Chlorite is present in some samples replacing plagioclase, volcanic glass (OD233), pyroxene or olivine (OJ105). The chlorite is usually grassy-green, fibrous and poorly crystalline. Chlorite is present in peridotite associated with serpentine. Four analyses from dolerite (OD204) are all pycnochlorites (Deer, Howie & Zussman, 1966). Smectite is found in several samples (OD202, OD201, OD203 OD212 and OJ76) and in some is associated with pumpellyite. It appears to be an alteration product of plagioclase or pyroxene. Zeolite is present filling amygdales in basalt (OR50) from Wobo Island at the south of Obi Latu Island.

4.8 Geochemistry

Rocks from the Ophiolitic Basement Complex selected for chemical analysis were basalts, dolerites and diorites. The main purpose of the whole rock chemistry study was to characterise volcanic and plutonic rock types and utilise published tectonic discrimination diagrams to identify the tectonic setting of formation of the ophiolite complex. Both major and trace elements were analysed to identify element mobility due to alteration in order to use appropriate tectonic discrimination diagrams. Discussion of the magmatic source and the processes of magmatic modification (e.g. assimilation, fractional crystallisation, partial melting, contamination) are beyond the scope of this study. Chemical analysis data are given in Table in Appendix C.

4.8.1 Major Elements

Significant major element mobility, reflecting alteration of the basalts, is shown by their relatively high SiO_2 contents (52-62 wt %), variable K_2O (0.1-1.6 wt %), enrichment in Na_2O (3.4-7.6 wt %), and variable depletion of CaO (4.4-12.0 wt %), and MgO (3.3-11.0 wt %). Loss on ignition (LOI) for all these rocks is also significant (2.0-5.3 wt %). Similar variations are seen in the analyses of dolerites. They resemble the basalts in the large range of their SiO_2 contents

(47.4-57.6 wt %), enrichment in Na_2O (0.9-6.9 wt %), and loss on ignition (0.5-4.5 wt %). One dolerite sample, has a SiO_2 content of 70.3 wt %. Most of the dolerites fall in the low-K tholeiite field (Fig. 4.10) on the diagram of Taylor *et al.* (1981), and they scatter in the fields between basalts and trachy-andesites on Na_2O+K_2O-SiO_2 diagram (Fig. 4.11) of Le Bas & Streckeisen (1991), but little confidence can be placed in these diagrams for classification purposes in view of the textural and chemical evidence for alteration.

The diorite also show a significant variation in major element compositions, suggesting alteration. However, they have generally low LOI and are, as expected, significantly richer in SiO_2 than most of the dolerites and basalts, consistent with at least some of their compositional variation being primary. These rocks closely resemble the fresh andesitic rocks of the Woi Formation and Guyuti Formation in their major element compositions.

4.8.2 Trace Elements

The basalts plot in a reasonably coherent manner on the MORB-normalised trace element diagrams (Fig. 4.12). They have generally flat patterns similar to ocean ridge basalts. Most are enriched in K and Rb, although one (OR191) is very depleted relative to MORB. All show significant Nb depletion suggesting an arc-related character. Two subgroups are suggested by the Ti-Zr-Y triangular plot (Fig. 4.13). Four of the six basalts fall in the MORB field on the diagram and the remaining two (OR50, OR56) plot in the arc field and are relatively enriched in Ce, P and ZR relative to Ti. On the Mn-Ti-P triangular diagram the basalts fall in the island arc tholeiite field (Fig. 4.14). Various other trace element ratios emphasise the similarities to both MORB and island arc basalts (Fig. 4.15).

The dolerites resemble the basalts and on the Ti-Zr-Y triangular diagram (Fig. 4.13) most plot in the MORB field. There are two extreme samples (OD208, OD233). On the Mn-Ti-P triangular diagram (Fig. 4.14) many dolerites fall in the island arc tholeiite field, but several samples plot in the ocean island fields. The MORB-normalised trace element diagrams also show their resemblance to the basalts (Fig.4.12). OD201, OD203 and OD220 are most similar to MORB, although they differ from MORB in their enrichment in K and Rb and depletion in Nb. OD207, 212 and 235 have similar patterns but are depleted in K, Rb and Ba. There is some correlation of trace element contents with SiO_2 contents; OD204, OD208 and OD209 are most depleted in the elements between Ce and Y and these have the lowest SiO_2 (47.4-51.2 wt %).

The diorites as a group have very coherent similar patterns on the MORB-normalised trace element diagram (Figs. 4.16 and 4.17) and they resemble typical arc andesites, as noted above for their major element compositions. On the triangular diagrams and trace element variation diagrams (Figs. 4.18 and 4.20) they fall mainly in the calc-alkaline basalt fields. They are very enriched in K, Rb and Ba, are notably depleted in Nb compared to most other elements, and have

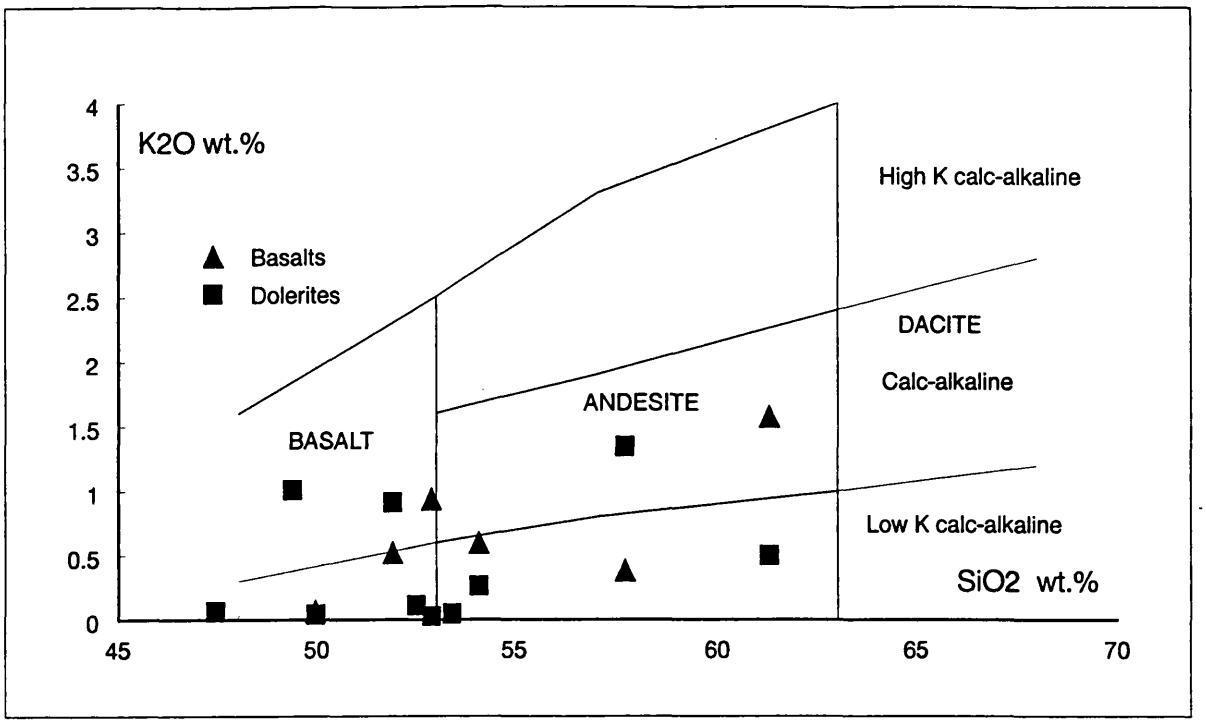

Fig. 4.10 Plot of K_2O versus SiO_2 for basalts and dolerites of the ophiolite. Compositional fields from Taylor et al. (1981).

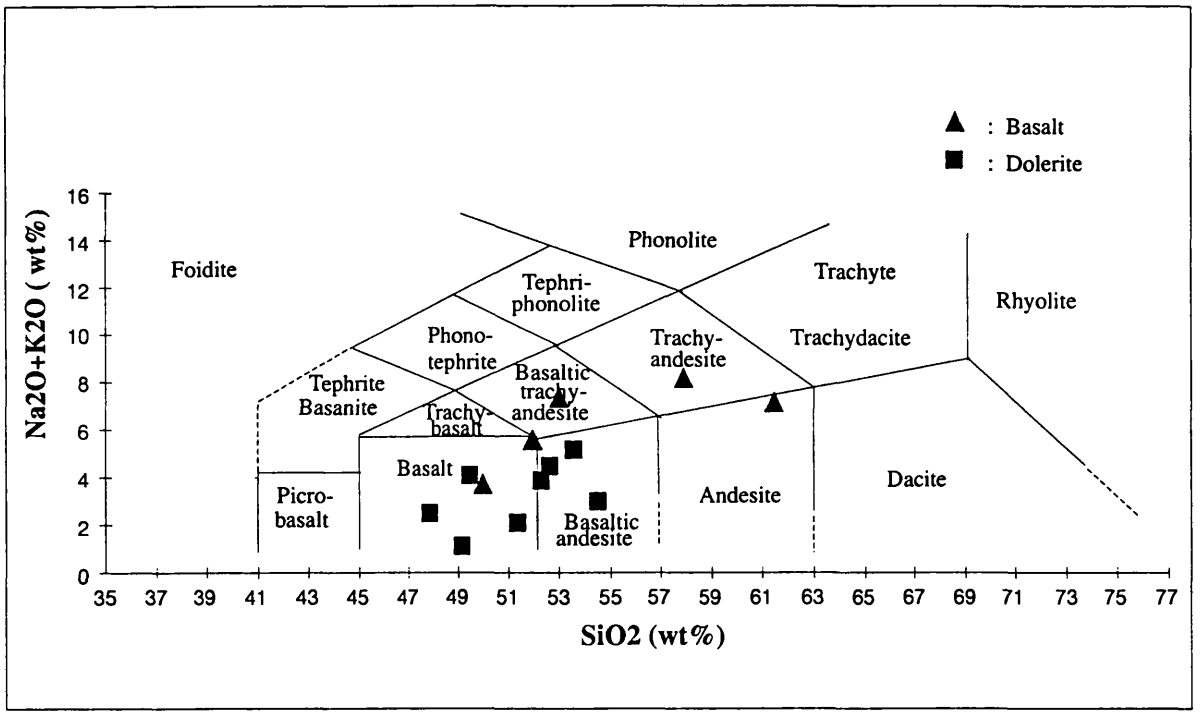

Fig. 4.11 Plot of Na_2O+K_2O versus SiO_2 for basalts and dolerites of the ophiolite. Compositional fields from Le Bas & Streckeisen (1991).

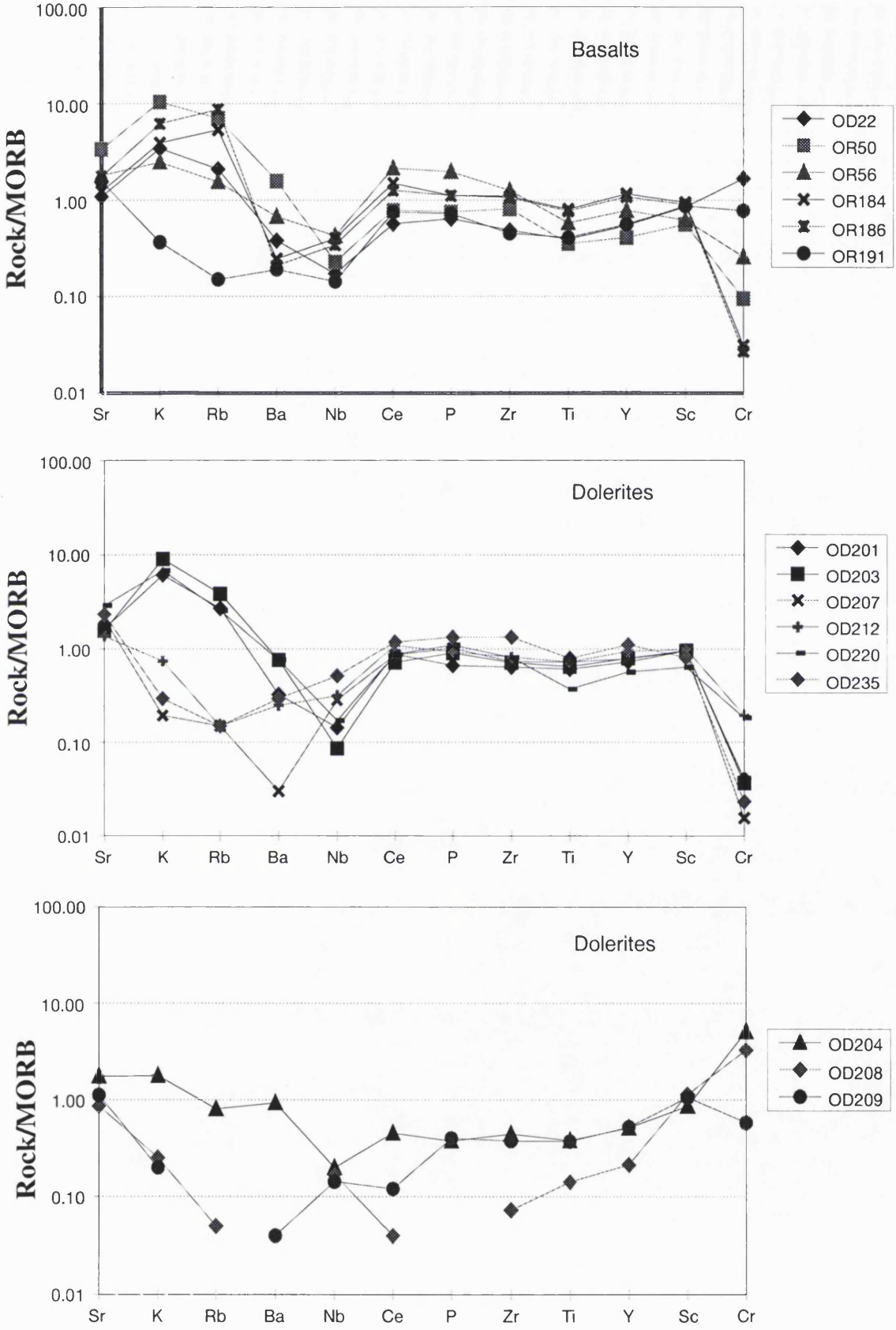

Fig. 4.12 MORB-normalised trace element spidergrams for basalts and dolerites of the ophiolite. Normalising factors from Pearce *et al.* (1984)

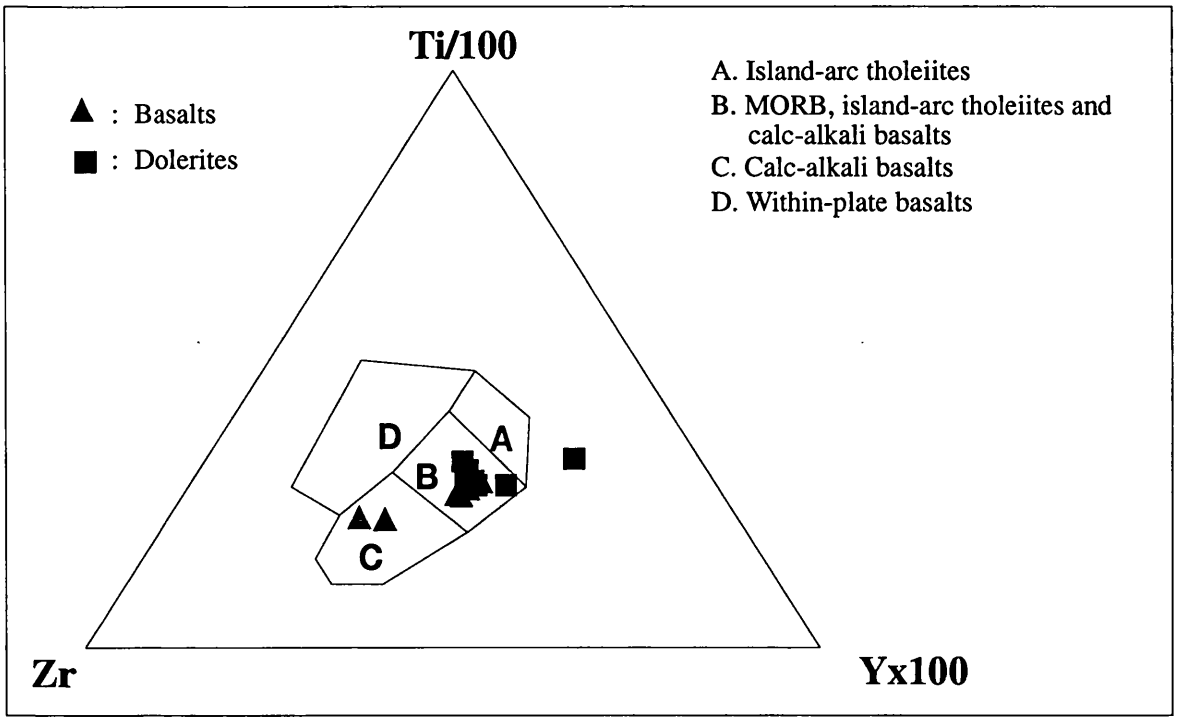

Fig. 4.13 Ti-Zr-Y discriminant diagram for basalts and dolerites of the ophiolite (after Pearce and Cann, 1973)

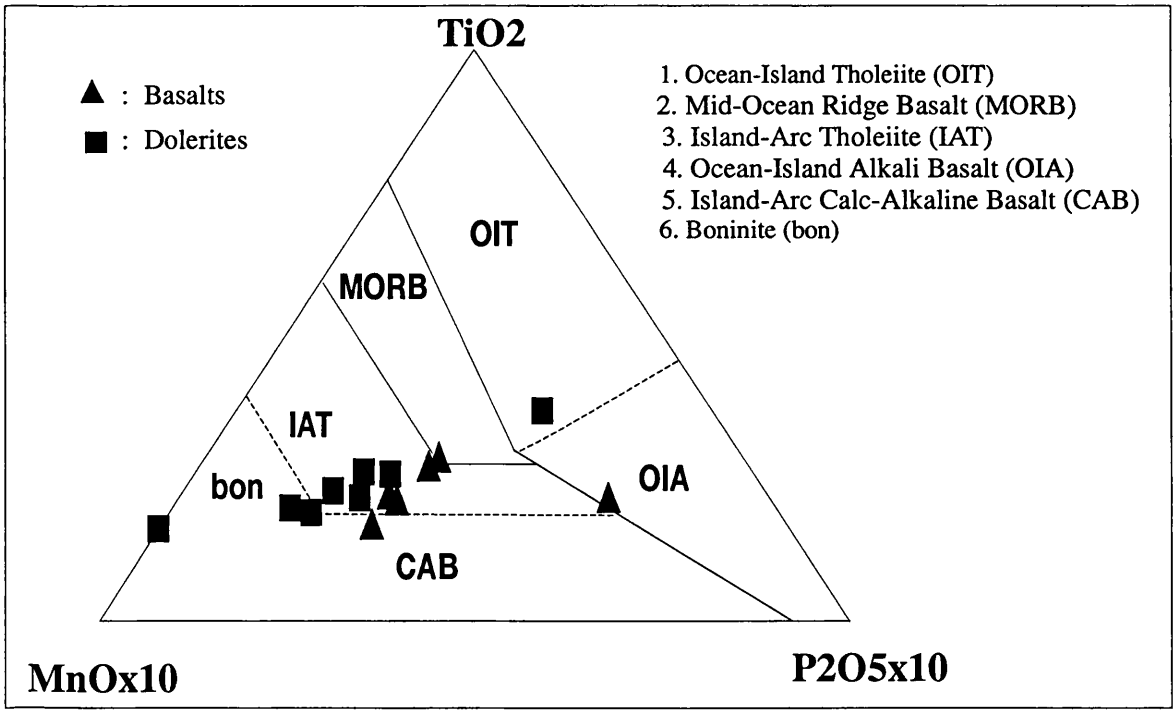

Fig. 4.14 Mn-Ti-P discriminant diagram for basalts and dolerites of the ophiolite (after Mullen, 1983)

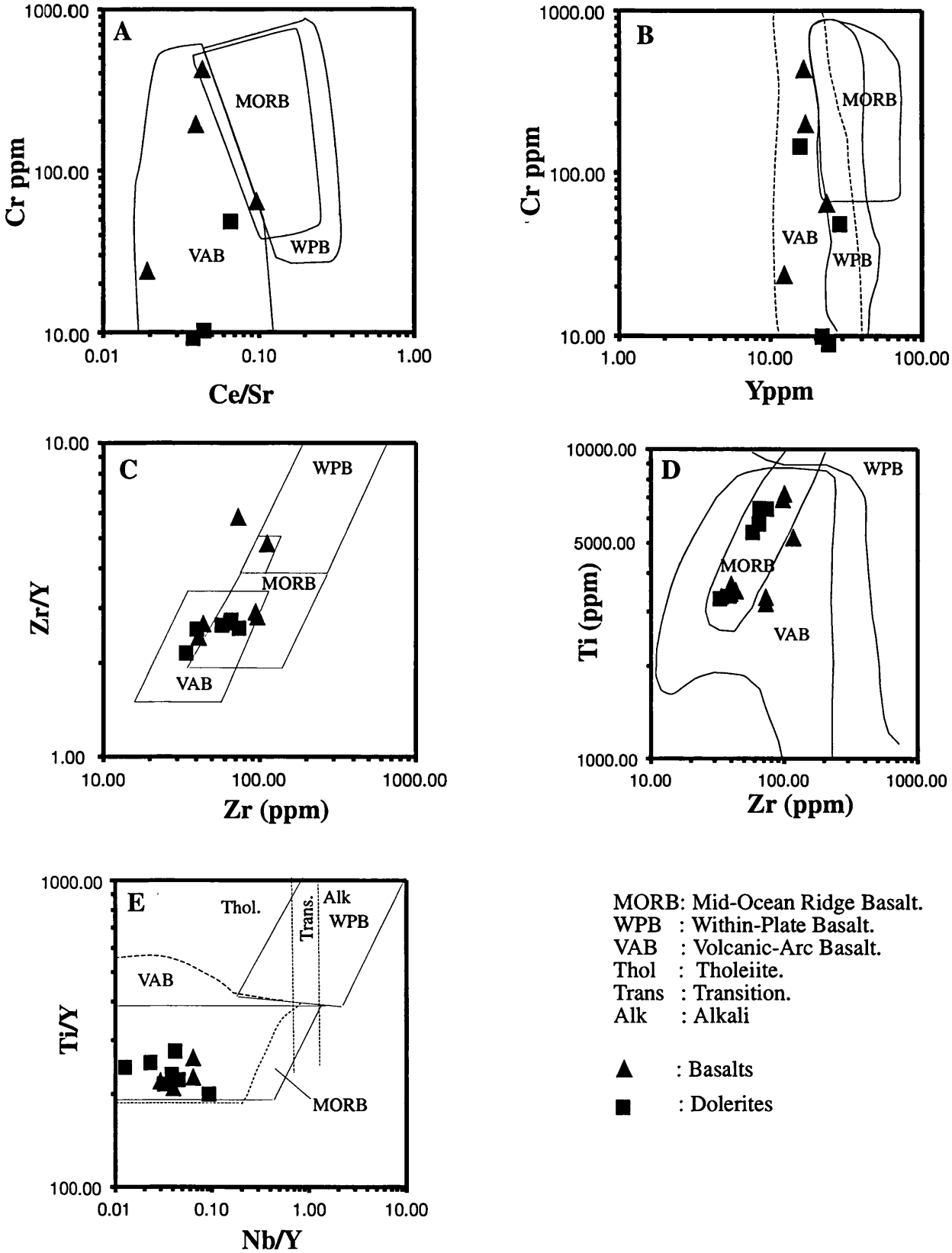

Fig. 4.15 Trace element covariation diagrams for basalt and dolerites of the ophiolite used to decipher their tectonic setting of formation. A, B, D and E after Pearce (1982). C after Pearce & Norry (1979).

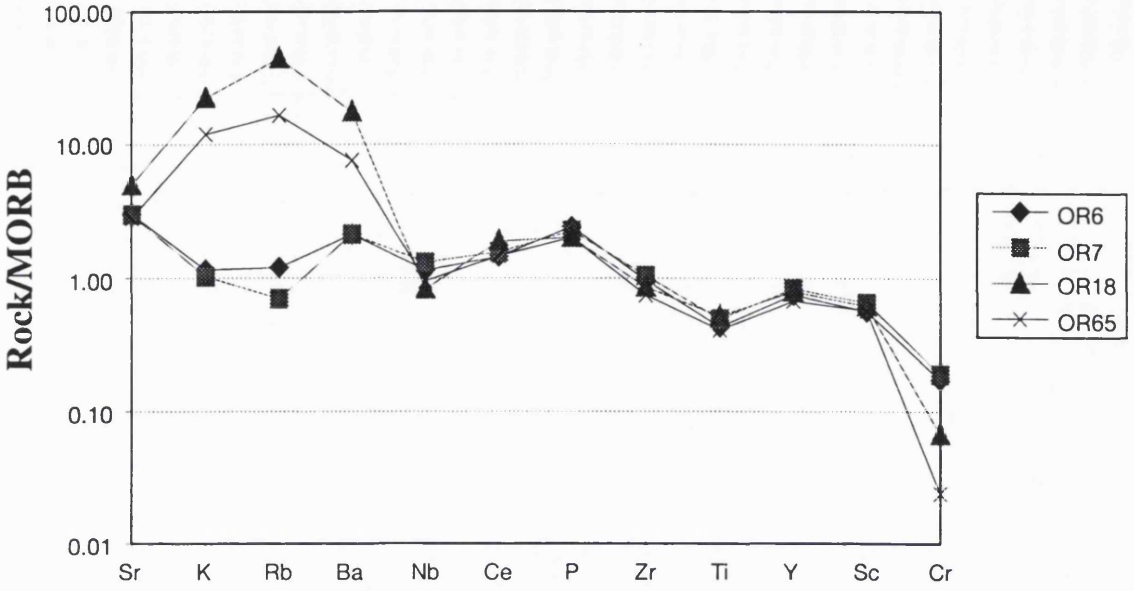

Fig. 4.16 MORB-normalised trace element spidergram for diorites intruding the ophiolite. Normalising factors from Pearce *et al.*, (1984)

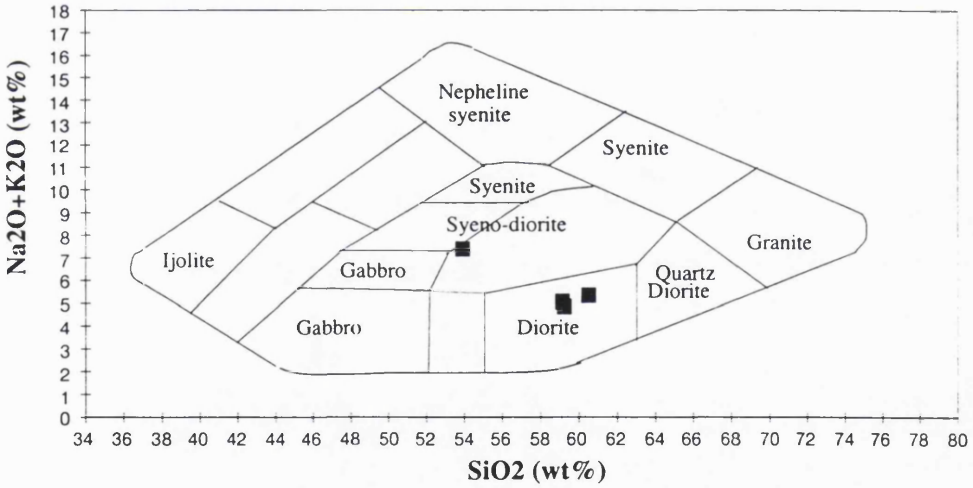

Fig. 4.17 Plot of Na_2O+K_2O versus SiO_2 for diorites intruding the ophiolite. Compositional fields from Cox *et al.* (1979)

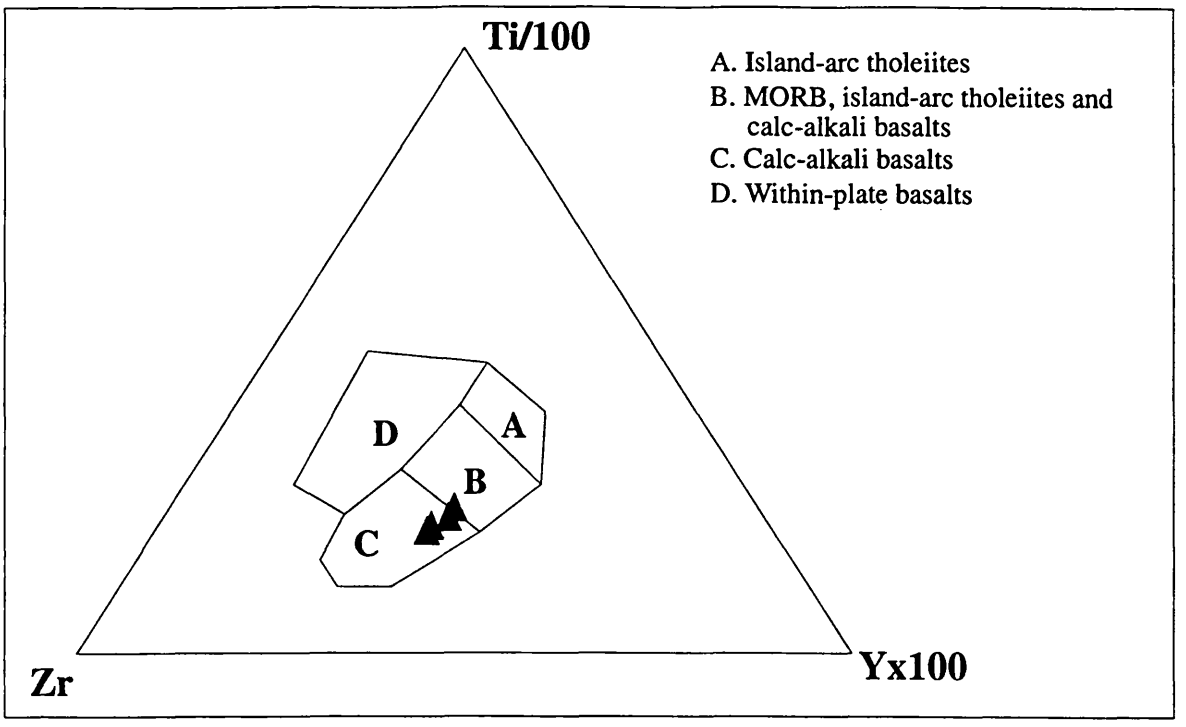

Fig. 4.18 Ti-Zr-Y discriminant diagram for diorites intruding the ophiolite (after Pearce and Cann, 1973)

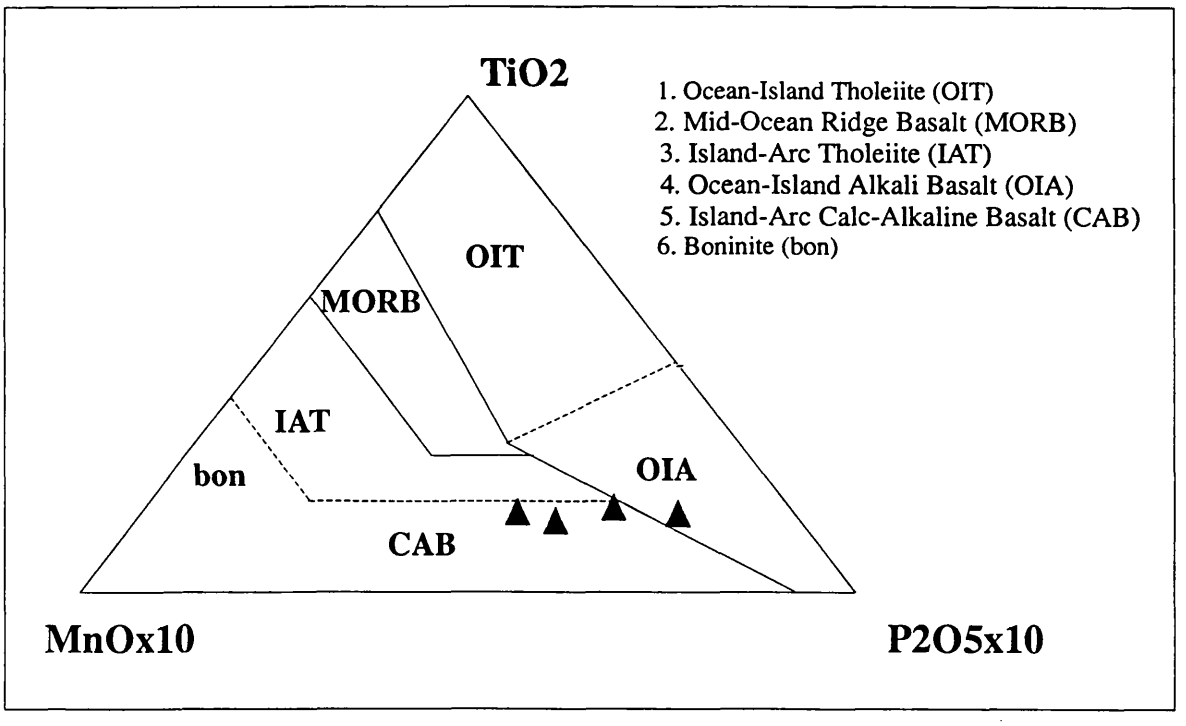

Fig. 4.19 Mn-Ti-P discriminant diagram for diorites intruding the ophiolite (after Mullen, 1983).

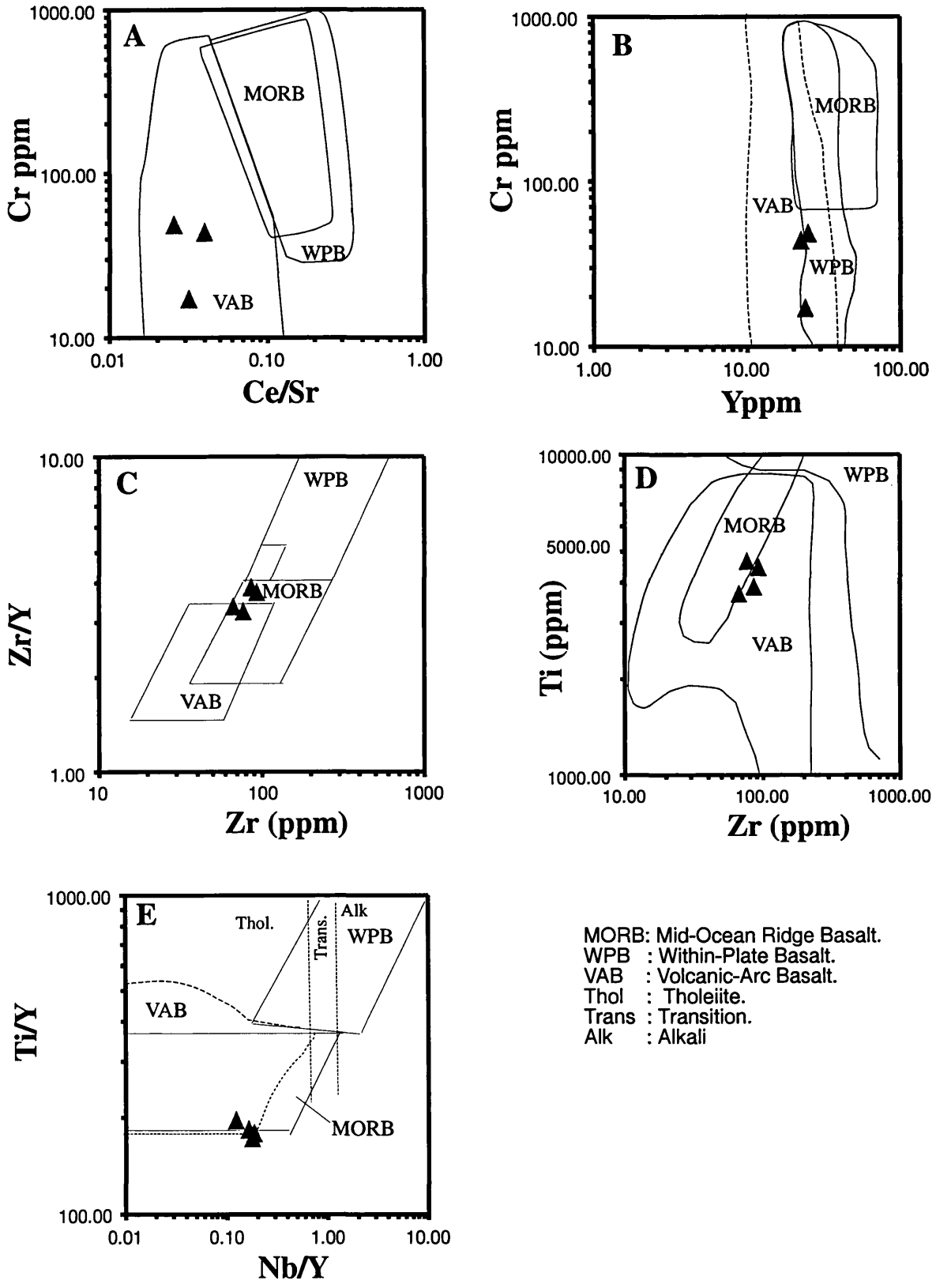

Fig. 4.20 Trace element covariation diagrams for diorites intruding the ophiolite. A, B, D and E after Pearce (1982). C after Pearce &Norry, 1979.

sloping patterns for the more immobile elements, being relatively enriched in the elements Ce-Y and depleted in Ti.

4.8.3 Discussion

The Obi basalts and dolerites are among the first MORB-like rocks discovered in the Halmahera group of islands, probably reflecting the more extensive exposures of the upper levels of the ophiolite. Despite significant alteration their trace element compositions are consistent and suggest an arc-related setting indicated by their consistent depletion in Nb. MORB-like rocks with an arc chemical signature are known from back-arc basins and forearc regions, and are similar to many of the ophiolites known from the western Pacific marginal basins. An arc setting for the formation of the ophiolite is consistent with the interpretation of the Halmahera ophiolite, based largely on the chemistry and mineralogy of the ophiolitic plutonic rocks, by Ballantyne (1990). The diorites suggest a younger episode of magmatism, with true arc magmas intruding the ophiolite, consistent with the K-Ar isotopic ages from the Obi rocks and similar age relationships demonstrated by Ballantyne (1990). Mobility of major elements and more mobile trace elements is interpreted to be the result of ocean-floor metamorphism (as suggested above based on mineralogy) and later alteration due to intrusion of arc diorites, probably reflecting Late Cretaceous and Tertiary arc magmatism recorded stratigraphically on Obi, and elsewhere in the Halmahera region, and described in Chapter 5.

CHAPTER 5

CRETACEOUS AND TERTIARY SEDIMENTARY AND VOLCANIC ROCKS

5. CRETACEOUS AND TERTIARY SEDIMENTARY AND VOLCANIC ROCKS

5.1 Introduction

The north, NE and SE parts of Obi are underlain by ophiolitic rocks which constitute the basement. They are interpreted to be overlain unconformably by Upper Cretaceous volcaniclastic sediments and pelagic limestones. These rocks are covered by Tertiary volcanic and sedimentary rocks. An inferred unconformity separates the Mesozoic rocks from the volcanic and volcaniclastic rocks of Oligocene age. The Cretaceous and Paleogene arc rocks are folded and overlain locally by Neogene limestones and younger Neogene rocks. The Neogene volcanic and volcaniclastic rocks are considered to represent the earliest activity of the Halmahera arc following eastward subduction of the Molucca Sea plate. Volcanic activity ceased in the Pliocene and currently there is no volcanic activity on the island. Plio-Pleistocene and Quaternary limestones and clastic sediments overlie all the older rocks. All of these sedimentary and volcanic rocks are described in this chapter.

5.2 Leleobasso Formation

The Leleobasso Formation includes coarse to fine grained volcaniclastic sedimentary rocks and rare pelagic limestones (fig. 5.1). It is interpreted as a sequence of rocks deposited in a deep basin situated close to an active arc. It comprises breccias and conglomerates, volcaniclastic sandstones and siltstones, red mudstones and pelagic limestones.

5.2.1 Synonymy

This formation name was introduced by Sudana & Yasin (1983) with a type locality at Tanjung Leleobasso. However, these rocks were considered to be Jurassic in age and were correlated with Jurassic shales reported only as float from southern Obi (Wanner, 1913). New dating (Hall *et al.*, 1992, see below) shows that the rocks at Tanjung Leleobasso are Upper Cretaceous and the descriptions below show that they are very different from the Jurassic shales (see Chapter 3). Here therefore, the Jurassic shales and siltstones of south Obi are assigned to the Gomumu Formation and the Leleobasso Formation is redefined from its original type locality.

5.2.2 Aerial Photography and Topographic Interpretation

It is difficult to map the Leleobasso Formation on aerial photographs and it is known from only a small area. However it can be distinguished from surrounding formations since it has a darker grey colour and a smoother surface than them.

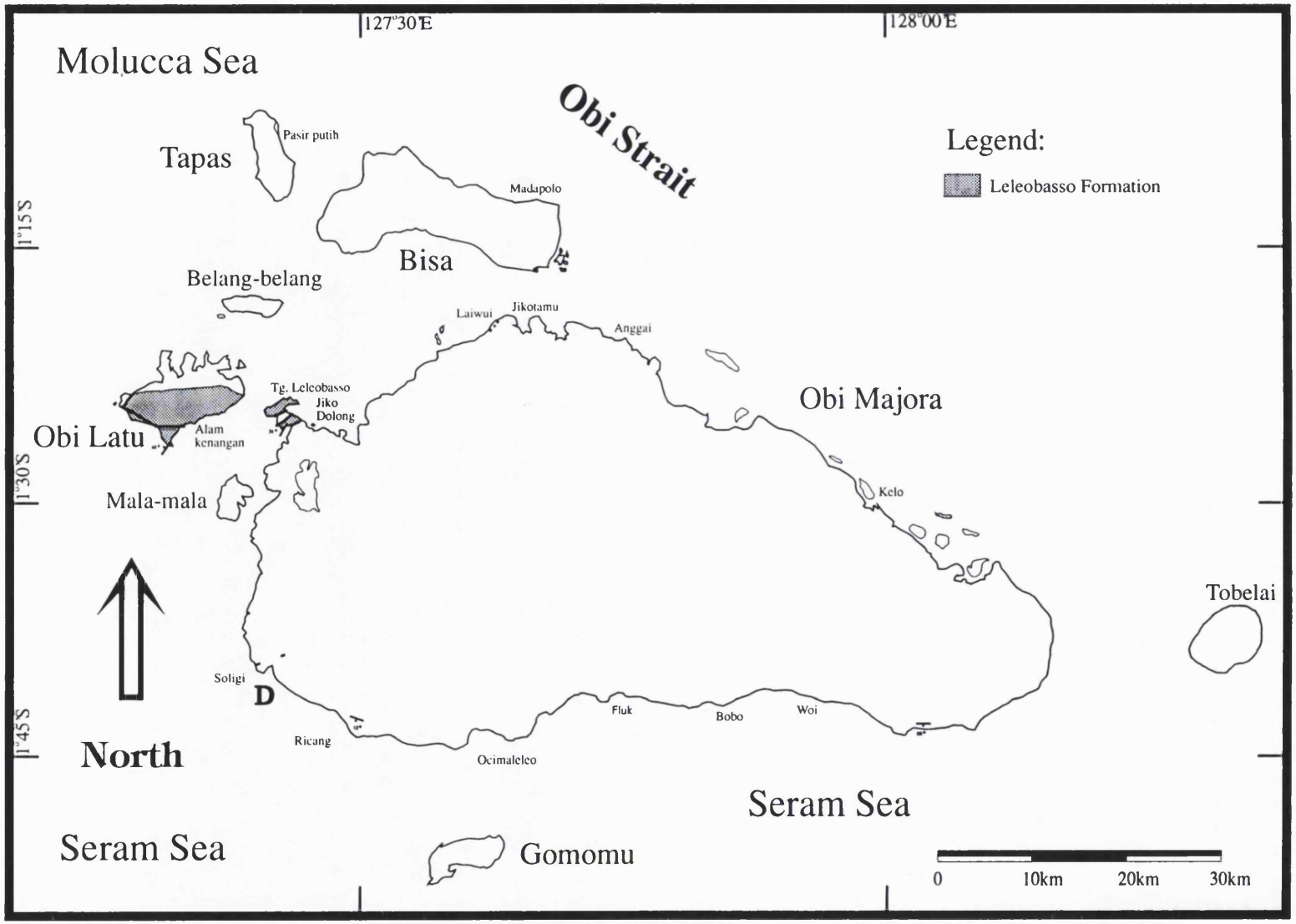

Fig. 5.1 Distribution of the Leleobasso Formation.

5.2.3 Type Section

The type section is Tanjung Leleobasso, situated at the NW end of Obi Major, where there is a series of well bedded green volcaniclastic conglomerates, sandstones and mudstones (Figs. 5.2 and 5.3). The finer grained rocks contain a variety of sedimentary structures characteristic of turbidites. In the whole of this area the rocks are very hard and splintery which appears to be the result of intrusion of the hornblende diorite body which forms most of south Obi Latu. At the north end of Tanjung Leleobasso is the unexposed contact between diorite and sedimentary rocks. On the south coast of Obi Latu there are similar well bedded, poorly sorted conglomerates interbedded with sandstones and fine calcareous mudstones. There are also rare pelagic limestones which are typically white or pale creamy blue in colour with locally thin sandy seams, and thin shaly partings. All are very highly indurated and splintery suggesting baking by the diorite intrusion.

5.2.4 Age

Upper Cretaceous (Campanian-Maastrichtian). Fossils have been found in only two samples of the formation and have been identified by F. T. Banner (Hall *et al.* 1992). Sample OR13 is a fine mudstone, collected at Tanjung Leleobasso and contains two recrystallised planktonic foraminifera indicating contains two recrystallised planktonic foraminifera (*Globotruncana cf. lapparenti* Brotzen and a pyritized *Pullenia* sp.) indicating a Campanian-Middle Maastrichtian age. Sample OR27 collected on the south side of the bay south of Tanjung Leleobasso contains a very small number of small planktonic foraminifera (very rare *Archeoglobigerina cf. blowi* Pessagno and heterohelicids) indicating a Coniacian-Maastrichtian age range. All other samples were barren although vague 'ghosts' of probable planktonic foraminifera can be discerned in some samples suggesting recrystallisation due to contact metamorphism.

5.2.5 Thickness

No complete measured section is possible for the Leleobasso Formation, since it is exposed in small coastal outcrops which are likely to be separated from one another by small faults. Measured sections indicate several tens of metres as a minimum and a thickness of several hundred metres is suggested by its distribution on Obi Latu island. This is similar to the thickness of the Gowonli Formation on Halmahera (Hall *et al.*, 1992), which is of similar age and lithology.

5.2.6 Distribution

The Leleobasso Formation is known from the type section at Tanjung Leleobasso which is situated at the NW tip of Obi Major and forms most of this small peninsula. It is moderately well exposed all along the south coast of Obi Latu and underlies most of the southern half of the island.

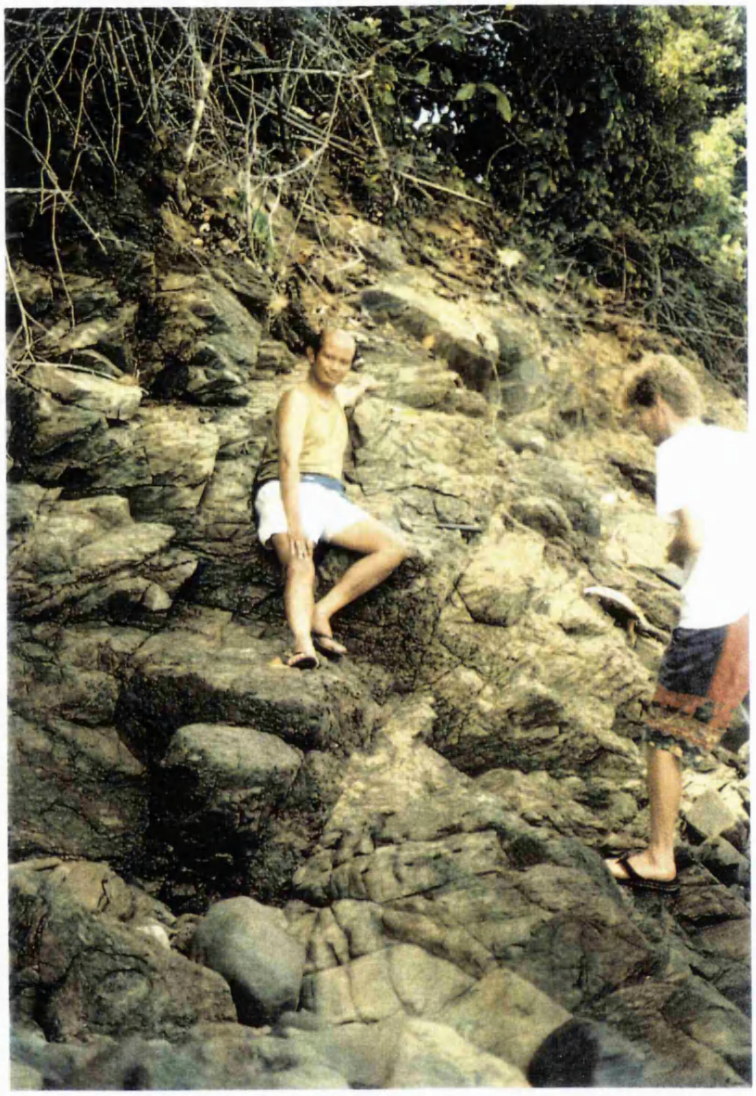

Fig. 5.2 Bedded volcaniclastic conglomerates and sandstones of the Leleobasso Formation at Tanjung Leleobasso, NW Obi Major. Bedding dips gently away from the observer and the trace of the bedding can be seen running from left to right across the photo from the foot of Spencer Roberts (right hand side of photo).

Fig. 5.3 Fractured foraminifera-bearing calcareous mudstones of the Leleobasso Formation at Tanjung Leleobasso, NW Obi Major.

5.2.7 Lower and Upper Contacts

The upper and lower stratigraphic contact is not observed. All contacts with adjacent units are faults, except for the inferred intrusive contact with a diorite body at the type locality. The contact intrusions are found on south coast Obi Latu Island.

5.2.8 Description

At the type locality, there are well-bedded green volcaniclastic conglomerates, sandstones and mudstones. The finer grained rocks show a variety of sedimentary structures including cross-bedding, grading, load casts, flame structures, mudstone rip-up clasts, burrows, and syn-sedimentary faults. All the rocks are the right-way up although dips are typically steep. On the south side of the bay south of Tanjung Leleobasso the sandstones are cut by narrow basaltic dykes. In the whole of this area the rocks are very hard and splintery which appears to be the result of intrusion of the hornblende diorite body which forms much of south Obi Latu. At the north end of Tanjung Leleobasso is the unexposed contact between the diorite and sedimentary rocks.

Along the south coast of Obi Latu there are similar rocks. There are well bedded, poorly sorted conglomerates, interbedded with sandstones and fine calcareous mudstones. There are rare pelagic limestones which are typically white or pale creamy blue in colour with locally thin sandy seams, and thin shaly partings. All are very highly indurated and splintery suggesting baking by the diorite intrusion.

A section has been measured on the coast south of Alam Kenangan village, Obi Latu (Fig. 5.4) with a total thickness of about 11.5 m. The section shows a repeating sequence of truncated Bouma Ta, Tb and Tc sequences. The lowest ~ 1 m is a greenish-grey massive calcarenite grading up to calcilutite interpreted as a calciturbidite grading into a pelagic interval. Above is ~ 4 m of greenish-grey calcareous sandstones representing a fine debris flow. At the base of the sandstones are load casts and there are thin parallel laminations (Tb) higher in the sandstones. In some places minor syn-depositional normal faults cut the section.

The upper part of the section, which begins at a minor normal fault, consists of grey conglomerates, grey siltstone and yellowish mudstone. A clast-supported conglomerate at the bottom is thickly bedded (~ 1m). Clasts range from 30-50 mm and have sub-rounded shapes, are poorly sorted and show alignment (organised conglomerate). This conglomerate fines upwards (Ta). It is overlain by 3 m of thick grey siltstone which shows parallel lamination, cross lamination, wavy lamination (Tb-Te), and is compact and hard. A coarse sandstone deposited above the siltstone consists of pebble mudstone clasts which are subangular to subrounded,

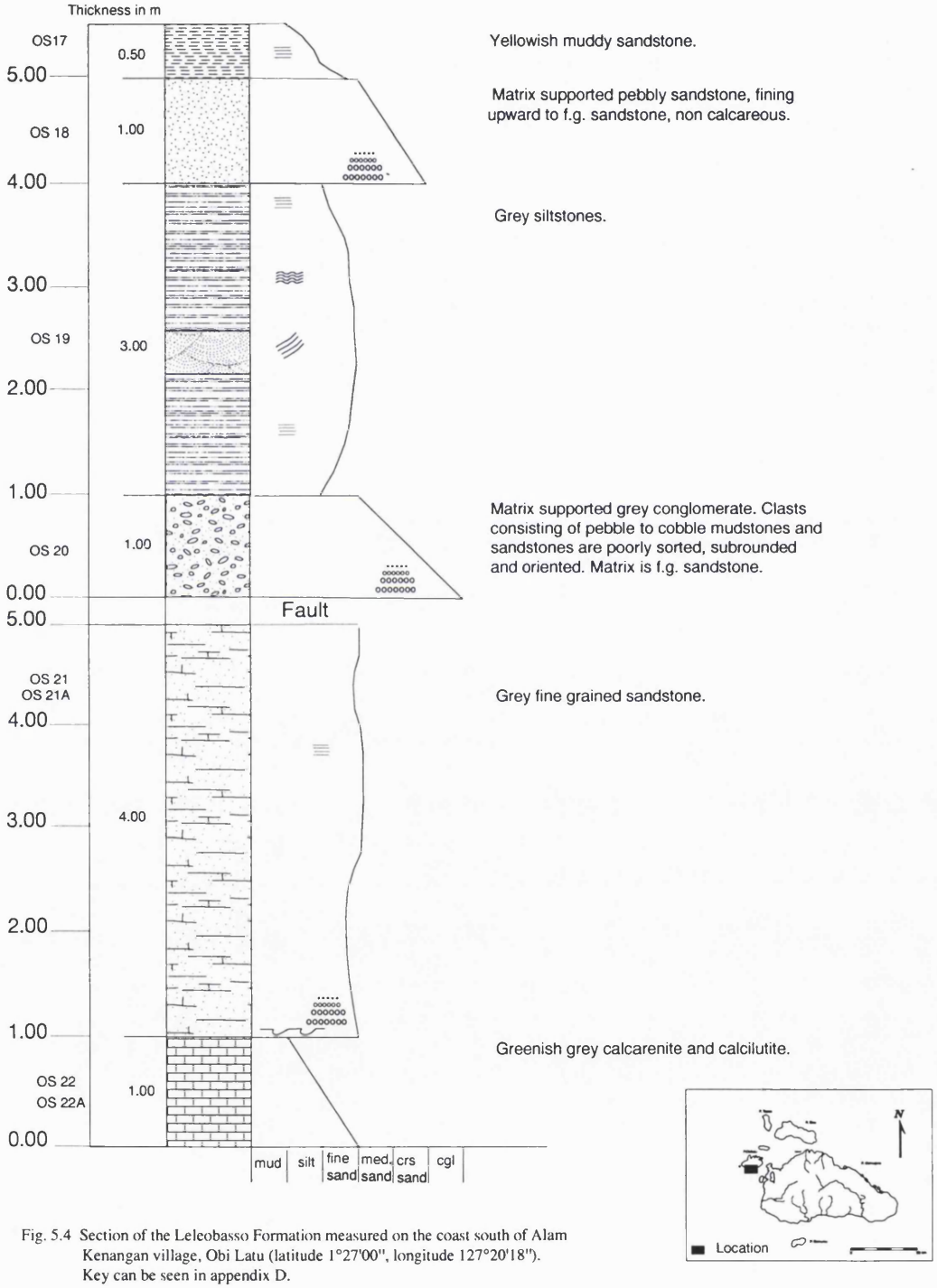

Fig. 5.4 Section of the Leleobasso Formation measured on the coast south of Alam Kenangan village, Obi Latu (latitude 1°27'00", longitude 127°20'18"). Key can be seen in appendix D.

poorly sorted and fine upwards (Ta). At the top of this section is yellowish mudstone with parallel lamination (Te).

The sandstones have a grain-supported fabric. Sorting is poorly to moderate and grains are subangular to subrounded. The grains consist of basaltic lithic fragments (partly replaced by clay, ~ 40 %), plagioclase (most are replaced by carbonate and clay, ~ 30 %), and opaque minerals (~ 10 %). Planktonic foraminifera fragments are very rare (~ 1 %).The matrix consists of clay and carbonate.

5.2.9 Depositional Environment

The pelagic limestones indicate deposition in a deep marine basin with frequent turbidites and debris flows bringing volcaniclastic material from the edge of the basin. On the basis of the foraminifera F. T. Banner (written communication, 1992) suggested that the Leleobasso Formation was probably deposited in poorly oxygenated bottom waters.

5.3 Anggai River Formation

The Anggai River Formation consists of minor volcanic rocks with coarse to fine volcaniclastic sedimentary rocks probably deposited as turbidites in a volcanic arc basin. It includes conglomerates, volcaniclastic sandstones, siltstones and mudstones (Fig. 5.5).

5.3.1 Synonymy

The Anggai River Formation is a new stratigraphic name introduced by Hall *et al.* (1992) for coarse to fine volcaniclastic sedimentary rocks, locally interbedded with volcanic rocks, probably representing igneous rocks and turbidites deposited in a volcanic arc basin.

5.3.2 Aerial Photography and Topographic Interpretation

In central Obi the Anggai River Formation forms undulating hills with elevations of 1000-1500 m above sea level. Most of the rivers dissect this landscape deeply and form V-shaped valleys. The slopes of the valley sides are steep, and they form gorges in places. On the aerial photos the formation usually shows rough surfaces and sharp ridges on the hills in central Obi. Nearer to the coast the Anggai Formation displays smoother surfaces cut by lineaments interpreted as faults with predominant NW-SE and subordinate NE-SW orientations.

5.3.3 Type section

The type area for this formation is the Anggai River, north Obi Major, where there are basaltic andesites, volcaniclastic conglomerates, sandstones, siltstones and mudstones.

5.3.4 Age

Oligocene-Lower Miocene. The sequence in the type locality is badly recrystallized and fossils are very rare. Nannofossils from two samples (OD39B, OD41B) indicate Middle to Upper

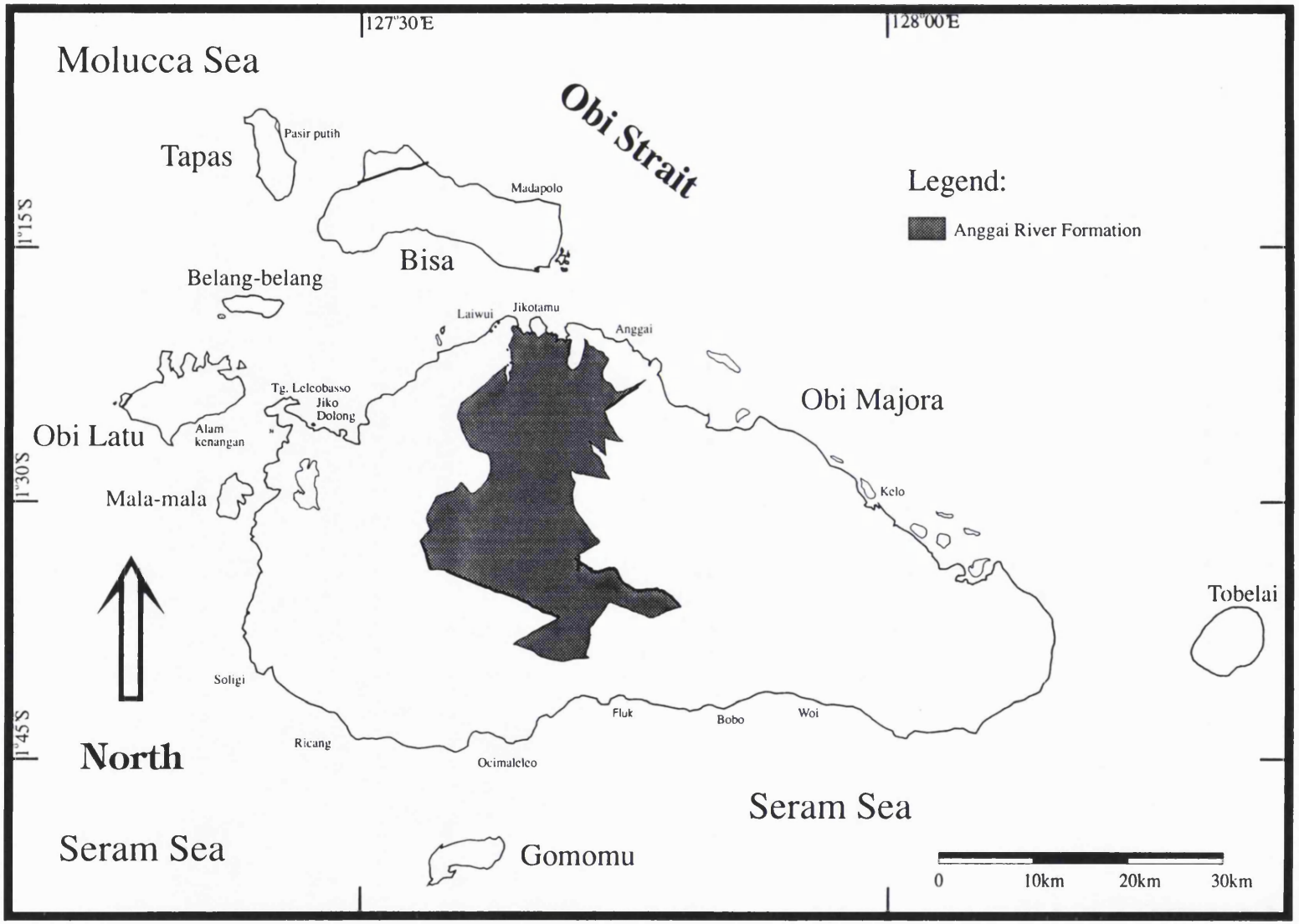

Fig. 5.5 Distribution of the Anggai River Formation

Oligocene ages. One float sample from the Anggai River (OD42Z) contains *Lepidosemicyclina, Amphistegina* spp, *Miogypsina borneensis, Cycloclypeus* spp, *Nephrolepidina* spp, *Heterostegina*, and valvulinids which indicate an Upper Oligocene to Lower Miocene age. Several samples assigned to the Anggai River Formation (Hall *et al.*, 1992) collected in south Obi (OR130-133, OR139, OR140) yielded Upper Oligocene to Lower Miocene ages.

5.3.5 Thickness

The exact thickness is unknown but, on the base of the sequences in the Anggai River, and interpretation of cross-sections, it is thought to be several hundred metres thick.

5.3.6 Distribution

This formation is known from the area of the Anggai River and from aerial photographs is interpreted to be exposed over a wide area of northeast and central Obi as far south as the upper waters of the Nike River.

5.3.7 Lower and Upper Contacts

The lower contact has not been observed. The upper contact is an angular unconformity and the formation is overlain by younger Neogene rocks.

5.3.8 Description

In the Anggai River section there are indurated calcareous volcaniclastic sandstones and siltstones with occasional conglomerates and breccias (Figs. 5.6 and 5.7). The sandstones are medium to fine grained with beds up to 1.5 m thick. Prominent parallel and wavy laminations are present, and sets of planar cross-stratification indicate a current direction broadly towards the south. Several units of coarser immature sandstones are interbedded with the other rocks in the sequence and load structures are found at the base of these and coarser units. The siltstones have a brown to purple colour with parallel lamination and are up to 80 cm thick. The conglomerates are well-sorted with a population of rounded pebble-size andesite clasts supported by a well-sorted sandstone matrix. This marine clastic sequence is characterised by steep dips of bedding.

The basaltic andesites contain plagioclase laths and pyroxene phenocrysts, with a dark glass matrix. The contacts between volcanic and sedimentary rocks are not clear, but previous mapping (Gondwana Company, 1985) reported that a 1.5 m andesite was intercalated with sandstones in the Laiwui River with a normal stratigraphic contact.

In the Nike River there are well lithified tuffs and tuffaceous sandstones and siltstones, some feldspar-phyric basalts/dolerites, and limestones (the limestones are found as very large blocks which makes it difficult to be certain whether or not they are outcrop).

Fig. 5.6 Bedded, steeply dipping, coarse and fine volcaniclastic sandstones of Anggai River Formation in the Anggai River, north Obi Major..

Fig. 5.7 Gently dipping, volcaniclastic sandstones of the Anggai River Formation in the Anggai River, north Obi Major.

5.3.8.1 Measured Sections

Two sections were measured in the type area of the Anggai River (Figs. 5.8 and 5.9), although these sections are not continuous. They are ~ 12 m and ~ 20 m thick. Lithologies in these sections include alternating conglomerates, sandstones, siltstones and mudstones and locally they show Bouma Ta, Tb, Tc and Td and probably Te.

The first section was measured in the Anggai River (Fig. 5.8). This section is dominated by siltstones with intercalations of sandstones and mudstones, except at the top where there are conglomerates. Sedimentary structures include parallel, planar and trough cross laminations interpreted as Bouma Tc and Td sequences. In some of the sandstone units are parallel laminations, cross laminations, ripple laminations and dewatering structures. These rocks show Ta, Tb, Tc and Td sequences. These suggest deposition as coarse-grained turbidites (Lowe, 1982) by high-density turbidity currents with grain flow, fluidized or liquefied flow mechanisms during the final stages of deposition. At the top of this section is yellowish grey conglomerates more than 4 m thick showing fining upward of clasts from pebbles to granules (Ta). Clasts consist of subrounded and poorly sorted of andesites and mudstones, supported by sandstone matrix. This unit is interpreted as a debris flow.

The second section has been measured close to the first measured section in the Anggai River (Fig. 5.9). This section consists of alternating sandstones and siltstones with several repeating Bouma sequences Ta, Tb, Tc and Td.

5.3.8.2 Petrography

The tuffaceous sandstone unit has a grain-supported fabric. Sorting is poor to moderate and grains are subangular to subrounded. They consist of volcanic glass (partly replaced by clay, ~ 60%), opaque mineral (~ 20%), plagioclase (broken, showing complex twinning, ~5%) and pyroxene (clinopyroxene, ~ 3%). The matrix consists of brown clay. The volcaniclastic siltstones are well sorted and similar but contain fewer opaque grains (~10%) and pyroxenes (very rare, ~1%), more plagioclase (~10%) and rare basaltic lithic fragments (~1%). Several thin siltstones contain carbonate.

The principal features of grey basaltic andesites are their porphyritic texture with both mafic and felsic phenocrysts in a microcrystalline or glassy groundmass. The phenocrysts are subhedral to euhedral and generally elongate and rectangular. The modal proportion of phenocrysts is between 15-25% and feldspars are usually more abundant than the mafic phenocrysts. Plagioclase feldspar is present as phenocrysts and in the groundmass. The modal percentage of plagioclase phenocrysts ranges from 10-20%; most are altered to clay minerals. Augite phenocrysts (2-5 modal %) are commonly twinned. Fe-Ti oxides occur in the groundmass and as inclusions in the phenocrysts. The groundmass also contains plagioclase and pyroxene microlites,

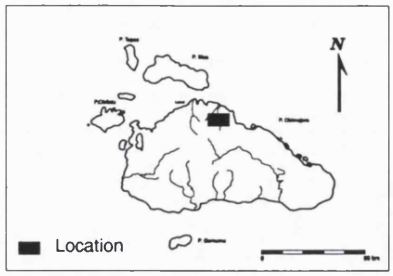

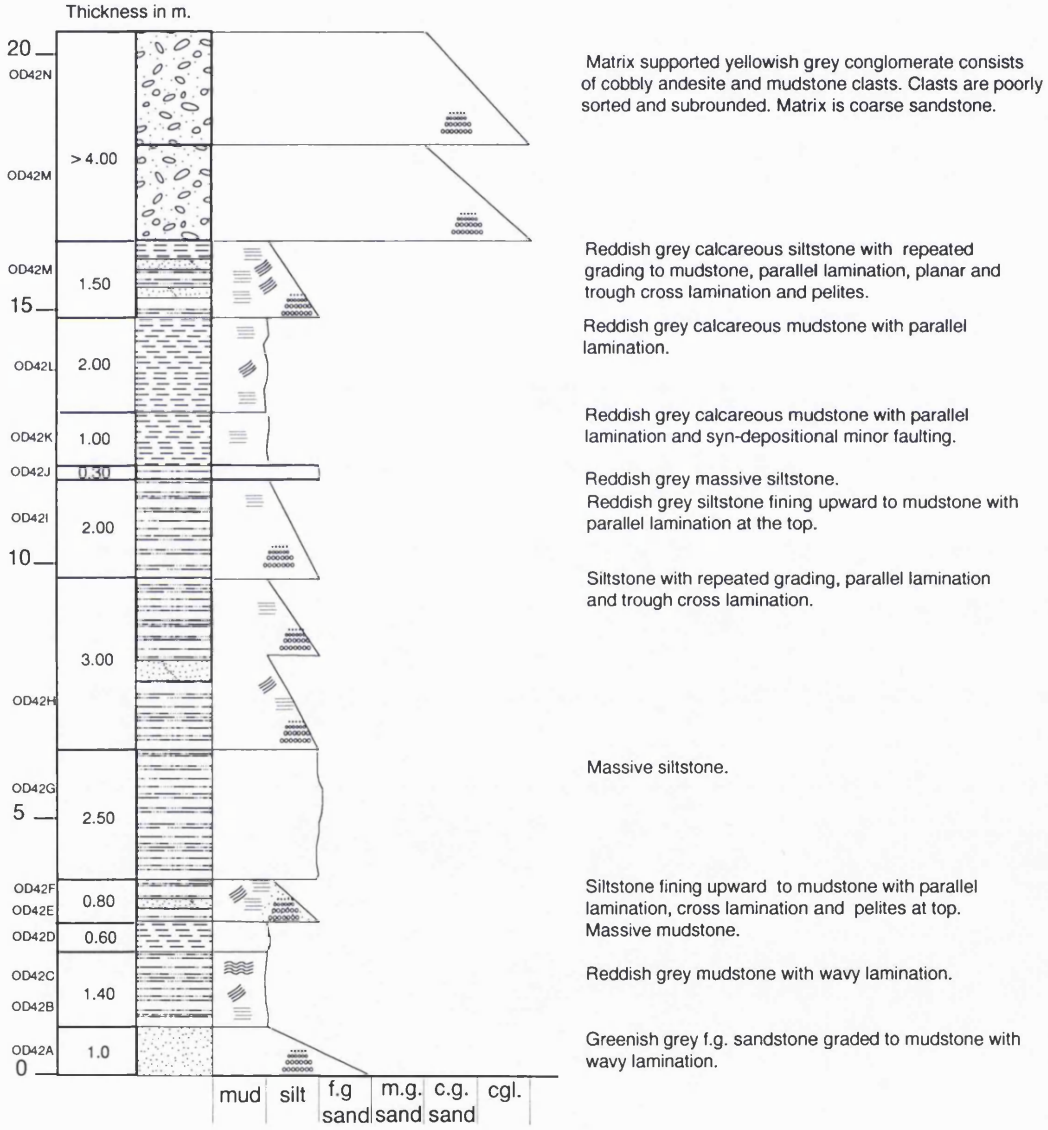

Fig. 5.8. Section of the Anggai River Formation measured in the type area of the Anggai River (latitude1°24'32", longitude 127°43'13"). Key can be seen in appendix D.

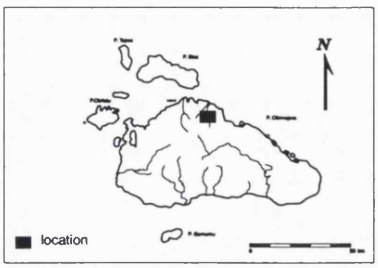

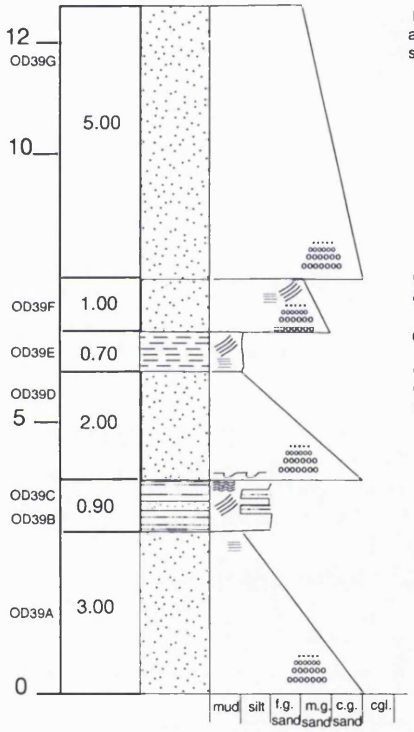

Matrix supported coarse grained sandstone. Sandstone fines upward, and consists of andesite and volcanic glass clasts. Clasts are poorly sorted and they have subangular - subrounded shapes. Matrix is fine grained sandstone.

Medium grained sandstone fines upward, consists of andesite and opaque mineral clasts and clay matrix. Parallel and cross laminations are present at the top.

Grey mudstone with parallel laminations and trough cross laminations.

Clast supported grey sandstone contains volcanic glass and opaque mineral clasts. Clasts are poorly sorted and subangular. This rock fines upward to mudstone with load structures at the base.

Alternating siltstone and mudstone with normal grading, cross and wavy laminations, and flame structures at the base.

Dark grey sandstone composed of plagioclase, volcanic glass and opaque mineral clasts which are supported by a mud matrix. This rock fines upward to mudstone with parallel laminations at the top.

Fig. 5.9 Section of the Anggai River Formation measured in the type area of the Anggai River (latitude 1°23'51", longitude 127°43'13"). Key can be seen in appendix D.

and glass, typically altered to clay minerals. The plagioclase grains are acicular and lath-shaped, showing simple twinning. The clinopyroxene crystals are usually colourless in plane polarised light and small (<0.1 mm in length). Secondary minerals such as smectite, chlorite, epidote and quartz infill amygdales in the rock.

5.3.9 Whole Rock Chemistry

A selection of samples from the Anggai River Formation have been analysed. These include three volcanic rocks (OD34, OD103 and OD106). OD34 is a fresh olivine basalt whereas OD103 and OD106 are altered andesites. OD103 contains abundant epidote and quartz, filling amygdales and OD106 contains chlorite. The remaining samples are probably sedimentary rocks, although they may include some ash deposits.

5.3.9.1 Major Elements

For all the samples except one there is a small range of SiO_2 (52.3-58.4 wt %) typical of andesites. The exception is a float sample (OD104) with extremely high SiO_2 which contains altered feldspar and has an igneous appearance; it may be a reworked ash or a primary pyroclastic interval. Alteration is suggested by the considerable variation in Fe_2O_3 (5.5-12.3 wt %), MgO (3.0-6.8 wt %), CaO (2.0-8.4 wt %), Na_2O (2.2-7.5 wt %) and K_2O (0.1-4.6 wt %). LOI is also very variable (1.8-8.3 wt %). The analyses scatter across the low-K tholeiite to high-K fields on the Taylor *et al.* (1981) diagram (Figs. 5.10 and 5.11).

5.3.9.2 Trace Elements

The igneous and sedimentary rocks are plotted separately on MORB-normalised diagrams (Figs. 5.12). The basalt and andesites are rather different, particularly for the more mobile elements. The basalt (OD34) has a typical arc character with a humped pattern for the elements Sr to Ba, depletion in Nb and sloping pattern for the immobile elements. OD103 and OD106 are considerably depleted in the elements Sr to Ba, but they resemble the basalt in their immobile element contents, notably Zr to Y. Among the supposed sedimentary rocks OD104 is clearly distinct with a spiky MORB-normalised pattern suggesting a mixed provenance. However, the remainder of the sedimentary rocks are strikingly similar to the fresh basalt suggesting they were derived from an arc basaltic source and have been little modified, at least for trace elements, by deposition. This similarity is also shown on the triangular plots, such as that for Ti-Zr-Y, in which the sedimentary and igneous rocks cluster in a small area in the arc field (Figs. 5.13 -5.15).

5.3.10 Depositional Environment

Interbedded with the volcanic rocks are volcaniclastic and hemipelagic rocks. The presence of Bouma sequences Tabcd in the sedimentary rocks indicates a turbidite origin. They are thought to represent the deposits of a moderately deep marine basin in a volcanic arc region.

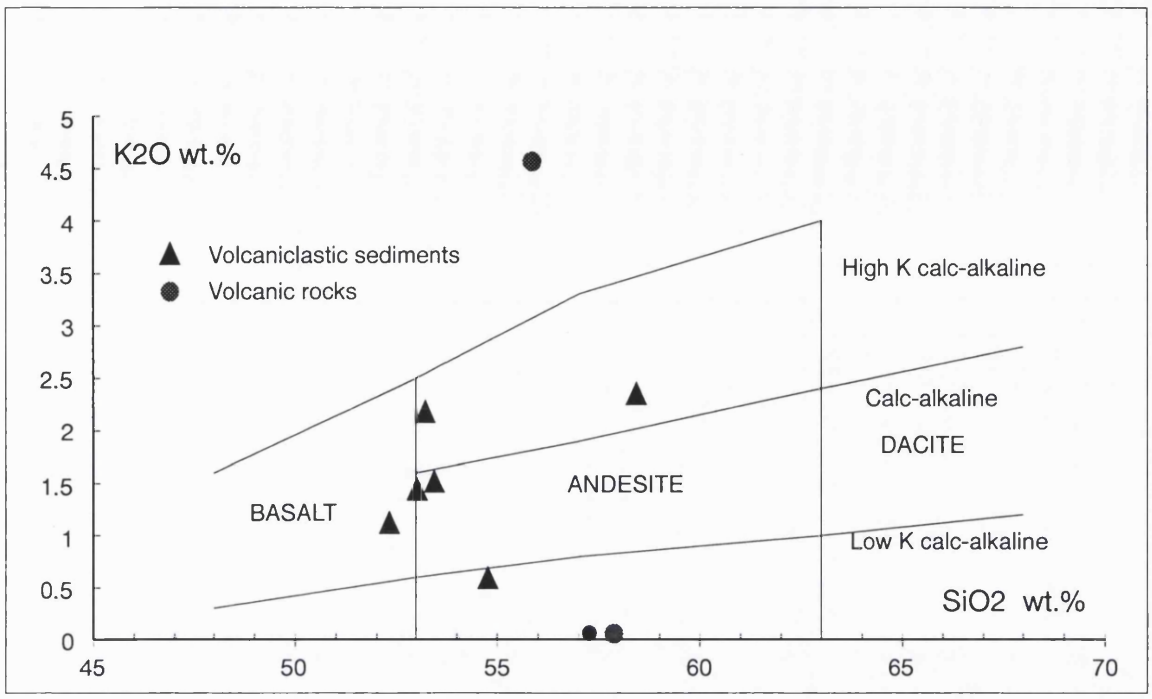

Fig. 5.10 Plot of K_2O versus SiO_2 for volcanic and volcaniclastic sedimentary rocks of the Anggai River Formation. Compositional fields from Taylor et al. (1981).

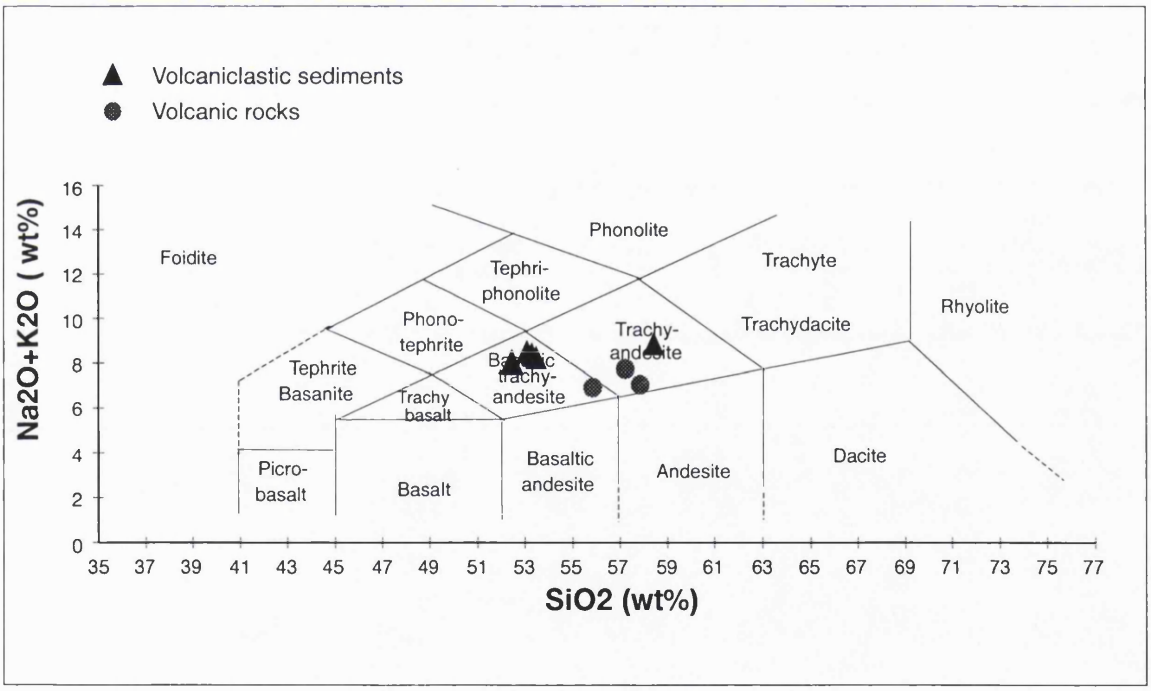

fig. 5.11 Plot of Na_2+K_2O versus SiO_2 for volcanic and volcaniclastic sedimentary rocks of the Anggai River Formation. Compositional fields from Le Bas & Streckeisen (1991).

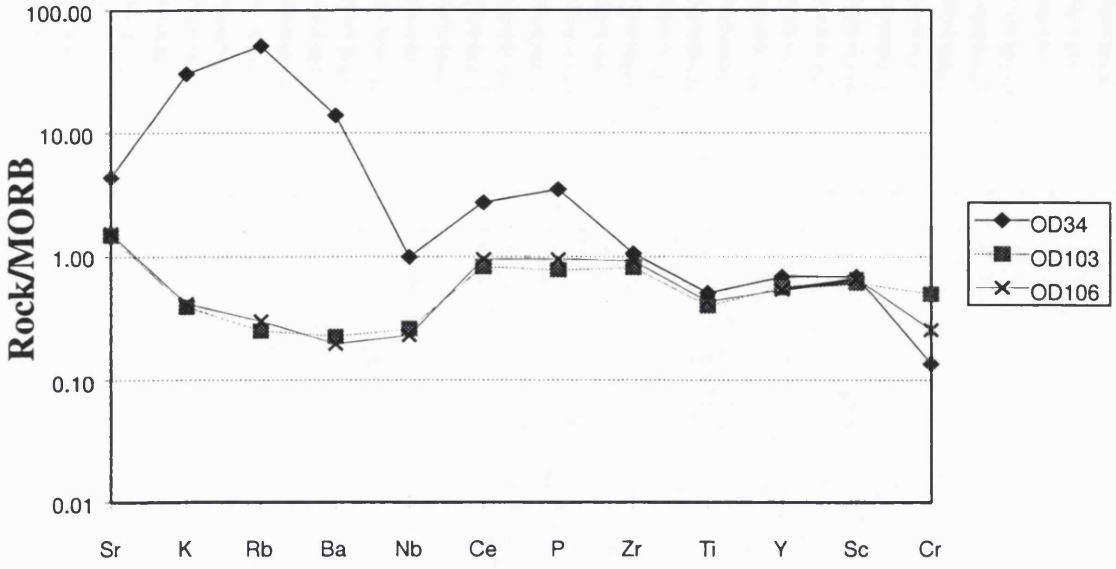

Fig. 5.12 MORB-normalised trace element spidergrams for volcanic rocks (above) and volcaniclastic sedimentary rocks (below) of the Anggai River Formation. Normalising factors from Pearce *et al.* (1984)

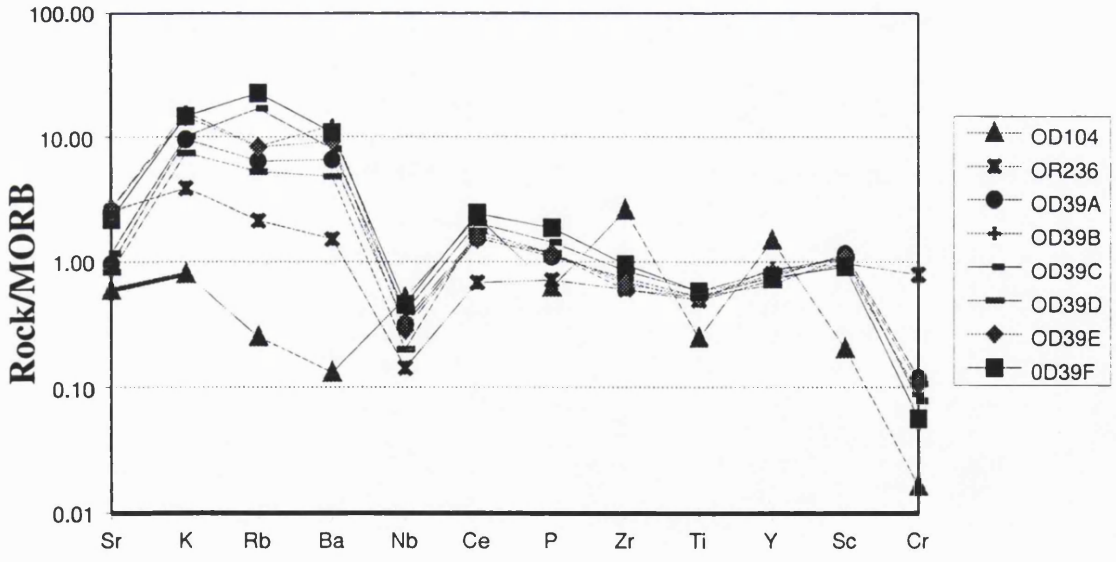

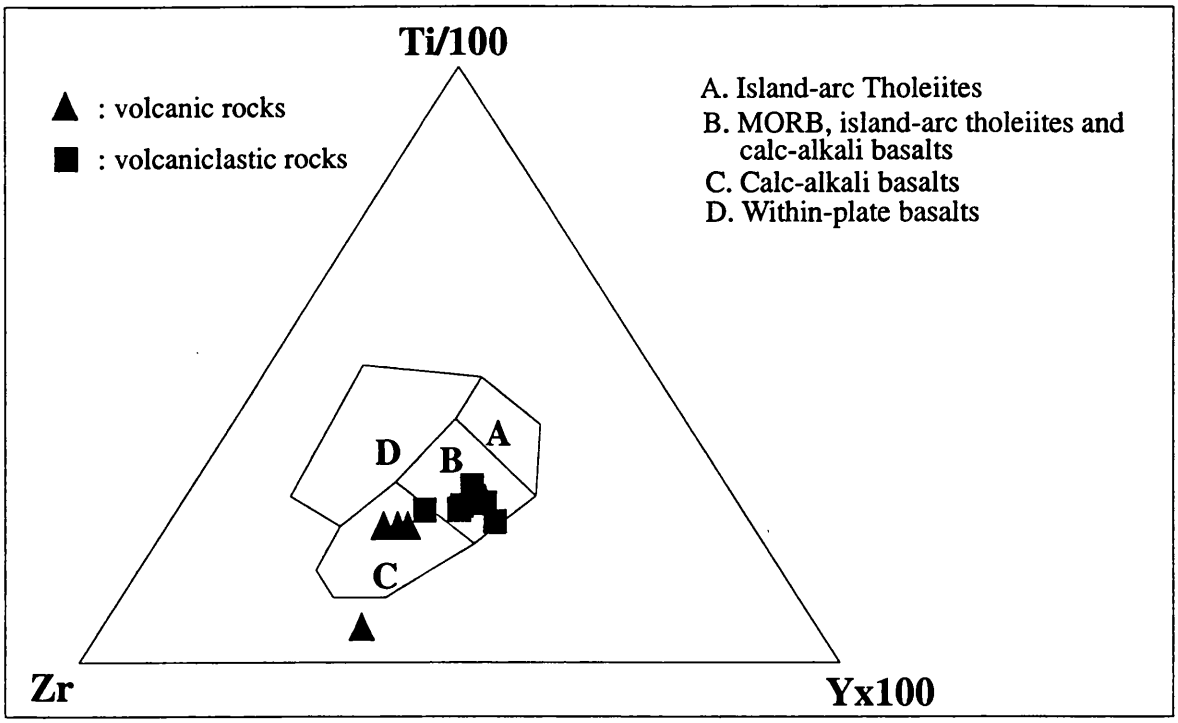

Fig. 5.13 Ti-Zr-Y discriminant diagram for volcanic and volcaniclastic sedimentary rocks of the Anggai River Formation (after Pearce and Cann, 1973)

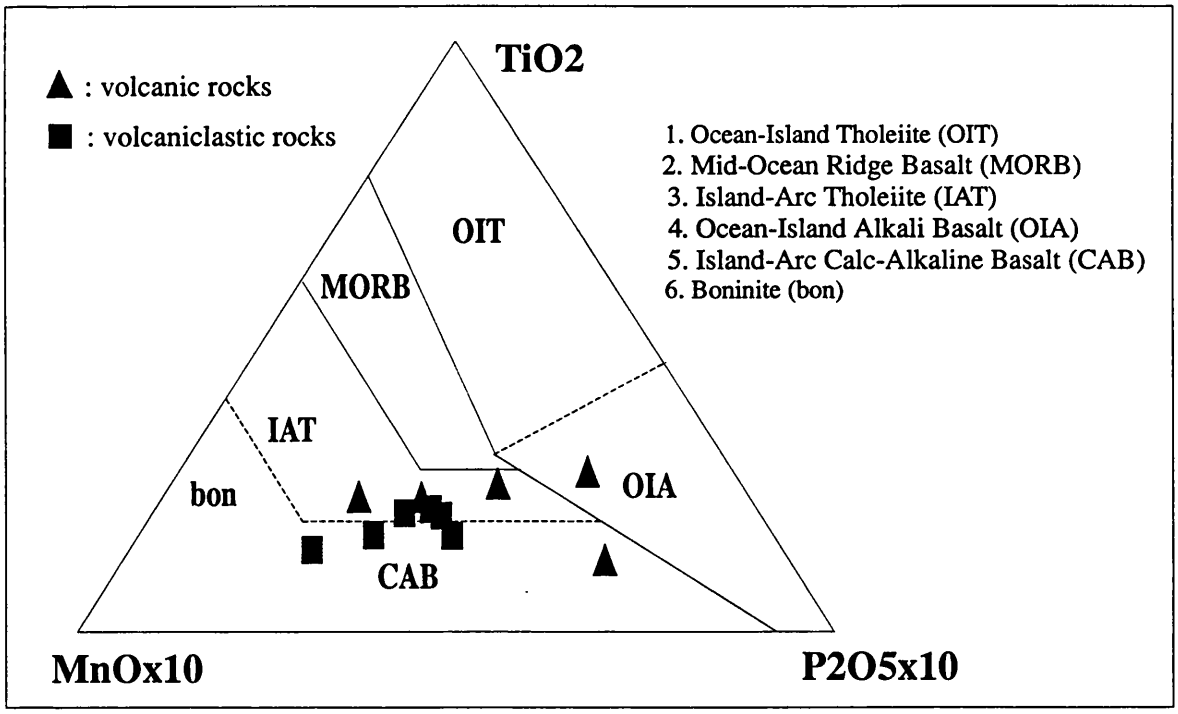

Fig. 5.14 Mn-Ti-P discriminant diagram for volcanic and volcaniclastic sedimentary rocks of the Anggai River Formation (after Mullen, 1983)

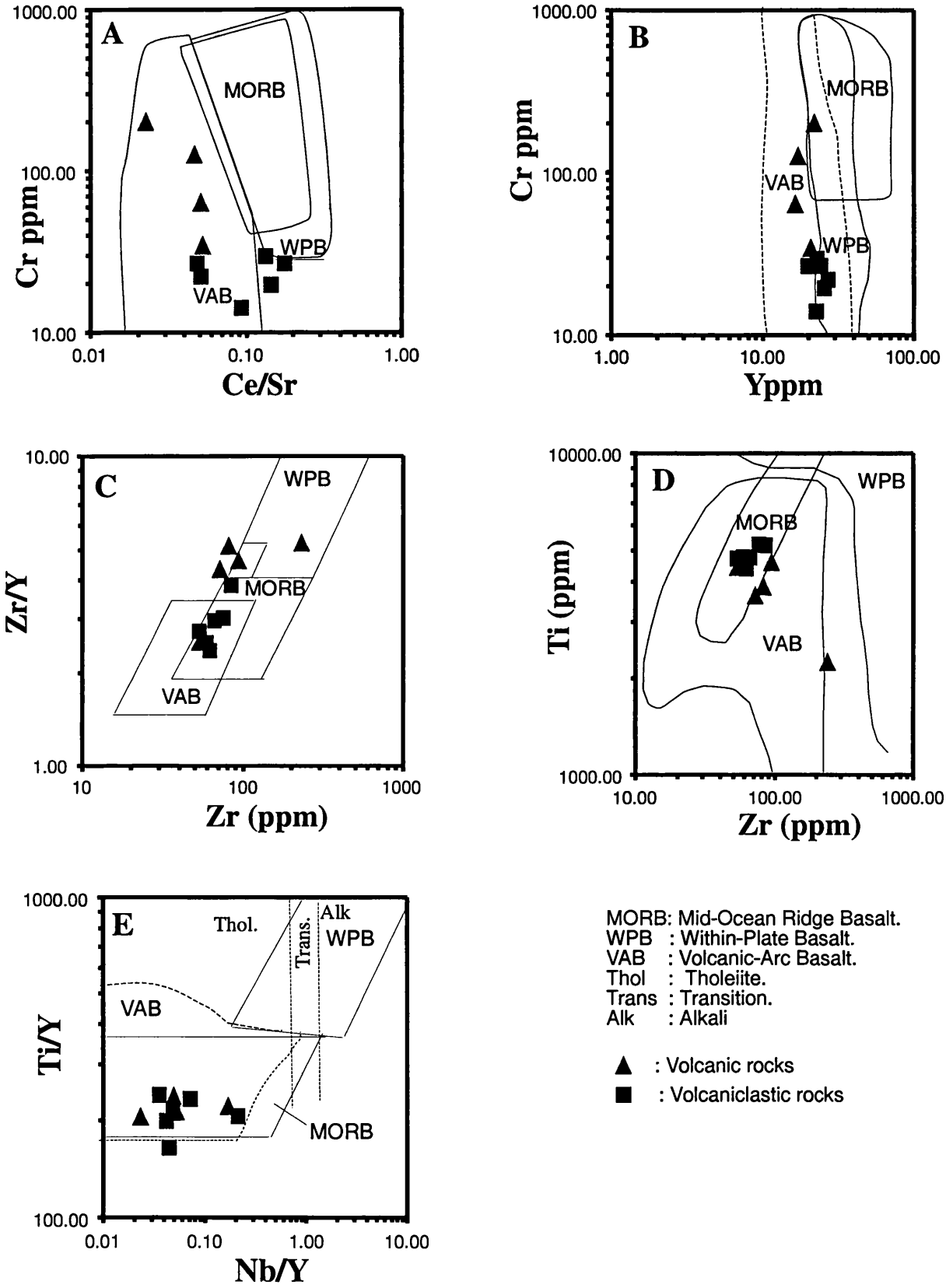

Fig. 5.15 Trace element covariation diagrams for volcanic and volcaniclastic sedimentary rocks of the Anggai River Formation. A, B, D and E after Pearce (1982). C after Pearce & Norry, 1979.

5.4 Fluk Formation

The Fluk Formation consists of shallow water limestones present in small areas throughout south Obi (Fig. 5.16).

5.4.1 Synonymy

This formation name was proposed by Sudana & Yasin (1983) who described it as alternating sandstones, claystones and shales with intercalations of conglomerates and limestone. No type locality was indicated and Hall *et al.* (1992) found that in the Fluk River, assumed to be the type locality, limestones were predominant and were of similar age to that assigned to the Fluk Formation by Sudana & Yasin (1983); the other rocks assigned to the Fluk Formation were discovered to be of different age. The formation was therefore restricted to the limestones.

5.4.2 Aerial Photography and Topographic Interpretation

The areas of Fluk Formation limestones are limited, but they can be recognised from their rough karst topography.

5.4.3 Type Locality

The type locality of the Fluk Formation is in the Fluk River, south Obi Major, although the limestones are not well exposed in the river. Many limestone boulders are found in the upstream part of the river, derived from the top of the hills above the river valley.

5.4.4 Age

Lower-Middle Miocene. Many samples are fossiliferous but few provided suitable material for dating. Two samples were dated using foraminifera (OT39, OT52) and yielded Lower-Middle Miocene ages (Hall *et al.*, 1992).

5.4.5 Thickness

No sections were measured in the Fluk Formation, but from consideration of elevations and distribution, it is thought to be at least 100 m thick.

5.4.6 Distribution

The distribution of the Fluk formation is very limited. It appears as limestone remnants on hilltops with limited exposures in the valleys of the Fluk, Nike and Anggai Rivers.

5.4.7 Lower and Upper Contacts

The limestones rest unconformably upon basement rocks in the type area. The upper contact was not observed but is interpreted to be an unconformity. Erosion is thought to have occurred before deposition of the volcanic and marginal marine Woi Formation and Guyuti Formation.

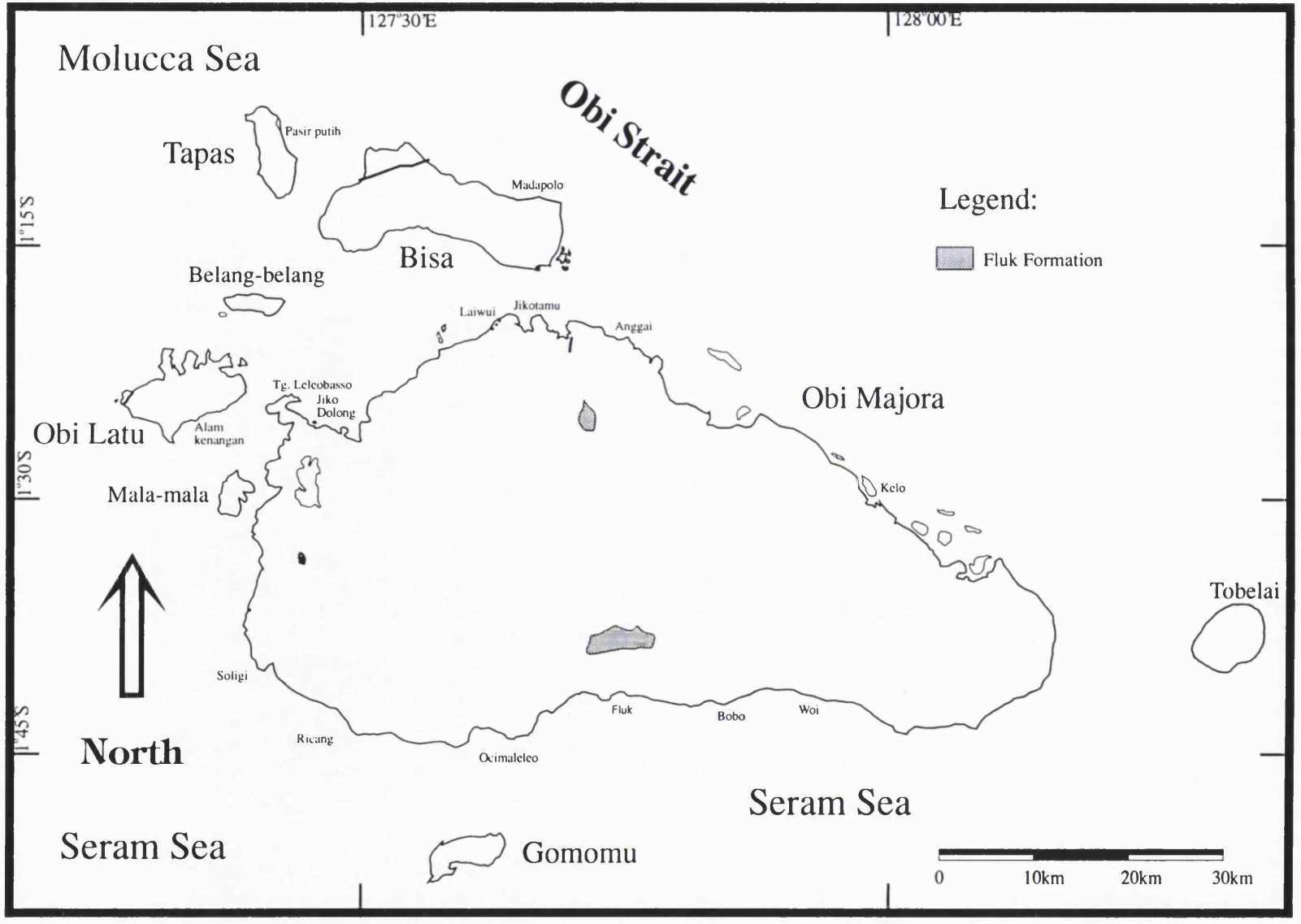

Fig. 5.16 Distribution of the Fluk Formation

5.4.8 Description

In the field the limestones are typically massive, locally contain reefal material, and are poorly bedded. They are often extremely hard and form a rough karst and often form cliffs. In the area of the Fluk River, a thick limestone unit with abundant foraminifera rests unconformably on older rocks and forms high cliffs.

A variety of limestone types can be recognised in the field. Most are packstones with subordinate wackestones (Dunham, 1962) and contain a diverse bioclastic assemblage dominated by large coral, algae, and miliolid fragments. Other bioclastic constituents are planktonic foraminifera, bryozoans, bivalves and brachiopods, and lithoclasts of limestone. Larger fragments are abraded, whereas smaller ones are sometimes found intact. Embedded fragments in a sparry matrix are seen in this rock. The abundance of coral and coralline algae, coexisting with benthic, planktic foraminifera and brachiopod indicate deposition in a normal salinity, shallow marine (10-100 m) environment (Flugel, 1982). Abraded clasts represent original deposition in high energy environment, thought to be an open marine platform.

5.4.9 Depositional Environment

This formation was deposited on a shallow marine shelf. The ages are typical of the interval of widespread carbonate deposition throughout the region and suggest that these limestones were once more widely distributed. Late Neogene uplift and volcanic activity resulted in their removal by erosion, or covering of the limestones by younger Neogene rocks.

5.5 Woi Formation

The Woi Formation consists of volcanic rocks, and volcaniclastic sediments deposited subaerially and in shallow water (Fig. 5.17). It includes andesites, volcanic breccias and conglomerates, tuffs, sandstones and mudstones.

5.5.1 Synonymy

This formation was named first by Sudana & Yasin (1983) who described the Woi Formation as consisting of sandstones, conglomerates and marls with an Upper Miocene to Pliocene age. Unfortunately neither type locality nor stratotype was given. The Gondwana Company (1985) used the term Woi Formation to include interbedded conglomerate with calcareous volcanic arenite, limestone, sandstone, calcareous claystone and sandy tuff and suggested a Pliocene to Pleistocene age, but they also did not identify a type locality. They measured some sections in Obi, but none in the Woi River or surrounding area. They focused particularly on outcrops in the rivers Akelamo, Airpati and Nike where the lithological sequences are very different from those in the Woi River area. Hall *et al.* (1992) used the Sudana & Yasin

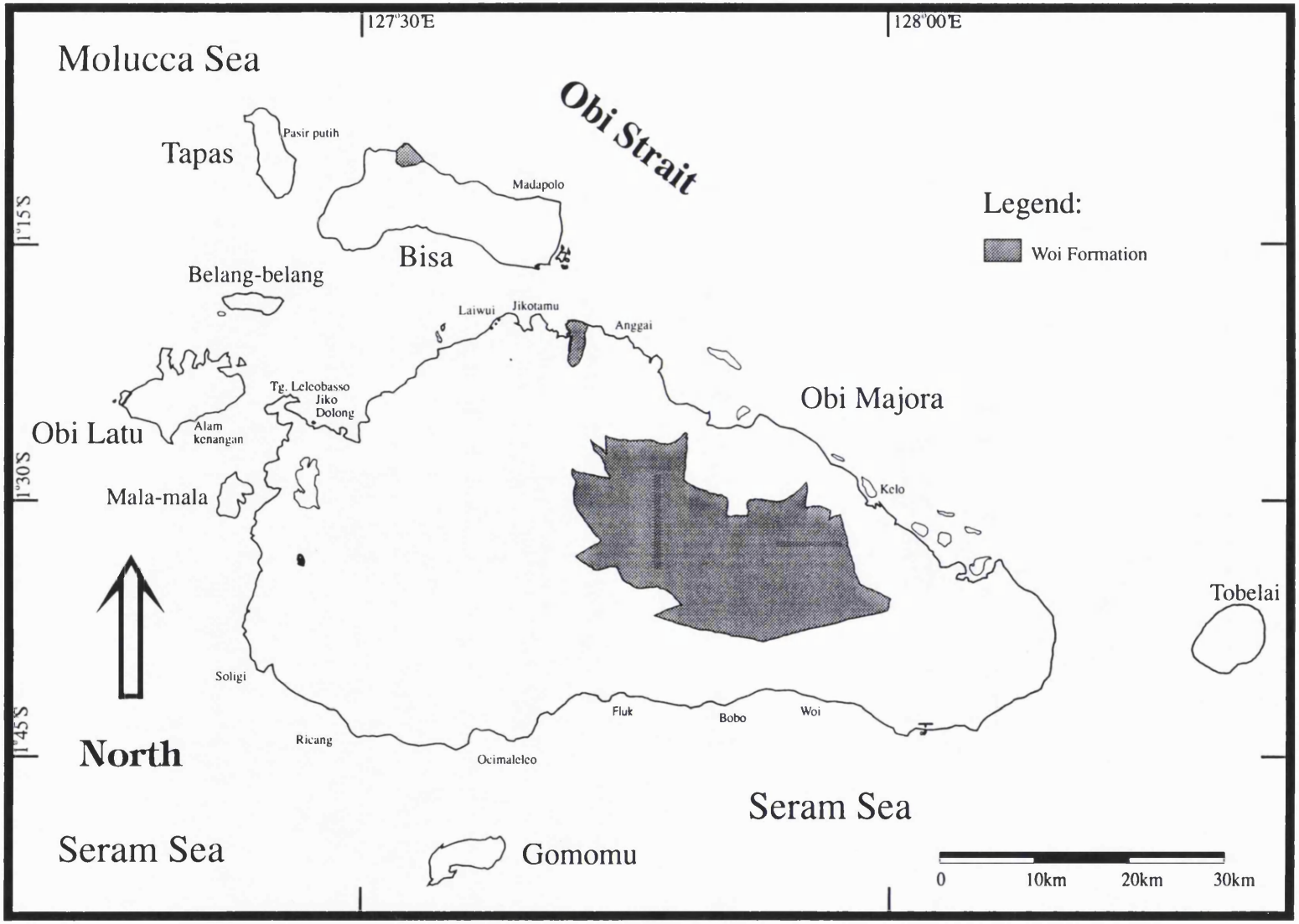

Fig. 5.17 Distribution of the Woi Formation.

(1983) map to redefine the Woi Formation in the area shown on their map and that is the usage followed here.

5.5.2 Aerial Photography and Topographic Interpretation

Topographically, the Woi Formation forms an undulating mountainous region dissected deeply by V-shaped valleys with steep-sided slopes, and gorges in places. The top of the mountainous area is about 1000 m above sea level. On aerial photographs the formation appears grey and quite smooth with NE-SW and east-west lineaments.

5.5.3 Type Section

The type section was chosen at a well exposed sequence near to a former logging company base camp about 26 km north of Bobo village in a river descending to the north to the main Woi River. The section consists of andesite, well bedded carbonaceous sandstone and conglomerates. The type area includes the lateral equivalents of this section which are well exposed in the high valleys above the Woi River.

5.5.4 Age

Micropalaeontological determinations and K-Ar dating of samples from the Woi Formation indicate a Middle Miocene to Lower Pliocene age. Fifteen calcareous mudstones and siltstones have been dated using foraminifera. Foraminifera identified include: *Amphistegina* spp, *Heterostegina cf. depressa, Sphaeroidinellopsis seminula, Orbulina suturalis, Paragloborotalia cf. mayeri, Orbulina universa, Globorotalia minardii,* globigerinids, *Lepidocyclina (Neprolepidina) ferreroi, Operculinella, Sphaeroidinellopsis kochi, Globoquadrina dehiscens, Globorotalia cf. periheroacuta, Globorotalia cf. praeminardi and Dentoglobigerina altispira globosa.* The assemblages found indicate Middle Miocene (N10-N11) and Mio-Pliocene ages (N16-N17).

One calcareous mudstone dated using nannofossils yielded an Upper Miocene to Lower Pliocene age (NN11-NN15) based on the presence of *Reticulofenestra pseudoumbilica, Discoaster surculus, Discoaster brouweri* and *Discoaster asymmetricus.*

Eleven samples have been dated using the K-Ar technique (Table 5.1) and they fall into three groups of ages: Middle-Upper Miocene (11.3-10.7 Ma), Upper Miocene (9.7-8.7 Ma), and Lower Pliocene (4.2-3.3 Ma). The ages suggest significant Late Miocene volcanic activity with some activity continuing through into the Pliocene.

Table 5.1 Summary of K-Ar results from Woi Formation volcanic rocks (wr: whole rock, bi: biotite, px: pyroxene).

Sample	Material	Grain size (μm)	%K (1σ error)	Wt for Ar (g)	$^{40}Ar^*$ nl/g (1σ error)	$^{40}Ar_{atm}$	Age Ma (2σ error)
OJ40	bi±px	125-250	0.834 ± 1	1.0418	0.3473 ± 2.16%	65.33	10.7 ± 0.5
OJ58	wr	125-250	1.792 ± 1	0.733	0.7443 ± 3.21%	75.1	10.7 ± 0.7
OD15	bi	125-250	4.762 ± 5.46	0.1403	2.095 ± 2.35%	67.48	11.3 ± 1.3
OD169	wr	125-300	0.55 ± 1	2.003	0.0896 ± 12.66%	92.43	4.19 ± 1.06
OD180	wr	125-300	0.793 ± 1	2.2166	0.1019 ± 6.91%	87.02	3.3 ± 0.46
OR303	wr	125-500	1.632 ± 1.5	1.0283	0.5565 ± 6.63%	86.41	8.75 ± 1.19
OR306	wr	125-500	2.010 ± 1.3	1.232	0.7476 ± 3.95%	78.96	9.54 ± 0.79
OR310	wr	125-300	2.18 ± 1	1.5779	0.8206 ± 6.84%	86.37	9.7 ± 1.32
OD310	wr	125-300	2.18 ± 1	2.7108	0.7918 ± 6.09%	84.73	9.3 ± 1.13

5.5.5 Thickness

Based on the height of the hills and geological cross sections, the minimum thickness of this formation is estimated to be ~1000 m.

5.5.6 Distribution

This formation is exposed in eastern Obi, from north of Bobo village to the eastward and north almost as far as the north coast near Kelo village. The formation dips NE at ~15-20°. Volcanic rocks on Bisa Island are also assigned to this formation.

5.5.7 Lower and Upper Contacts

The formation is interpreted to rest unconformably on folded pre-Neogene rocks and possibly on Miocene Limestones. However, where the basal contact is observed in the Woi River area, it is a thrust. The formation is conformably overlain by shallow water limestones of the Anggai Formation.

5.5.8 Description

The Woi Formation is well exposed, though difficult to reach, in the tributaries and upstream sections of the River Woi, a major river which runs NW-SE across eastern Obi. The main rock units exposed are lavas, agglomerates and tuffs, all either close to horizontal or with very low dips. The lavas are dark, contain phenocrysts of feldspar, hornblende and biotite, and are andesites and basaltic andesites (Fig. 5.18). There are two kinds of volcanic rocks discovered in Woi Formation; the lower part of the Woi formation commonly contains biotite andesites,

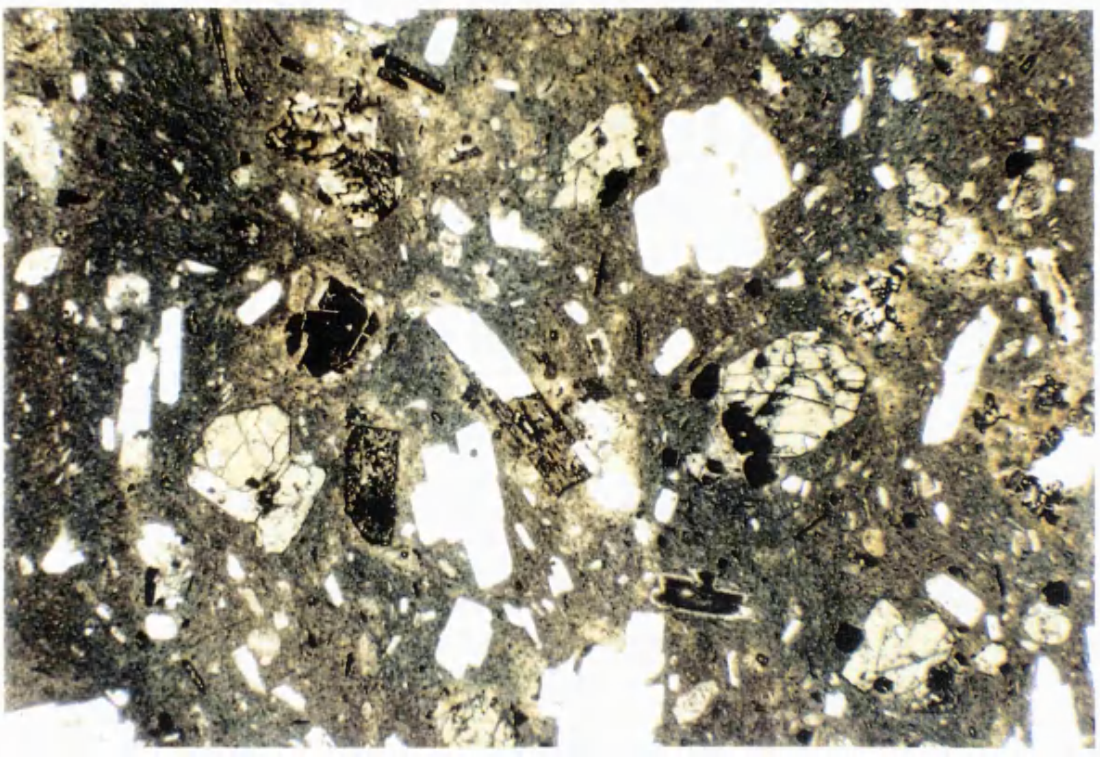

Fig. 5.18 A. (above) Photomicrograph of biotite andesite (OD14), containing brown biotite, clinopyroxene and plagioclase phenocrysts in a finer matrix. Plane polarised light. Width of photograph is 1.6 mm. B. (below) crossed polars.

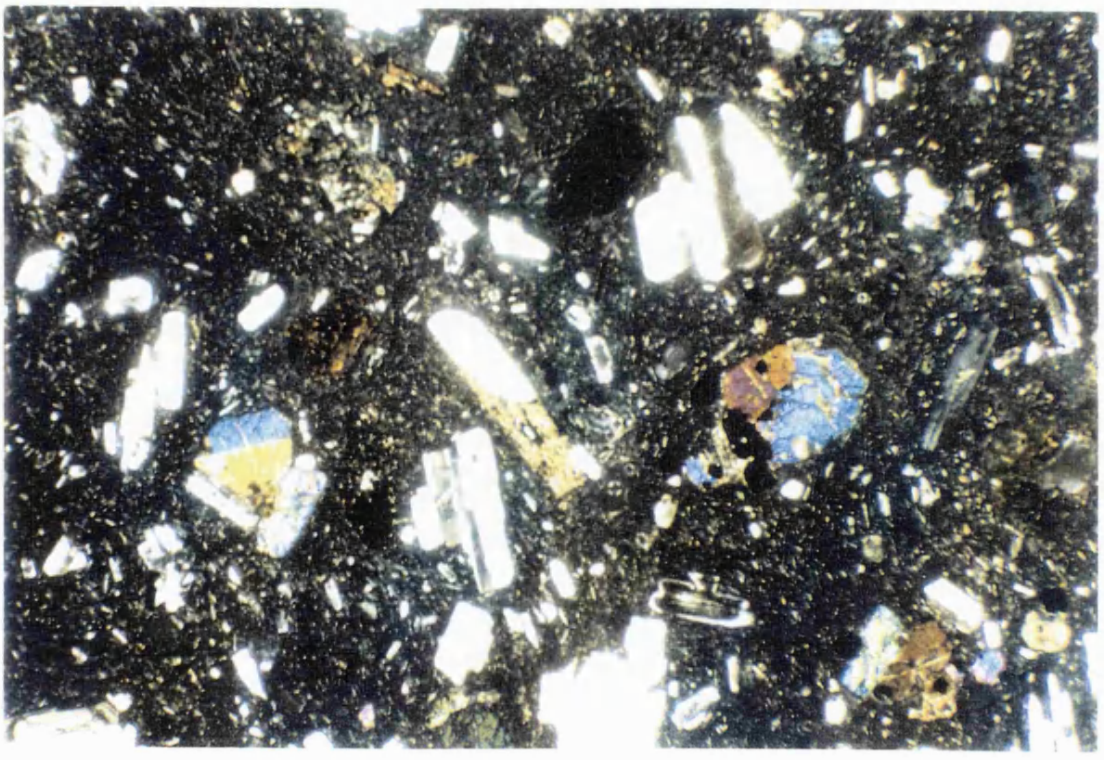

Whereas in the upper part of the Woi Formation pyroxene andesites without biotite are more common.

Basaltic andesite lavas in the Sesepe River near Kelo show bedded or flow banding structures (Figs. 5.19 and 5.20). Exposures behind spectacular waterfalls suggest that the lavas are in units metres to tens of metres thick. They are interbedded with metre-thick beds of coarse breccias of volcanic debris which are thought to be primary pyroclastic deposits; the clasts are all very similar to the composition of the lavas. In a river section close to the end of the Bobo logging road (the Bobo waterfall section) the upper 30 m of a long section in sub-horizontal rocks exposes a 20 m thick andesitic lava flow conformably above well bedded sandstones and siltstones. The sandstones form beds up to 20 cm thick with low angle cross bedding and contain large clasts of hard limestones and coral debris.

The tuffaceous parts of the sequence are frequently weathered and poorly exposed in most streams, although road cuts made by the logging operations expose fresh sections several metres thick. The colour of the tuffs is highly variable. The least altered material is pale green with abundant crystals of feldspar and biotite; these occur in massive units up to several metres thick and may be primary pyroclastic deposits. More commonly, the colour ranges through yellow, brown, grey, orange and red, occurring in sub-horizontal layers or as a mottling of the material. The most strongly reddened exposures are soft and clayey, but the volcanic origin of the material is evident from the crystals of feldspar and biotite in red mudstones. These colour variations and the breakdown of minerals to clay is attributed to pedogenic processes. This pedogenesis may have taken place contemporaneously with the deposition of the tuffs or may be a result of Quaternary soil processes. There are two lines of evidence to suggest the former. Firstly, the thickness and occurrence of the pedogenic profiles does not appear to be related to the present day land surface. Secondly, distinct, repeated profiles can be observed within the tuff beds. Within these profiles there are concentrations of carbonised wood, solidified resin and seed pods and the tuffs display parallel and wavy laminations indicative of aqueous reworking of the ash. The occurrence of these features within the beds of tuff indicate that the reworking and soil forming processes were going on during the period of volcanic activity.

The lower thrust contact of the Woi Formation is exposed in a major south-flowing tributary of the Woi River where the formation rests unconformably upon the Guyuti Formation. The contact is exposed in the small gorge of the Guyuti River where there is a sudden change from folded Guyuti Formation to poorly sorted highly angular andesitic breccias of the Woi Formation. These are probably lava breccias, approximately 20 m thick, with clasts which range up to 2 m across, although most are less than 30 cm, of fresh pyroxene andesites in an andesitic matrix. Immediately above the breccias is about 1 m of well bedded limestone, then a further 5 m of andesitic breccias followed by 5 m of andesitic conglomerate, partly bedded, with shallow

Fig. 5.19 Bedded basaltic andesitic lavas of the Woi Formation in the lower Sesepe River, northeast Obi Major.

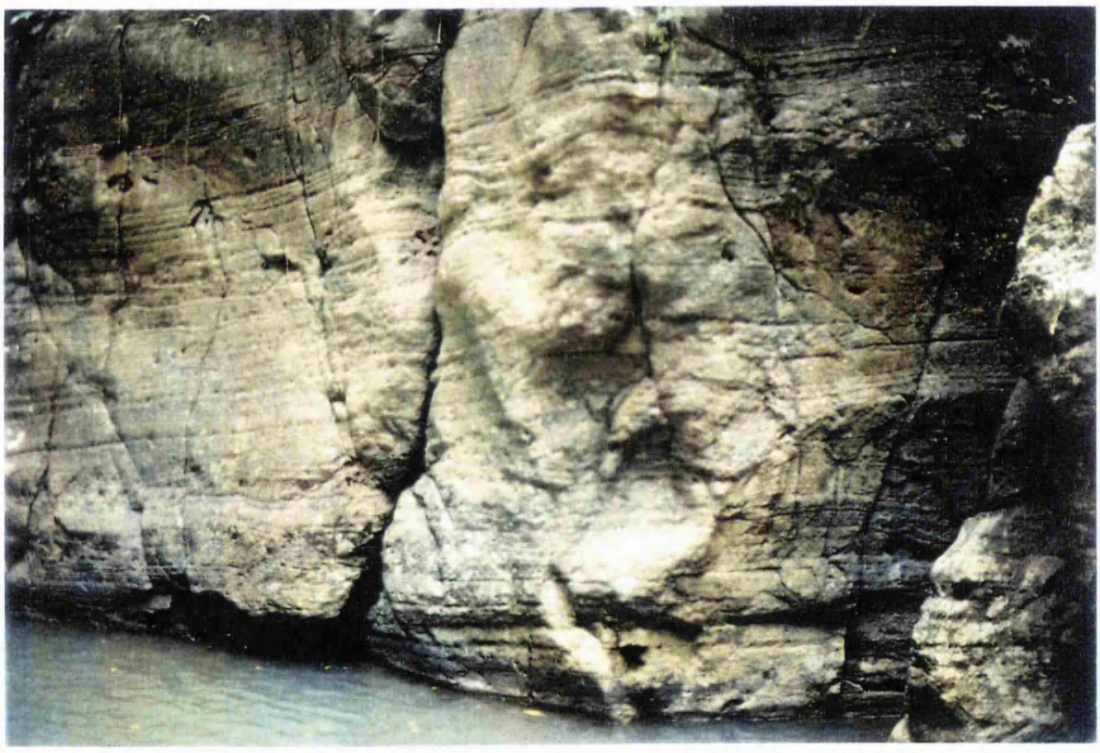

Fig. 5.20 Flow-banded andesitic lavas of the Woi Formation in the upper Sesepe River, northeasth Obi Major.

water limestone debris in the matrix. The carbonate debris includes corals and shelly material. Although the breccias lack bedding the two bedded limestone intervals indicate that the sequence dips east at ~20°. The sequence continues with a long section, at least 30 m thick of andesitic breccias.

Above this, the next part of the Woi Formation is very difficult to examine as it is exposed in vertical and near vertical cliffs forming high waterfalls in the headwaters of the south-flowing Woi tributaries. At the tops of these waterfalls are thick andesitic lava flows; observations in the Bobo waterfall section on the south side of the Woi valley suggest that this section is composed of interbedded lavas and shallow marine sedimentary rocks. The summits of the peaks on the north side of the Woi valley are composed almost entirely of several hundred metres of massive, deeply weathered andesites, probably almost entirely lavas with subordinate pyroclastic rocks. The logging roads south of the Sesepe River descend to the north down the north-dipping dip slope of the formation, locally descending deeper into the Woi Formation and elsewhere climbing into the overlying Anggai Formation. The upper part of the Woi Formation is dominated by pyroclastic arenites, with some thin coal seams and increasing amounts of dark shales up-section. In several places there are green muddy limestones above the shales which contain beds of white calcarenite with benthonic forams, abundant coral debris, bivalve shells, and elongate algal mat-like material. These may be the transition to the limestones of the Anggai Formation above the Woi Formation although there are shallow water limestones similar to those elsewhere in the area that are within the Woi Formation.

Most of Bisa is underlain by gently south-dipping limestones of the Pliocene Anggai Formation and Quaternary age. However, on its north coast of Bisa there is a single area with relatively good exposure over a few tens of metres where there are low cliffs of some unusual acid igneous rocks. These are acid volcanic (possibly minor intrusive) rocks of probable rhyolitic composition locally with flow banding. Their colour is typically pale green, grey or almost white. The paler samples form well jointed outcrops, generally featureless, but locally with preferred orientation of flow features and possible pumice or glass fragments. Elsewhere there are xenoliths, mostly of reddened acid volcanic rocks, but with a very small number of xenoliths of coarse amphibolite/hornblendite similar to those exposed on the nearby island of Tapas. These rocks are quite unlike anything found elsewhere on Obi or Bacan and have yielded late Miocene K-Ar ages (OR303, OR306 and OR310, Table 5.1) of 8.7-9.7 Ma.

Samples from the Woi Formation have now been dated by a variety of methods (foraminifera, nannofossils and K-Ar) indicating an age range for the formation of upper Middle to Early Pliocene. So far, there is insufficient stratigraphic and structural control to demonstrate clearly variation in age of the formation across its outcrop width. It is expected to young north-

east. The similarities of lithology and age indicate the Woi Formation is the equivalent of the Kaputusan Formation of the Bacan Islands.

5.5.8.1 Measured Sections

Three sections have been measured in the Woi Formation (Figs. 5.21, 5.22 and 5.23). One section was measured in the Guyuti River and the other sections were measured in north Obi. These sections consist of a variety of conglomerates, breccias, limestones and sandstones. They appear to have be deposited in marginal marine to shallow marine environments.

The section (Fig. 5.21) in the Guyuti River tributary is above the thrust separating it from the Guyuti Formation. The lithological succession consists of andesitic breccias with an intercalation of thin well bedded limestone, andesitic conglomerate and andesitic breccia. At the bottom, dark grey andesitic breccias are composed of andesitic-basaltic clasts in a calcareous sandstone matrix. These rocks are matrix-supported. Clasts are typically 20-30 cm across and are angular. Thin well bedded limestones consist of lithoclasts of limestone (10%), skeletal and coralline debris, and large benthonic foraminifera (10%) in a micritic matrix. A wackestone-packstone (OD172) contains andesitic clasts, plagioclase, corals and benthic foraminifera in micritic matrix. These rocks are covered by andesitic conglomerate which contains corals and shallow water limestone debris as clasts in a fine grained calcareous sandstone matrix. Clasts are subrounded and poorly sorted. At the top of this section, andesite breccias with veins up to 0.5 m thick lie on the andesitic conglomerate and are similar to andesitic breccias at the bottom of the section.

The second section is in a small river with waterfall beside the former base camp of the logging road north of Bobo village (Fig. 5.22). This section consists of andesitic breccias, sandstone and andesitic lava. At the bottom, a dark grey monomict breccia is matrix supported with subangular to angular pyroxene andesitic clasts, up to 60 mm long and wide. It is poorly sorted and massive. The matrix is coarse grained sandstone. Thick well bedded sandstones overlie the breccia, and has fine to coarse, poorly sorted, andesitic clasts, with pyrite and plant fragments. Reverse grading, parallel laminations, normal grading and burrows are present in these sandstone beds. A calcareous sandstone (OG2) is matrix supported, poorly sorted and contains subrounded grains. The grains consist of basaltic andesite fragments (partly replaced by clay, ~ 30%), plagioclase (fresh, ~10%), opaque (5%) and sometimes planktic foraminifera (3%).The matrix consists of clay and carbonate (~ 57%). A tuffaceous sandstone (OD26J) is grain-supported with moderately sorted, angular to subangular grains. The grains consist of plagioclase (fresh, simple twinning, 25%), pyroxene (fresh, but part altered to carbonate, 2%), biotite (brown, fresh, 1%), volcanic glass (38%) and opaque mineral (5%). The matrix consists of clay and carbonate. These sandstones are covered by breccia which consists of andesite and coralline limestone clasts in a matrix of fine grained sandstone. Clast are poorly sorted, angular to subangular and up to 9 cm across. At the top, an andesitic lava flow contains agate-lined

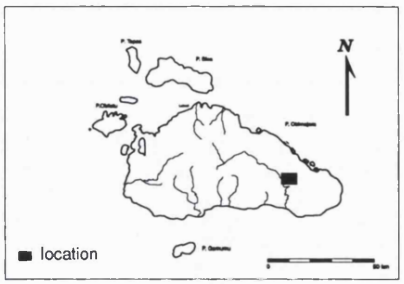

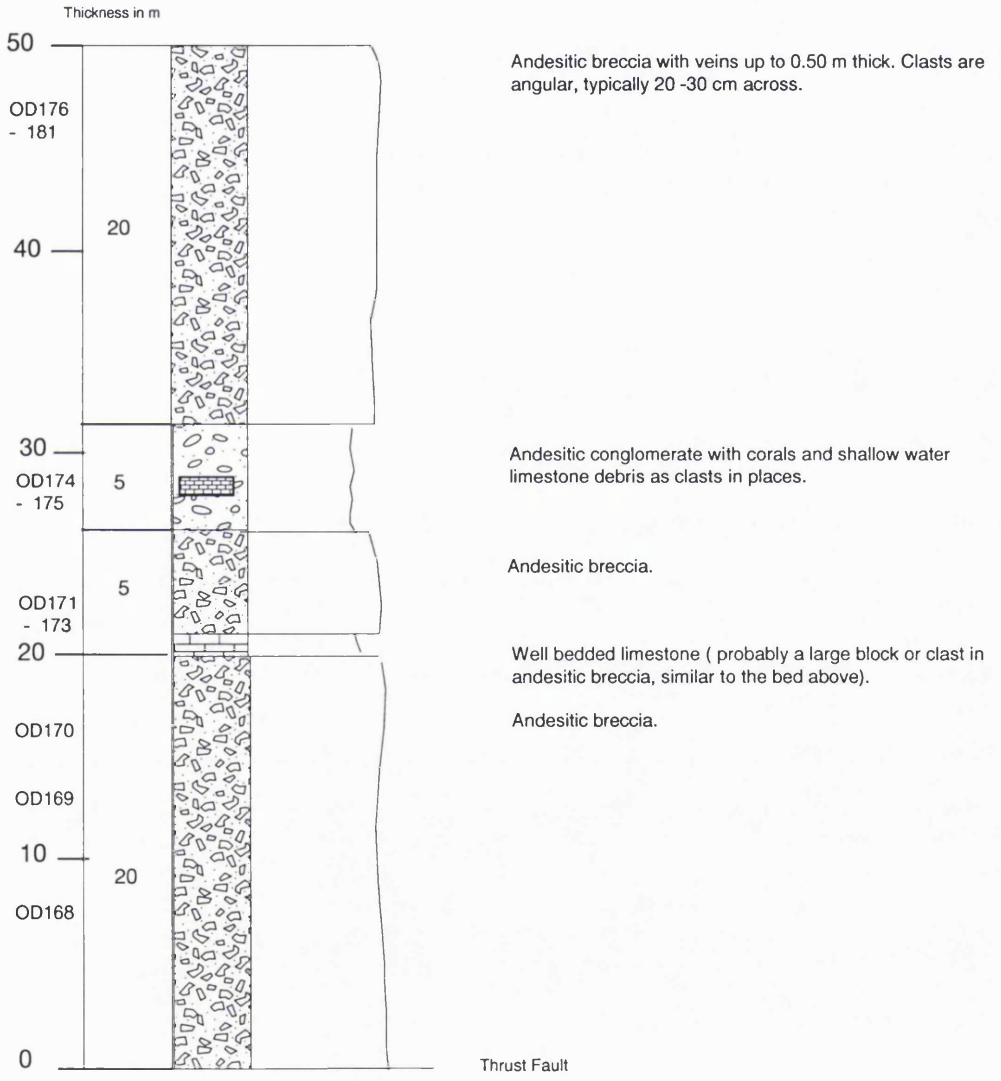

Fig. 5.21 Section of part of the Woi Formation measured in the Guyuti River in south Obi (latitude 1°36'08", longitude 127°57'08"). Location shown on inset map. Key can be seen in appendix D.

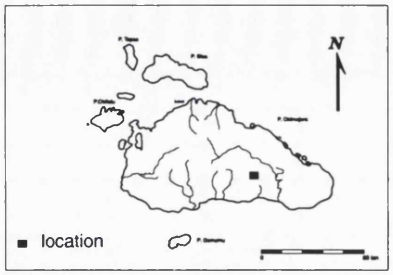

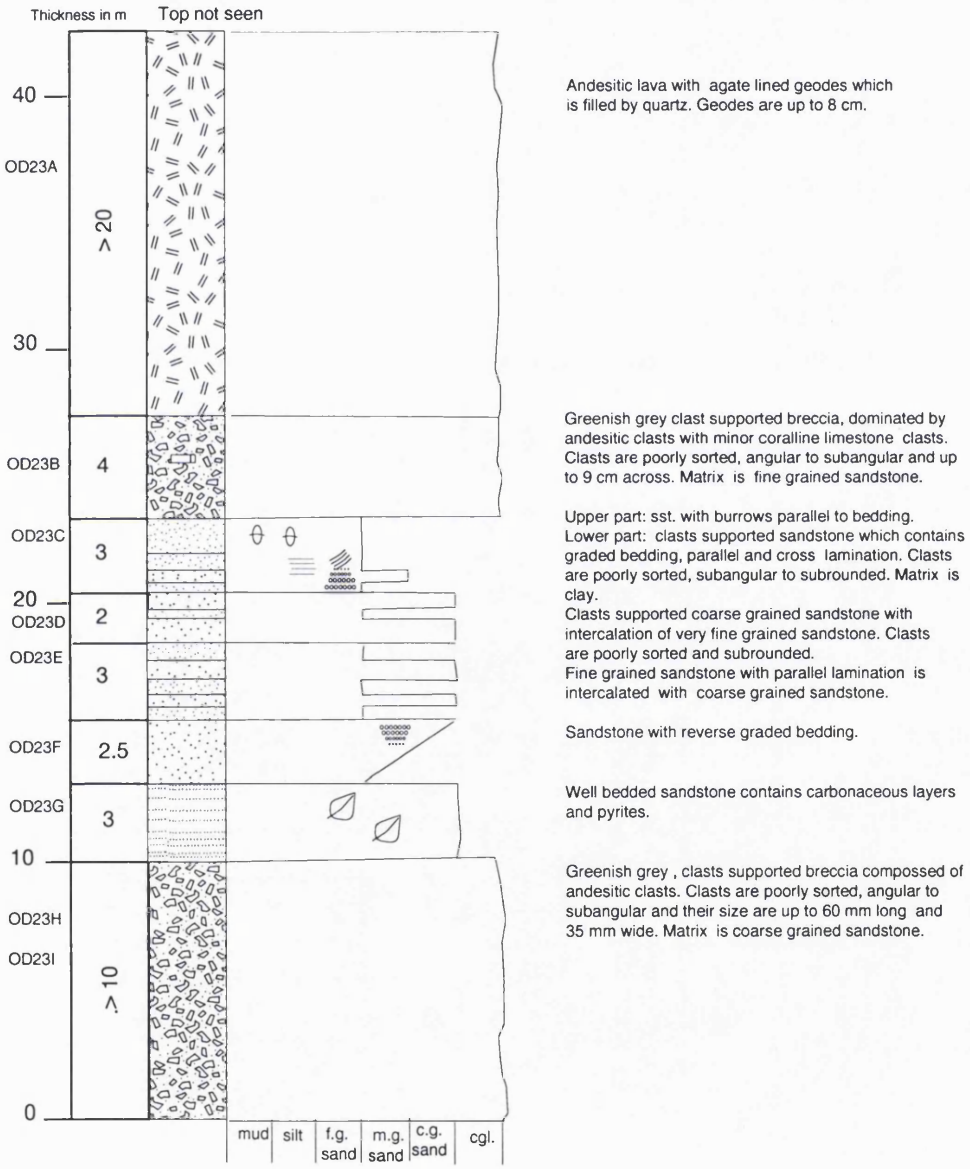

Fig. 5.22 Section of part of the Woi Formation measured below the waterfall near the former logging camp north of Bobo in south Obi (latitude 1°36'49", longitude 127°54'57") . Location shown on inset map. Key can be seen in appendix D.

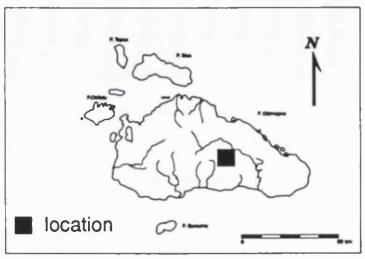

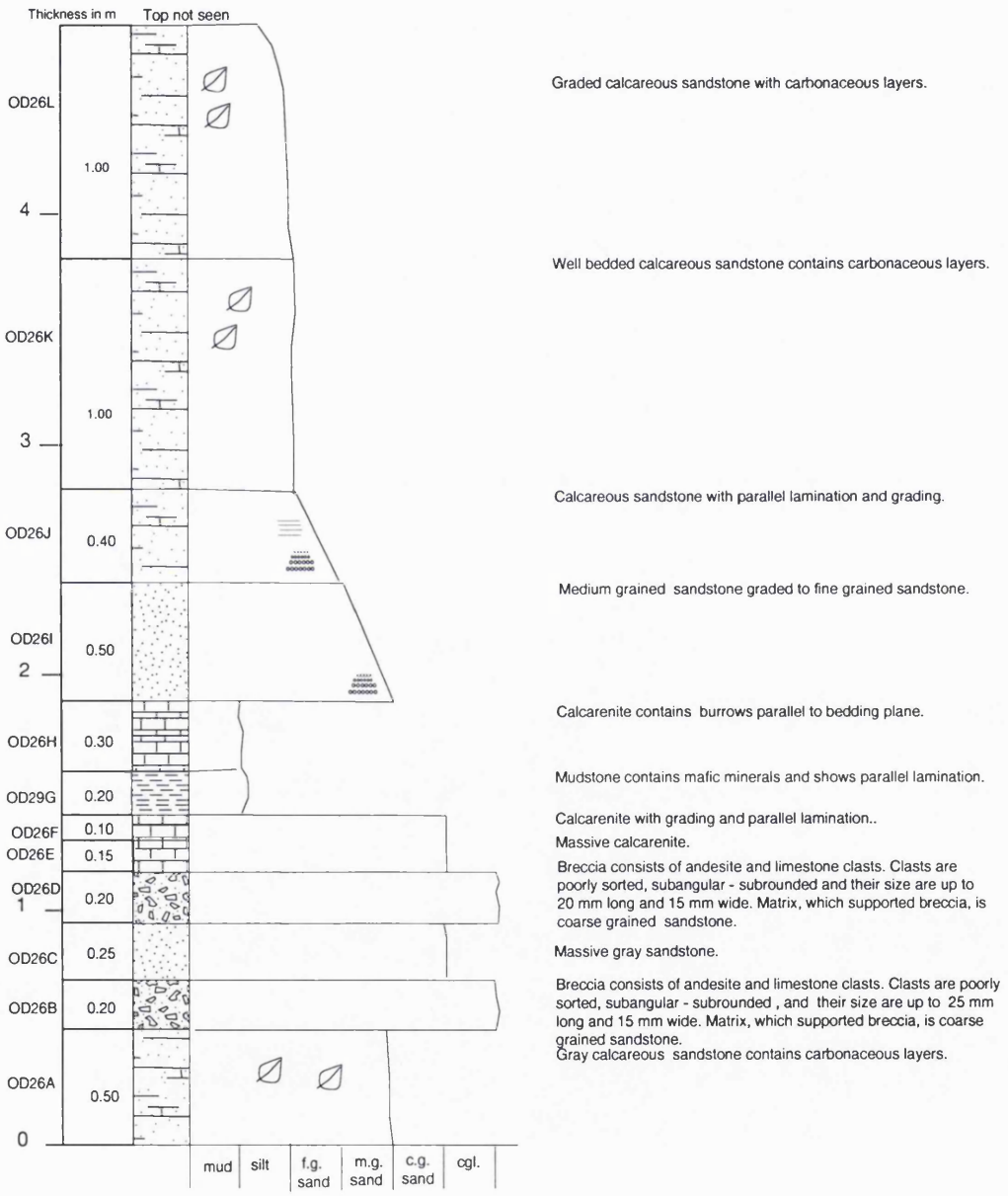

Fig. 5.23 Section of part of the Woi Formation measured in a tributary of the Woi River, south Obi (latitude 1°35'43", longitude 127°54'32"). Location shown on inset map. Key can be seen in appendix D.

geodes.

The last section was measured in a tributary of the Woi River (Fig. 5.23). This section is comprised of calcareous sandstones with intercalations of thin beds of breccias, mudstones and calcarenites. Well bedded grey fine to medium grained calcareous sandstones contain carbonaceous layers and normal grading in some beds. Breccias are clast-supported, poorly sorted and contain subangular to subrounded clasts of andesite and limestone in a coarse grained sandstone matrix. Calcarenites show grading, parallel lamination and burrows parallel to bedding planes.

5.5.8.2 Petrography and Mineral Chemistry of Volcanic Rocks

Volcanic rocks exposed in the Sesepe River are basalts and andesites (OD4, OD15, OD17 and OD 18). One sample (OD4) has been analysed by microprobe. They have a porphyritic texture with both mafic and felsic phenocrysts in plagioclase-rich microcrystalline and glassy matrix (Fig. 5.3). The mafic and felsic phenocrysts are subhedral to euhedral and have generally elongate and rectangular shapes with simple twinning and zoning. The modal proportion of phenocrysts is between 25% and 30%. Most phenocrysts and microcrystalline grains are fresh. Compositions of fresh plagioclase are between labradorite and bytownite (An_{67-84}). Pyroxene phenocrysts constitute ~10 modal % and have subhedral to euhedral shapes. Clinopyroxenes are magnesium-rich augites. Othopyroxenes are ferroan enstatite, but they are rare. Plagioclases and pyroxenes are commonly embayed and often form glomerocrysts. Brown biotite represents up to 5 modal % in some samples with tiny opaque minerals concentrated at the rim of grains. Accessory minerals in all samples are abundant Fe-Ti oxides. The groundmass contains plagioclase and pyroxene microcrystalline grains, Fe-Ti oxides and a glassy matrix. The microcrystalline grains are oriented in a pilotaxitic texture.

Volcanic rocks exposed in the Guyuti River and north of Bobo village are basaltic andesites (OD179 and OD180). They have porphyritic textures with plagioclase, pyroxene and opaque phenocrysts in a plagioclase microlite-rich and volcanic glass matrix. The modal proportion of phenocrysts is ~30%. Phenocrysts are often embayed. Plagioclase is the most abundant phase and shows simple twinning and zoning. Usually both phenocryst and matrix phases are fresh. Some small inclusions of plagioclase and pyroxene appear within plagioclase phenocrysts. The matrix is glassy and plagioclase microlites are oriented to form a pilotaxitic texture.

Andesites and dacites exposed on north coast of Bisa Island (OD303, OD306 and OD310) contain xenoliths of older volcanic rocks. These andesites are pale grey to grey with porphyritic textures and contain both mafic and felsic phenocrysts in a plagioclase-rich microcrystalline matrix. The modal percentage of plagioclase is between 40% and 60%. There is about 15% to 20 modal % of pyroxene. Fe-Ti oxides are present as accessory minerals. Other minerals present include probable smectites and carbonates which partly replace plagioclase.

5.5.9 Whole Rock Chemistry

5.5.9.1 Major Elements

A Ph.D. study by E. Forde on the geochemistry of the Neogene volcanic rocks is currently in its final stages and a large number of rocks from the Woi Formation have been analysed for major, trace elements and isotopes. The results reported here are therefore intended simply to identify the principal chemical features, in particular the compositional ranges of the Woi Formation volcanic rocks.

Analyses of nineteen samples of Woi Formation volcanic rocks are reported in Appendix C. All are relatively fresh as indicated by their small LOI (0.6-2.8 wt %). On the Na_2O-K_2O-SiO_2 diagram of Le Bas & Streckeisen (1991) they range between basaltic andesite and dacite in composition (Fig. 5.24). On the K_2O-SiO_2 diagram of Taylor *et al.* (1981) the majority plot in the high-K field with a smaller number plotting in or very close to the medium K calcalkaline fields (Fig. 5.25). The high K samples are clearly linked to different volcanic centres. The majority come from the Kelo area where there are no low- or medium-K samples. In the Guyuti River both medium and high K samples are found but the high-K samples were all collected in one small area, possibly indicating a centre erupting high-K magmas at some times and low- to medium K magmas at other. As noted earlier similar subsets of high-K and calc-alkaline rocks are known from Neogene volcanic centres elsewhere in the Halmahera arc (Hakim, 1989; E. Forde, pers. comm., 1994).

5.5.9.2 Trace Elements

The volcanic rocks have very similar patterns on the MORB-normalised trace element diagrams and resemble typical arc volcanics (Fig. 5.26). They are enriched in K, Rb and Ba, depleted in Nb, and have sloping patterns for the more immobile elements, being relatively enriched in the elements Ce-Y and depleted in Ti. On most of the discriminant diagrams they plot in the calcalkaline and volcanic arc fields (Figs. 5.27, 5.28 and 5.29).

5.5.10 Depositional Environment

The presence of foraminifera, shelly and coralline debris, burrows, and plant material suggest that the part of Woi Formation was deposited in an oxygen-rich, nearshore, shallow marine environment. The presence of coal-bearing strata and resin in alternating mudstones and fine-grained sandstones, indicates that other parts of the formation were deposited in a subaerial setting, such as swamps or lakes. These non-marine sequences are interbedded with volcanic ash, and there are rapid transitions, and often no transition, to fresh volcanic rocks including volcanic breccias and lava flows. Lavas are interbedded in many sections with both non-marine and marine sedimentary rocks. Volcanic activity on Obi was in progress at the end of the Middle Miocene and continued into the Late Miocene (about 11.3 to 8.7 Ma). There is evidence of further volcanic activity in the Early Pliocene (4.2 to 3.3 Ma). The evidence from the sequences

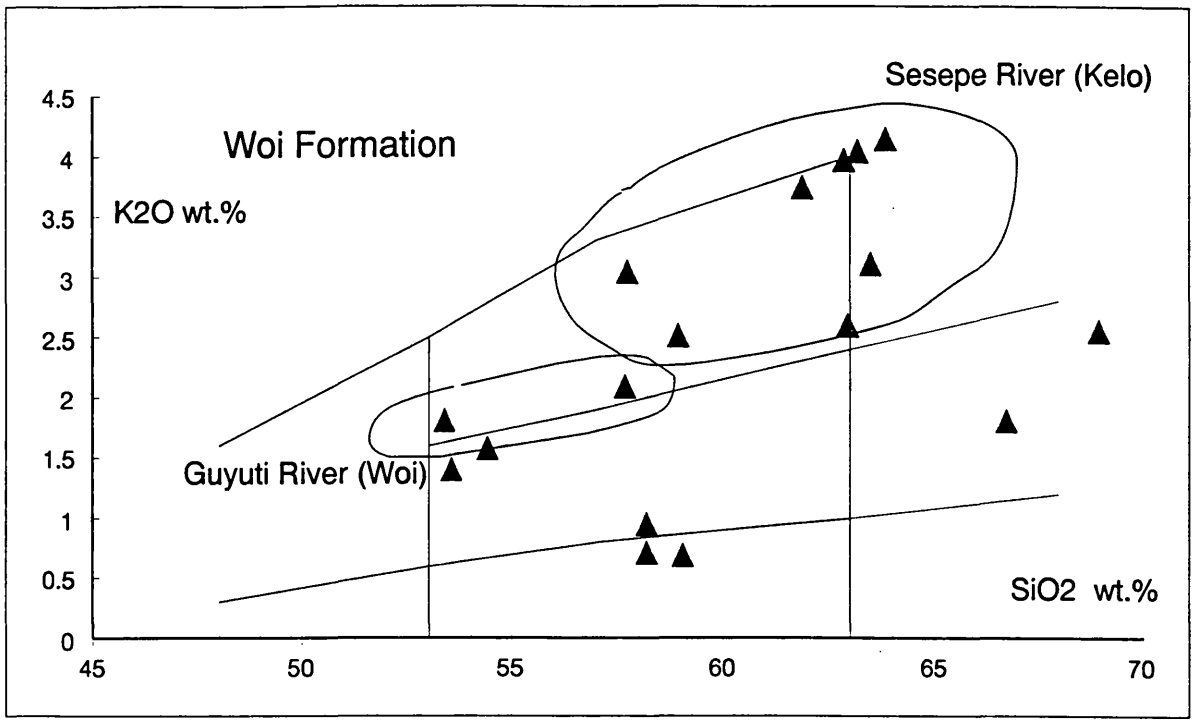

Fig. 5.24 Plot of K_2O versus SiO_2 for volcanic rocks of the Woi Formation. Compositional fields from Taylor *et al.* (1981). Areas identified are those in which the high-K rocks were collected.

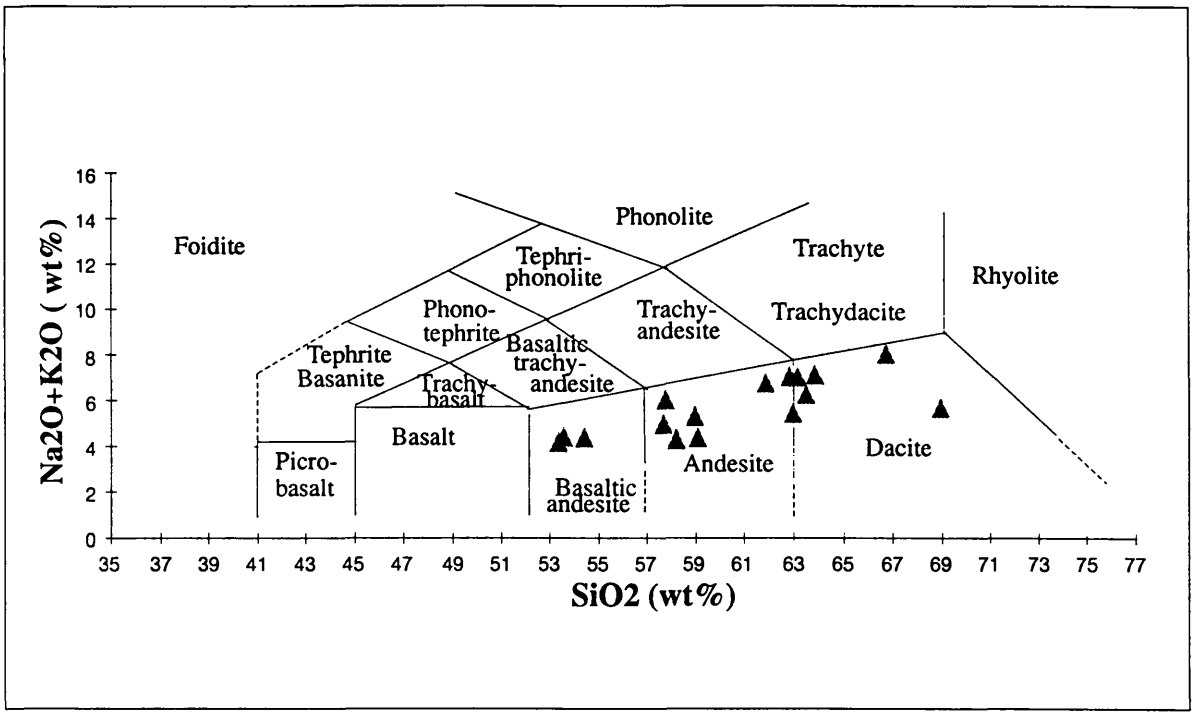

Fig. 5.25 Plot of Na_2O+K_2O versus SiO_2 for volcanic rocks of the Woi Formation. Compositional field from after Le Bas & Streckeisen, (1991).

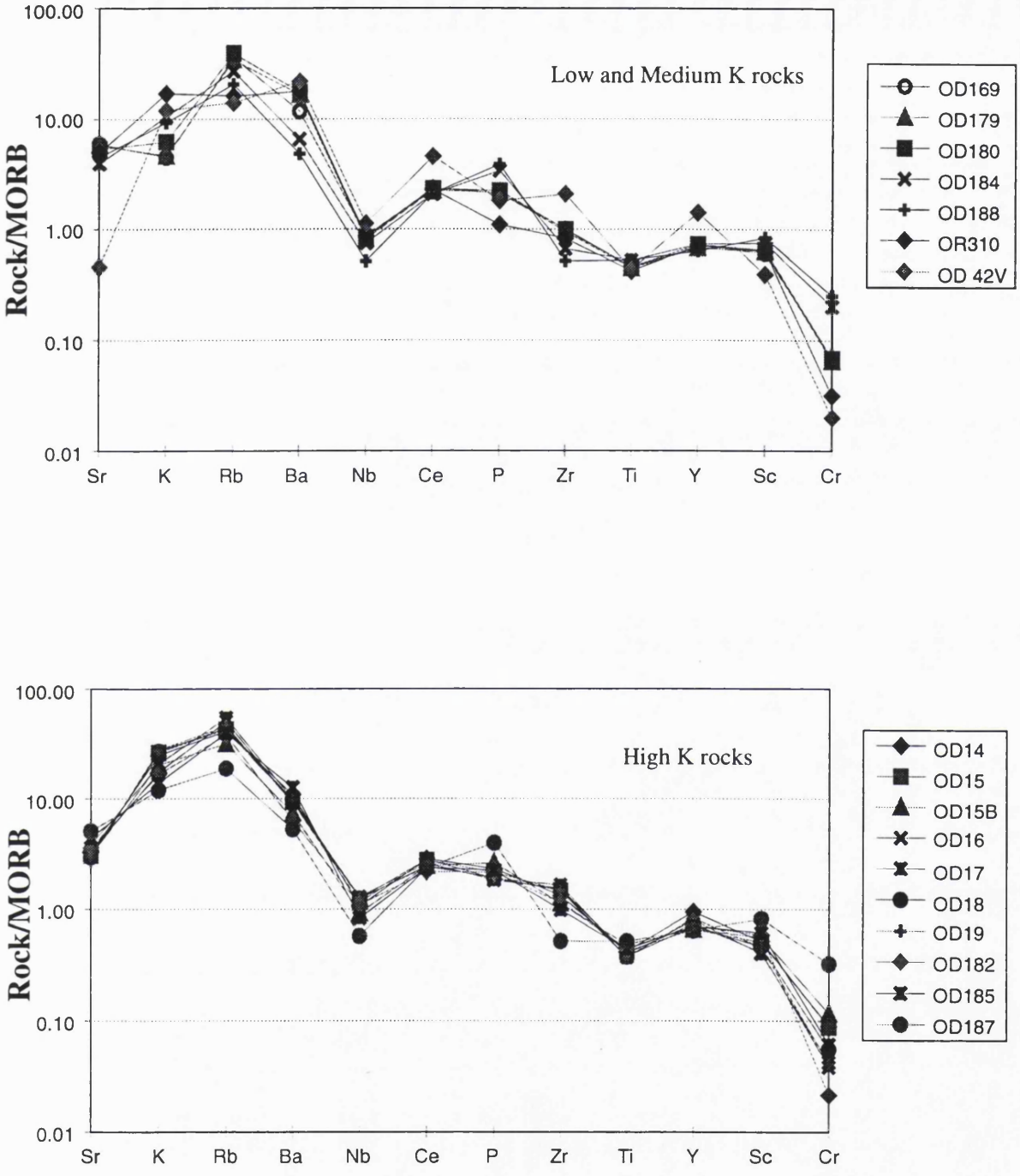

Fig. 5.26 MORB-normalised trace element spidergrams for volcanic rocks of the Woi Formation. Normalising factor from Pearce et al. (1984)

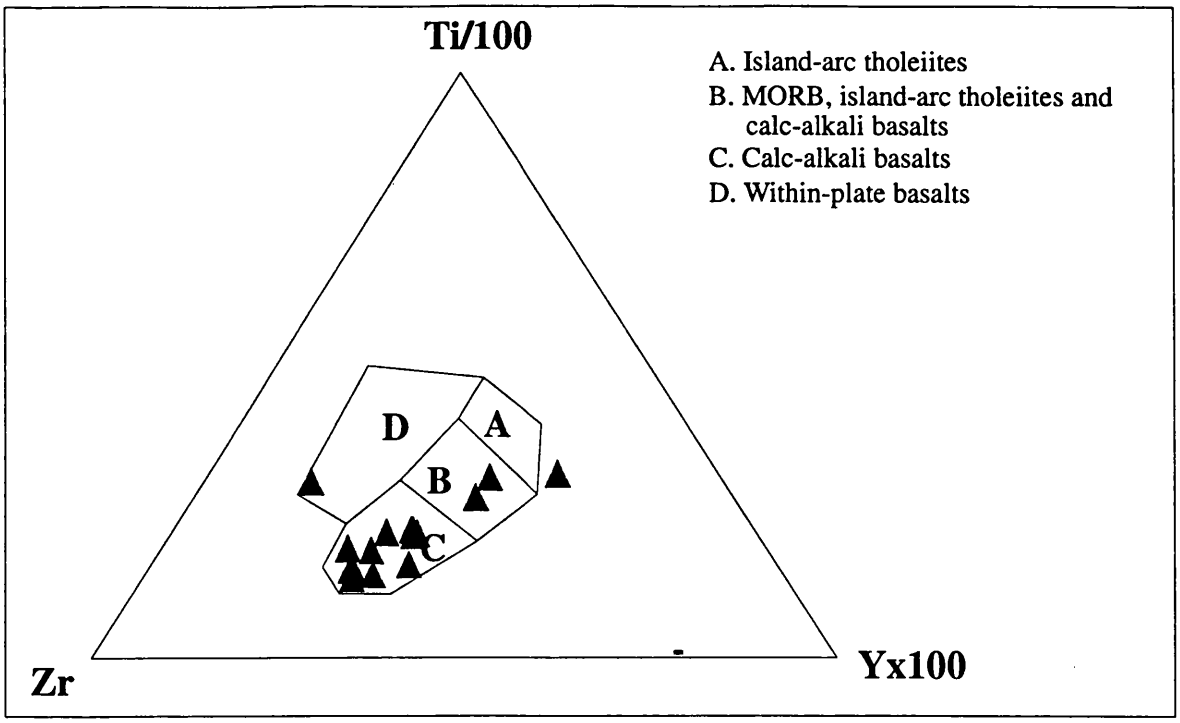

Fig. 5.27 Ti-Zr-Y discriminant diagram for volcanic rocks of the Woi Formation (after Pearce and Cann, 1973)

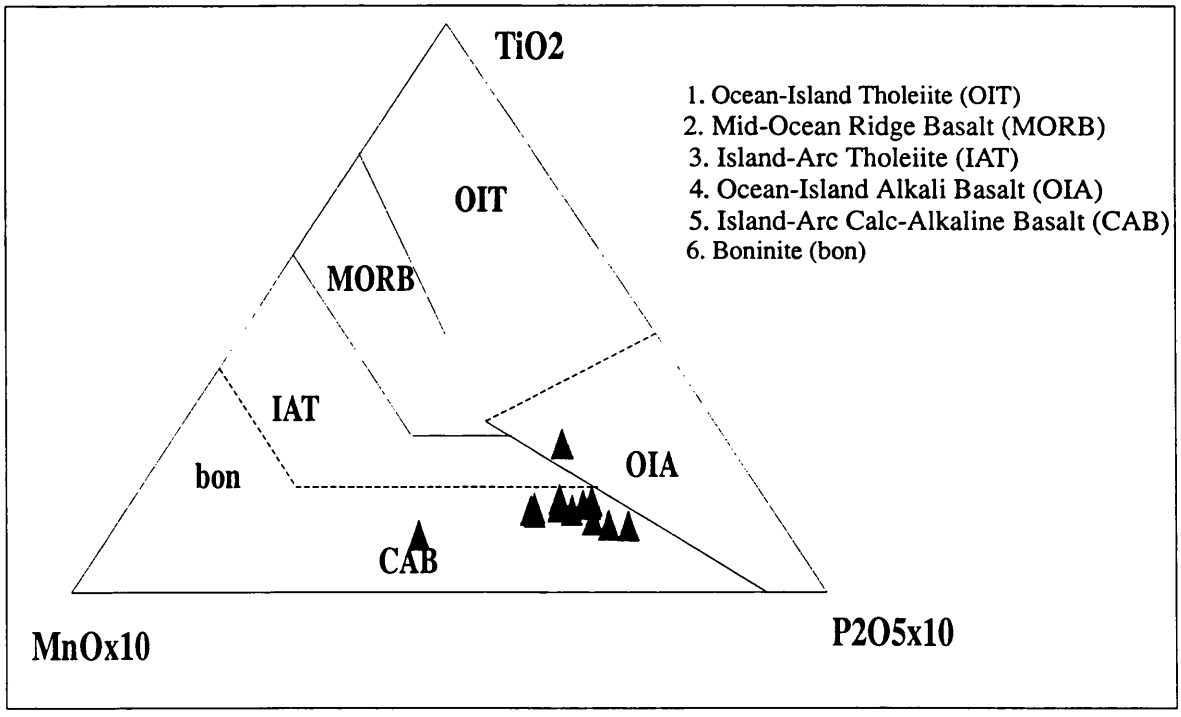

Fig. 5.28 Mn-Ti-P discriminant diagram for volcanic rocks of the Woi Formation (after Mullen, (1983)

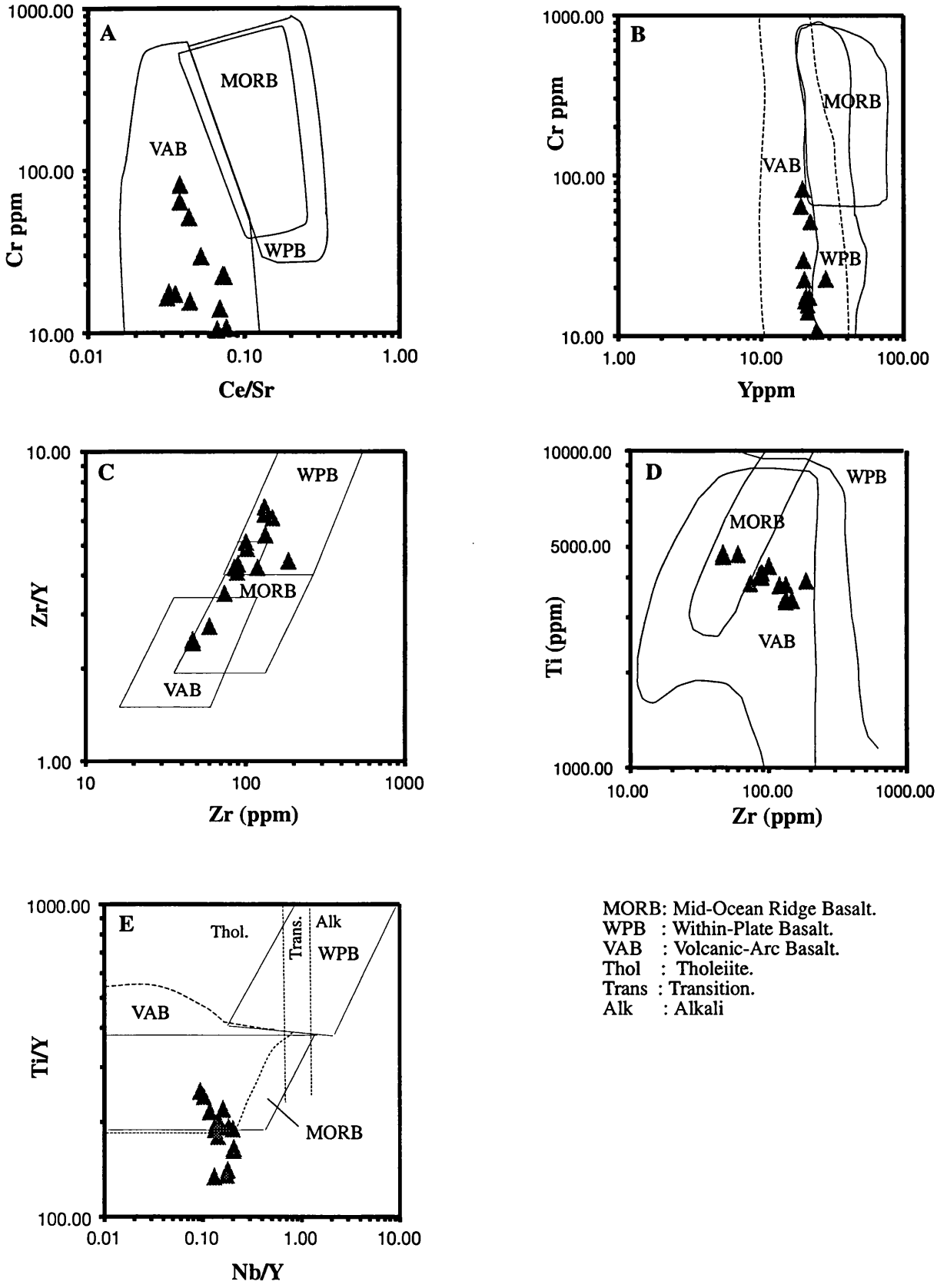

MORB: Mid-Ocean Ridge Basalt.
WPB : Within-Plate Basalt.
VAB : Volcanic-Arc Basalt.
Thol : Tholeiite.
Trans : Transition.
Alk : Alkali

Fig. 5.29 Trace element covariation diagrams for volcanic rocks of the Woi Formation. A, B, D and E after Pearce (1982). C after Pearce & Norry, 1979

examined suggest that the Woi Formation represents a subaerial volcanic arc and its emergent to marginal marine flanks. Sequences of marine strata may represent intervals of volcanic inactivity or may represent areas away from volcanic centres.

5.6 Guyuti Formation

The Guyuti Formation consists of interbedded breccio-conglomerates, sandstones and siltstones interpreted as debris flow deposits and associated turbidites, derived from a source area of volcanic rocks and shallow water limestones (fig.5.30).

5.6.1 Synonymy

This formation name is a new one. Rocks in the type area were shown as part of the Fluk Formation on the map of Sudana & Yasin (1983). Fieldwork during the 1992 expedition and subsequent dating showed that this formation is the age equivalent of the overlying Woi Formation and the contact between the two is interpreted as a thrust.

5.6.2 Aerial Photography and Topographic Interpretation

The Guyuti Formation is difficult to distinguish from the Woi Formation since formations include similar lithologies. On aerial photographs the Guyuti Formation appears to have smoother surfaces than the Woi Formation.

5.6.3 Type Section

The Woi River, at the junction with its tributary the Guyuti River in southeast Obi. In this area there is complete exposure in the Woi gorge although it is difficult to access.

5.6.4 Age

Middle to Upper Miocene. Dating is based on K-Ar dating of an andesitic clast from a breccio-conglomerate (OD194, 11.1 ± 0.3 Ma), and a brecciated andesite (OD155, 7.47 ± 0.37 Ma). Micropalaeontological analyses of limestone clasts (OD191, OD198 and OD199) yielded Middle Miocene or younger ages, with evidence of reworking and redeposition. Recognisable foraminifera are: *Carpentaria, Orbulina suturalis, O. universa, Amphistegina* and *Gypsina* (F. T. Banner, pers. comm., 1993). One sample (OD200) dated using nannofossils yielded a possible Neogene age, but this is uncertain since only two specimens of *Calcidicus macintyrei* were found in the sample (E. M. Finch, pers. comm., 1993).

5.6.5 Thickness

At least 100 metres, which is the thickness of the section observed. Cross section constructions suggest the formation is more than 500 m thick.

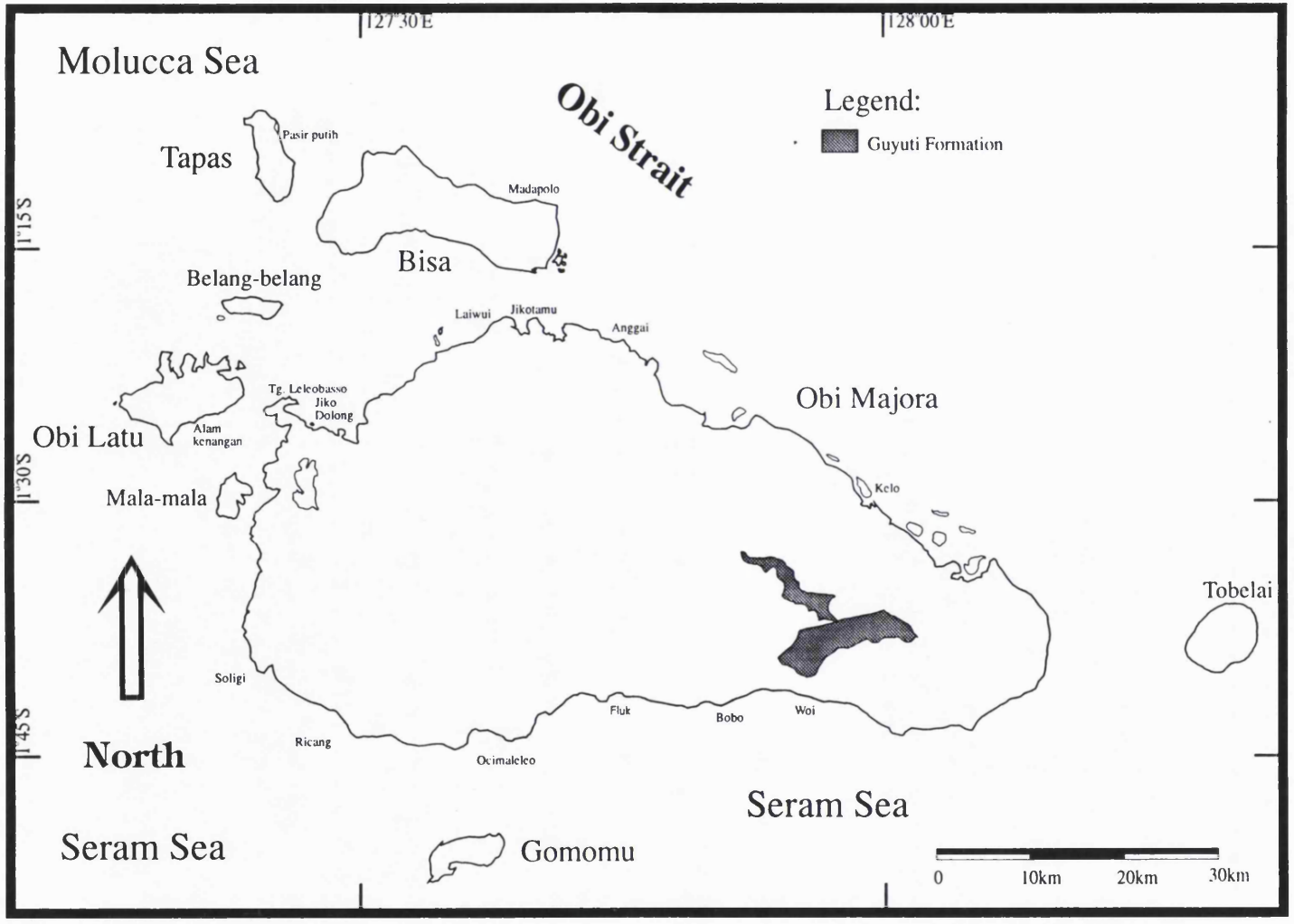

Fig. 5.30 Distribution of the Guyuti Formation

5.6.6 Distribution

The exposure of this formation is limited. Because it is overlain by the Woi Formation it is exposed only in the bed of the deeply incised Woi River, in tributaries such as the Guyuti River, and in nearby low-lying areas.

5.6.7 Lower and Upper Contacts

Neither upper nor lower stratigraphic contacts are observed. In the Woi River this formation is overthrust by the Woi Formation, which rests upon folded, moderately steeply dipping rocks of the Guyuti Formation. It is interpreted to rest unconformably upon Fluk Formation limestones and older rocks.

5.6.8 Description

Although the contact is not exposed the Guyuti Formation is interpreted to rest unconformably upon the ophiolite and the contact can be traced roughly NW-SE on the aerial photographs. On the logging road to the Woi River the Guyuti Formation dip gently, typically less than 30°, to both north and south. Near to the Woi River dips change locally quite quickly and the rocks are folded on approximately E-W axes. Due to weathering, exposures along the road are rather poor but in the Woi River and its tributaries they are excellent. In one tributary of the Woi River running N-S from the north these rocks are overlain by volcanic rocks and interbedded limestones of the Woi Formation. The contact is a thrust.

At the type locality, there are breccio-conglomerates interbedded with alternating sandstone and siltstone. The matrix-supported breccio-conglomerate consists of andesitic, microdiorite and limestone clasts at the base, with increasing amount of andesite and decreasing amount of microdiorite and limestone towards the top. The clasts are subrounded to rounded with maximum clast sizes of 4 m at the base and of 0.3 m at the top. The matrix consists of coarse-grained sandstone, which is similar to the overlying sandstone units. It is well bedded, with bed thickness at least 4 metres at the base, down to 10 mm thick at the top, although typically beds are about 0.5 m thick. This unit is cut by numerous veins, filled by a white mineral. The breccio-conglomerate is interbedded with 0.1-0.5 m thick sandstone and siltstone beds. The coarse grained volcanic clastic sandstone is graded with local small basal load structures. The top of some beds have burrows parallel to bedding surfaces (typically 0.2 - 0.3 m long and 10 mm wide). Locally there are dewatering and load structures (showing the sequence is the right way up). Some sandstone beds have conglomeratic bases, and locally the sandstone beds also contain breccia intervals, with andesitic and laminated sedimentary clasts (up to 20 cm long). There are finer grained dark sandstones alternating with fine siltstone and sandstone on a mm scale. The

siltstone is grey and carbonaceous. It may be either parallel laminated or extensively disturbed by bioturbation. Locally it contains ripples. Bedding thickness are < 10 cm thick.

The sequence in the Woi River is dominated by andesitic conglomerates with subordinate sandstones and mudstones. The conglomerates include both clast- and matrix-supported types, they are generally poorly sorted but well bedded. Different beds have very different clast sizes. In the main Woi River the conglomerates are well exposed in the wall of the gorges. Andesite boulders are the predominant rock type and in places they are up to 2 m, although typically between 0.5 and 1 m, across. Large compact limestone clasts are found in these conglomerates; some are very large and one not untypical block was 4m x 2m x 2m (Fig. 5.31). The limestones contain shallow water debris including corals. Some contain a few planktonic foraminifera and lithic grains of andesite in a micritic matrix forming ~ 80% of the total rock volume, locally recrystallized to spar. Mudstones contains ~ 5% planktic foraminifera and a few lithic fragments in a micritic matrix. Spar has replaced skeletal material and fills some veins. Sandstones and thin mudstones interbedded with the conglomerates are typically thinner (< 1 m) beds and usually medium to finely bedded. Sedimentary structures include normal grading, load casts, flame structures, ripple cross lamination, rippled tops to silty beds, and bedding parallel burrows on some bed tops. The size, shape, distribution and type of clasts, the well bedded character of the conglomerates and the internal variation from matrix to clast-supported types suggests these rocks are debris flows, probably deposited in deep water. The finer grained sediments are interpreted as volcaniclastic turbidites.

5.6.8.1 Measured section

A section was measured in the lower Guyuti River (Fig. 5.32). The thickness of this section is about 50 m, and although the thickness of the formation seen is more than 100 m the measured section is typical of the entire formation. It includes brecciated andesite overlain by conglomerates and alternating sandstones and siltstones.

At the base a grey breccia 4 m thick contains clasts of andesite and microdiorite of pebble to cobble size. The clasts are subangular to angular and have a sandy matrix. Some quartz veins cut this rock. Above there are dark grey to light grey sandstones 3 m to 10 m thick with dewatering and load structures at the coarse sandstone base. These are overlain by breccias within locally bedded intervals and they have clasts in a largely sandy matrix. Carbonaceous layers and layers of silt on scales of a few mm are intercalated in this unit. Above are beds with a coarse sandstone matrix containing abundant clasts of andesites, up to ~ 0.2-0.3 m size in places. Some andesite clasts are the size of boulders yet have well rounded shapes. Further up section, well bedded sandstones alternate with siltstones which contain bedding-parallel burrows typically 0.2-0.3 m in length. At the top are well bedded conglomerates 0.5-1 m thick which consist of sub-rounded andesitic clasts (~ 0.2 m across) floating in a coarse sandy matrix. At the base of this unit the

Fig. 5.31 Andesitic conglomerates of the Guyuti Formation in the Woi River include large compact limestone blocks containing shallow water debris including corals.

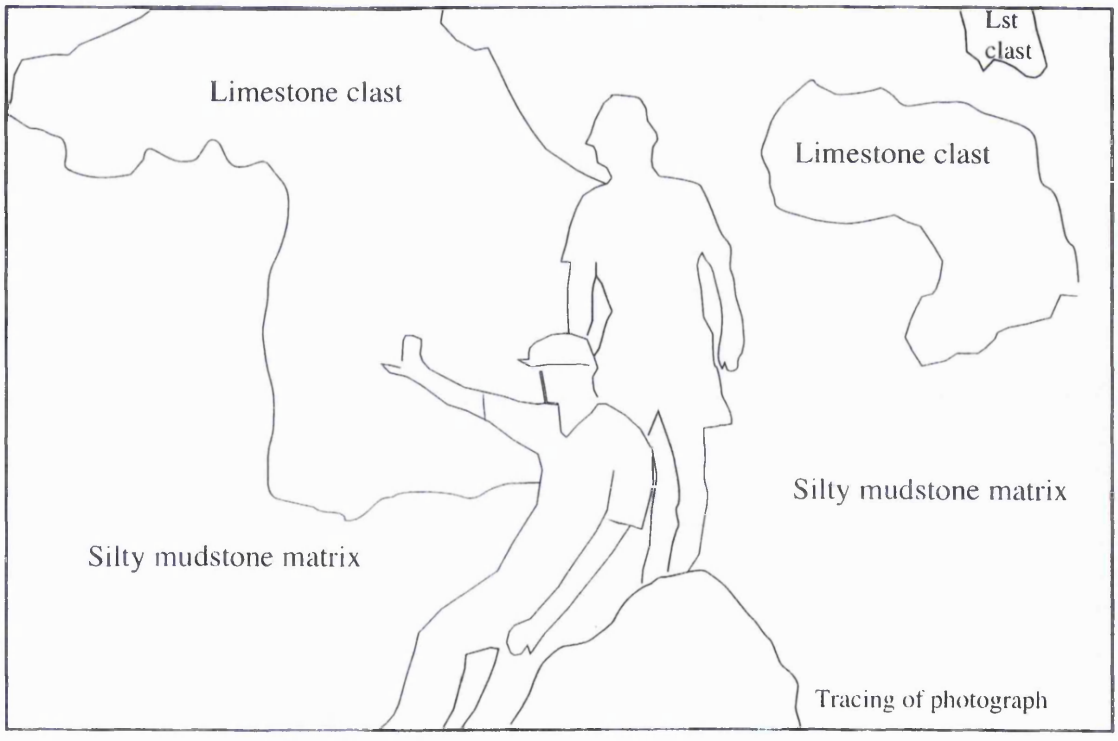

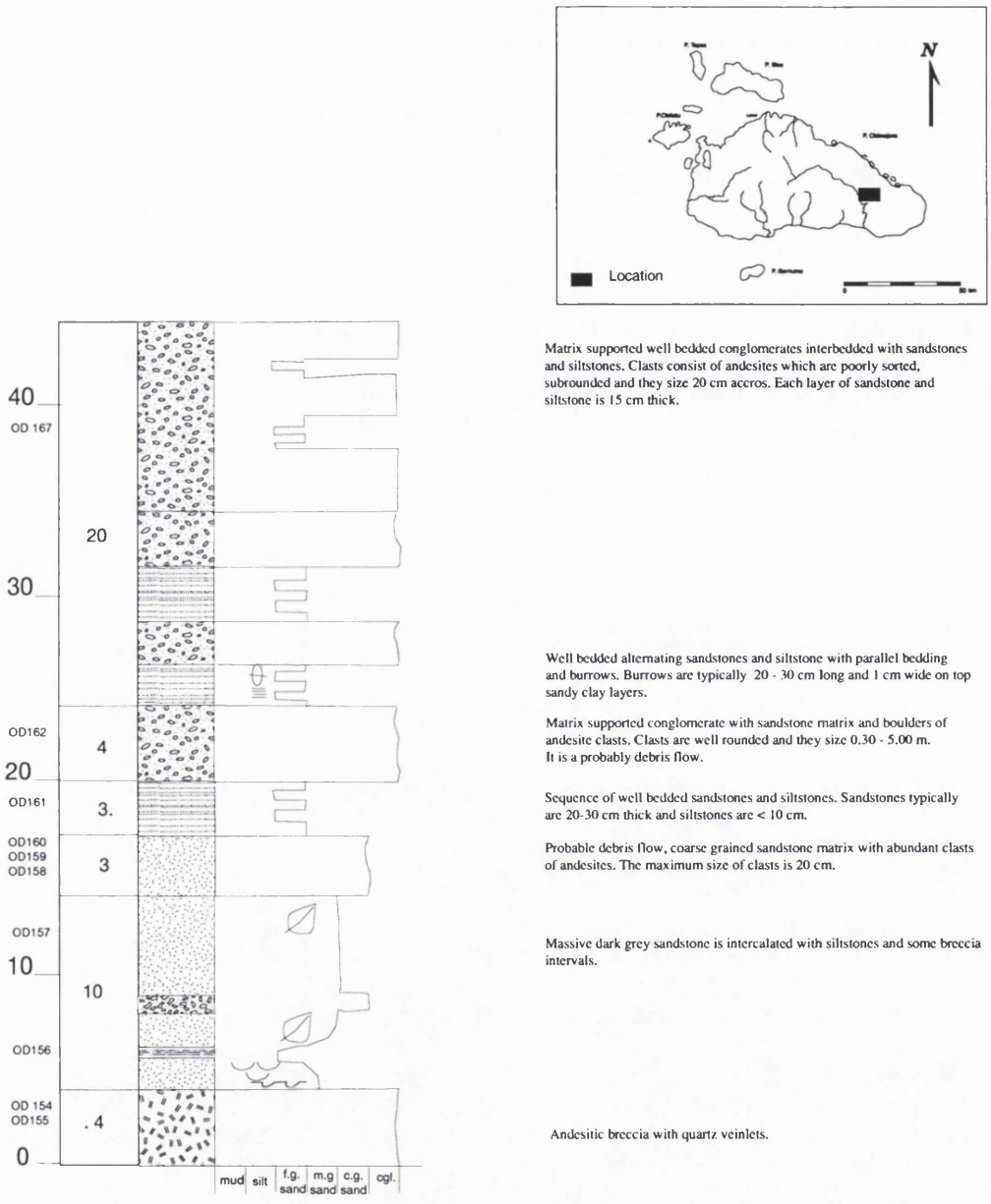

Fig. 5.32 Section of part of the Guyuti Formation measured in the Guyuti River in south Obi (latitude 1°36'33", longitude 127°56'51"). Location shown on inset map. Key can be seen in appendix D.

conglomerates are interbedded with sandstones and siltstones. The thickness of the conglomerates is about 20 m. This section is interpreted as a rapidly deposited sequence of debris flows and turbidites, sourced from an active volcanic area. The size of material suggests a proximal setting with high energies and a steep slope. Bedding parallel burrows indicate intervals of non-deposition.

5.6.8.2 Petrography and Mineral Chemistry of Volcanic Rocks

Petrographically, the volcanic rock clasts in the Guyuti Formation resemble basalts of the Woi Formation. Three samples (OD154, OD160 and OD194) were analysed by microprobe. The basalts have porphyritic textures with mafic and felsic phenocrysts in a microcrystalline to glassy matrix (Fig. 5.33). The mafic and felsic phenocrysts are subhedral to euhedral and generally elongate and rectangular. The modal proportion of phenocrysts in the basalts is between 30% to 40%. Plagioclase represents ~25-35 modal %. Phenocrysts have subhedral to euhedral shapes and are zoned. Plagioclases have bytownite to labradorite compositions (OD154 An_{56-86}; OD194 An_{60-82}; OD160 An_{58-71}). Pyroxene content is about 10% of total rock volume. They are magnesium-rich augites with enstatites in sample OD154. Both plagioclases and pyroxenes have embayed crystals and sometimes form glomerocrysts. Oxide phenocrysts represents ~ 5 modal %. The groundmass consists of microcrystalline plagioclase, pyroxene, opaques and a glassy matrix.

5.6.9 Whole Rock Chemistry

5.6.9.1 Major Elements

Only four samples of andesite have been analysed but all are relatively fresh as indicated by their small LOI (0.9-2.1 wt %). On the K_2O-SiO_2 diagram of Taylor *et al.* (1981) there appear to be two sub-groups: three samples falling in the calc-alkaline field and two falling in the high-K field (Figs. 5.34 and 5.35). Similar subsets of high-K and calc-alkaline rocks are known from Neogene volcanic centres elsewhere in the Halmahera arc (Hakim, 1989; E. Forde, pers. comm., 1994). Otherwise the four samples from the Guyuti Formation are typical of island arc andesites.

5.6.9.2 Trace Elements

The andesites have very similar patterns on the MORB-normalised trace element diagrams and resemble typical arc andesites (Fig. 5.36). They are enriched in K, Rb and Ba, depleted in Nb, and have sloping patterns for the more immobile elements, being relatively enriched in the elements Ce-Y and depleted in Ti. On most of the discriminant diagrams they plot in the calalkaline and volcanic arc fields (Figs. 5.37 and 5.39).

5.6.10 Depositional Environment

The Guyuti Formation is interpreted as a series of turbidites and subaqueous debris flows. These were derived from a volcanic source terrain with a vegetation cover providing the common carbonaceous material. The size of the clasts in parts of the sequence suggests a significant slope,

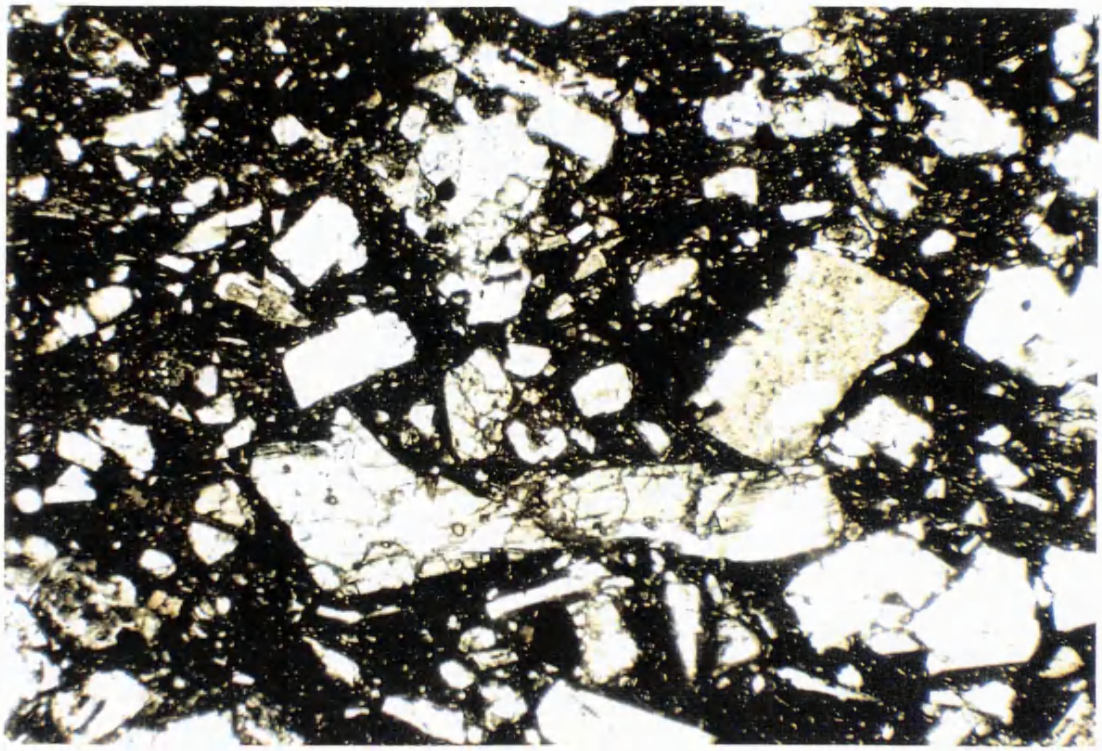

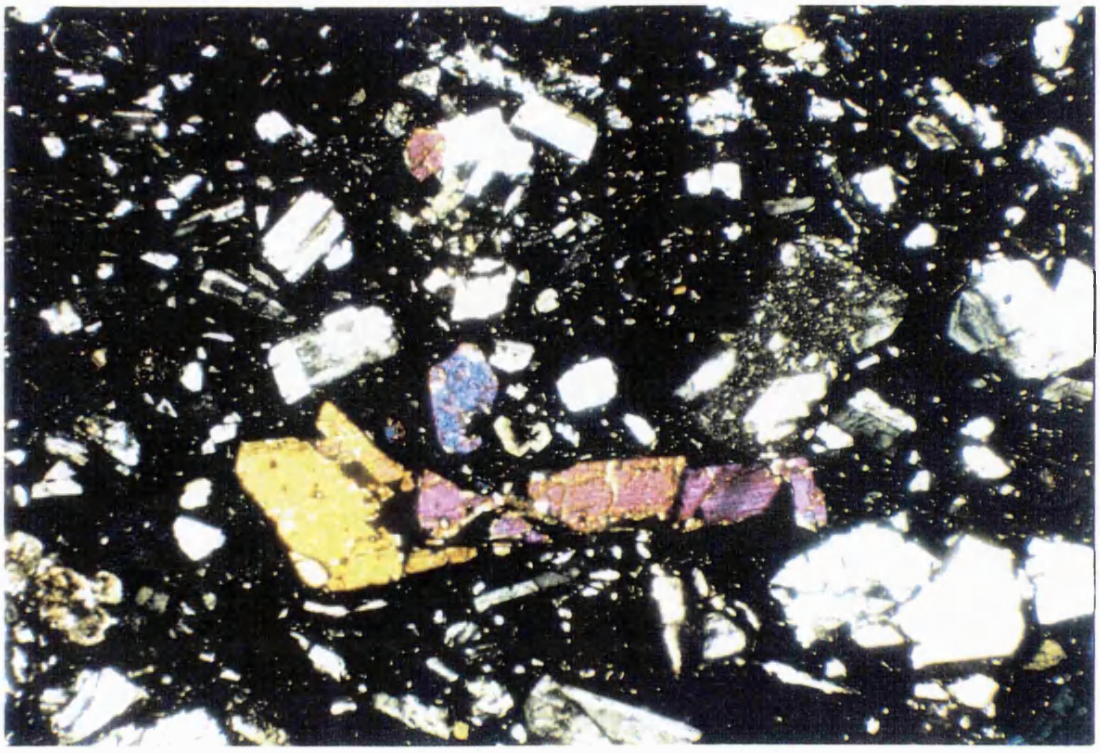

Fig. 5.33 A. (above) Photomicrograph of basalts (OD199) from the Guyuti Formation, containing clinopyroxene and plagioclase phenocrysts in a finer matrix. Plane polarised light. Width of photograph is 1.6 mm. B. (below) crossed polars.

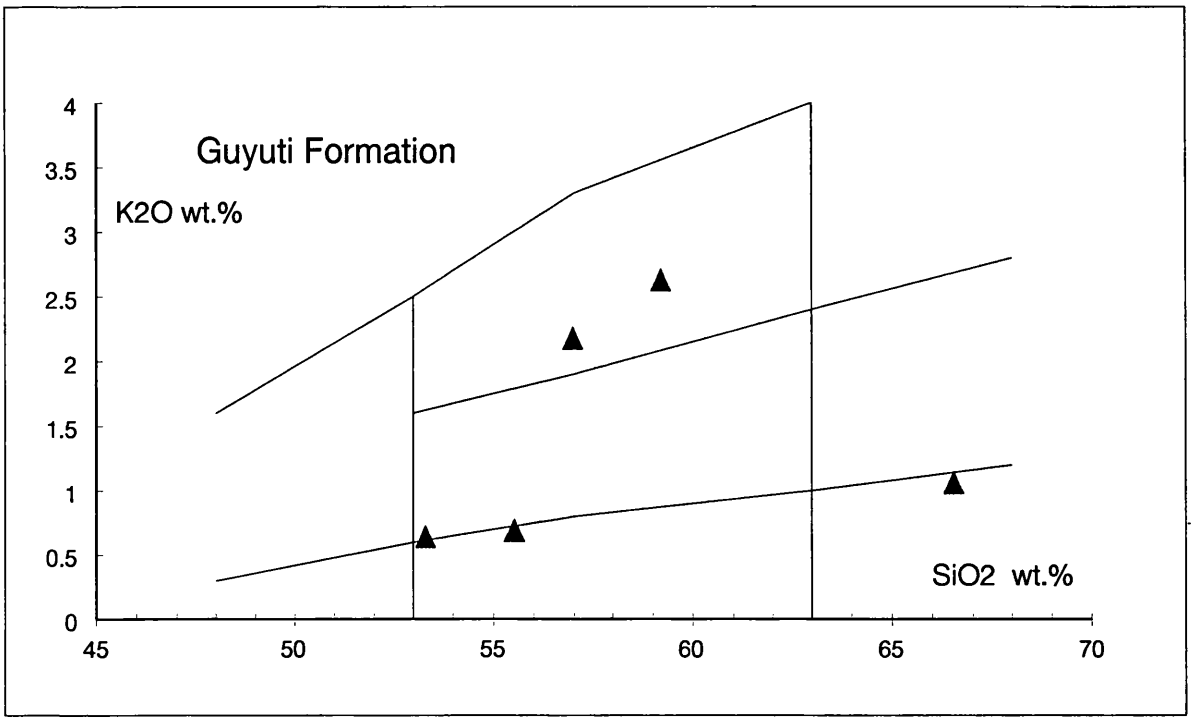

Fig. 5.34 Plot of K_2O versus SiO_2 for volcanic rocks of the Guyuti Formation. Compositional fields from Taylor *et al.* (1981).

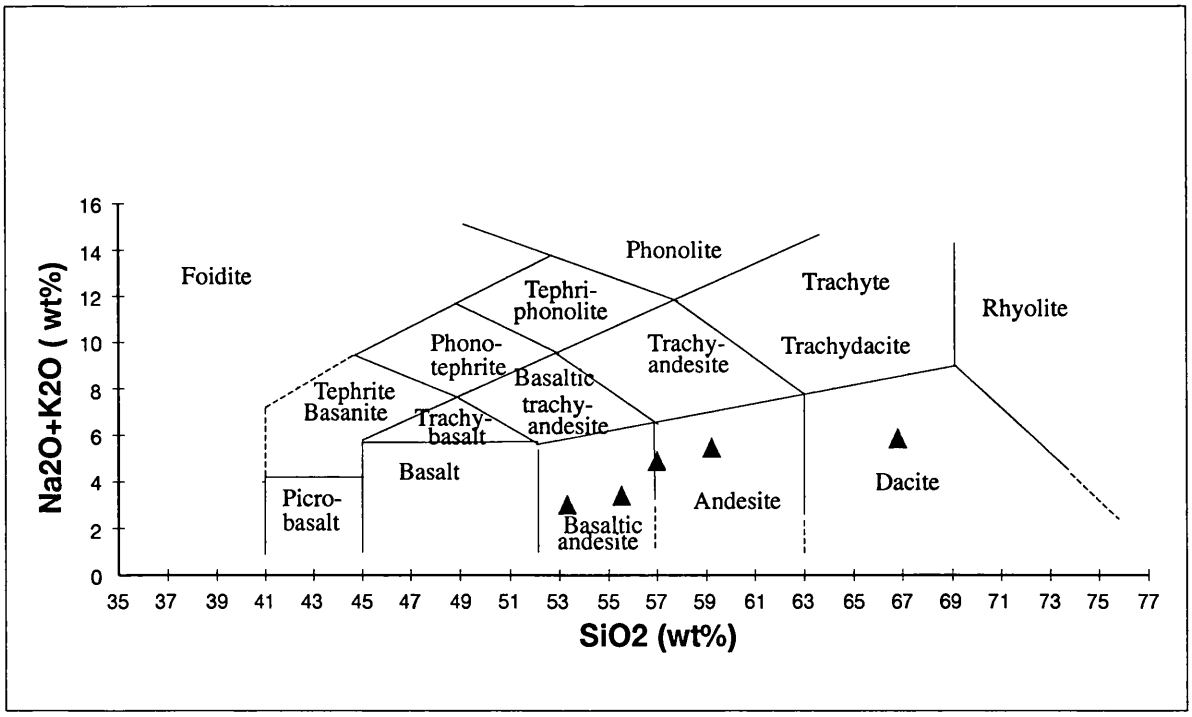

Fig. 5.35 Plot of Na_2O+K_2O versus SiO_2 for volcanic rocks of the Guyuti Formation. Compositional fields from Le Bas & Streckeisen (1991).

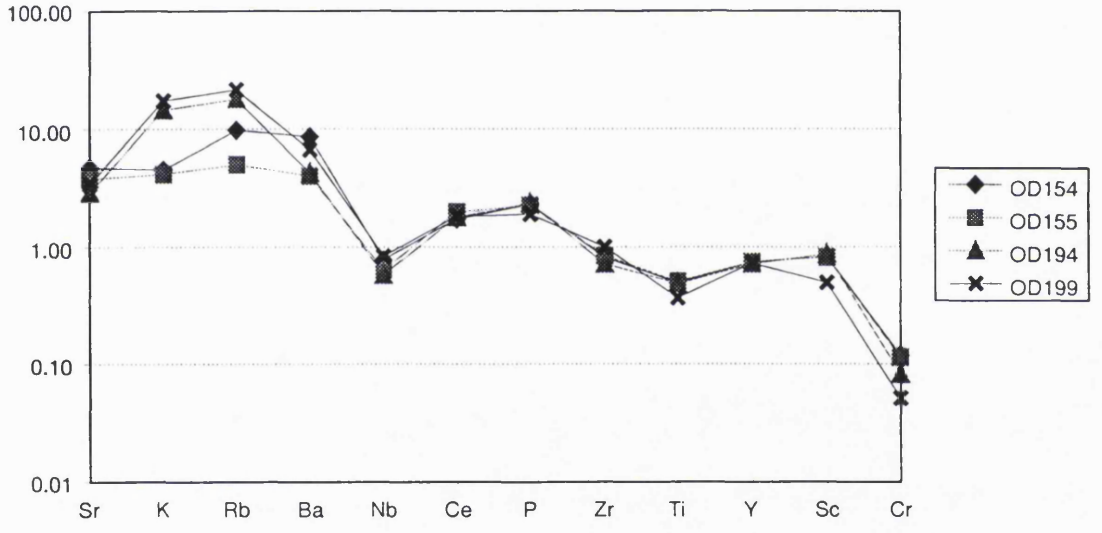

Fig. 5.36 MORB-normalised trace element spidergram for volcanic rocks of the Guyuti Formation. Normalising factors from Pearce et al. (1984).

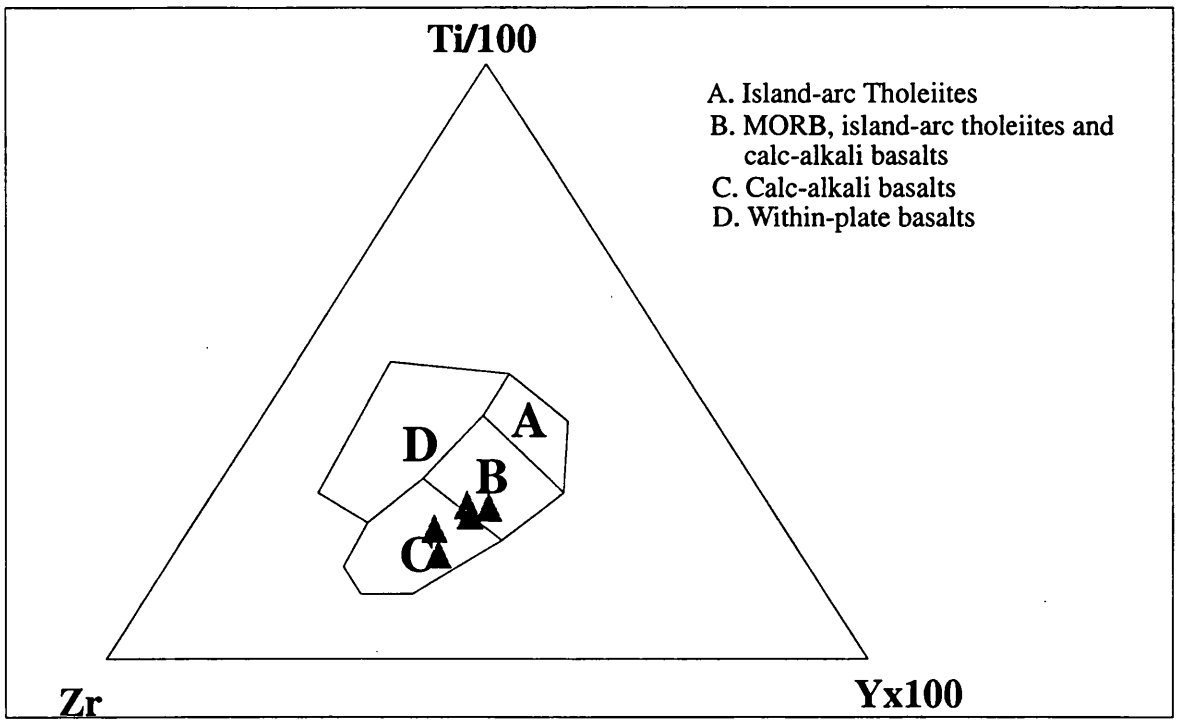

Fig. 5.37 Ti-Zr-Y disciminant diagram for volcanic rocks of the Guyuti Formation (after Pearce and Cann, 1973)

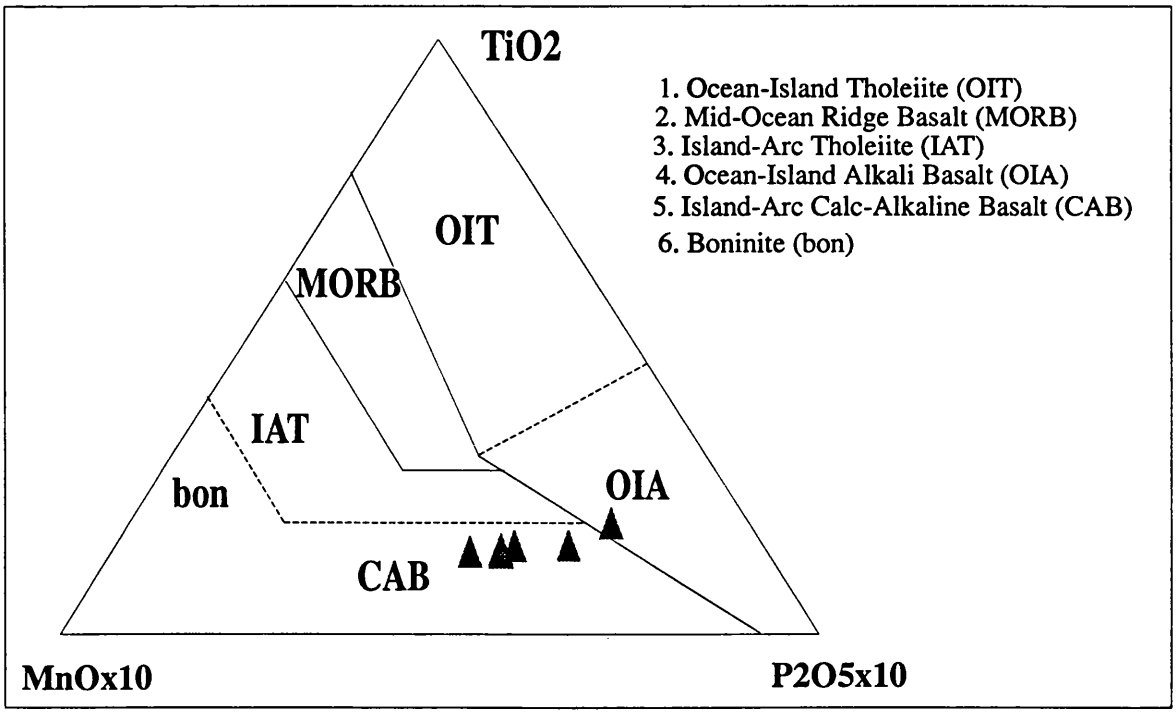

Fig. 5.38 Mn-Ti-P disciminant diagram volcanic rocks of the Guyuti Formation (after Mullen, 1983)

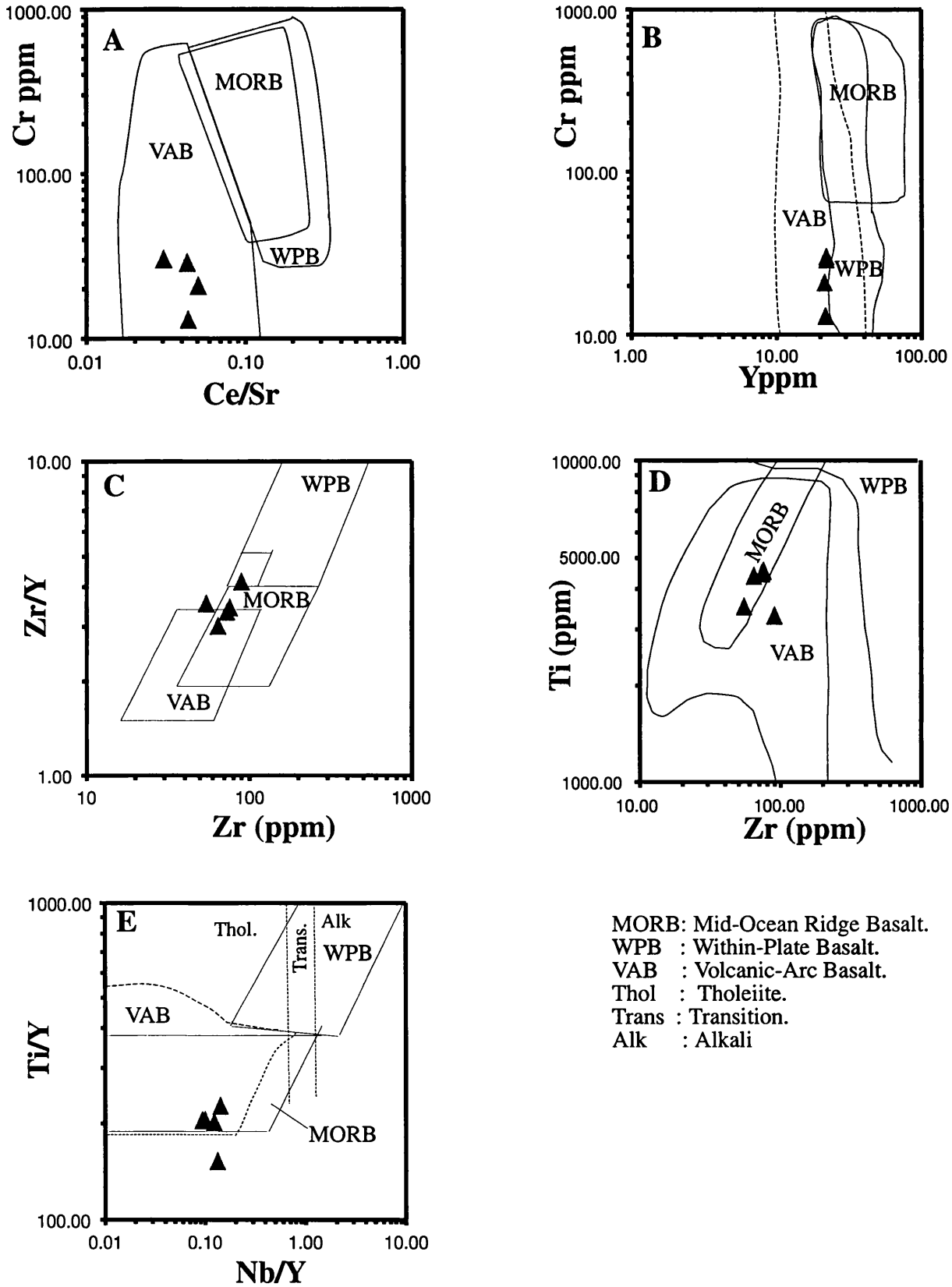

Fig. 5.39 Trace element covariation diagrams for volcanic rocks of the Guyuti Formation. A-Band D-E after Pearce (1982). C after Pearce and Nory (1979).

a considerable depth of water and a significant erosive force in order to move them. Between debris flows, quieter periods are represented by mudstones and burrowed tops to beds. From their position west of, and overthrust by, the Woi Formation the Guyuti Formation is considered to represent a proximal forearc deposit. This formation can probably be correlated with the Loku Formation in Halmahera.

5.7 Anggai Formation

The eastern part of Obi is occupied by shallow marine limestones which are characterised by a karst topography (Fig. 5.40).

5.7.1 Synonymy

This formation name was introduced by Sudana & Yasin (1983). According to their report, the age of this formation is about Late Miocene to Pliocene. Gondwana Company (1985) reported that this formation has a Pliocene to Pleistocene age and was deposited in shallow water environment.

5.7.2 Aerial Photography and Topographic Interpretation

The Anggai Formation forms a ridge which extends NW to SE along the northern coast where elevations reach 1000 m above sea level. On aerial photographs the Anggai Formation appears pale grey and has a karst surface with conical hills. These limestones can be separated easily from Quaternary limestones which are lighter grey and are terraced.

5.7.3 Type Section

Along the logging road from Kelo on the northeast coast, west of the Sesepe River. The lithologies consist of reef limestone and bioclastic limestone.

5.7.4 Age

Pliocene-?Pleistocene. The age of these limestones may vary; one nannofossil date (OR110) indicates an age range of Upper Miocene-Lower Pliocene; since the underlying volcanic and volcaniclastic rocks have yielded Upper Miocene to Lower Pliocene dates the Anggai Formation is considered to be Pliocene (-Pleistocene) in age. The formation is overlain with a sharp boundary visible from a distance and on aerial photographs by Quaternary limestones which have a different character.

5.7.5 Thickness

The thickness of this formation is approximately 200 m, deduced from geological cross section.

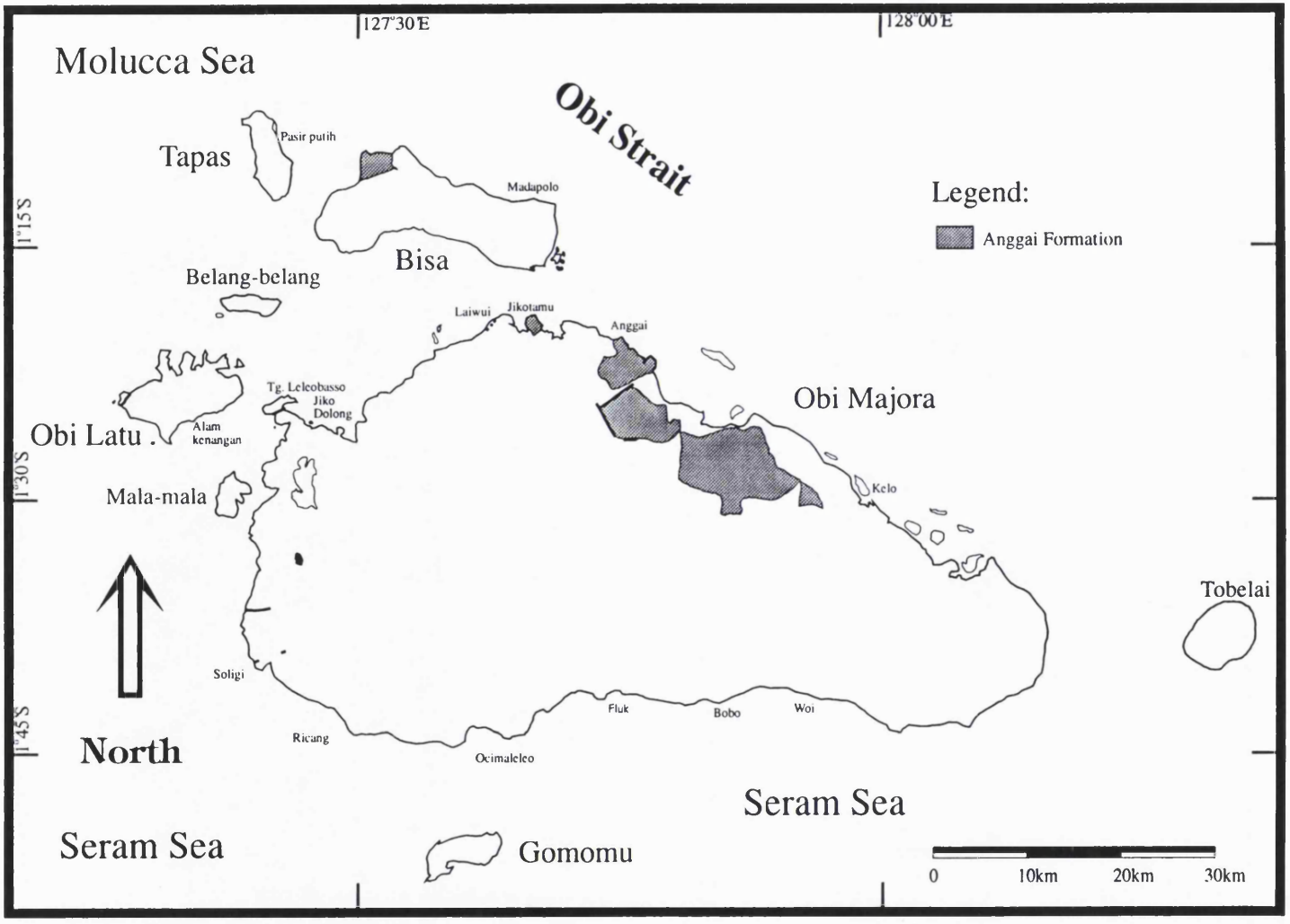

Fig. 5.40 Distribution of the Anggai Formation.

5.7.6 Distribution

This formation occupies are large area parallel to the coast of northeastern Obi Major (Fig. 5.40). A small area of limestones assigned to this formation are found in northwest Bisa Island.

5.7.7 Lower and Upper Contacts

The lower contact is an unconformity with older Neogene formations. The formation is unconformably overlain with a slight angular discordance by Quaternary limestones.

5.7.8 Description

In north Obi, unconformably on top of the volcaniclastic rocks, lie beds of shallow marine limestone. At the abandoned Kelo logging camp, 10 km from the coast, the base of the limestone is at over 300 m above sea level, but towards the coast in the east, the limestone is found at progressively lower elevations. This suggests that there is an offlap relationship between the limestones and the underlying rocks and that the limestones were deposited over a long period when the island of Obi was steadily emergent.

5.7.8.1 Petrography

No section was measured in this formation but samples were collected along the logging road. Microfacies study has enabled the limestone to be grouped into major types which reflect their depositional environment.

Coral skeletal packstones (OD20, OD22, OD163 and OD124) are composed of coralline algae, large bivalves, echinoids, planktonic and encrusting benthonic foraminifera, in a micritic matrix (Fig.5.41). These rocks are grain supported and poorly sorted. The matrix is micrite with ~5% sparite. A planktonic foraminiferal grainstone to packstone (OR105) is composed of ~60% bioclasts of planktonic foraminifera) in a micritic matrix. It is well sorted and grain supported. A benthonic foraminiferal packstone to wackestone (OR117) is composed of ~30% benthonic and planktonic foraminifera, coral fragments, and bryozoa, in a micritic matrix. It is poorly sorted and mud supported.

5.7.9 Depositional Environment

These rocks are interpreted as deposited in a foreslope, open marine environment with high to moderate energies. The existence of planktonic and benthonic foraminifera, coralline algae and echinoids indicates 10-100 m water depths, with a normal salinity environment.

5.8 South Obi Formation

Clastic sedimentary rocks, probably fluviatile to shallow marine in origin. Lithologies include conglomerates, sandstones and mudstones (Fig. 5.42)

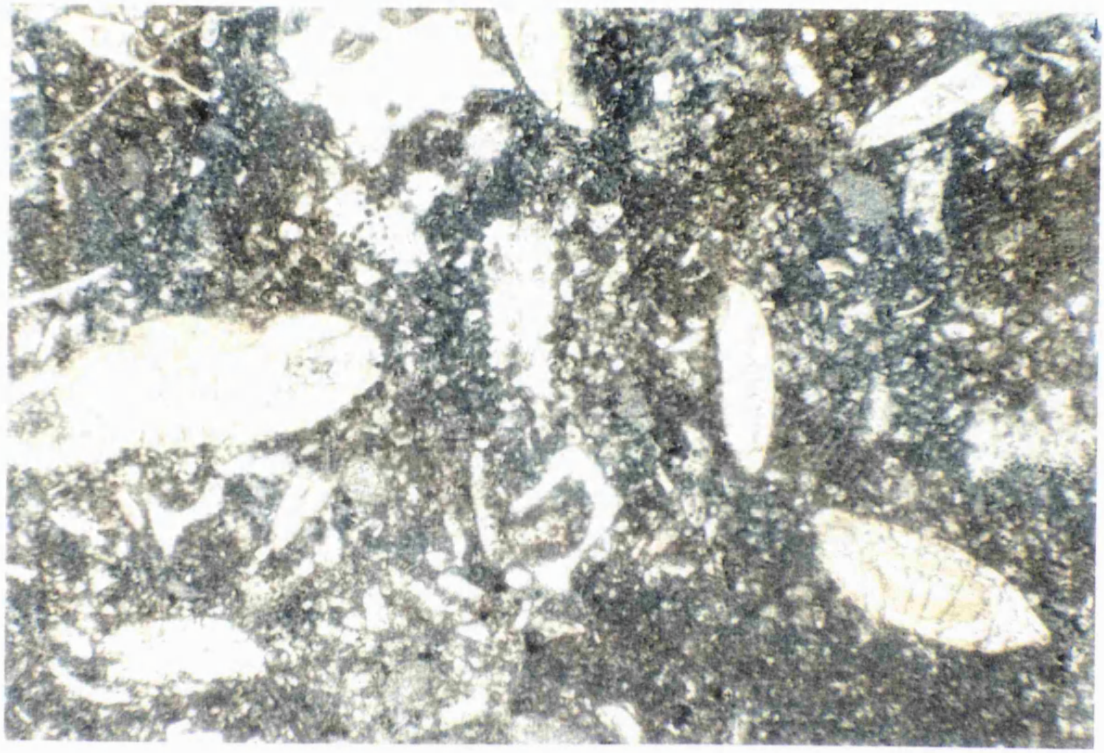

Fig. 5.41 Limestone from the Anggai Formation (OD124) from Kelo logging road containing shallow water debris including coral.

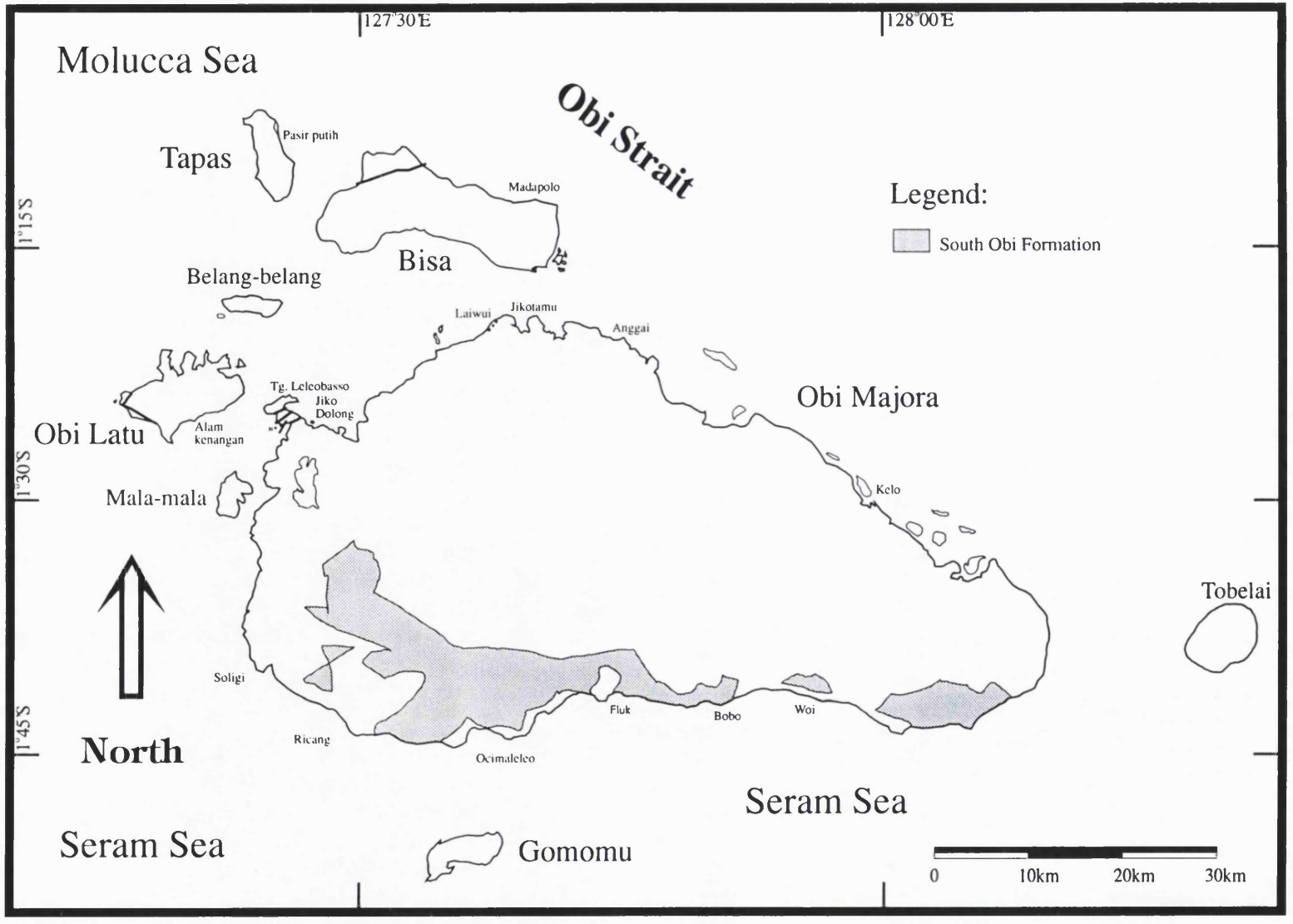

Fig. 5.42 Distrbution of the South Obi Formation.

5.8.1 Synonymy

This formation name is a new one. This formation was introduced by Hall *et al.* (1992). Previously, Sudana & Yasin (1983) and Gondwana Company (1985) had mapped these rocks as part of the Woi Formation.

5.8.2 Aerial Photography and Topographic Interpretation

On aerial photography this formation has a grey, rough but soft surface with a dendritic to rectangular drainage pattern. At higher elevations rocks are harder, probably calcareous conglomerates and sandstones, whereas at lower elevations they are softer and probably mainly siltstones and mudstones.

5.8.3 Type Section

South Obi along the logging road between Ricang and Airpati River.

5.8.4 Age

Pliocene-Pleistocene. One sample (OR100) dated using nannofossils yielded a Pliocene-Pleistocene age.

5.8.5 Thickness

No measured section has been done in this formation, but on the basis of geological cross sections it is estimated to be up to ~300 m thick.

5.8.6 Distribution

This formation is found in south Obi, where it extends parallel to the south coast from Ricang village until around Bobo village.

5.8.7 Lower and Upper Contacts

The lower contact is an unconformity with pre-Neogene and probably Neogene formations.

5.8.8 Description

Large areas of the pre-Neogene rocks in south Obi are overlain by a thick sequence of conglomerates and sandstones assigned to the South Obi Formation. These rest unconformably on Jurassic shales in SW Obi and on ophiolitic rocks in other parts of south Obi. The conglomerates appear to be fluviatile, possibly alluvial fan deposits. There is an overall gradual fining-up character to the formation. At the base of the formation there are coarse, poorly sorted boulder conglomerates but most of the formation is well bedded, with well rounded and generally well sorted clasts. Beds are typically ~1 m thick with clasts a few cm across with locally thicker beds up to 5 m with boulder sized clasts which are less well sorted. Almost all of the clasts in the

conglomerates are derived from the ophiolite (~75%) and the Leleobasso Formation (~20%), with a small proportion of soft sandstones, probably intraformational clasts. Fragments of Woi Formation volcanic rocks are notably absent as are clasts similar to the Anggai Formation limestones.

In most places the conglomerates are interbedded with sandstones but these constitute a relatively small proportion of the sequence, probably less than 20%. In some places the conglomerates show a crude normal grading and at the top of each bed are thin mudstones and a thin plant-rich organic layer which probably represent soils; there are several repetitions of these conglomerate-mudstone units, each about 1 m thick. Near the top of the formation the conglomerates are finer, and there is an increasing proportion of sandstone which is increasingly calcareous nearer to the top of the formation. Thin-medium bedded impure calcarenites are interbedded with conglomerates and sandstones near the top of the formation and contain abundant very large bivalves, small gastropods and ?echinoid fragments.

In most all places the sequence dips southward at 20-30° although there are locally steeper dips near the base of the formation and close to faults. In a few places dips are northward or the beds are subhorizontal suggesting large scale low amplitude open folds with approximately E-W fold axes. Near the coast the conglomerates are overlain by Quaternary limestones and in a few places the conglomerates are overlain unconformably by Quaternary boulder conglomerates and gravels which are largely composed of clasts reworked from the South Obi Formation.

5.8.9 Depositional Environment

The sequence appears to represent a largely terrestrial environment, probably an alluvial fan, with a marginal marine character close to the top of the formation. Samples were collected for dating but the conglomerates and sandstones which constitute the major part of the formation have proved difficult to date. The formation is definitely pre-Quaternary and has yielded one Pliocene age. The significant southward dips mirror the northward dip of the Anggai Formation in north Obi and suggest that this formation may be its age equivalent. If so the absence of Woi Formation clasts suggests that either there was a barrier to southward transport of material or that the Woi Formation has been eroded from south Obi before the deposition of the South Obi Formation.

5.9 Quaternary Limestone

Quaternary deposits have not been considered in any detail in this work, but where appropriate they have been included in mapping of the region. Quaternary limestones fall into two groups: uplifted masses of reef limestone presently exposed on land, and actively forming or very recently formed coral reefs which occur around the coastline. The appearance of the limestones is very distinctive on aerial photographs. The degree of uplift may be considerable;

locally over 100 m. It has not been possible to date these limestones precisely within the Quaternary and so rates of uplift and tilting cannot be determined. Wave-cut platforms of dead coral are locally present around coasts of all orientations. This indicates that uplift is going on at the present day, but the pattern of uplift and subsidence is not clear.

5.10 Quaternary Alluvium

The deposits of present day rivers and raised beach deposits form significant areas of alluvium throughout the area; in many cases controlled by young faults.

CHAPTER 6
STRUCTURE AND REGIONAL TECTONICS

6. STRUCTURE AND REGIONAL TECTONICS

6.1 Introduction

The islands of the Obi group lie at the boundary of three plates, the Philippine Sea, Molucca Sea and Australian plates, and within strands of the Sorong Fault system (Chapter 1). The Molucca Sorong Fault (Hamilton, 1979) separates Obi from the Bacan islands to the north, and the North Sula Sorong Fault separates Obi from the islands of the north Banda arc to the south.

The principal aim of this study was to establish the stratigraphy and large scale structures of the Obi region. Structural observations were made during this study but detailed structural studies, for example of microstructures, have not been made because of lack of time and because of limitations of exposures. In this thesis, the structural geology of Obi is summarised on the basis of mapping of fault structures, lineaments, and a number of small folds, based on aerial photographic interpretation, field mapping and interpretation of geological cross sections across the islands.

6.2 Structure

Fig. 6.1 shows the principal faults and lineaments identified from fieldwork and aerial photographic interpretation. Cross-sections illustrating the principal structures of the island are shown on Figs. 6.2 and 6.3. The major steep faults commonly have orientations between east-west and NW-SE, whereas less important steep lineaments have predominantly NE-SW directions. In most cases no sense of displacement can be determined directly, although in the case of several a large vertical displacement is clear. This need not preclude significant strike-slip displacement on these faults. Comparison with the geological map (Fig. 2.1) shows that many of these faults do not cut the boundaries between Quaternary rocks and older rocks, and that even where a fault does cut Quaternary contacts there is no significant displacement. These observations suggest that most of the faults are older than Quaternary. In contrast, significant offsets are interpreted on faults which cut Pliocene formations (the Anggai and South Obi Formations) indicating relatively young movements on many structures.

The cross-sections of Figs. 6.2 and 6.3 show the importance of thrusting in the structure of Obi. A major thrust separates the Woi Formation from the underlying Guyuti and the Anggai River Formations (all cross sections). The other major thrusts bring the Anggai River Formation and the ophiolite over the South Obi Formation (all cross sections). The formations involved in the thrusting include those well-dated as Upper Miocene to Lower Pliocene, indicating that the thrusting is younger than early Pliocene.

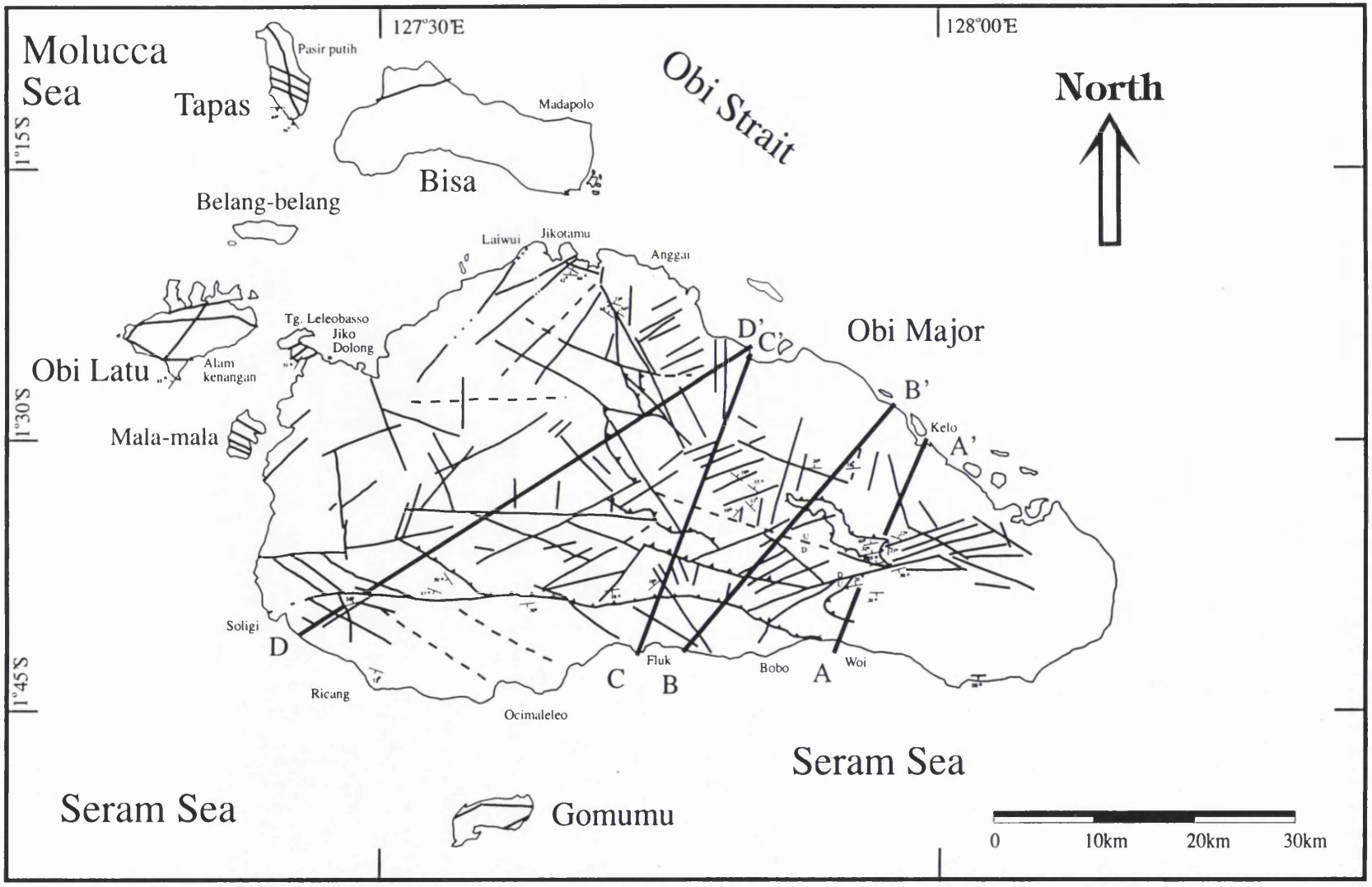

Fig. 6.1 Principal structures of the Obi islands based on this study.

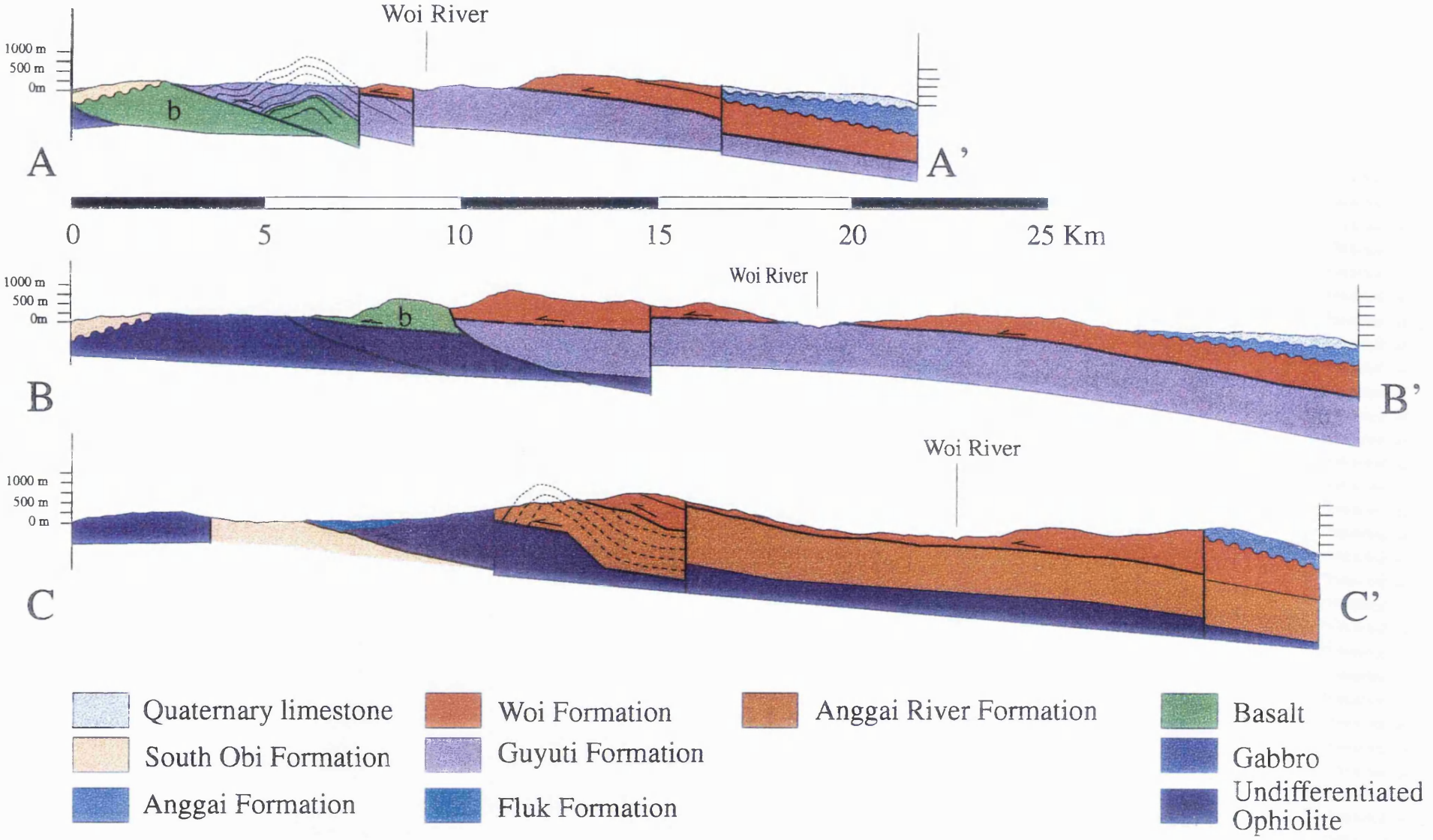

Fig. 6.2 Cross-sections of Obi Island. The location of the profiles are shown on Fig. 6.1

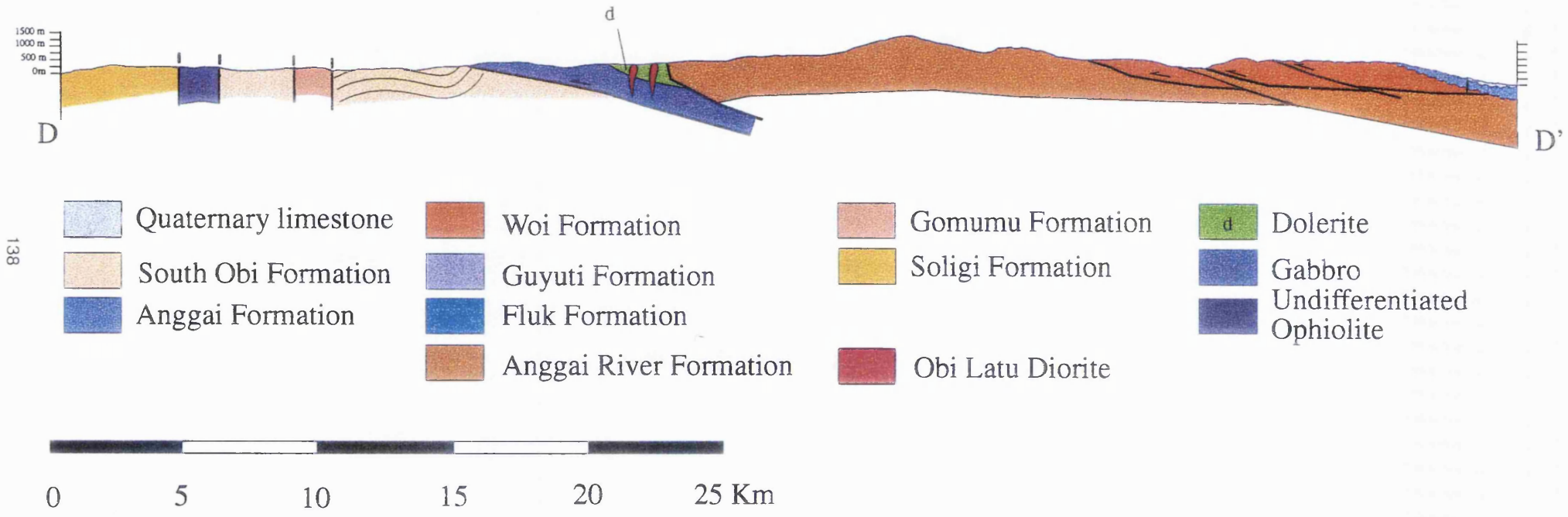

Fig. 6.3 Cross-section of Obi Island. The location of the profile is shown on Fig. 6.1.

There are few identifiable folds in the Obi region. Small ramp anticlines are associated with thrusting of the Guyuti Formation and Anggai River Formation (cross sections AA' and CC'). These folds have approximately east-west axial traces.

The direction of thrusting is uncertain but can be inferred from the orientation of the orientation of ramp anticlines to be south-directed. Normally, lateral ramps give a more precise indication of thrusting direction. One fault which appears to be a lateral ramp can be identified between sections C and B (terminating the ramp anticline in the Anggai River Formation at its east end), and a second truncates the east end of the Guyuti Formation window beneath the Woi Formation almost in the middle of section AA'. Both of these faults have orientations of about 060° and there are several other faults with similar orientations that terminate at their south ends in thrusts, suggesting they are lateral ramps. These therefore indicate thrusting parallel to 060°.

6.2.1 Cross sections

Four cross sections (Figs 6.2 and 6.3) have been drawn across the geological map of Obi from the south coast to north coast. These have been made for the purpose of estimating thicknesses of formations, understanding the contacts between each formation, and interpreting the structural geology of the island.

Cross section AA' is from Woi to Kelo and the section cuts the South Obi, Guyuti, Woi and Anggai Formations. At the southern end of the section the South Obi Formation unconformably overlies pillow basalt of the ophiolite. The thickness of this formation is at least 200 m. The Guyuti Formation is inferred to be thrust over the pillow basalts just west of the line of section. The logging road to the Woi River crosses a wide area of the Guyuti Formation which consists of alternating well bedded sandstone, siltstone and mudstone. An asymmetrical anticline with an approximately east-west axial trace is suggested by measurements of dips along the logging road and is interpreted as a ramp anticline above the thrust carrying the Guyuti Formation over the ophiolite. Further to the north, the section line crosses the steep fault forming a lateral ramp of the thrust sheet to the northwest in which the Guyuti Formation is overthrust by the Woi Formation which forms a narrow window trending WNW-ESE along the Woi River valley. North of this the Woi and Anggai Formations dip gently northwards.

Section BB' runs from the south coast close to Fluk northward to Kelo. The line of section BB' is closer to the inferred transport direction than section AA'. This section appears simpler and cuts the South Obi Formation, the ophiolitic rocks, the Guyuti, Woi and Anggai Formations, and Quaternary limestone. As on AA' the South Obi Formation unconformably overlies the ophiolite. Several thrusts are interpreted at the southern end of the section which are shown with listric character since they appear relatively straight on aerial photographs implying a steep near-surface dip. A thrust brings the Woi Formation over the Guyuti Formation which has an uncertain thickness, since it is exposed only exposed in the main Woi River and some tributaries, and its

base is not seen. The Anggai Formation is interpreted to be ~ 200 m thick and covered by Quaternary limestone which is at least ~25 m thick.

Section CC' is drawn from Fluk to the north coast and cuts almost all formations which are found in Obi Major. Ophiolites are found near the coast and form hills which are interpreted to be bounded by a steep fault to the north. Further north the South Obi Formation is not well exposed. It forms low-lying land and consist of almost horizontal light grey calcareous silty mudstones. The thickness of this formation is unknown. The ophiolitic rocks consist of peridotites, layered gabbros, dolerites and basalts which are exposed in the Fluk River. The Fluk Formation is interpreted to rest unconformably on the ophiolitic rocks, and has a gentle dip northward with a minimum thickness of ~ 100 m. Both the Fluk Formation and the ophiolitic rocks are interpreted as thrust south onto the South Obi Formation. The Anggai River Formation is interpreted from surface dips and aerial photographs to form a narrow east-west trending ramp anticline above a thrust which carries it over the ophiolite. The Anggai River Formation is in turn overthrust by the Woi Formation. Note that the Guyuti Formation is missing on this section as shown by mapping at the western edge of the Woi Formation outcrop area implying the Guyuti Formation thins westwards between sections BB' and CC'. At the northeast end of the section the Anggai Formation unconformably overlies the Woi Formation. The thickness of the Anggai River Formation is about 150 m.

Section DD' crosses the island from Soligi to the northeast coast. This section also cut almost all the formations which are found in the island: the Soligi, Gomumu, South Obi, Anggai River, Woi and Anggai Formations, Quaternary limestones, and ophiolitic rocks. There is no clear indication of the nature of the contact between the Soligi and Gomumu Formations (Chapter 3), or their contacts with the ophiolitic rocks further north. The continental rocks are poorly exposed but seem from aerial photographs to be restricted to steep fault-bounded zones trending WNW-ESE. E. Forde (1994, pers. comm.) reports that no continental material contaminates any of the volcanic rocks of the Woi Formation indicating that the continental rocks are not structurally below the ophiolite. This implies the steep faults separating the area of continental rocks in SW Obi from the remainder of the islands are strike-slip faults which represent splays of the Sorong Fault system with sinistral displacement. Further to the northeast, as the contact with the ophiolites is approached, the dip of the South Obi Formation increases to 50° below the thrust bringing the ophiolites south. The ophiolites are shown as part of a single thrust slice, with an uncertain geometry at depth, tectonically overlain by the Anggai River Formation. At the northern end of the section the Anggai River and Woi Formations are imbricated together.

6.2.2 Stratigraphic Considerations

Because of the lack of markers and the difficulty of structural work in rainforest the amount of shortening is difficult to assess. The nature of the original contacts between the Anggai River

Formation and the underlying ophiolites are uncertain and there could be an early Miocene thrust contact between them. The sections imply at least 20 km of Pliocene contraction although a fully balanced section is not possible. On stratigraphic grounds this seems likely to be a minimum estimate. The Woi Formation clearly represents a volcanic arc and includes rocks such as coals, and shallow water limestones representing periods of time, or places, without volcanic activity which were situated at or close to sea level. In contrast, the Guyuti Formation which is overthrust by the Woi Formation, but is its age equivalent, represents debris flow deposits and turbidites formed at the base of steep submarine slope, which by analogy with the Loku Formation of Halmahera (Nichols & Hall, 1991) represent a forearc sequence. Thus, during the Pliocene the Woi arc was thrust over its Guyuti forearc. The dimensions of present arc-forearc regions also suggest that the 20 km contraction inferred from cross-sections is likely to be a minimum.

6.3 Palaeomagnetic Rotations

Palaeomagnetic work carried out in the Obi region and areas around the Sorong Fault zone have been reported recently. The islands of Halmahera, Bacan, Obi and Waigeo form the southern boundary of the Philippine Sea plate (Ali & Hall, 1995). The islands in the area north of the Sorong Fault include the oldest rocks within the Philippine Sea plate and provide a record of Philippine Sea plate motion which can be used as a reference to distinguish local rotations within the Sorong Fault Zone. Hall *et al.* (1995a,b) have shown that the very large area north of the Sorong Fault system has a distinctive and consistent rotation history. There was approximately 40° of clockwise rotation after ~25 Ma at an approximately constant rate, no significant rotation between ~25 and ~40 Ma, approximately 45° of clockwise rotation between ~40 and ~50 Ma, and ~90° rotation between the Late Cretaceous and the Early Eocene.

In contrast to the area north of the Sorong Fault system, in north Obi Tertiary rocks record counter-clockwise rotations increasing with age whereas in south Obi sites record small clockwise rotations (Fig. 6.4). Sites in north and south Obi in the Woi Formation are of almost identical ages yet record quite different declinations. The geological mapping based on aerial photographs and fieldwork shows that these two groups of sites are separated by the WNW-ESE fault (dashed on Fig. 6.1) shown with a north-side-up displacement on sections AA', BB' and CC'. This fault post-dates thrusting, although it cannot be clearly traced through the flat area of Quaternary alluvium and limestones in SE Obi. There are several other young WNW-ESE faults and all are similar in orientation to Pliocene splays of the Sorong Fault system further north. Seismic lines (Hamilton, 1979; Letouzey *et al.*, 1983) and GLORIA data (Masson *et al.*, 1988) show that Obi is separated from the islands further north by a major submarine fault strand, the Molucca-Sorong Fault, and is bounded on its southern side by the North Sula-Sorong Fault. Thus, these faults may be linked to the Sorong system, implying left lateral motion as well as vertical offset. Ali & Hall (1995) consider it most likely that the differences in rotation history between parts of Obi and the

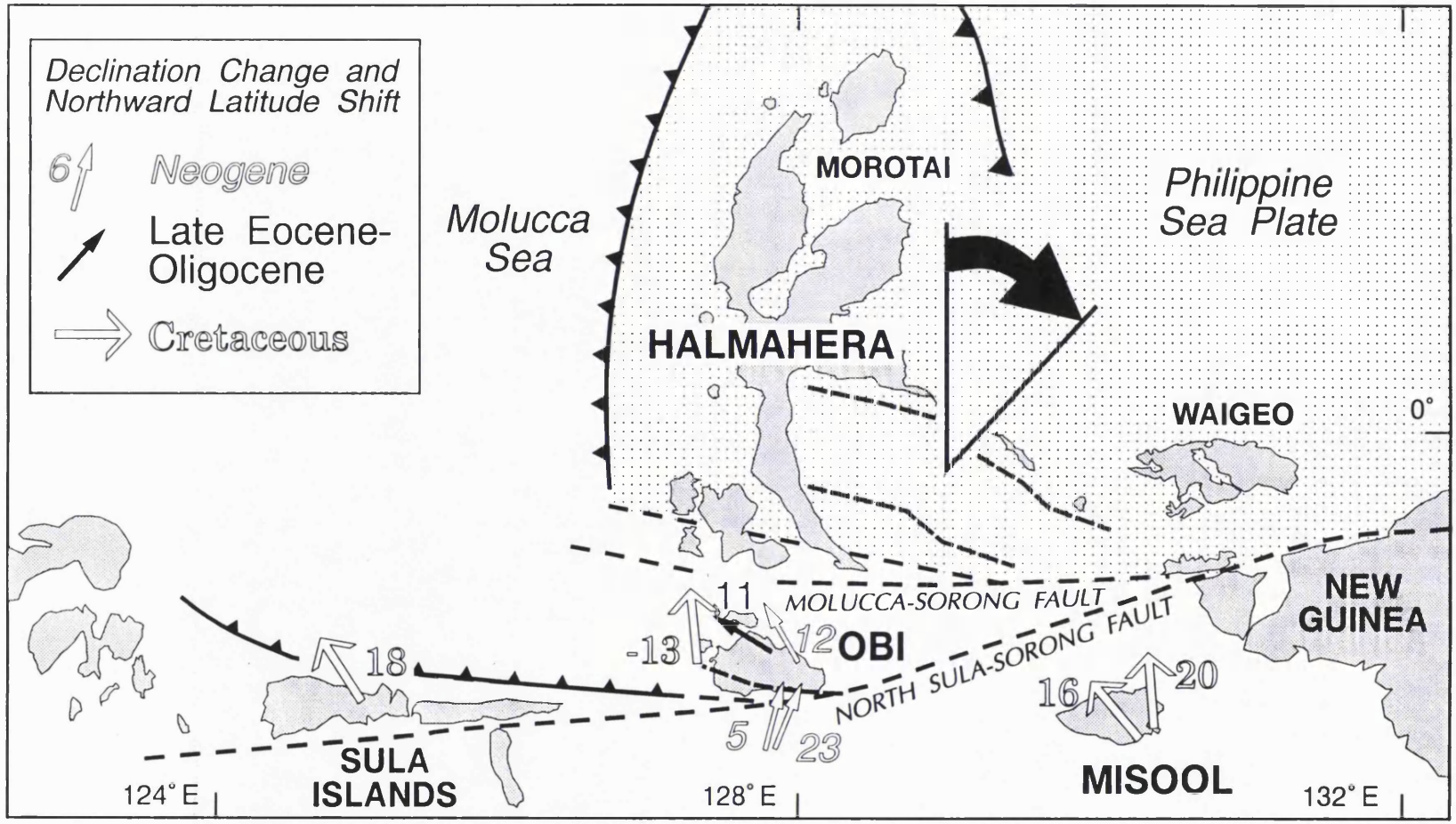

Fig. 6.4 Palaeomagnetic rotations in the Sorong Fault Zone, from Ali & Hall (1995).

Philippine Sea plate to the north are attributable to movements within the Sorong Fault system. The counter-clockwise rotations from sites in north Obi are consistent with shear in a left-lateral fault system. The clockwise rotations of other sites on Obi indicate that there have been significant local rotations on fault-bounded blocks within the Sorong Fault system and that these are likely to have been accommodated by the array of faults identified during this study of Obi.

6.4 Tectonic Evolution

To elucidate the tectonic development of the Obi region, the geology of each formation described earlier is first briefly summarised. Following this, an attempt will be made to synthesise these observations with regional tectonic events and the large scale tectonic evolution of eastern Indonesia to provide a model of the tectonic evolution of the Obi region.

6.4.1 Continental Crust

6.4.1.1 Tapas Metamorphic Complex.

The oldest rocks in the Obi region are thought to be the Tapas Metamorphic Complex. This complex resembles medium to high-grade metamorphic rocks on Bacan (Sibela Metamorphic Complex) of supposed Palaeozoic or greater age (Hamilton, 1979; Malaihollo, 1993; Vroon *et al.*, 1996). The Tapas Complex includes continental phyllites, schists, and gneisses of greenschist to amphibolite facies with a strong foliated fabric and with polyphase metamorphic fabrics, typical of regional metamorphism. Attempts at dating Sibela rocks by K-Ar and Ar-Ar methods yielded very young ages interpreted to be related to Neogene volcanic and hydrothermal activity (Malaihollo, 1993; Baker & Malaihollo, 1996). Hornblende-rich rocks of the Tapas Complex resemble probable cumulates of the Sibela ophiolitic suite which yielded isotopic ages of ~ 100 Ma interpreted as part of the Philippine Sea plate (Malaihollo, 1993).

All workers agree that the metamorphic rocks in Obi and Bacan represent Australian continental fragments brought from New Guinea although there are differences of opinion concerning their site of origin. Hamilton (1979) and Silver *et al.* (1985) derive these fragments from the Bird's Head whereas Pigram & Panggabean (1984) suggest an origin in central Papua New Guinea. Vroon *et al.* (1996) noted that their isotopic characteristics indicate derivation from a Proterozoic basement, not represented in present-day sediments derived from the Bird's Head region. The juxtaposition of the Tapas continental metamorphic rocks (splinters of the Australian plate) and parts of the Philippine Sea plate is thought to have occurred in the Neogene.

6.4.1.2 Soligi Formation

In southwest Obi the Soligi Formation consists of micaceous sandstone with *Pentacrinus* moulds indicating a Lower Jurassic age. This formation is considered part of the Australian continental margin which was displaced into south Obi via the Sorong Fault system. Unconformably beneath this formation may be the Tapas Metamorphic rocks.

6.4.1.3 Gomumu Formation

Other Mesozoic sedimentary rocks exposed in south Obi and on the north coast of Gomumu Island belong to the Gomumu Formation consisting of black shales and dark siltstones containing ammonite fragments, aptychi, belemnites and bivalves and deposited in an open marine setting. The formation is Middle-Upper Jurassic. The contact with the Soligi Formation was not found, but it is thought to be conformable.

6.4.2 Ophiolitic Basement Complex

Ophiolitic rocks are interpreted to be the basement of northern and central Obi. They include serpentinites, gabbros, dolerites, and pillow lavas interpreted as the oldest rocks of the Philippine Sea plate (Hall *et al.*, 1991, 1992). The presence of zeolites, calcite, epidote, chlorite and smectite in pillow lavas indicate these rocks have suffered ocean floor-type hydrothermal metamorphism of zeolite facies. In some dolerites and gabbros, pumpellyite-actinolite and epidote-actinolite facies assemblages are typical of that associated with submarine hydrothermal metamorphism. K-Ar dating of basalts, dolerites and gabbros yielded a wide range of ages from 15-84 Ma. Younger ages are thought to reflect reheating associated with Miocene-Pliocene volcanic activity. Other ages may also reflect older Tertiary and late Cretaceous volcanic activity recorded stratigraphically. Dolerite dykes on Gag similar to those of Obi are Upper Jurassic (Pieters *et al*, 1979; Hall *et al.* 1995b).

6.4.3 Cretaceous and Tertiary Sedimentary and Volcanic Rocks

6.4.3.1 Leleobasso Formation

The Leleobasso Formation probably lies unconformably above ophiolitic rocks. It comprises turbiditic volcaniclastic conglomerates, sandstones and mudstones which contain some calcareous fossils representing an arc-related sequence. Its age is Upper Cretaceous (Campanian-Maastrichtian). Later diorite intrusion caused mineralisation and hornfelsing.

6.4.3.2 Obi Latu Diorite

Diorites intrude the ophiolitic rocks and the Leleobasso Formation on Obi Latu and in parts of central Obi. These rocks comprise plagioclase, hornblende and quartz. Their age of formation is uncertain. They could be plutonic rocks associated with the Oligocene Anggai River Formation; this interpretation is based on K-Ar dating of sample OR66 (30-26 Ma). They could also represent early Tertiary or Cretaceous episodes of igneous activity as dated elsewhere in the region (Ballantyne, 1990; Baker, pers. comm. 1994).

6.4.3.3 Anggai River Formation

The Anggai River Formation consists of volcanic rocks with coarse to fine volcaniclastic sedimentary rocks probably deposited as turbidites in deep marine volcanic arc basin. Based on fossil contents this formation ranges from Middle Oligocene to Lower Miocene. This formation can be correlated with the Marikapal Member of the Tawali Formation of Bacan (Malaihollo,

1993), the Tawali Formation in NW Halmahera and the Rumai Formation in Waigeo (Hall *et al.*, 1992). The Anggai River, Tawali, Rumai and South Bacan Formations are arc-related volcanic and sedimentary sequences which record arc volcanism at the edge of the Philippine Sea plate due to the subduction of the leading edge of the Indian-Australian plate under the Philippine Sea plate (Hall *et al.* 1992; Malaihollo, 1993; Hall, 1996).

6.4.3.4 Fluk Formation

The Lower-Middle Miocene Fluk Formation probably lies unconformably above the Anggai River Formation and older rocks. Most limestones are packstones with subordinate wackestones and contain a diverse bioclastic assemblage. These represent deposition in a high energy environment on an open marine shelf, forming a shallow marine platform. The platform carbonates extend throughout the Bacan (Ruta Formation), Halmahera (Subaim Formation) and Waigeo (Waigeo Formation) region (Hall *et al.*, 1992). Uplift and erosion of a possibly more extensive carbonate platform on Obi has left only remnants of limestones and was followed by volcanic activity of the Woi Formation.

6.4.3.5 Woi and Guyuti Formations

The Woi Formation was deposited unconformably above the Fluk Formation. This formation consists of basalts and andesites, tuffs, agglomerate, conglomerates, breccias, sandstone, siltstone and mudstone with coal-bearing strata indicating a subaerial to marginal marine environment. The petrography, mineral chemistry, whole rock major and trace element chemistry of volcanic rocks are typical of island arc medium- to high-K calc-alkaline suites. The earliest volcanic activity began in the late Middle Miocene. The Guyuti Formation represents products of the same volcanic arc, deposited as debris flow and associated turbidites derived from a source area of volcanic rocks and shallow water limestones. The volcanic activity may have ceased in the late Miocene, but sedimentation appears to have been continuous in shallow marine settings with deposition of conglomerates, sandstones and mudstones which contain calcareous and carbonaceous material. In the Early Pliocene the volcanic arc was active again, forming volcanic rocks in the upper part of the Woi Formation. The Upper Woi Formation is considered similar to the Kaputusan Formation described from the Bacan region (Malaihollo, 1993). An important difference between the Neogene Kaputusan and Woi Formations is that $^{86}Sr/^{87}Sr$ and $^{143}Nd/^{144}Nd$ ratios show that the former has been contaminated by continental material, while the latter is typical of intra-oceanic arcs (E. Forde pers. comm. 1994).

6.4.3.6 Anggai Formation

The Anggai Formation lies unconformably above the Woi Formation. This is probably only a local unconformity. This formation consists of coral skeletal packstone, planktonic foraminiferal grainstones and benthonic foraminiferal packstones to wackestones. These represent deposition on

foreslope, forming part of a shallow marine carbonate platform. The deposition of the Anggai Formation is considered to have occurred between Late Pliocene and Pleistocene.

6.4.3.7 South Obi Formation

The South Obi Formation rests unconformably on Jurassic shales in SW Obi and on ophiolitic rocks in other parts of south Obi. It consists of polymict conglomerates, calcareous sandstone, calcareous siltstone and calcareous mudstone. The conglomerates commonly contain pebbles of ophiolitic rocks and Leleobasso Formation. It notably lacks clasts from the Woi Formation, and the Soligi and Gomumu Formations which are even closer to its present position. The position of the South Obi Formation, and its structure (section DD') suggests that it represents a foreland basin southwest of the advancing thrust sheet. The absence of Woi Formation debris would therefore reflect the northward dip of the thrust sheets and a similar topographic barrier to southward transport of Woi Formation debris as that of the present day. Currently, all rivers crossing the Woi Formation drain northwards or into the Woi River which emerges in SE Obi. Thus, the age of the South Obi Formation suggests deformation began in the mid to late Pliocene.

6.4.3.8 Quaternary deposits

Volcanic activity ceased in the Pliocene and currently there is no volcanic activity on the island. Quaternary deposits consist of alluvium and limestone. Quaternary limestone occurs along the coast and in northeast Obi is marked by terrace levels indicating recent uplift and emergence with a slight northeast dip.

6.5 Correlation with Regional Events

As noted above, the Obi region lies at the junction of three major plates: the Philippine Sea plate to the northeast, moving westward relative to Eurasia, the Eurasian plate (including the Molucca Sea plate) to the west, and the Indo-Australian plate including Irian Jaya and Misool, currently moving northeast.

6.5.1 Early Mesozoic

The upper Palaeozoic-Mesozoic sequences of the Australian continental margin record the start of break-up at about 230 Ma and post-break-up unconformity related to the initiation of sea floor spreading dated at about 185 Ma in Papua New Guinea and 170 Ma in Irian Jaya (Pigram & Panggabean, 1984). Subduction-related volcanism occurred in some places around SE Asia at this time. Rifting occurred between Burma and Australia and India and Antarctica which was followed by sea floor spreading in the Cretaceous (Parker & Gealey, 1983). The spreading of the Tethys Ocean III resulted in northward drift of continental fragments of northern Australia-central New Guinea (Audley-Charles *et al.*, 1988). The ophiolitic rocks of the north, NE and SE parts of Obi

are thought to be older than 94 Ma, and are possibly Jurassic. At this time they were situated somewhere in the Pacific region at sub-equatorial latitudes (J. R. Ali, pers. comm., 1995).

6.5.2 Mid Cretaceous to Late Cretaceous 100 - 70 Ma

The separation of Australia from Antarctica has been estimated as mid-Cretaceous (Veevers, 1988; Cande & Mutter, 1982) with slow spreading lasting until the Eocene (43 Ma) accompanied by early northward movement of Australia. In the Late Cretaceous, island arc volcanism occurred in what was to become the oldest part of the Philippine Sea plate. The ophiolitic rocks are interpreted to be overlain unconformably by Cretaceous volcaniclastic turbidite sediments and pelagic limestones of the Leleobasso Formation (Fig. 6.5) recording the activity of this arc.

6.5.3 Eocene - Oligocene 56 - 23 Ma

The Australian plate moved northward from 55 Ma (Early Eocene) and changed direction from northward to northeastward at approximately 45-42 Ma (Struckmeyer *et al.*, 1993). An Eocene regional unconformity may mark a 45 Ma plate reorganisation in the Pacific (Uyeda & Ben Avraham, 1972; Seno & Maruyama, 1984). On Obi an unconformity is inferred, based on observations elsewhere in the Halmahera region (Hall *et al.*, 1992), to separate Cretaceous arc rocks from the arc volcanic and volcaniclastic rocks of Oligocene age.

During the Oligocene there was an extensive arc throughout the Halmahera region, which was thought to include Obi and Bacan (Sukamto *et al.*, 1981). Arc activity occurred in Halmahera, Waigeo, and the Gauttier, Biak, Tosem and Yapen terranes of northern New Guinea (Struckmeyer *et al.*, 1993). The Oligocene-Lower Miocene Anggai River Formation is considered similar to the Tawali Formation in Bacan (Hall *et al.*, 1992). Both include volcaniclastic sediments (Fig. 6.6) which are products of repeated, high density and distal turbidity currents. These volcanic products were derived from a volcanic arc at the edge of the Philippine Sea plate produced by the subduction of the Indo-Australian plate under the Philippine Sea plate (Hall *et al.*, 1992; Malaihollo, 1993). The Obi Latu Diorite may represent the plutonic parts of the same arc, but also could be older. Diorites intrude the ophiolitic rocks and the Leleobasso Formation, but have not yet been found to intrude other formations including the Anggai River Formation.

6.5.4 Oligocene - Early Miocene ~22-15 Ma

The Cretaceous and Paleogene arc rocks are folded and overlain by Neogene limestones. This regional unconformity is considered to mark the collision of the Philippine Sea plate arc with the Australian margin (Hall *et al.*, 1992, 1995a,b; Ali & Hall, 1995). Volcanic activity ceased due to the ending of subduction of the Australian plate margin under the Philippine Sea plate. Continental crust on Obi could therefore be the result of the arc-continent collision but this hypothesis seems to be ruled out by the absence of evidence for continental contamination of

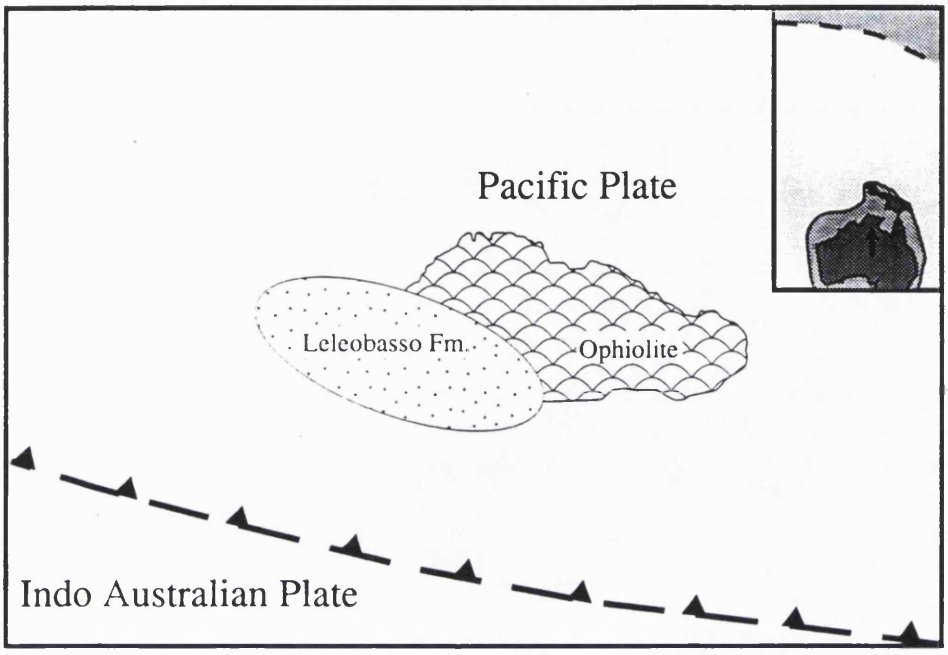

Fig.6.5. Simplified tectonic setting of the Obi region during the Middle to Late Cretaceous

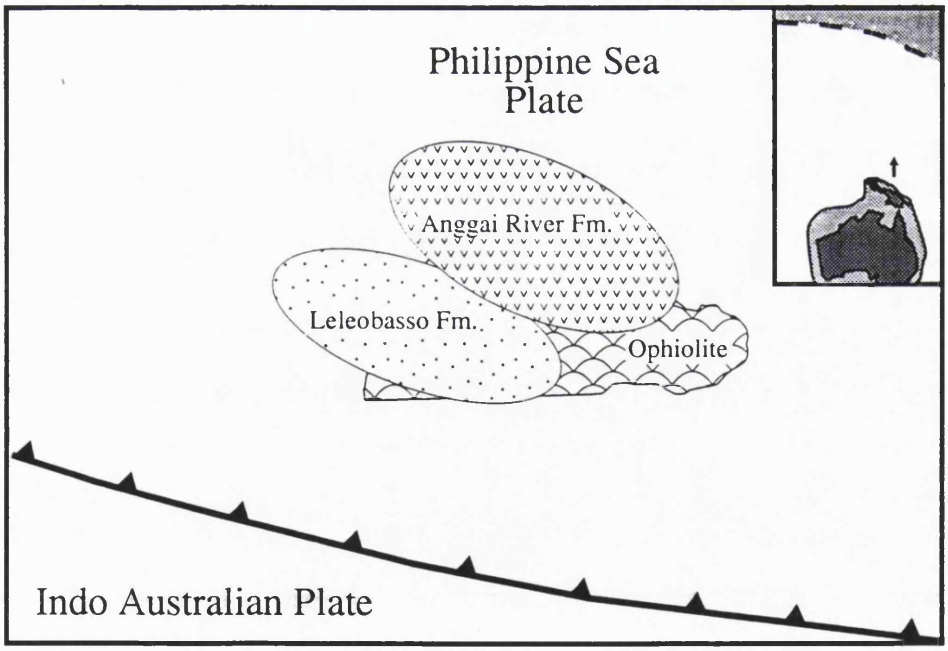

Fig.6.6. Simplified tectonic setting of the Obi region during the Late Oligocene to Early Miocene.

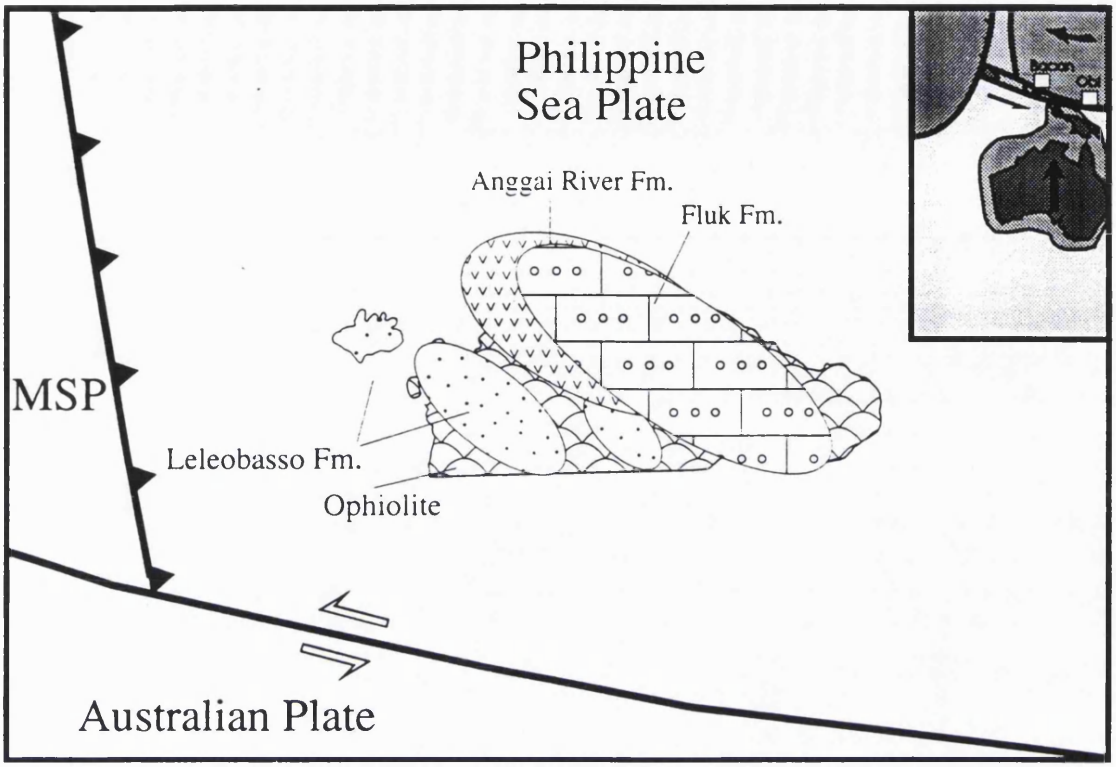

Fig.6.7. Simplified tectonic setting of the Obi region during the Early to Middle Miocene.
MSP : Molucca Sea Plate.

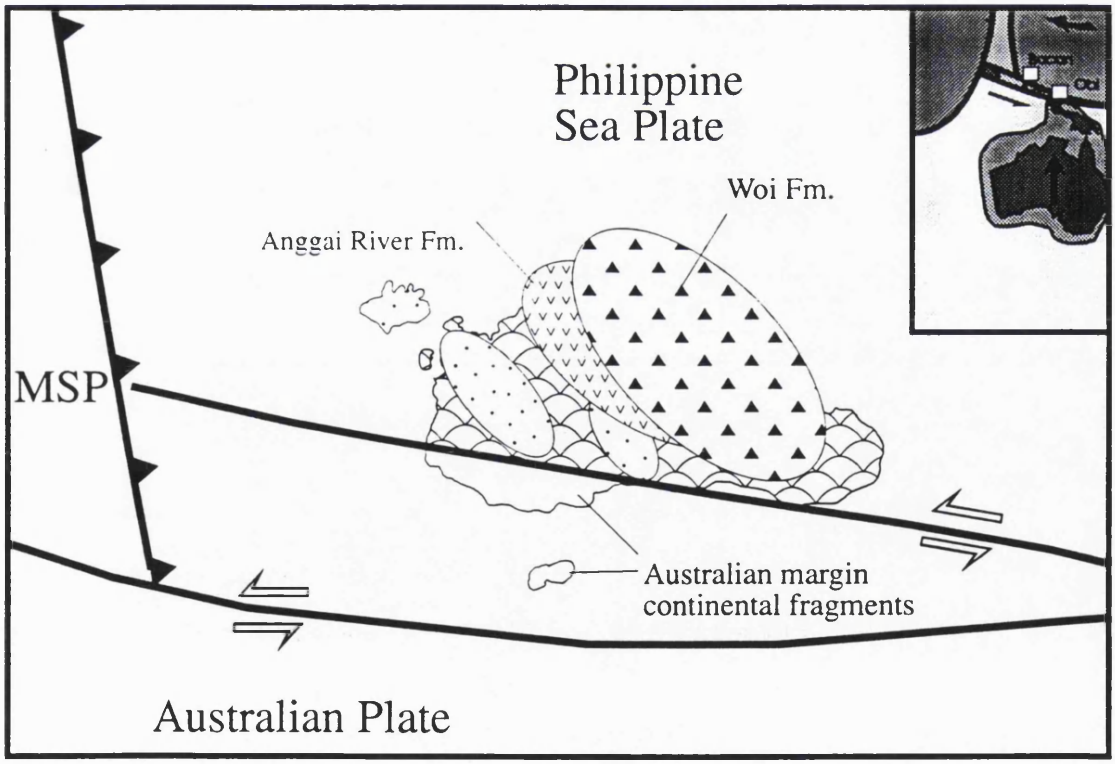

Fig.6.8. Simplified tectonic setting of the Obi region during the Late Miocene.
MSP : Molucca Sea Plate.

Neogene volcanics beneath north Obi (E. Forde, pers. comm., 1994). The plate boundary between the Australian and Philippine Sea plates changed to a left-lateral strike-slip fault at the beginning of the Neogene (Hall *et al.*, 1995; Hall, 1996). Hall *et al.* (1992) estimate the age of the unconformity initiating activity on the Sorong Fault as about 22 Ma (Oligocene-Miocene boundary) and since then there is evidence for movement of crustal fragments of Australian and Philippine Sea plate origin within the fault zone. Thus, continental crust could have arrived in Obi by movement on strands of the fault. Volcanic activity was succeeded by Early-Middle Miocene carbonate platform development represented on Obi by the Lower-Middle Miocene Fluk Formation (Fig 6.7).

6.5.5 Middle Miocene 15 Ma

In the late Middle Miocene the Halmahera arc was initiated, following the beginning of eastward subduction of the Molucca Sea plate under the Philippine Sea plate at about 15 Ma (Baker & Malaihollo, 1996). Carbonate deposition ceased. Parts of Obi were uplifted above sea level, eroding the carbonates; carbonate clasts of the Fluk Formation are found in the oldest parts of the Woi Formation.

6.5.6 Late Miocene - Early Pliocene 11 - 3 Ma

The Woi volcanic arc is interpreted as the product of the eastward subduction of the Molucca Sea plate under Halmahera, Bacan and Obi (the Philippine Sea plate). K-Ar dating indicates the Woi Formation volcanic arc was active on Obi from approximately 11 to 8 Ma and was active again from 4 to 3 Ma (Fig. 6.8). During periods of volcanic inactivity calcareous sedimentary rocks were deposited in shallow marine environments in northeastern Obi (Fig. 6.9). At the same time the Guyuti Formation was deposited by debris flows and turbidity currents in deeper water further south or southwest.

6.5.7 Late Pliocene to Present 3 - 0 Ma

Subduction of the Molucca Sea plate under Obi Island ceased. Ending of volcanic activity led to development of the Anggai Formation which consists of shallow marine limestones, particularly in northeast Obi, Bisa and Tapas Islands. It was probably at about this time that the Australian margin continental fragments were juxtaposed with the Philippine Sea plate crust in south Obi via a branch of the Sula Sorong Fault (Fig 6.10). Thrusting of the ophiolitic rocks and younger cover must have occurred at about this time, tilting the formations of north Obi such as the Pliocene-Pleistocene Anggai River Formation, and over-riding the South Obi Formation which are terrestrial to shallow marine products of erosion of older rocks (the ophiolitic rocks and the Leleobasso Formation). During the Quaternary uplift and erosion occurred in Obi.

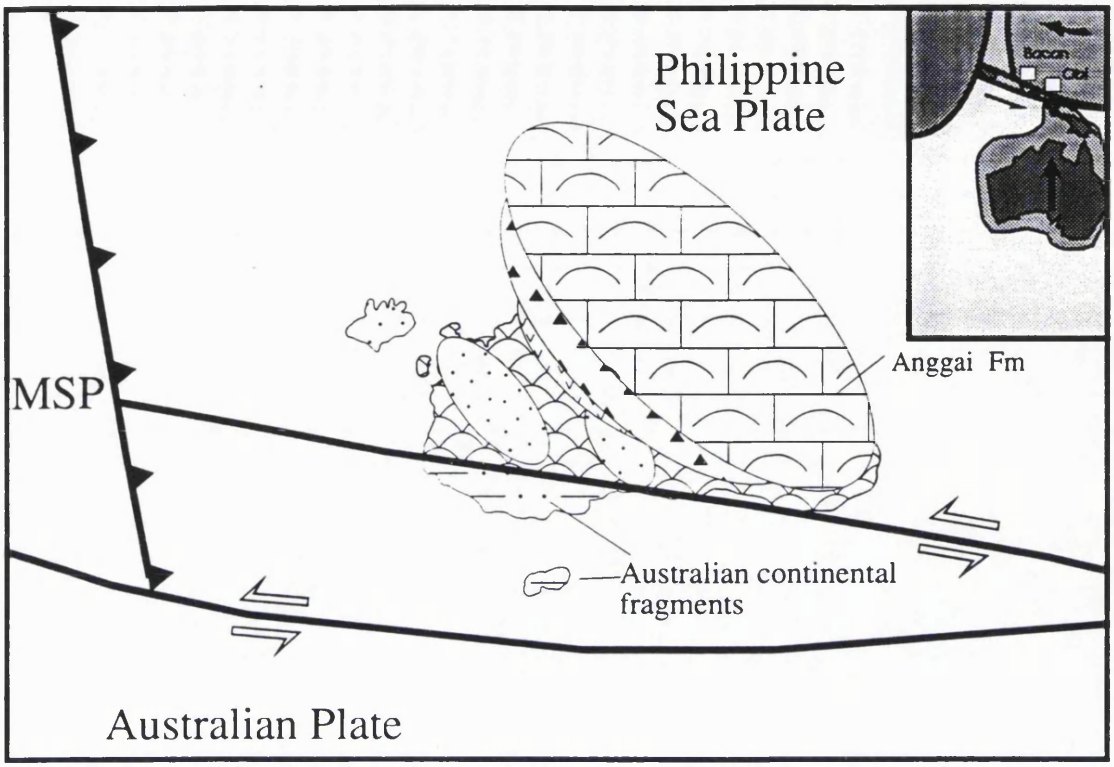

Fig.6.9. Simplified tectonic setting of the Obi region during the Early Pliocene.
MSP : Molucca Sea Plate.

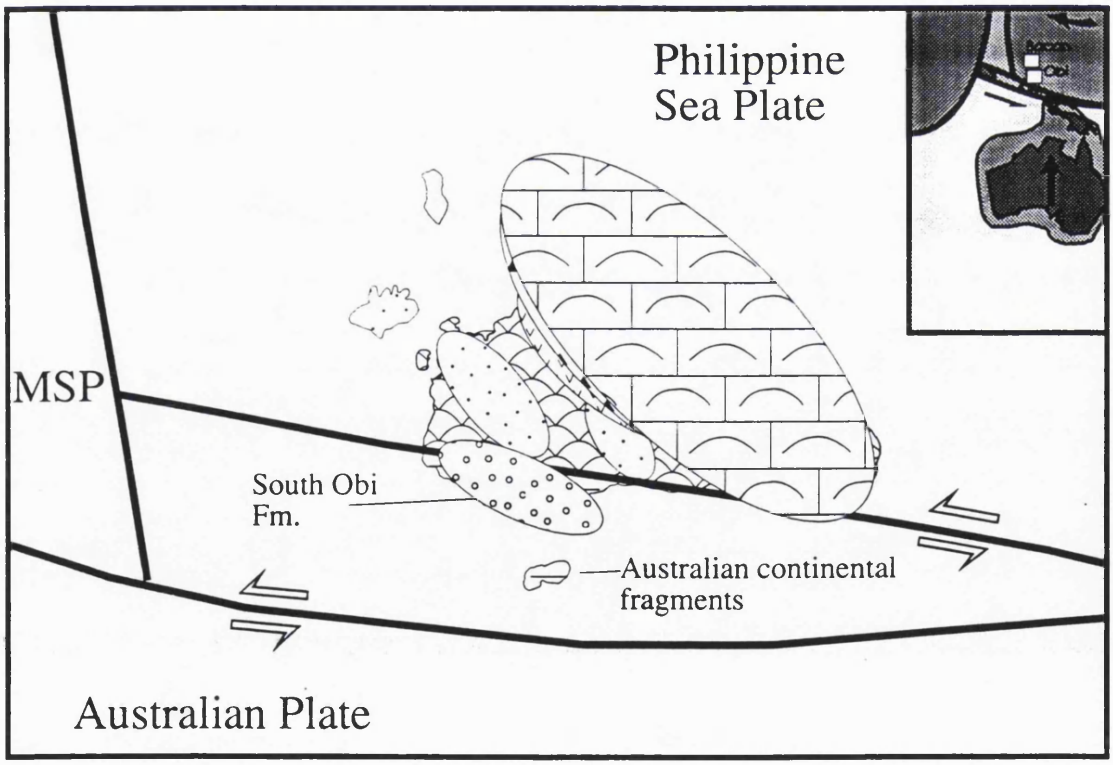

Fig.6.10. Simplified tectonic setting of the Obi region during the Late Pliocene to Pleistocene.
MSP: Molucca Sea Plate.

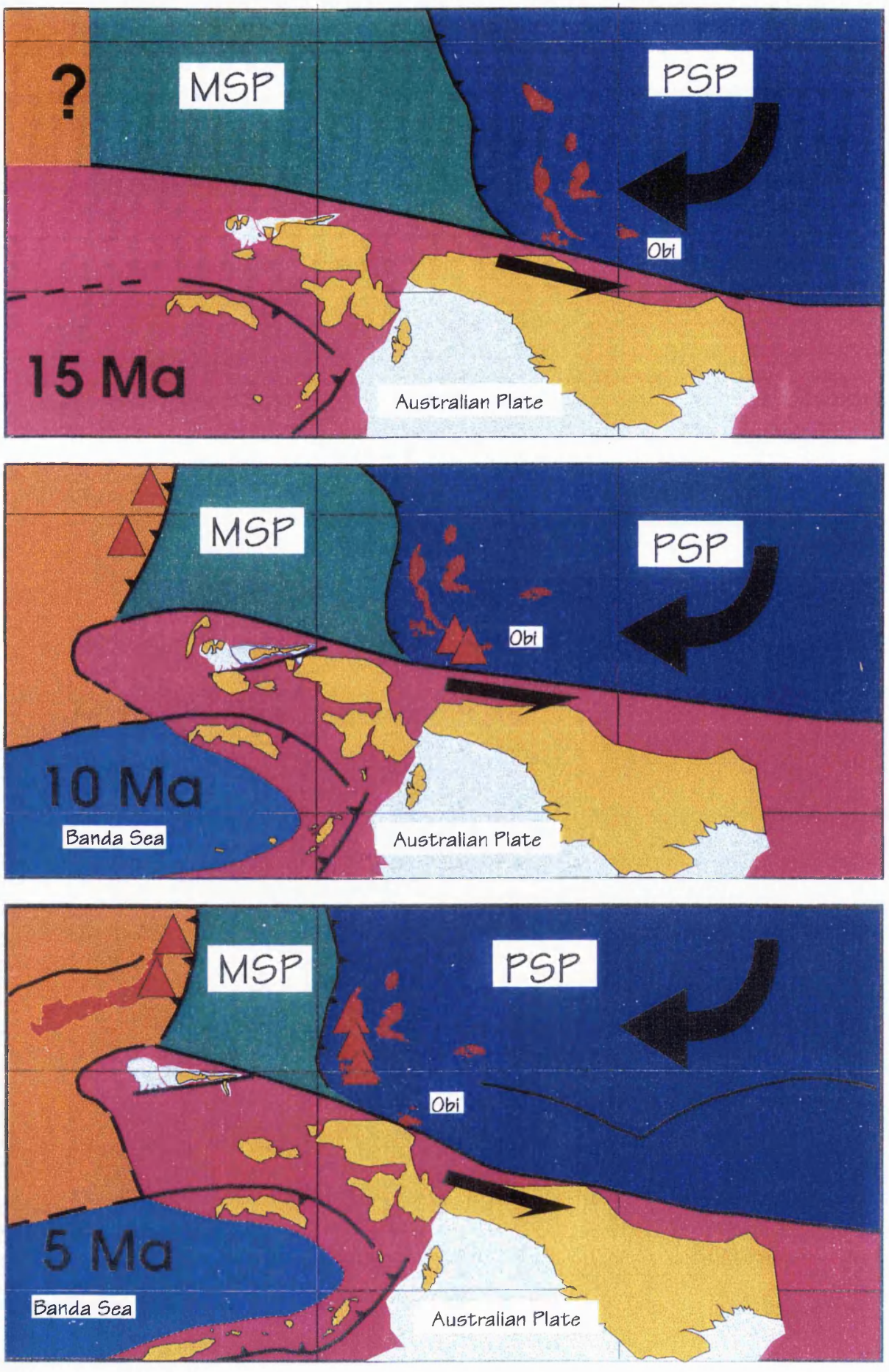

Fig. 6.11. Neogene tectonic development of the Obi region at the boundary of the Philippine Sea and Australian plates, modified from Hall (1996).

6.6 Conclusions

In tectonic models of eastern Indonesia the Sorong Fault occupies a critical position. This project was part of the investigation of the Sorong fault system initiated in 1992. As a result of this mapping a sound new stratigraphy for the island has been established providing the basis for palaeomagnetic work and isotopic work completed or in progress. Until recently there has been little evidence concerning the age of its initiation, the amount of displacement and the origin of fragments within the fault zone. The geological mapping of Obi has helped to identify several important features in the history of the region (Fig. 6.11).

- Similarities between the stratigraphies of east Halmahera, Waigeo and other islands of the North Moluccas, showing an older ophiolitic basement overlain by Cretaceous arc volcaniclastic and sedimentary rocks, consistent with a common origin as part of a single plate.
- The regional distribution of Oligocene-early Miocene arc rocks suggest this arc was part of the Philippine Sea plate and show that this Philippine Sea plate arc system collided with the Australian margin at about 25 Ma.
- Pliocene thrusting on Obi, as on Halmahera, has dramatically contracted the late Neogene arc, and on Obi carried the Woi arc over its own Guyuti forearc. The very young age of this thrusting was a great surprise.
- The new stratigraphy has provided the basis for mapping the distribution of different basement types using trace element and isotope geochemistry (E. Forde, in progress, 1995).
- New palaeomagnetic results show significant rotations implying movement of parts of Obi as separate fragments within the Sorong fault system. On a small scale Obi can be described as a terrane in the sense that it is now a relatively large fragment separated from the adjacent plates by splays of the Sorong Fault system.
- During the Neogene Obi moved north with the Philippine Sea Plate. At the same time the northern part of the island has rotated counter-clockwise whereas the southern part has rotated clockwise. Obi is a composite fragment, including crust of Philippine Sea Plate and Australian origin, and has been deformed within a shear zone marking the boundary between the plates.

Further work on Obi will be able to take advantage of this new stratigraphic and structural framework to further develop our understanding of this complex plate boundary.

References

7. REFERENCES

ALI, J. R. & HALL, R. 1995. Evolution of the boundary between the Philippine Sea Plate and Australia: palaeomagnetic evidence from eastern Indonesia. *Tectonophysics*, **251**, (1-4), 251-275.

AUDLEY-CHARLES, M. G., BALLANTYNE, P. D. & HALL, R. 1988. Mesozoic-Cenozoic rift-drift sequence of Asian fragments from Gondwanaland. *Tectonophysics*, **155**, 317-330.

BAKER , S. & MALAIHOLLO , J. 1996. Dating of Neogene igneous rocks in the Halmahera region: arc initiation and development. In: HALL, R. & BLUNDELL, D. J. (eds.) *Tectonic Evolution of SE Asia*. Geological Society of London Special Publication, **106**, 499-509.

BALLANTYNE, P. D. 1990. *The Petrology of the Ophiolitic Rocks of Eastern Halmahera, Indonesia*. Ph. D. Thesis, University of London. 263 pp.

BEARD, J. S. 1986. Characteristic mineralogy of arc-related cumulate gabbros: implications for the tectonic setting of gabbroic plutons and for andesite genesis. *Geology* **14**, 848-851.

BROUWER, H. A. 1924. Bijdrage tot de geologie der Obi-eilanden. *Jaarboek Mijnwesen Nederlandsch Oost-Indie 1923* **52**, 1-62.

CANDE, S. C. & MUTTER, J. C. 1982. A revised identification of the oldest sea-floor spreading anomalies between Australia and Antarctica. *Earth and Planetary Science Letters*, **58**, 151-160.

CARDWELL, R. K. & ISACKS, B. L. 1978. Geometry of the subducted lithosphere beneath the Banda Sea in Eastern Indonesia from seismicity and fault plane solutions. *Journal of Geophysical Research* **83**, 2825-2838.

CARDWELL, R. K., ISACKS, B. L. & KARIG, D. E. 1980. The spatial distribution of earthquakes, focal mechanism solutions and subducted lithosphere in the Philippine and northeastern Indonesian islands. In: HAYES, D. E. (ed.) *The tectonic and geologic evolution of South-east Asian seas and islands. American Geophysical Union Monograph* **23**, 1-35.

COX, K. G., BELL, J. D. & PANKHURST, R. J. 1979. *The Interpretation of Igneous Rocks*. George Allen and Unwin, 450 pp.

DALY, M. C., COOPER, M. A., WILSON, I., SMITH, D. G. & HOOPER, B. G. D. 1991. Cenozoic plate tectonics and basin evolution in Indonesia. *Marine and Petroleum Geology* **8**, 2-21.

DEER, W. A, HOWIE, R. A. & ZUSSMAN, J. 1966. *An Introduction to the Rock-Forming Minerals*. Longmans, 528 pp.

DOW, D. B. & SUKAMTO, R. 1984. Western Irian Jaya: the end-product of oblique plate convergence in the late Tertiary. *Tectonophysics* **106**, 109-139.

DUNHAM, R. G. 1962. Classification of carbonate rocks according to depositional texture. In: HAM, W. E. (ed.) *Classification of Carbonate Rocks*. American Association of Petroleum Geologists Memoir, **1**, 106-121.

FITCH, T. J. 1972. Plate convergence, transcurrent faults and internal deformation adjacent to South-east Asia and the Western Pacific. *Journal of Geophysical Research* **77**, 4432-4460.

FLÜGEL, E. 1982. *Microfacies Analysis of Limestones*. Springer-Verlag, Berlin, 633 pp.

GONDWANA COMPANY, 1984. *The Geology of Obi, Maluku*. Litbang EP Pertamina. Dinas Evaluasi & Pengembangan Geology, 99 pp.

GONDWANA COMPANY, 1985. *Geological map of Obi Island, North Maluku*. Appendix to *The Geology of Obi, Maluku*. Litbang Pertamina. Dinas Evaluasi & Pengembangan Geology.

HAKIM, A. S. 1989. *Tertiary Volcanic Rocks from the Halmahera Arc, Indonesia: Petrology, Geochemistry and Low Temperature Alteration*. M.Phil. Thesis, University of London, 292 pp.

HAKIM, A. S. & HALL, R. 1991. Tertiary volcanic rocks from the Halmahera Arc, eastern Indonesia. *Orogenesis in Action Proceedings, Journal of SE Asian Earth Sciences* 6, 271-287.

HALL, R. 1987. Plate boundary evolution in the Halmahera region, Indonesia. *Tectonophysics* **144**, 337-352.

HALL, R. 1989. *1989 Sorong Fault Zone Field Report*. University of London SE Asia Research Group, Report **81**, 9 pp.

HALL, R. 1992. *Expedition to the Molucca Sea 1992*. University of London SE Asia Research Group, Report **116**, 15 pp.

HALL, R. 1995. Plate tectonic reconstructions of the Indonesian region. *Proceedings of the Indonesian Petroleum Association 24th Annual Convention*, 71-84.

HALL, R. 1996. Reconstructing Cenozoic SE Asia. In: HALL, R. & BLUNDELL, D. J. (eds.) *Tectonic Evolution of SE Asia.* Geological Society of London Special Publication, **106**, 153-184.

HALL, R. & NICHOLS, G. J. 1990. Terrane amalgamation at the boundary of the Philippine Sea Plate. *Tectonophysics* **181**, 207-222.

HALL, R., AUDLEY-CHARLES, M. G., BANNER, F. T., HIDAYAT, S. & TOBING, S. L. 1988a. The basement rocks of the Halmahera region, east Indonesia: a Late Cretaceous-Early Tertiary forearc. *Journal of the Geological Society of London* **145**, 65-84.

HALL, R., AUDLEY-CHARLES, M. G., BANNER, F. T., HIDAYAT, S. & TOBING, S. L. 1988b. Late Paleogene-Quaternary Geology of Halmahera, Eastern Indonesia: initiation of a volcanic island arc. *Journal of the Geological Society of London* **145**, 577-590.

HALL, R., NICHOLS, G. J., BALLANTYNE, P. D., CHARLTON, T. & ALI, J. 1991. The character and significance of basement rocks of the southern Molucca Sea region. *Journal of SE Asian Earth Sciences* **6**, 249-258.

HALL, R., ALI, J. R., ANDERSON, C. D., BAKER, S., MALAIHOLLO, J. F. A., ROBERTS, S. J., FINCH, E., AGUSTIYANTO, D. A., MILSOM, J. S. & NICHOLS, G. J. 1992. *The Sorong Fault Zone Project: processes and rates of terrane amalgamation.* University of London SE Asia Research Group, Report **111**, 217 pp.

HALL, R., ALI, J. R. & ANDERSON, C.D. 1995a. Cenozoic motion of the Philippine Sea plate: palaeomagnetic evidence from eastern Indonesia. *Tectonics*, **14**, 1117-1132.

HALL, R., ALI, J. R. ANDERSON, C. D. & BAKER, S. J. 1995b. Origin and motion history of the Philippine Sea Plate. *Tectonophysics*, **251**, (1-4), 229-250.

HALL, R., FULLER, M., ALI, J. R. & ANDERSON, C. D. 1995c. The Philippine Sea Plate: Magnetism and Reconstructions. In: TAYLOR, B. & NATLAND, J. H. (eds.) *Active Margins and Marginal Basins: A Synthesis of Western Pacific Drilling Results.* American Geophysical Union Monograph, **88**, 371-404.

HAMILTON, W. 1979. Tectonics of the Indonesian region. *U. S. Geological Survey Professional Paper* **1078**, 345 pp.

HARTONO, H. M. S. & TJOKROSAPOETRO, S. 1984. Preliminary account and reconstruction of Indonesian terranes. *Proceedings of the Indonesian Petroleum Association 13th Annual Convention*, 185-226.

HATHERTON, T. & DICKINSON, W. 1969. The relationship between andesitic volcanism and seismicity in Indonesia, the Lesser Antilles and other island arcs. *Journal of Geophysical Research* **74**, 5301-5310.

HASTON, R. B. & FULLER, M. 1991. Paleomagnetic data from the Philippine Sea Plate and their tectonic significance. *Journal of Geophysical Research* **96**, 6073-6078.

JÄGER , E., CHEN, W. J., HURFORD, A. J., LIU, R. X., HUNZIKER, J. C. & LI, D. M. 1985. A Quaternary age standard for K-Ar dating. *Chemical Geology*, **52**, 275-279.

KUENEN, P. H. 1935. Contributions to the geology of the East Indies from the Snellius expedition. Part I. Volcanoes. *Leidsche Geologische Mededeelingen* **7(2)**, 273-331.

LE BAS , M. J. & STRECKEISEN, A. L. 1991. The IUGS systematics of igneous rocks. *Journal of the Geological Society of London*, **148**, 825-833.

LETOUZEY, J., DE CLARENS, J., GUIGNARD, J. & BERTHON, J-L. 1983. Structure of the North Banda-Molucca area from multichannel seismic reflection data. *Proceedings Indonesian Petroleum Association 12th Annual Convention 1983*, 143-156.

LOWE D. R. 1982. Sediment gravity flows: II. Depositional model with special reference to the deposit of high-density turbidity currents. In: *Sedimentary Environments and Facies.* READING, H. G. (ed.) 339-444. Scientific Publications. Second Edition. Blackwells, Oxford & London.

MALAIHOLLO, J. F. A. 1993. *The Geology and Tectonics of the Bacan Region, Eastern Indonesia.* Ph.D. thesis, University of London.

MARTIN, 1903. Jungtertiäre kalksteine von Batjan und Obi. *Samml. Geologisch. Reichsmuseum*, **1(7)**, 225-230.

MASSON, D. G., DWIYANTO, B., KALLAGHER, H., MILSOM, J. S. NICHOLS, G. J., PARSONS, L. & SIKUMBANG, N. 1988. Active margin tectonics in eastern Indonesia - a study with GLORIA and underway geophysics. *Institute of Oceanographic Sciences Cruise Report*, **202**, 20 pp.

MOORE, G. F., KADARISMAN, D., EVANS, C. A. & HAWKINS, J. W. 1981. Geology of the Talaud Islands, Molucca Sea collision zone, northeast Indonesia. *Journal of Structural Geology* **3**, 467-475.

MORRIS, J. D., JEZEK, P. A., HART, S. R. & GILL, J. B. 1983. The Halmahera island arc, Molucca Sea collision zone, Indonesia: a geochemical survey. *In:* HAYES, D. E. (ed.) *The tectonic and geologic evolution of South-east Asian seas and islands. Part 2. American Geophysical Union Monograph* **23**, 373-387.

MULLEN, E. D. 1983. $MnO-TiO_2-P_2O_5$: a minor element discriminant for basaltic rocks of oceanic environments and its implications for petrogenesis. *Earth and Planetary Science Letters*, **62**, 53-62.

NICHOLS, G. J. & HALL, R. 1991. Basin formation and Neogene sedimentation in a backarc setting, Halmahera, eastern Indonesia. *Marine and Petroleum Geology*, **8**, 50-61.

NICHOLS, G. J., HALL, R., MILSOM, J., MASSON, D., PARSON, L., SIKUMBANG, N., DWIYANTO, B. & KALLAGHER, H. 1990. The southern termination of the Philippine Trench. *Tectonophysics* **183**, 289-303.

PARKER, E. S. & GEALEY, W. K. 1983. Plate tectonic evolution of the western Pacific-Indian Ocean region. In*: Geology and Hydrocarbon Potential of the Soputh China Sea and Possibilities of Joint Development.* Proceedings of the "nd EAPI/CCOP Workshop, 249-261.

PEARCE, J. A. & CANN, J. R. 1973. Tectonic setting of basic volcanic rocks determined using trace element analysis. *Earth and Planetary Science Letters*, **19**, 290-299.

PEARCE, J. A. & NORRY, M. J. 1979. Petrogenetic implications of Ti, Zr, Y and Nb variations in volcanic rocks. *Contributions to Mineralogy and Petrology*, **69**, 33-47.

PEARCE, J. A., LIPPARD, S. J. & ROBERTS, S. 1984. Characteristic and tectonic significance of supra-subduction zone ophiolites. In: KOKELAAR, B. P. & HOWELLS, M. F. (eds.) *Marginal Basin Geology: Volcanic and Associated Sedimentary and Tectonic Processes in Modern and Ancient Marginal Basins.* Geological Society of London, Special Publication **16**, 77-94.

PIETERS, P. E., RYBURN, R. J. & TRAIL, D. S., 1979. *Geological reconnaissance in Irian Jaya, 1976 and 1977.* Geological Research and Development Centre, Indonesia, unpublished report: 1979/19.

PIGRAM, C. J. & PANGGABEAN, H. 1984. Rifting of the northern margin of the Australian continent and the origin of some microcontinents in Eastern Indonesia. *Tectonophysics* **107**, 331-353.

SENO, T. & MARUYAMA, S. 1984. Paleogeographic reconstruction and origin of the Philippine Sea. *Tectonophysics*, **102**, 53-84.

SILVER, E. A. & MOORE, J. C. 1978. The Molucca Sea collision zone, Indonesia. *Journal of Geophysical Research* **83**, 1681-1691.

SILVER, E. A. & SMITH, R. B. 1983. Comparison of terrane accretion in modern Southeast Asia and the Mesozoic North American cordillera. *Geology* **11**, 198-202.

SILVER, E. A., GILL, J. B., SCHWARTZ, H., PRASETYO, H. & DUNCAN, R. A. 1985. Evidence for a submerged and displaced continental borderland, north Banda Sea, Indonesia. *Geology*, **13**, 687-691.

SOERIA ATMADJA, R. 1981. Ophiolites in the Halmahera paired belts, East Indonesia. *In:* BARBER, A. J. AND WIRIOSUYONO, S. (eds.) *The Geology and Tectonics of Eastern Indonesia. Geological Research and Development Centre Bandung, Indonesia, Special Publication* **2**, 363-372.

STRUCKMEYER, H. I. M., YEUNG, M. & PIGRAM, C. J. 1993. Mesozoic to Cainozoic plate tectonic and palaeogeographic evolution of the New Guinea Region. In: CARMAN, G. J. AND CARMAN, Z. (eds.) *Proceedings of the Second Papua New Guinea Petroleum Convention, Port Moresby*, 261-290.

SUDANA, D. & YASIN, A., 1983. Geological map of the Obi quadrangle, North Maluku. Geological Research and Development Centre Bulletin (Indonesia).

SUKAMTO, R., APANDI, T., SUPRIATNA, S. & YASIN, A. 1981. The geology and tectonics of Halmahera Island and surrounding areas. *In:* BARBER, A. J. AND WIRYOSUJONO, S. (eds.) *The Geology and Tectonics of Eastern Indonesia.* Geological Research and Development Centre, Bandung, Indonesia, Special Publication **2**, 349-362.

TAYLOR, S. R., ARCULUS, R., PERFIT, M. R. & JOHNSON, R. W. 1981. Island arc basalts. *In: Basaltic volcanism on the terrestrial planets: Basaltic volcanism study project.* Pergamon Press, New York, 193-213.

THIRLWALL, M. F. & MARRINER, G. F. 1986. *A guide to Rock Analysis using the Philips PW1400 X-ray Fluorescence Spectrometer.* Unpublished Report, Department of Geology, Royal Holloway and Bedford New College, University of London.

TOMASSON, J. & KRISTMANNSDOTTIR, H. 1972. High temperature alteration minerals and thermal brines, Reykyanes, Iceland. *Contributions to Mineralogy and Petrology*, **36**, 123-134.

UYEDA, S. & BEN-AVRAHAM, Z. 1972. Origin and development of the Philippine Sea. *Nature Physical Sciences*, **240**, 176-178.

VAN BEMMELEN, R. W. 1949. *The Geology of Indonesia.* The Government Printing Office, The Hague. 732 pp.

VEEVERS, J. J. 1988. Morphotectonics of Australia's northwestern margin - a review. In: PURCELL, P. G. & R. R. (eds.) *The North West Shelf, Australia.* Proceedings of Petroleum Exploration Society Australia Symposium, Perth, 1988, 19–27.

VROON, P. Z. 1992. *Subduction of continental material in the Banda Arc, Eastern Indonesia: Sr-Nd-Pb isotope and trace-element evidence from volcanics and sediments.* Ph.D. Thesis University of Utrecht, *Geol. Ultraiectina*, **90**, 205 pp.

VROON, P. Z. , VAN BERGEN, M. J. & FORDE , E. J. 1996. Pb and Nd isotope Constraints on the Provenance of Tectonically Dispersed Continental Fragments in East Indonesia. In: HALL, R. & BLUNDELL, D. J. (eds.) *Tectonic Evolution of SE Asia.* Geological Society of London Special Publication, **106**, 445-453

WANNER, J. 1913. Zur Geologie der Inseln Obimajora und Halmahera in den Molukken. *Neues Jahrbuch fur Geologie und Palaontologie* **36**, 560-585.

YARDLEY, B. W. D. 1989. *An Introduction to Metamorphic Petrology.* Longman Earth Science, 248 pp.

ZEN, E.-AN. 1961. The zeolite facies: an interpretation. *American Journal of Science*, **259**, 401-409.

APPENDIX A

ISOTOPIC DATING METHODS

APPENDIX A

ISOTOPIC DATING METHODS

A.1 Introduction

K-Ar dating was carried out at the NERC Isotope Geology Laboratory (NIGL) at Keyworth, Nottingham. Most of the samples were analysed by Simon Baker with a few subsequent analyses by G. Nowell. Samples were chosen from various volcanic, plutonic and metamorphic rocks. Rock crushing, milling and mineral separation were performed in the UCL and Birkbeck laboratories.

A.2 Sample Selection Procedure

Samples for K-Ar dating should fulfil several requirements before analysis. Criteria used in selecting samples are: a) samples are as fresh as possible, b) *in situ* samples are preferred to ensure that they represent the rock formation being dated, c) minerals such as mica and hornblende are ideal for K-Ar dating due to their high potassium content and are therefore preferred. Whole rock analyses can be carried out, although there is a risk of mixing argon from a variety of minerals.

A.3 Rock Crushing and Mineral Separation

The rock samples were crushed using a Sturtevant jaw crusher and then milled in a disc mill. The resulting ground rock was sieved through 1 mm, 500, 250 and 125 μm meshes. The ground rock with a size of 250 to 180 micron was chosen for potassium argon analysis. This size was chosen because it gives the best balance between sample heterogeneity and contamination with atmospheric argon (Jäger *et al.*, 1985). Below this size problems of high atmospheric argon contamination can occur, whereas above this size it appears that there is some mineral fractionation that can lead to large variations in apparent K content and radiogenic argon. However, the effects seem to be systematic and do not affect the ages obtained.

The samples for analysis were washed in de-ionised water and stirred until the water became clear indicating that the sieve fraction has been cleaned from dust particles.

Mineral separation was performed with some or all of the following methods: a) heavy liquid/density separation b) hand separation techniques and c) magnetic separation. For the heavy liquid method Bromoform or Di-iodomethane were used. Bromoform (SG 2.87) will separate most mafic from felsic minerals, whilst Di-iodomethane (SG 3.2) is used to further separate heavier mafic minerals. Hand separation is done under a microscope by picking minerals that will be analysed.

A.4 Analytical Procedure

A quantity of powdered sample (~0.2-0.3 g for amphibole, ~0.08-0.10 g for biotite) was placed in a 25 ml platinum crucible and dissolved using ~2 ml concentrated perchloric and 8 ml

40% hydrofluoric acids. Then the crucibles were heated overnight at 150°C on a hot plate below a fume hood in order to evaporate the samples to dryness. Hydrofluoric acid breaks down the silicate lattice to form silicon tetrafluoride.

The residue was diluted with de-ionised water (6M HCl was added to aid dissolution). This solution was transferred to a clean volumetric flask (100, 250, 500 ml depending on the expected K content, as flame photometry works best for 5 - 25 ppm concentration). After thorough mixing, a 5 ml aliquot was mixed with 5 ml of standard lithium solution (~200 ppm Li). The photometer was calibrated against a standard K solution and a pure water blank and the sample solutions were fed into the machine which provided a direct readout of the K concentration.

Argon analysis was by the isotope dilution method on a Micromass 1200 gas source mass spectrometer connected to VG Systems Argon Analysis software. Up to several grams of sample were weighed into a molybdenum crucible and covered with a little quartz wool to prevent spraying during high-frequency radio induction heating. Fusion of the sample liberated all argon present, a known volume (spike) of ^{38}Ar was added and the gaseous mixture was passed through a liquid nitrogen cold-trap and over a cooling titanium 'getter'. The 'clean up' procedure purified the argon, since other gases are either adsorbed onto the titanium sponge or frozen by the cold trap. The argon passes through the gas extraction line to the mass spectrometer. A static analysis was used (i.e. an appropriate amount of sample was admitted to the mass spectrometer which was then isolated) and the relative proportions of the argon isotopes (36,38,40) were measured over a fixed time by scanning with a Faraday detector. These results were fed into the analytical software and the ratio of argon 36/38 and argon 40/38 at time zero were calculated by extrapolation backwards. After correction for atmospheric argon 40 the decay constants, values for radiogenic argon and potassium 40 are substituted into the age equation and a direct print-out of the age of the sample is obtained.

APPENDIX B

MICROPROBE ANALYSES

Appendix B

Tapas Metamorphic rock : Mica schist

Feldspar composition data
filename: or250plg.dat

	1 plg2	2 plg3	3 plg4	4 plg9	5 plg6
SiO2	68.97	69.05	69.90	68.68	68.47
Al2O3	19.05	19.36	19.85	19.51	20.18
Fe2O3	0.00	0.00	0.43	0.00	0.00
CaO	0.00	0.21	0.00	0.00	0.44
Na2O	11.61	10.64	10.60	10.80	10.37
Sum:	99.63	99.26	100.78	99.00	99.46

feldspar cation numbers on the basis of 8 oxygens

Si	3.017	3.021	3.012	3.013	2.991
Al	0.982	0.998	1.008	1.009	1.039
Fe3	-	-	0.014	-	-
Ca	-	0.010	-	-	0.021
Na	0.985	0.902	0.886	0.919	0.878
inCAT#:	4.984	4.931	4.920	4.941	4.929
mg:	0.00	0.00	0.00	0.00	0.00
Al4:	-	-	-	-	0.009
Al6:	0.982	0.998	1.008	1.009	1.030
Or:	0.000	0.000	0.000	0.000	0.000
Ab:	100.000	98.925	100.000	100.000	97.719
An:	0.000	1.075	0.000	0.000	2.281

Appendix B

Tapas Metamorphic rock : Mica schist

Amphibole composition data of
file-name: or250amp.dat
Number of samples: 8

	1 amp2	2 amp3	3 amp4	4 amp9	5 amp10	6 amp11	7 amp13	8 amp16
SiO2	51.58	50.54	51.33	51.99	52.45	50.98	50.01	52.74
TiO2	0.19	0.32	0.27	0.18	0.24	0.00	0.00	0.00
Al2O3	4.91	5.90	6.30	5.16	5.05	6.21	6.82	4.92
FeO	15.29	15.80	16.08	15.06	15.47	15.28	16.10	14.73
MnO	0.42	0.00	0.00	0.36	0.00	0.27	0.00	0.00
CaO	9.96	8.97	9.17	9.61	9.81	9.56	9.60	9.12
MgO	12.41	11.69	12.05	12.57	12.50	11.69	11.40	12.70
K2O	0.20	0.23	0.22	0.22	0.22	0.19	0.29	0.14
Na2O	1.51	2.24	2.37	1.71	1.97	2.13	2.18	2.08
TOTAL:	96.48	95.69	97.80	96.87	97.71	96.31	96.39	96.43
	Amphibole ion numbers on the basis of 23 (24) oxygens							
Si	7.521	7.435	7.385	7.523	7.564	7.470	7.347	7.635
Al4	0.479	0.565	0.615	0.477	0.436	0.530	0.653	0.365
	8.000	8.000	8.000	8.000	8.000	8.000	8.000	8.000
Al6	0.364	0.458	0.454	0.403	0.422	0.542	0.527	0.475
Ti	0.021	0.035	0.030	0.020	0.026	-	-	-
Fe3+	0.494	0.525	0.573	0.534	0.339	0.342	0.429	0.451
Mg	2.698	2.563	2.583	2.710	2.686	2.553	2.495	2.742
Fe2+	1.371	1.419	1.360	1.289	1.527	1.530	1.549	1.332
Mn	0.052	-	-	0.044	-	0.033	-	-
	5.000	5.000	5.000	5.000	5.000	5.000	5.000	5.000
Fe2+	-	-	0.001	-	-	-	-	-
Ca	1.557	1.414	1.414	1.490	1.515	1.501	1.511	1.414
Na	0.427	0.586	0.585	0.479	0.485	0.499	0.489	0.584
	1.984	2.000	2.000	1.969	2.000	2.000	2.000	1.998
Na	-	0.054	0.076	-	0.066	0.107	0.132	-
K	0.038	0.044	0.040	0.041	0.041	0.036	0.054	0.025
	0.038	0.098	0.116	0.041	0.107	0.143	0.186	0.025
mg:	0.591	0.569	0.572	0.598	0.590	0.577	0.558	0.606
mg-Fe2:	0.663	0.644	0.655	0.678	0.638	0.625	0.617	0.673
SUMOX:	23.000	23.000	23.001	23.000	23.000	22.999	23.000	22.999
orCAT#:	15.184	15.271	15.306	15.186	15.219	15.258	15.328	15.172
Ca+Na)B	1.984	2.000	1.999	1.969	2.000	2.000	2.000	1.998
(Na)B	0.427	0.586	0.585	0.479	0.485	0.499	0.489	0.584
(Na+K)A	0.038	0.098	0.116	0.041	0.107	0.143	0.186	0.025

IMA name:
1 amp2 - Calcic Amphibole - Actinolite
2 amp3 - Calcic Amphibole - Actinolitic-Hornblende
3 amp4 - Calcic Amphibole - Actinolitic-Hornblende
4 amp9 - Calcic Amphibole - Actinolite
5 amp10 - Calcic Amphibole - Actinolite
6 amp11 - Calcic Amphibole - Actinolitic-Hornblende
7 amp13 - Calcic Amphibole - Actinolitic-Hornblende
8 amp16 - Calcic Amphibole - Actinolite

Appendix B

Metamorphic rock : Mica schist

Chlorite composition data
filename: or250sil.dat

	1 sil3	2 sil4	3 sil5	4 sil6
SiO2	26.71	26.10	26.16	22.27
Al2O3	20.11	20.00	19.98	18.33
FeO	24.72	24.32	24.07	28.59
MnO	0.34	0.34	0.37	0.36
MgO	15.63	15.27	14.73	13.52
Sum:	87.52	86.03	85.31	83.07
Si	5.613	5.581	5.632	5.141
Al	4.982	5.040	5.071	4.987
Fe3	-	-	-	-
Fe2	4.344	4.350	4.335	5.518
Mn	0.061	0.062	0.068	0.070
Mg	4.897	4.867	4.727	4.650
inCAT#:	19.896	19.899	19.833	20.366
mg:	52.99	52.81	52.16	45.73

Appendix B

Tapas Metamorphic rock : Mica schist

Epidote composition data
filename: or250unk.dat

	1 unk1	2 unk2	3 unk3	4 unk4	5 unk5	6 unk6
SiO2	37.75	37.92	38.30	38.60	38.14	37.73
TiO2	0.00	0.00	0.20	0.00	0.00	0.20
Al2O3	24.27	24.18	24.29	24.87	25.08	23.95
Fe2O3	10.32	10.24	9.99	10.35	9.43	10.02
CaO	23.38	23,30	23.36	23.39	23.43	23.02
Sum:	95.72	95.64	96.14	97.21	96.08	94.92
Si	3.164	3.178	3.189	3.178	3.171	3.183
Ti	-	-	0.013	-	-	0.013
Al	2.397	2.388	2.383	2.413	2.457	2.382
Fe3	0.651	0.646	0.626	0.641	0.590	0.636
Ca	2.099	2.092	2.084	2.063	2.087	2.081
inCAT#:	8.312	8.305	8.294	8.295	8.305	8.295
mg:	0.00	0.00	0.00	0.00	0.00	0.00

Appendix B

Tapas Metamorphic rock : Mica schist

Plagioclase composition data
filename: or262pl.dat

	1 pl1	2 pl2	3 pl3	4 pl18	5 pl19	6 pl10	7 pl11	8 pl13
SiO2	67.36	69.29	67.71	69.38	68.78	66.67	66.00	68.52
Al2O3	20.88	20.46	21.48	20.64	21.56	21.52	22.19	20.35
CaO	1.10	1.10	2.24	1.32	1.91	2.68	3.05	1.16
K2O	0.00	0.00	0.00	0.00	0.00	0.11	0.00	0.13
Na2O	9.86	8.98	8.89	8.95	8.51	8.85	9.26	9.32
Sum:	99.20	99.83	100.32	100.29	100.76	99.83	100.50	99.49

feldspar cation numbers on the basis of 8 oxygens

Si	2.955	3.002	2.937	2.995	2.959	2.916	2.878	2.989
Al	1.079	1.045	1.098	1.050	1.093	1.109	1.140	1.046
Ca	0.052	0.051	0.104	0.061	0.088	0.125	0.142	0.054
K	-	-	-	-	-	0.006	-	0.007
Na	0.839	0.754	0.748	0.749	0.710	0.751	0.783	0.789
inCAT#:	4.924	4.852	4.887	4.855	4.850	4.908	4.943	4.885
mg:	0.00	0.00	0.00	0.00	0.00	0.00	0.00	0.00
Al4:	0.045	-	0.063	0.005	0.041	0.084	0.122	0.011
Al6:	1.034	1.045	1.035	1.045	1.052	1.025	1.018	1.035
Or:	0.000	0.000	0.000	0.000	0.000	0.714	0.000	0.870
Ab:	94.204	93.668	87.779	92.482	88.961	85.075	84.603	92.744
An:	5.796	6.332	12.221	7.518	11.039	14.211	15.397	6.386

Appendix B

Tapas Metamorphic rock : Mica schist

Amphibole composition data
file-name: or262amp.dat
Number of samples: 9

	1 amp1	2 amp2	3 amp3	4 amp6	5 amp10	6 amp11	7 amp12	8 amp13
SiO2	42.00	42.66	43.03	42.04	41.54	42.08	41.55	42.38
TiO2	1.25	1.10	1.12	1.86	1.75	1.29	1.82	1.33
Al2O3	14.36	14.36	14.25	13.95	14.69	14.28	14.75	14.53
FeO	15.08	15.20	15.00	15.19	14.82	15.12	13.29	17.19
MnO	0.26	0.22	0.00	0.29	0.00	0.29	0.35	0.00
CaO	11.27	11.30	11.27	11.63	11.35	11.52	11.70	11.20
MgO	10.61	10.58	10.98	10.52	10.09	10.54	11.34	9.05
K2O	0.69	0.68	0.69	0.80	0.86	0.71	0.81	0.71
Na2O	2.45	2.55	2.44	2.19	2.22	2.25	2.16	2.36
TOTAL:	97.99	98.65	98.78	98.47	97.32	98.08	97.75	98.75
	Amphibole ion numbers on the basis of 23 (24) oxygens							
Si	6.169	6.225	6.246	6.176	6.166	6.182	6.096	6.234
Al4	1.831	1.775	1.754	1.824	1.834	1.818	1.904	1.766
	8.000	8.000	8.000	8.000	8.000	8.000	8.000	8.000
Al6	0.654	0.696	0.683	0.591	0.735	0.655	0.646	0.753
Ti	0.138	0.121	0.122	0.206	0.195	0.143	0.201	0.147
Fe3+	0.525	0.456	0.506	0.387	0.297	0.476	0.413	0.381
Mg	2.324	2.302	2.374	2.302	2.231	2.308	2.479	1.985
Fe2+	1.328	1.399	1.315	1.478	1.542	1.382	1.218	1.733
Mn	0.031	0.026	-	0.036	-	0.036	0.043	-
	5.000	5.000	5.000	5.000	5.000	5.000	5.000	4.999
Fe2+	-	-	-	-	0.001	-	-	-
Mn	0.001	0.001	-	-	-	-	0.001	-
Ca	1.773	1.767	1.753	1.830	1.805	1.813	1.839	1.765
Na	0.226	0.232	0.247	0.170	0.194	0.187	0.160	0.235
	2.000	2.000	2.000	2.000	2.000	2.000	2.000	2.000
Na	0.473	0.489	0.440	0.454	0.444	0.453	0.453	0.437
K	0.130	0.126	0.128	0.150	0.163	0.134	0.151	0.133
	0.603	0.615	0.568	0.604	0.607	0.587	0.604	0.570
mg:	0.557	0.554	0.566	0.552	0.548	0.554	0.603	0.484
mg-Fe2:	0.636	0.622	0.644	0.609	0.591	0.625	0.671	0.534
SUMOX:	23.000	23.001	23.000	23.000	23.000	23.000	23.001	22.998
orCAT#:	15.782	15.770	15.741	15.737	15.708	15.750	15.745	15.701
Ca+Na)B	1.999	1.999	2.000	2.000	1.999	2.000	1.999	2.000
(Na)B	0.226	0.232	0.247	0.170	0.194	0.187	0.160	0.235
(Na+K)A	0.603	0.615	0.568	0.604	0.607	0.587	0.604	0.570

IMA name:

1	amp1	-	Calcic Amphibole - Ferroan-Pargasite
2	amp2	-	Calcic Amphibole - Ferroan-Pargasite
3	amp3	-	Calcic Amphibole - Ferroan-Pargasite
4	amp6	-	Calcic Amphibole - Ferroan-Pargasite
5	amp10	-	Calcic Amphibole - Ferroan-Pargasite
6	amp11	-	Calcic Amphibole - Ferroan-Pargasite
7	amp12	-	Calcic Amphibole - Ferroan-Pargasite
8	amp13	-	Calcic Amphibole - Ferroan-Pargasite

	9
	amp14
SiO2	41.76
TiO2	1.96
Al2O3	14.78
FeO	13.82
MnO	0.00
CaO	12.03
MgO	11.71
K2O	0.78
Na2O	2.42
TOTAL:	99.26

Amphibole ion numbers on the basis of 23 (24) oxygens

Si	6.054
Al4	1.946
	8.000
Al6	0.580
Ti	0.213
Fe3+	0.378
Mg	2.531
Fe2+	1.297
	4.999
Ca	1.868
Na	0.132
	2.000
Na	0.548
K	0.144
	0.692
mg:	0.602
mg-Fe2:	0.661
SUMOX:	22.998
orCAT#:	15.822
Ca+Na)B	2.000
(Na)B	0.132
(Na+K)A	0.692

IMA name:
9 amp14 - Calcic Amphibole - Ferroan-Pargasite

Appendix B

Tapas Metamarphic rock : Mica schist

Epidote composition data
filename: or262ep.dat

	1 ep5	2 ep6	3 ep7	4 ep9	5 ep10	6 ep12	7 ep16
SiO2	38.36	39.09	40.23	39.10	39.15	38.82	39.41
Al2O3	24.24	26.48	27.50	23.91	26.27	25.27	27.68
Fe2O3	10.69	8.02	6.96	11.67	8.78	9.41	7.39
FeO	0.00	0.00	0.00	0.00	0.00	0.00	0.00
MnO	0.00	0.25	0.00	0.00	0.00	0.34	0.00
CaO	23.27	23.86	23.29	23.97	23.47	22.98	24.16
Sum:	96.56	97.70	97.98	98.65	97.67	96.82	98.65
Si	3.185	3.179	3.230	3.191	3.185	3.197	3.163
Al	2.372	2.538	2.603	2.299	2.519	2.453	2.618
Fe3	0.668	0.491	0.421	0.716	0.537	0.583	0.447
Fe2	-	-	-	-	-	-	-
Mn	-	0.017	-	-	-	0.024	-
Ca	2.070	2.080	2.003	2.095	2.046	2.027	2.077
inCAT#:	8.295	8.306	8.257	8.301	8.287	8.284	8.305
mg:	0.00	0.00	0.00	0.00	0.00	0.00	0.00

Appendix B

Tapas Metamorphic rock : Mica schist Muscovite

filename: or262mic.dat

	1 mica2	2 mica3	3 mica4	4 mica5	5 mica6	6 mica7
SiO2	50.32	51.15	48.84	51.43	51.54	48.10
TiO2	0.00	0.20	0.00	0.00	0.00	0.00
Al2O3	34.59	32.27	36.30	32.68	33.65	35.82
FeO	1.37	2.84	0.97	3.12	2.17	1.49
MgO	0.34	0.92	0.28	1.49	0.74	0.96
K2O	9.04	9.52	9.91	9.86	9.10	9.02
Na2O	0.93	1.25	0.22	0.36	1.48	0.79
Sum:	96.59	98.15	96.52	98.94	98.68	96.17

mica cation numbers on the basis of 22 oxygens

Si	6.508	6.593	6.335	6.574	6.564	6.272
Ti	-	0.020	-	-	-	-
Al	5.272	4.902	5.549	4.924	5.052	5.505
Fe2	0.148	0.306	0.105	0.333	0.231	0.162
Mg	0.065	0.176	0.053	0.283	0.140	0.186
K	1.492	1.566	1.639	1.609	1.479	1.500
Na	0.233	0.311	0.056	0.090	0.366	0.199
inCAT#:	13.718	13.874	13.738	13.813	13.831	13.825
mg:	30.66	36.50	33.66	45.95	37.60	53.50
Al4:	1.492	1.407	1.665	1.426	1.436	1.728
Al6:	3.780	3.495	3.884	3.498	3.616	3.777
Fe3T:	-	-	-	-	-	-
T site:	8.000	8.000	8.000	8.000	8.000	8.000
Y site:	3.994	3.997	4.042	4.115	3.987	4.125
Z site:	1.724	1.877	1.696	1.698	1.844	1.699
Anions:	0.000	0.000	0.000	0.000	0.000	0.000

Appendix B

Tapas Metamorphic rock : Mica scist

Chlorite composition data
filename: or262sil.dat

	1 sil2	2 sil3	3 sil6	4 sil7
SiO2	28.38	27.40	27.28	25.80
Al2O3	20.43	19.55	19.68	19.02
FeO	21.37	22.12	23.70	21.05
MgO	19.01	17.54	17.53	17.38
CaO	0.00	0.00	0.14	0.00
Sum:	89.18	86.61	88.34	83.25
Si	5.713	5.726	5.638	5.612
Al	4.848	4.813	4.794	4.875
Fe2	3.598	3.866	4.098	3.828
Mg	5.704	5.461	5.402	5.635
Ca	-	-	0.032	-
inCAT#:	19.863	19.867	19.964	19.951
mg:	61.32	58.55	56.86	59.55

Appendix B

Ophiolitic rock : gabbro

Feldspar composition data
filename: or70pl.dat

	1 pl1	2 pl2	3 pl3	4 pl4	5 pl5	6 pl6	7 pl10	8 pl11
SiO2	43.97	44.57	44.08	43.99	43.10	43.49	43.47	44.23
TiO2	0.00	0.00	0.00	0.00	0.00	0.00	0.23	0.00
Al2O3	35.53	35.46	35.53	35.36	35.34	35.27	35.27	34.82
FeO	0.00	0.34	0.38	0.23	0.34	0.27	0.00	0.43
CaO	19.41	19.28	19.93	19.89	19.84	19.56	19.79	19.20
Na2O	0.72	0.57	0.32	0.38	0.33	0.97	0.39	0.54
Sum:	99.63	100.22	100.24	99.85	98.95	99.56	99.15	99.22

feldspar cation numbers on the basis of 8 oxygens

Si	2.042	2.057	2.039	2.042	2.022	2.029	2.031	2.063
Ti	-	-	-	-	-	-	0.008	-
Al	1.945	1.929	1.937	1.934	1.954	1.939	1.942	1.915
Fe2	-	0.013	0.015	0.009	0.013	0.010	-	0.017
Ca	0.966	0.953	0.988	0.989	0.997	0.978	0.991	0.960
Na	0.065	0.051	0.029	0.034	0.030	0.088	0.035	0.049
inCAT#:	5.017	5.004	5.007	5.008	5.016	5.045	5.007	5.003
mg:	0.00	0.00	0.00	0.00	0.00	0.00	0.00	0.00
Al4:	0.958	0.943	0.961	0.958	0.978	0.971	0.969	0.937
Al6:	0.987	0.986	0.976	0.976	0.976	0.969	0.973	0.978
Or:	0.000	0.000	0.000	0.000	0.000	0.000	0.000	0.000
Ab:	6.288	5.078	2.814	3.333	2.921	8.231	3.441	4.839
An:	93.712	94.922	97.186	96.667	97.079	91.769	96.559	95.161

	9 pl15	10 pl16
SiO2	43.86	45.27
TiO2	0.00	0.00
Al2O3	34.93	33.81
FeO	0.32	0.43
CaO	19.51	18.90
Na2O	0.49	1.17
Sum:	99.11	99.58

feldspar cation numbers on the basis of 8 oxygens

Si	2.050	2.105
Ti	-	-
Al	1.925	1.853
Fe2	0.013	0.017
Ca	0.977	0.942
Na	0.044	0.105
inCAT#:	5.009	5.021
mg:	0.00	0.00
Al4:	0.950	0.895
Al6:	0.975	0.958
Or:	0.000	0.000
Ab:	4.346	10.068
An:	95.654	89.932

Appendix B

Ophiolitic rock : gabbro

Pyroxene composition data
file-name: or70pxa.dat
Number of samples: 8

	1 px1	2 px2	3 px3	4 px4	5 px5	6 px6	7 px7	8 px8
SiO2	54.24	54.08	54.35	53.59	52.90	52.62	53.00	53.64
TiO2	0.00	0.25	0.00	0.23	0.14	0.34	0.42	0.00
Al2O3	0.64	0.60	1.14	1.14	0.96	1.27	2.14	0.97
FeO	3.84	4.49	4.81	4.38	4.15	4.17	5.78	4.70
MnO	0.00	0.00	0.00	0.23	0.24	0.00	0.40	0.25
MgO	15.98	16.12	15.89	15.75	15.17	15.17	15.75	15.48
CaO	24.55	24.92	24.55	24.35	25.25	24.90	22.65	24.06
Sum	99.25	100.46	100.74	99.67	98.81	98.47	100.14	99.10
T site								
Si4+	1.9972	1.9764	1.9796	1.9730	1.9689	1.9637	1.9469	1.9868
AlIV	0.0028	0.0236	0.0204	0.0270	0.0311	0.0363	0.0531	0.0132
Fe3+	-	-	-	-	0.0000	-	-	-
TOTAL:	2.0000	2.0000	2.0000	2.0000	2.0000	2.0000	2.0000	2.0000
M1 site								
AlVI	0.0249	0.0021	0.0285	0.0224	0.0109	0.0195	0.0395	0.0291
Fe3+	-	0.0069	-	-	0.0117	-	-	-
Ti4+	-	0.0068	-	0.0063	0.0039	0.0095	0.0116	-
Mg2+	0.8770	0.8781	0.8626	0.8643	0.8416	0.8438	0.8623	0.8546
Fe2+	0.0981	0.1061	0.1089	0.1070	0.1175	0.1272	0.0866	0.1163
Mn2+	-	-	-	-	0.0075	-	-	-
TOTAL:	1.0000	1.0000	1.0000	1.0000	0.9931	1.0000	1.0000	1.0000
M2 site								
Fe2+	0.0201	0.0242	0.0376	0.0278	-	0.0029	0.0909	0.0292
Mn2+	-	-	-	0.0071	-	-	0.0124	0.0078
Ca2+	0.9685	0.9757	0.9580	0.9605	1.0069	0.9956	0.8914	0.9548
TOTAL:	0.9886	0.9999	0.9956	0.9954	1.0069	0.9985	0.9947	0.9918
iCAT#:	3.9886	4.0023	3.9956	3.9954	4.0039	3.9985	3.9947	3.9918
OXNUM:	5.9997	5.9994	5.9997	5.9994	5.9996	5.9996	5.9995	5.9997
mg#:	0.88	0.87	0.85	0.87	0.88	0.87	0.83	0.85
Q:	1.9637	1.9841	1.9671	1.9596	1.9660	1.9695	1.9312	1.9549
J:	0.0000	0.0000	0.0000	0.0000	0.0000	0.0000	0.0000	0.0000
En:	44.6606	44.1035	43.8514	43.9467	42.3937	42.8434	44.3661	43.5421
Wo:	49.3202	49.0055	48.7011	48.8382	50.7203	50.5509	45.8633	48.6473
Fs:	6.0192	6.8910	7.4475	7.2151	6.8860	6.6057	9.7705	7.8107
ZrAe	-	-	-	-	-	-	-	-
Ae	-	-	-	-	-	-	-	-
Jd	-	-	-	-	-	-	-	-
Nept	-	-	-	-	-	-	-	-
Kosm	-	-	-	-	-	-	-	-
Ka	-	-	-	0.7133	-	-	1.2466	0.7864
CaTi	-	1.3601	-	1.2658	0.7854	1.9029	2.3324	-
CaCr	-	-	-	-	-	-	-	-
CaTs	2.5187	0.2100	2.8626	2.2504	1.0976	1.9529	3.9710	2.9341
Ess	-	0.6901	-	-	1.1781	-	-	-
F2F3	-	-	-	-	-	-	-	-
FeAl	-	-	-	-	-	-	-	-
Jo	-	-	-	-	0.7552	-	-	-
Di	88.7113	87.1387	86.6412	85.4832	84.3520	83.5553	83.3116	85.3801
Hd	6.7368	8.1808	6.7196	7.4945	11.8316	12.2984	-	7.9552
En	-	-	-	-	-	-	-	-
Fs	2.0332	2.4202	3.7766	2.7928	-	0.2904	8.7061	2.9441
Fs-En	-	-	-	-	-	-	0.4323	-
inSUM:	0.9886	0.9999	0.9956	0.9954	0.9931	0.9985	0.9947	0.9918
resAlT	-0.0221	0.0010	-0.0081	-0.0080	0.0007	-0.0022	-0.0096	-0.0159

IMA names:
px1 - Ferroan DIOPSIDE
px2 - Ferroan DIOPSIDE
px3 - Ferroan DIOPSIDE
px4 - Ferroan DIOPSIDE
px5 - Ferroan DIOPSIDE
px6 - Ferroan DIOPSIDE
px7 - Ferroan DIOPSIDE
px8 - Ferroan DIOPSIDE

Appendix B

Ophiolitic rock : gabbro

Amphibole composition data
file-name: or70ama.dat
Number of samples: 5

	1 amp1	2 amp2	3 amp3	4 amp4	5 amp5
SiO2	42.82	42.80	46.84	49.22	43.57
Al2O3	11.09	10.98	9.08	7.62	11.12
TiO2	2.19	2.24	0.63	0.76	2.25
FeO	10.13	10.22	11.01	9.56	10.27
MnO	0.27	0.00	0.00	0.00	0.00
MgO	14.53	14.95	14.64	16.18	14.92
CaO	11.26	11.58	12.62	12.93	11.75
Na2O	1.89	1.79	1.23	1.11	2.02
K2O	1.13	1.16	0.51	0.32	0.94
TOTAL:	95.31	95.72	96.56	97.70	96.84

Amphibole ion numbers on the basis of 23 (24) oxygens

Si	6.334	6.305	6.838	7.041	6.350
Al4	1.666	1.695	1.162	0.959	1.650
	8.000	8.000	8.000	8.000	8.000
Al6	0.267	0.211	0.400	0.326	0.260
Ti	0.244	0.248	0.069	0.082	0.247
Fe3+	0.588	0.603	0.230	0.141	0.481
Mg	3.203	3.282	3.186	3.450	3.241
Fe2+	0.665	0.655	1.114	1.001	0.771
Mn	0.033	-	-	-	-
	5.000	4.999	4.999	5.000	5.000
Fe2+	-	-	-	0.002	-
Mn	0.001	-	-	-	-
Ca	1.784	1.828	1.974	1.982	1.835
Na	0.215	0.172	0.026	0.016	0.165
	2.000	2.000	2.000	2.000	2.000
Na	0.327	0.339	0.322	0.292	0.406
K	0.213	0.218	0.095	0.058	0.175
	0.540	0.557	0.417	0.350	0.581
mg:	0.719	0.723	0.703	0.751	0.721
mg-Fe2:	0.828	0.834	0.741	0.775	0.808
SUMOX:	23.001	22.999	22.997	23.003	23.000
orCAT#:	15.741	15.763	15.495	15.395	15.745
Ca+Na)B	1.999	2.000	2.000	1.998	2.000
(Na)B	0.215	0.172	0.026	0.016	0.165
(Na+K)A	0.540	0.557	0.417	0.350	0.581

IMA name:
1 amp1 - Calcic Amphibole - magnesio hastingsitic-Hornblende
2 amp2 - Calcic Amphibole - magnesio hastingsitic-Hornblende
3 amp3 - Calcic Amphibole - Magnesio-Hornblende
4 amp4 - Calcic Amphibole - Magnesio-Hornblende
5 amp5 - Calcic Amphibole - magnesio hastingsitic-Hornblende

Appendix B

Ophiolitic rock : Gabbro

feldspar composition data
filename: oj101pl.dat

	1 pl1r	2 pl2r	3 pl2c	4 pl3c	5 pl6c	6 pl6m	7 pl6m1	8 pl6m3
SiO2	45.35	47.02	47.40	46.96	46.49	45.73	46.19	45.44
Al2O3	33.72	32.80	32.74	33.19	33.39	33.51	33.32	33.79
FeO	0.40	0.40	0.47	0.41	0.42	0.36	0.43	0.36
CaO	18.06	17.12	16.88	17.28	17.59	18.12	17.92	18.27
Na2O	1.29	2.07	2.03	1.98	1.64	1.36	1.61	1.30
Sum:	98.82	99.41	99.52	99.82	99.53	99.08	99.47	99.16
feldspar cation numbers on the basis of 8 oxygens								
Si	2.118	2.178	2.190	2.167	2.152	2.130	2.143	2.116
Al	1.857	1.791	1.783	1.805	1.822	1.840	1.822	1.855
Fe2	0.016	0.015	0.018	0.016	0.016	0.014	0.017	0.014
Ca	0.904	0.850	0.836	0.854	0.873	0.904	0.891	0.912
Na	0.117	0.186	0.182	0.177	0.147	0.123	0.145	0.117
inCAT#:	5.011	5.019	5.009	5.019	5.010	5.011	5.018	5.014
mg:	0.00	0.00	0.00	0.00	0.00	0.00	0.00	0.00
Al4:	0.882	0.822	0.810	0.833	0.848	0.870	0.857	0.884
Al6:	0.975	0.969	0.973	0.972	0.974	0.970	0.965	0.971
Or:	0.000	0.000	0.000	0.000	0.000	0.000	0.000	0.000
Ab:	11.443	17.953	17.867	17.171	14.436	11.956	13.981	11.408
An:	88.557	82.047	82.133	82.829	85.564	88.044	86.019	88.592

	9 pl6m4	10 pl6r	11 pl7c	12 pl8r	13 pl8m1	14 pl8c	15 pl9c	16 pl10
SiO2	45.84	45.04	47.03	47.71	48.59	48.90	46.53	46.89
Al2O3	33.96	33.81	33.72	32.51	32.46	32.25	33.56	33.22
FeO	0.42	0.45	0.51	0.52	0.35	0.41	0.34	0.42
CaO	18.18	18.28	17.65	16.31	16.46	16.09	17.56	17.46
Na2O	1.58	1.25	1.80	2.29	2.28	2.48	1.68	1.92
Sum:	99.98	98.83	100.71	99.34	100.14	100.13	99.67	99.91
feldspar cation numbers on the basis of 8 oxygens								
Si	2.119	2.107	2.153	2.206	2.225	2.238	2.150	2.163
Al	1.850	1.864	1.819	1.771	1.752	1.740	1.828	1.806
Fe2	0.016	0.018	0.020	0.020	0.013	0.016	0.013	0.016
Ca	0.900	0.916	0.866	0.808	0.808	0.789	0.869	0.863
Na	0.141	0.113	0.160	0.205	0.202	0.220	0.150	0.172
inCAT#:	5.027	5.018	5.017	5.011	5.000	5.002	5.011	5.020
mg:	0.00	0.00	0.00	0.00	0.00	0.00	0.00	0.00
Al4:	0.881	0.893	0.847	0.794	0.775	0.762	0.850	0.837
Al6:	0.969	0.971	0.972	0.977	0.977	0.977	0.978	0.969
Or:	0.000	0.000	0.000	0.000	0.000	0.000	0.000	0.000
Ab:	13.582	11.006	15.576	20.255	20.042	21.806	14.756	16.596
An:	86.418	88.994	84.424	79.745	79.958	78.194	85.244	83.404

Appendix B

Ophiolitic rock : gabbro

Pyroxene composition data
file-name: oj101cp.dat
Number of samples: 10

	1 cp1c	2 cp1r	3 cp2	4 cp4	5 cp4c	6 cp5c	7 cp6r	8 cp6c
SiO2	51.35	51.33	52.25	51.76	51.77	51.68	52.06	53.29
TiO2	0.56	0.54	0.61	0.37	0.33	0.44	0.37	0.21
Al2O3	2.51	2.18	2.48	2.30	1.72	2.48	2.42	1.26
FeO	7.62	7.21	7.47	7.35	7.40	7.72	7.43	6.54
MnO	0.00	0.00	0.00	0.29	0.00	0.00	0.28	0.00
CaO	22.57	22.37	22.38	22.27	22.18	22.08	22.74	23.66
MgO	14.59	14.63	14.74	14.74	14.92	14.81	14.76	14.97
Na2O	0.00	0.52	0.47	0.37	0.34	0.54	0.40	0.00
Sum	99.19	98.78	100.38	99.46	98.67	99.75	100.45	99.93
T site								
Si4+	1.9192	1.9168	1.9225	1.9224	1.9370	1.9110	1.9146	1.9706
AlIV	0.0808	0.0832	0.0775	0.0776	0.0630	0.0890	0.0854	0.0294
Fe3+	0.0000	-	-	-	-	-	-	-
TOTAL:	2.0000	2.0000	2.0000	2.0000	2.0000	2.0000	2.0000	2.0000
M1 site								
AlVI	0.0296	0.0125	0.0298	0.0231	0.0129	0.0190	0.0193	0.0253
Fe3+	0.0189	0.0772	0.0466	0.0594	0.0552	0.0834	0.0736	-
Ti4+	0.0158	0.0152	0.0167	0.0103	0.0093	0.0122	0.0101	0.0058
Mg2+	0.8126	0.8145	0.8081	0.8161	0.8322	0.8165	0.8089	0.8250
Fe2+	0.1231	0.0806	0.0988	0.0911	0.0904	0.0689	0.0881	0.1439
TOTAL:	1.0000	1.0000	1.0000	1.0000	1.0000	1.0000	1.0000	1.0000
M2 site								
Fe2+	0.0963	0.0674	0.0844	0.0778	0.0859	0.0865	0.0666	0.0583
Mn2+	-	-	-	0.0092	-	-	0.0087	-
Ca2+	0.9038	0.8950	0.8821	0.8864	0.8893	0.8747	0.8958	0.9374
Na+	-	0.0376	0.0335	0.0266	0.0249	0.0388	0.0287	-
TOTAL:	1.0001	1.0000	1.0000	1.0000	1.0001	1.0000	0.9998	0.9957
iCAT#:	4.0063	4.0259	4.0156	4.0199	4.0185	4.0280	4.0247	3.9957
OXNUM:	5.9998	5.9997	5.9994	5.9994	5.9995	5.9995	5.9993	5.9995
mg#:	0.79	0.85	0.82	0.83	0.83	0.84	0.84	0.80
Q:	1.9358	1.8575	1.8734	1.8714	1.8978	1.8466	1.8594	1.9646
J:	0.0000	0.0752	0.0670	0.0532	0.0498	0.0776	0.0574	0.0000
En:	41.5716	42.0995	42.0885	42.0670	42.6114	42.3057	41.6594	41.9933
Wo:	46.2373	46.2604	45.9427	45.6907	45.5351	45.3212	46.1348	47.7145
Fs:	12.1911	11.6400	11.9688	12.2423	11.8536	12.3731	12.2058	10.2922
ZrAe	-	-	-	-	-	-	-	-
Ae	-	3.7600	3.3500	2.6600	2.4900	3.8800	2.8706	-
Jd	-	-	-	-	-	-	-	-
Nept	-	-	-	-	-	-	-	-
Kosm	-	-	-	-	-	-	-	-
Ka	-	-	-	0.9200	-	-	0.8702	-
CaTi	3.1600	3.0400	3.3400	2.0600	1.8600	2.4400	2.0204	1.1650
CaCr	-	-	-	-	-	-	-	-
CaTs	2.9600	1.2500	2.9800	2.3100	1.2900	1.9000	1.9304	2.5409
Ess	1.8900	3.9600	1.3100	3.2800	3.0300	4.4600	4.4909	-
F2F3	-	-	-	-	-	-	-	-
FeAl	-	-	-	-	-	-	-	-
Jo	-	-	-	-	-	-	-	-
Di	79.6800	79.9300	79.1400	79.6600	82.2900	78.6700	79.0258	82.2738
Hd	2.6900	1.3200	1.4400	1.3300	0.4600	-	2.1304	8.1651
En	-	-	-	-	-	-	-	-
Fs	9.6200	6.7400	8.4400	7.7800	8.5800	6.8900	6.6613	5.8552
Fs-En	-	-	-	-	-	1.7600	-	-
inSUM:	1.0000	1.0000	1.0000	1.0000	1.0000	1.0000	0.9998	0.9957
resAlT	0.0007	0.0007	0.0012	0.0011	0.0012	0.0010	0.0010	-0.0075

IMA names:
cp1c - Ferroan DIOPSIDE
cp1r - Ferroan DIOPSIDE
cp2 - Ferroan DIOPSIDE
cp4 - Ferroan DIOPSIDE
cp4c - Ferroan DIOPSIDE
cp5c - Ferroan DIOPSIDE
cp6r - Ferroan DIOPSIDE
cp6c - Ferroan DIOPSIDE

	9	10
	cp7	cp8
SiO2	51.62	52.02
TiO2	0.50	0.45
Al2O3	2.57	2.67
FeO	7.57	7.76
MnO	0.00	0.00
CaO	22.17	22.21
MgO	14.40	14.84
Na2O	0.39	0.52
Sum	99.22	100.47
T site		
Si4+	1.9240	1.9106
AlIV	0.0760	0.0894
Fe3+	-	0.0000
TOTAL:	2.0000	2.0000
M1 site		
AlVI	0.0369	0.0260
Fe3+	0.0386	0.0748
Ti4+	0.0139	0.0124
Mg2+	0.7998	0.8122
Fe2+	0.1108	0.0746
TOTAL:	1.0000	1.0000
M2 site		
Fe2+	0.0866	0.0889
Ca2+	0.8853	0.8740
Na+	0.0281	0.0371
TOTAL:	1.0000	1.0000
iCAT#:	4.0129	4.0251
OXNUM:	5.9996	5.9995
mg#:	0.80	0.83
Q:	1.8825	1.8497
J:	0.0562	0.0742
En:	41.6324	42.2032
Wo:	46.0830	45.4144
Fs:	12.2846	12.3824
ZrAe	-	-
Ae	2.8100	3.7100
Jd	-	-
Nept	-	-
Kosm	-	-
Ka	-	-
CaTi	2.7800	2.4800
CaCr	-	-
CaTs	3.6900	2.6000
Ess	1.0500	3.7700
F2F3	-	-
FeAl	-	-
Jo	-	-
Di	78.5900	78.5500
Hd	2.4200	-
En	-	-
Fs	8.6600	7.4600
Fs-En	-	1.4300
inSUM:	1.0000	1.0000
resAlT	0.0008	0.0009

IMA names:
cp7 - Ferroan DIOPSIDE
cp8 - Ferroan DIOPSIDE

Appendix B

Ophilitic rock : gabbro

Pyroxene composition data
file-name: oj101op.dat
Number of samples: 23

	1 op1	2 op2	3 op3r	4 op4r	5 op4c	6 op4m	7 op5r	8 op5c
SiO2	53.67	54.34	53.50	53.65	53.48	53.52	53.46	53.69
Al2O3	1.14	1.16	1.11	1.17	1.25	1.21	1.28	1.30
TiO2	0.00	0.00	0.22	0.26	0.21	0.00	0.00	0.00
FeO	17.53	17.55	17.93	17.31	17.58	17.26	17.45	17.54
MnO	0.30	0.43	0.33	0.25	0.36	0.44	0.47	0.41
MgO	25.79	25.54	25.83	25.88	25.81	25.65	25.28	25.18
CaO	0.92	0.92	0.95	0.86	0.88	0.92	1.00	1.20
Na2O	0.00	0.00	0.00	0.34	0.33	0.00	0.00	0.00
Sum	99.35	99.94	99.87	99.71	99.90	99.00	98.94	99.32
T site								
Si4+	1.9633	1.9781	1.9497	1.9499	1.9418	1.9647	1.9672	1.9694
AlIV	0.0367	0.0219	0.0476	0.0501	0.0535	0.0353	0.0328	0.0306
Fe3+	0.0000	-	0.0027	-	0.0047	0.0000	-	-
TOTAL:	2.0000	2.0000	2.0000	2.0000	2.0000	2.0000	2.0000	2.0000
M1 site								
AlVI	0.0124	0.0278	-	-	-	0.0170	0.0226	0.0256
Fe3+	0.0237	-	0.0377	0.0585	0.0689	0.0180	0.0093	0.0042
Ti4+	-	-	0.0060	0.0071	0.0057	-	-	-
Mg2+	0.9639	0.9722	0.9563	0.9344	0.9254	0.9650	0.9681	0.9702
TOTAL:	1.0000	1.0000	1.0000	1.0000	1.0000	1.0000	1.0000	1.0000
M2 site								
Mg2+	0.4422	0.4135	0.4468	0.4676	0.4714	0.4384	0.4184	0.4064
Fe2+	0.5125	0.5342	0.5060	0.4675	0.4603	0.5118	0.5277	0.5338
Mn2+	0.0093	0.0132	0.0102	0.0076	0.0110	0.0137	0.0146	0.0127
Ca2+	0.0360	0.0358	0.0371	0.0334	0.0342	0.0361	0.0393	0.0471
Na+	-	-	-	0.0239	0.0232	-	-	-
TOTAL:	1.0000	0.9967	1.0001	1.0000	1.0001	1.0000	1.0000	1.0000
iCAT#:	4.0079	3.9967	4.0135	4.0196	4.0247	4.0060	4.0031	4.0014
OXNUM:	5.9997	5.9997	5.9998	5.9994	5.9995	5.9999	5.9996	5.9996
mg#:	0.73	0.72	0.73	0.75	0.75	0.73	0.72	0.72
Q:	1.9546	1.9557	1.9462	1.9029	1.8913	1.9513	1.9535	1.9575
J:	0.0000	0.0000	0.0000	0.0478	0.0464	0.0000	0.0000	0.0000
En:	70.7436	70.3794	70.2674	71.2037	70.6918	70.7716	70.1173	69.7225
Wo:	1.8112	1.8183	1.8580	1.6963	1.7309	1.8205	1.9875	2.3855
Fs:	27.4452	27.8023	27.8746	27.1001	27.5773	27.4080	27.8952	27.8920
ZrAe	-	-	-	-	-	-	-	-
Ae	-	-	-	2.3900	2.3200	-	-	-
Jd	-	-	-	-	-	-	-	-
Nept	-	-	-	-	-	-	-	-
Kosm	-	-	-	-	-	-	-	-
Ka	0.9300	1.3244	1.0200	0.7600	1.1000	1.3700	1.4600	1.2700
CaTi	-	-	1.2000	1.4200	1.1400	-	-	-
CaCr	-	-	-	-	-	-	-	-
CaTs	1.2400	2.7892	-	-	-	1.7000	2.2600	2.5600
Ess	2.3600	-	2.5100	1.9200	2.2800	1.8000	0.9300	0.4200
F2F3	0.0100	-	1.2600	1.5400	2.2900	-	-	-
FeAl	-	-	-	-	-	-	-	-
Jo	-	-	-	-	-	-	-	-
Di	-	0.8026	-	-	-	0.1100	0.7400	1.7300
Hd	-	-	-	-	-	-	-	-
En	44.2200	41.4869	44.6800	46.7600	47.1400	43.8400	41.8400	40.6400
Fs	-	-	-	-	-	-	-	-
Fs-En	51.2400	53.5969	49.3300	45.2100	43.7300	51.1800	52.7700	53.3800
inSUM:	1.0000	0.9967	1.0000	1.0000	1.0000	1.0000	1.0000	1.0000
resAlT	0.0006	-0.0059	0.0006	0.0013	0.0011	0.0003	0.0009	0.0008

IMA names:
op1 - Ferroan ENSTATITE
0p2 - Ferroan ENSTATITE
op3r - Ferroan ENSTATITE
op4r - Ferroan ENSTATITE
op4c - Ferroan ENSTATITE
op4m - Ferroan ENSTATITE
op5r - Ferroan ENSTATITE
op5c - Ferroan ENSTATITE

	9	10	11	12	13	14	15	16
	op6c	op6m	op6r	op6r	op7r	op8c	op8r	op8r
SiO2	53.79	53.53	54.09	54.09	53.57	52.95	53.54	53.54
Al2O3	1.41	1.40	1.03	1.03	1.18	1.27	1.38	1.38
TiO2	0.23	0.00	0.00	0.00	0.00	0.00	0.00	0.00
FeO	17.45	17.70	17.08	17.08	17.27	17.20	17.24	17.24
MnO	0.35	0.43	0.43	0.43	0.36	0.40	0.52	0.53
MgO	25.69	26.07	25.38	25.38	26.12	25.41	25.22	25.22
CaO	0.95	0.76	0.85	0.85	0.90	0.89	0.86	0.86
Na2O	0.34	0.00	0.00	0.00	0.00	0.00	0.00	0.00
Sum	100.22	99.90	98.87	98.86	99.40	98.12	98.76	98.77
T site								
Si4+	1.9475	1.9463	1.9862	1.9862	1.9551	1.9612	1.9721	1.9719
AlIV	0.0525	0.0537	0.0138	0.0138	0.0449	0.0388	0.0279	0.0281
Fe3+	0.0000	-	-	-	-	-	-	-
TOTAL:	2.0000	2.0000	2.0000	2.0000	2.0000	2.0000	2.0000	2.0000
M1 site								
AlVI	0.0076	0.0062	0.0307	0.0307	0.0058	0.0166	0.0320	0.0318
Fe3+	0.0552	0.0469	-	-	0.0386	0.0213	-	-
Ti4+	0.0062	-	-	-	-	-	-	-
Mg2+	0.9310	0.9469	0.9693	0.9693	0.9556	0.9621	0.9680	0.9682
TOTAL:	1.0000	1.0000	1.0000	1.0000	1.0000	1.0000	1.0000	1.0000
M2 site								
Mg2+	0.4555	0.4659	0.4197	0.4198	0.4652	0.4407	0.4165	0.4163
Fe2+	0.4732	0.4914	0.5245	0.5245	0.4885	0.5116	0.5311	0.5311
Mn2+	0.0107	0.0131	0.0134	0.0133	0.0111	0.0125	0.0163	0.0165
Ca2+	0.0368	0.0296	0.0335	0.0334	0.0352	0.0352	0.0337	0.0339
Na+	0.0238	-	-	-	-	-	-	-
TOTAL:	1.0000	1.0000	0.9911	0.9910	1.0000	1.0000	0.9976	0.9978
iCAT#:	4.0185	4.0157	3.9911	3.9910	4.0129	4.0071	3.9976	3.9978
OXNUM:	5.9994	5.9997	5.9995	5.9994	5.9998	5.9995	5.9997	5.9997
mg#:	0.75	0.74	0.73	0.73	0.74	0.73	0.72	0.72
Q:	1.8965	1.9338	1.9470	1.9470	1.9445	1.9496	1.9493	1.9495
J:	0.0476	0.0000	0.0000	0.0000	0.0000	0.0000	0.0000	0.0000
En:	70.6533	70.8597	70.8529	70.8616	71.2466	70.7270	70.4365	70.4222
Wo:	1.8753	1.4846	1.7088	1.7038	1.7651	1.7747	1.7145	1.7243
Fs:	27.4715	27.6557	27.4383	27.4346	26.9883	27.4982	27.8490	27.8535
ZrAe	-	-	-	-	-	-	-	-
Ae	2.3800	-	-	-	-	-	-	-
Jd	-	-	-	-	-	-	-	-
Nept	-	-	-	-	-	-	-	-
Kosm	-	-	-	-	-	-	-	-
Ka	1.0700	1.3100	1.3520	1.3421	1.1100	1.2500	1.6339	1.6536
CaTi	1.2400	-	-	-	-	-	-	-
CaCr	-	-	-	-	-	-	-	-
CaTs	0.7600	0.6200	3.0976	3.0979	0.5800	1.6600	3.2077	3.1870
Ess	1.6800	2.3400	-	-	2.9400	1.8600	-	-
F2F3	1.4600	2.3500	-	-	0.9200	0.2700	-	-
FeAl	-	-	-	-	-	-	-	-
Jo	-	-	-	-	-	-	-	-
Di	-	-	0.2825	0.2725	-	-	0.1704	0.2105
Hd	-	-	-	-	-	-	-	-
En	45.5500	46.5900	42.3469	42.3612	46.5200	44.0700	41.7502	41.7218
Fs	-	-	-	-	-	-	-	-
Fs-En	45.8600	46.7900	52.9210	52.9263	47.9300	50.8900	53.2378	53.2271
inSUM:	1.0000	1.0000	0.9911	0.9910	1.0000	1.0000	0.9976	0.9978
resAlT	0.0011	0.0006	-0.0169	-0.0169	0.0005	0.0009	-0.0041	-0.0037

IMA names:
op6c - Ferroan ENSTATITE
op6m - Ferroan ENSTATITE
op6r - Ferroan ENSTATITE
op6r - Ferroan ENSTATITE
op7r - Ferroan ENSTATITE
op8c - Ferroan ENSTATITE
op8r - Ferroan ENSTATITE
op8r - Ferroan ENSTATITE

	17	18	19	20	21	22	23
	0p9c	0p10r	op11r	op12	op13	op14r	op14c
SiO2	53.23	53.94	53.99	53.42	53.90	53.85	53.75
Al2O3	1.39	1.22	1.17	1.12	1.29	1.23	1.28
TiO2	0.18	0.20	0.00	0.00	0.21	0.20	0.24
FeO	17.41	17.48	17.30	18.41	17.84	17.43	16.88
MnO	0.00	0.40	0.38	0.52	0.39	0.35	0.35
MgO	25.88	25.74	25.90	25.18	25.83	25.73	25.92
CaO	0.97	0.98	1.22	0.74	0.87	0.81	0.84
Na2O	0.35	0.00	0.33	0.00	0.34	0.00	0.00
Sum	99.41	99.96	100.29	99.39	100.67	99.61	99.26
T site							
Si4+	1.9383	1.9633	1.9508	1.9623	1.9438	1.9663	1.9657
AlIV	0.0596	0.0367	0.0492	0.0377	0.0548	0.0337	0.0343
Fe3+	0.0021	0.0000	0.0000	0.0000	0.0014	-	-
TOTAL:	2.0000	2.0000	2.0000	2.0000	2.0000	2.0000	2.0000
M1 site							
AlVI	-	0.0156	0.0006	0.0108	-	0.0191	0.0209
Fe3+	0.0754	0.0090	0.0707	0.0260	0.0678	0.0027	-
Ti4+	0.0049	0.0054	-	-	0.0057	0.0056	0.0066
Mg2+	0.9197	0.9700	0.9287	0.9632	0.9265	0.9726	0.9725
TOTAL:	1.0000	1.0000	1.0000	1.0000	1.0000	1.0000	1.0000
M2 site							
Mg2+	0.4850	0.4265	0.4662	0.4153	0.4619	0.4279	0.4402
Fe2+	0.4527	0.5231	0.4519	0.5395	0.4689	0.5295	0.5161
Mn2+	-	0.0123	0.0115	0.0162	0.0118	0.0108	0.0107
Ca2+	0.0378	0.0382	0.0472	0.0289	0.0336	0.0318	0.0327
Na+	0.0246	-	0.0231	-	0.0238	-	-
TOTAL:	1.0001	1.0001	0.9999	0.9999	1.0000	1.0000	0.9997
iCAT#:	4.0260	4.0030	4.0237	4.0087	4.0232	4.0009	3.9997
OXNUM:	5.9995	5.9994	5.9994	5.9994	5.9996	5.9997	5.9996
mg#:	0.76	0.73	0.76	0.72	0.75	0.73	0.73
Q:	1.8952	1.9578	1.8940	1.9469	1.8909	1.9618	1.9615
J:	0.0492	0.0000	0.0462	0.0000	0.0476	0.0000	0.0000
En:	71.2070	70.5624	70.5850	69.3027	70.4092	70.9006	71.6307
Wo:	1.9162	1.9302	2.3884	1.4529	1.7039	1.6099	1.6580
Fs:	26.8769	27.5075	27.0266	29.2444	27.8868	27.4895	26.7113
ZrAe	-	-	-	-	-	-	-
Ae	2.4600	-	2.3102	-	2.3800	-	-
Jd	-	-	-	-	-	-	-
Nept	-	-	-	-	-	-	-
Kosm	-	-	-	-	-	-	-
Ka	-	1.2300	1.1501	1.6202	1.1800	1.0800	1.0703
CaTi	0.9800	1.0800	-	-	1.1400	1.1200	1.3204
CaCr	-	-	-	-	-	-	-
CaTs	-	1.5600	0.0600	1.0801	-	1.9100	1.9506
Ess	2.8000	0.9000	4.6605	1.8102	2.2200	0.1500	-
F2F3	2.2800	-	0.1000	0.7901	2.1800	0.1200	-
FeAl	-	-	-	-	-	-	0.1400
Jo	-	-	-	-	-	-	-
Di	-	0.2800	-	-	-	-	-
Hd	-	-	-	-	-	-	-
En	48.5000	42.6500	46.6247	41.5341	46.1900	42.7900	44.0332
Fs	-	-	-	-	-	-	-
Fs-En	42.9800	52.3000	45.0945	53.1653	44.7100	52.8300	51.4854
inSUM:	1.0000	1.0000	0.9999	0.9999	1.0000	1.0000	0.9997
resAlT	0.0011	0.0013	0.0010	0.0009	0.0008	0.0007	0.0002

IMA names:
0p9c - Ferroan ENSTATITE
0p10r - Ferroan ENSTATITE
op11r - Ferroan ENSTATITE
op12 - Ferroan ENSTATITE
op13 - Ferroan ENSTATITE
op14r - Ferroan ENSTATITE
op14c - Ferroan ENSTATITE

Appendix B

Ophiolitic rock : gabbro

Amphibole composition data
file-name: oj101amp.dat
Number of samples: 4

	1 amp1	2 amp2	3 amp3	4 amp4
SiO2	45.95	45.10	45.91	48.82
TiO2	2.12	2.11	1.95	0.55
Al2O3	10.20	10.53	9.48	7.38
CaO	12.24	11.78	11.96	11.84
MgO	16.13	16.13	15.56	16.95
K2O	0.11	0.12	0.12	0.00
Na2O	1.82	1.90	1.59	1.56
FeO	9.62	9.49	10.56	9.50
TOTAL:	98.19	97.17	97.13	96.60

Amphibole ion numbers on the basis of 23 (24) oxygens

Si	6.517	6.437	6.590	6.964
Al4	1.483	1.563	1.410	1.036
	8.000	8.000	8.000	8.000
Al6	0.223	0.208	0.194	0.205
Ti	0.226	0.226	0.210	0.059
Fe3+	0.566	0.750	0.652	0.661
Mg	3.410	3.432	3.328	3.603
Fe2+	0.575	0.383	0.616	0.472
	5.000	4.999	5.000	5.000
Fe2+	0.001	-	0.000	0.000
Ca	1.861	1.801	1.839	1.810
Na	0.138	0.199	0.161	0.190
	2.000	2.000	2.000	2.000
Na	0.362	0.328	0.281	0.241
K	0.021	0.021	0.023	-
	0.383	0.349	0.304	0.241
mg:	0.749	0.752	0.724	0.761
mg-Fe2:	0.855	0.900	0.844	0.884
SUMOX:	23.001	22.997	23.000	23.000
orCAT#:	15.572	15.603	15.524	15.463
Ca+Na)B	1.999	2.000	2.000	2.000
(Na)B	0.138	0.199	0.161	0.190
(Na+K)A	0.383	0.349	0.304	0.241

IMA name:
1 amp1 - Calcic Amphibole - Magnesio-Hornblende
2 amp2 - Calcic Amphibole - Tschermakitic-Hornblende
3 amp3 - Calcic Amphibole - Magnesio-Hornblende
4 amp4 - Calcic Amphibole - Magnesio-Hornblende

Appendix B

Ophiolitic rock : gabbro

Fe-Ti oxide composition data
file-name: oj101ore.dat
Number of samples: 2

	1 ore1	2 ore2
SiO2	0.25	0.00
Al2O3	2.56	2.71
TiO2	5.34	3.74
Fe2O3	54.89	59.96
FeO	32.11	30.91
MgO	0.80	0.80
Na2O	0.54	0.54
Sum.:	96.49	98.66
Fe2O3:	54.89	59.96
FeO:	32.11	30.91
newSum:	151.38	158.62

Fe-Ti oxide cation numbers

Si	0.0096	-
Al	0.1165	0.1209
Ti	0.1550	0.1064
Fe3	1.5950	1.7080
Fe2	1.0369	0.9785
Mg	0.0460	0.0451
Na	0.0403	0.0396
cal Fe3	1.5950	1.7080
mg:	4.25	4.41
CAT#:	4.5944	4.7065
Usp%:	16.27	11.08
Ilm%:	-	-

End-members for spinels
Gabbro of the Ophiolitic rock

file-name: oj101ore.dat

	1 ore1	2 ore2
Spi	5.0093	4.9171
Her	1.3340	1.6736
Gah	-	-
Gal	-	-
Qua	-	-
Mfe	-	-
Cou	-	-
Tre	-	-
Fra	-	-
Jac	-	-
Usp	17.9244	11.6005
Nic	-	-
Mnc	-	-
Pic	-	-
Chr	-	-
Mag	75.7323	81.8088
SUM:	91.83	91.72

End-members for ilmenites
Gabbro of the Ophiolitic rock

Appendix B

Ophiolitic rock : gabbro

Pumphellyite composition data
filename: oj101pum.dat

	1 pum1
SiO2	37.41
Al2O3	25.36
FeO	8.82
MgO	2.29
CaO	20.70
Sum:	94.58
Si	3.431
Al	2.742
Fe2	0.677
Mg	0.313
Ca	2.034
inCAT#:	9.197
mg:	31.64

Appendix B

Ophiolitic rock : gabbro

Feldspar composition data
filename: oj107pl.dat

	1 pl3c	2 pl3r	3 pl4	4 pl4r	5 pl5c	6 pl6	7 pl7	8 pl8r
SiO2	46.42	46.74	46.05	45.72	46.90	47.07	46.35	47.04
Al2O3	34.01	34.02	33.94	33.86	34.14	34.20	34.17	34.12
FeO	0.21	0.27	0.23	0.23	0.22	0.00	0.29	0.32
MgO	0.31	0.32	0.00	0.00	0.00	0.00	0.26	0.00
CaO	17.58	17.46	17.37	17.52	17.91	17.45	18.00	17.64
Na2O	1.50	1.56	1.52	1.48	1.53	1.44	1.53	1.62
Sum:	100.03	100.64	99.38	98.81	100.92	100.16	100.92	100.74
feldspar cation numbers on the basis of 8 oxygens								
Si	2.135	2.138	2.133	2.129	2.141	2.155	2.120	2.149
Al	1.843	1.834	1.853	1.859	1.837	1.846	1.842	1.837
Fe3	0.007	0.009	0.009	0.008	0.007	-	0.011	-
Fe2	-	0.010	0.009	-	0.008	-	0.011	0.012
Mg	0.021	0.022	-	-	-	-	0.018	-
Ca	0.866	0.856	0.862	0.874	0.876	0.856	0.882	0.863
Na	0.134	0.138	0.137	0.134	0.135	0.128	0.136	0.143
inCAT#:	5.006	5.008	5.003	5.004	5.004	4.985	5.020	5.004
mg:	100.00	68.10	0.00	0.00	0.00	0.00	61.54	0.00
Al4:	0.865	0.862	0.867	0.871	0.859	0.845	0.880	0.851
Al6:	0.978	0.973	0.986	0.988	0.977	1.001	0.963	0.985
Or:	0.000	0.000	0.000	0.000	0.000	0.000	0.000	0.000
Ab:	13.371	13.911	13.669	13.257	13.389	12.989	13.331	14.245
An:	86.629	86.089	86.331	86.743	86.611	87.011	86.669	85.755

	9 pl9	10 pl10c	11 pl10r	12 pl11c	13 pl11m	14 pl11r
SiO2	46.72	46.96	46.19	46.05	46.52	45.94
Al2O3	33.76	33.51	33.95	33.66	33.58	33.82
CaO	17.19	17.14	17.54	17.38	17.45	17.36
Na2O	1.50	1.70	1.54	1.50	1.41	1.53
Sum:	99.17	99.31	99.22	98.82	98.96	98.65
feldspar cation numbers on the basis of 8 oxygens						
Si	2.161	2.169	2.140	2.143	2.158	2.140
Al	1.840	1.824	1.854	1.847	1.836	1.857
Fe3	-	-	-	-	-	-
Fe2	-	-	-	0.009	-	-
Ca	0.852	0.848	0.871	0.867	0.867	0.866
Na	0.134	0.152	0.138	0.135	0.127	0.138
inCAT#:	4.986	4.994	5.002	5.001	4.988	5.001
mg:	0.00	0.00	0.00	0.00	0.00	0.00
Al4:	0.839	0.831	0.860	0.857	0.842	0.860
Al6:	1.000	0.994	0.993	0.990	0.993	0.996
Or:	0.000	0.000	0.000	0.000	0.000	0.000
Ab:	13.629	15.212	13.708	13.503	12.757	13.750
An:	86.371	84.788	86.292	86.497	87.243	86.250

Appendix B

Ophiolitic rock : gabbro

Amphibole composition data
file-name: oj107amp.dat
Number of samples: 12

	1 amp1	2 amp2	3 amp3	4 amp4	5 amp5	6 amp6	7 amp7	8 amp9
SiO2	44.97	44.83	46.02	45.96	45.97	45.35	45.95	46.15
Al2O3	10.84	10.72	11.29	11.24	11.13	11.16	11.07	11.14
TiO2	1.56	1.68	1.74	1.59	1.49	1.63	1.67	1.74
FeO	9.24	9.05	9.20	9.04	9.65	9.09	9.46	9.43
MgO	15.92	15.40	16.01	16.02	16.18	15.94	15.76	16.15
CaO	10.99	11.19	11.38	11.49	11.43	11.23	11.41	11.41
Na2O	2.43	1.81	2.47	2.31	2.31	2.29	2.24	2.17
K2O	0.00	0.00	0.00	0.00	0.12	0.10	0.00	0.00
TOTAL:	95.95	94.68	98.11	97.65	98.28	96.79	97.56	98.19
	Amphibole ion numbers on the basis of 23 (24) oxygens							
Si	6.469	6.530	6.489	6.506	6.468	6.472	6.517	6.483
Al4	1.531	1.470	1.511	1.494	1.532	1.528	1.483	1.517
	8.000	8.000	8.000	8.000	8.000	8.000	8.000	8.000
Al6	0.307	0.370	0.365	0.381	0.314	0.349	0.367	0.327
Ti	0.169	0.184	0.185	0.169	0.158	0.175	0.178	0.184
Fe3+	0.821	0.727	0.661	0.655	0.804	0.742	0.674	0.797
Mg	3.413	3.343	3.365	3.380	3.393	3.391	3.332	3.381
Fe2+	0.290	0.375	0.424	0.415	0.331	0.343	0.449	0.311
	5.000	4.999	5.000	5.000	5.000	5.000	5.000	5.000
Ca	1.694	1.746	1.719	1.743	1.723	1.717	1.734	1.717
Na	0.306	0.254	0.281	0.257	0.277	0.283	0.266	0.283
	2.000	2.000	2.000	2.000	2.000	2.000	2.000	2.000
Na	0.372	0.257	0.394	0.377	0.353	0.351	0.350	0.308
K	-	-	-	-	0.022	0.018	-	-
	0.372	0.257	0.394	0.377	0.375	0.369	0.350	0.308
mg:	0.754	0.752	0.756	0.760	0.749	0.758	0.748	0.753
mg-Fe2:	0.922	0.899	0.888	0.891	0.911	0.908	0.881	0.916
SUMOX:	23.000	22.998	22.999	23.000	23.000	23.000	22.999	23.000
orCAT#:	15.651	15.502	15.619	15.599	15.648	15.621	15.578	15.578
Ca+Na)B	2.000	2.000	2.000	2.000	2.000	2.000	2.000	2.000
(Na)B	0.306	0.254	0.281	0.257	0.277	0.283	0.266	0.283
(Na+K)A	0.372	0.257	0.394	0.377	0.375	0.369	0.350	0.308

IMA name:
1 amp1 - Calcic Amphibole - Tschermakitic-Hornblende
2 amp2 - Calcic Amphibole - Magnesio-Hornblende
3 amp3 - Calcic Amphibole - Tschermakitic-Hornblende
4 amp4 - Calcic Amphibole - Magnesio-Hornblende
5 amp5 - Calcic Amphibole - Tschermakitic-Hornblende
6 amp6 - Calcic Amphibole - Tschermakitic-Hornblende
7 amp7 - Calcic Amphibole - Magnesio-Hornblende
8 amp9 - Calcic Amphibole - Tschermakitic-Hornblende

	9	10	11	12
	amp10	amp11	amp12	amp13
SiO2	46.12	46.35	46.29	45.74
Al2O3	11.28	11.15	11.39	11.09
TiO2	1.60	1.64	1.59	1.79
FeO	9.56	9.50	9.51	9.34
MgO	16.09	16.09	16.11	16.08
CaO	11.39	11.39	11.50	11.49
Na2O	2.36	2.22	2.43	2.36
K2O	0.00	0.10	0.00	0.17
TOTAL:	98.40	98.44	98.82	98.06

Amphibole ion numbers on the basis of 23 (24) oxygens

Si	6.475	6.503	6.479	6.468
Al4	1.525	1.497	1.521	1.532
	8.000	8.000	8.000	8.000
Al6	0.341	0.347	0.358	0.316
Ti	0.169	0.173	0.167	0.190
Fe3+	0.776	0.756	0.718	0.675
Mg	3.367	3.365	3.361	3.389
Fe2+	0.347	0.359	0.395	0.429
	5.000	5.000	4.999	4.999
Ca	1.713	1.712	1.725	1.741
Na	0.287	0.288	0.275	0.259
	2.000	2.000	2.000	2.000
Na	0.355	0.316	0.384	0.388
K	-	0.018	-	0.031
	0.355	0.334	0.384	0.419
mg:	0.750	0.751	0.751	0.754
mg-Fe2:	0.907	0.904	0.895	0.888
SUMOX:	22.999	22.999	22.998	22.998
orCAT#:	15.619	15.590	15.628	15.648
Ca+Na)B	2.000	2.000	2.000	2.000
(Na)B	0.287	0.288	0.275	0.259
(Na+K)A	0.355	0.334	0.384	0.419

IMA name:

9	amp10	-	Calcic Amphibole - Tschermakitic-Hornblende
10	amp11	-	Calcic Amphibole - Magnesio-Hornblende
11	amp12	-	Calcic Amphibole - Tschermakitic-Hornblende
12	amp13	-	Calcic Amphibole - Tschermakitic-Hornblende

Appendix B

Ophiolitic rock : dolerite

Feldspar composition data
filename: od204pl.dat

	1 pl3	2 pl5	3 pl8	4 pl14	5 pl17
SiO2	63.40	64.58	49.04	63.51	64.09
Al2O3	22.55	18.29	31.79	22.29	22.01
CaO	4.13	0.00	16.28	3.38	3.39
MgO	0.00	0.00	0.33	0.00	0.00
K2O	0.00	15.83	0.00	0.36	0.00
Na2O	8.17	0.55	2.37	8.45	8.49
FeO	0.27	0.00	0.99	0.42	0.24
Sum:	98.52	99.25	100.80	98.41	98.22

feldspar cation numbers on the basis of 8 oxygens

Si	2.830	3.001	2.237	2.841	2.862
Al	1.186	1.002	1.709	1.175	1.158
Ca	0.198	-	0.796	0.162	0.162
Mg	-	-	0.022	-	-
K	-	0.938	-	0.021	-
Na	0.707	0.049	0.210	0.733	0.735
Fe2	0.010	-	0.038	0.016	0.009
inCAT#:	4.930	4.991	5.012	4.948	4.926
mg:	0.00	0.00	37.16	0.00	0.00
Al4:	0.170	-	0.763	0.159	0.138
Al6:	1.016	1.002	0.947	1.016	1.020
Or:	0.000	94.990	0.000	2.239	0.000
Ab:	78.165	5.010	20.847	80.063	81.931
An:	21.835	0.000	79.153	17.697	18.069

Appendix B

Ophiolitic rock : dolerite

Pyroxene composition data
file-name: od204px.dat
Number of samples: 6

	1	2	3	4	5	6
	px1	px2	px3	px4	px5	px6
SiO2	47.81	49.82	49.24	49.03	50.41	56.03
TiO2	1.34	0.79	0.73	0.30	0.53	0.00
Al2O3	5.39	5.68	7.47	8.32	5.13	23.00
FeO	11.98	6.53	4.85	4.63	5.39	3.87
MnO	0.40	0.00	0.00	0.00	0.00	0.00
Cr2O3	0.00	0.24	0.00	0.00	0.00	0.00
CaO	19.54	22.16	23.65	23.31	22.57	4.92
MgO	12.41	14.22	14.21	13.26	15.13	5.76
Na2O	0.48	0.35	0.00	0.00	0.52	5.84
Sum	99.35	99.79	100.15	98.85	99.68	99.42
T site						
Si4+	1.8061	1.8389	1.8043	1.8178	1.8482	1.9158
AlIV	0.1939	0.1611	0.1957	0.1822	0.1518	0.0842
Fe3+	-	0.0000	0.0000	-	0.0000	-
TOTAL:	2.0000	2.0000	2.0000	2.0000	2.0000	2.0000
M1 site						
AlVI	0.0460	0.0860	0.1269	0.1813	0.0698	0.8426
Fe3+	0.1062	0.0487	0.0278	-	0.0890	-
Ti4+	0.0381	0.0219	0.0201	0.0083	0.0146	-
Cr3+	-	0.0070	-	-	-	-
Mg2+	0.6988	0.7823	0.7761	0.7327	0.8266	0.1574
Fe2+	0.1109	0.0541	0.0491	0.0777	-	-
TOTAL:	1.0000	1.0000	1.0000	1.0000	1.0000	1.0000
M2 site						
Mg2+	-	-	-	-	0.0002	0.1361
Fe2+	0.1614	0.0987	0.0716	0.0658	0.0762	0.1106
Mn2+	0.0128	-	-	-	-	-
Ca2+	0.7908	0.8763	0.9284	0.9259	0.8866	0.1802
Na+	0.0351	0.0250	-	-	0.0369	0.3871
TOTAL:	1.0001	1.0000	1.0000	0.9917	0.9999	0.8140
iCAT#:	4.0357	4.0163	4.0093	3.9917	4.0299	3.8140
OXNUM:	5.9998	5.9997	5.9996	5.9995	5.9995	5.9997
mg#:	0.72	0.84	0.87	0.84	0.92	0.73
Q:	1.7619	1.8114	1.8252	1.8021	1.7896	0.5843
J:	0.0702	0.0500	0.0000	0.0000	0.0738	0.7742
En:	37.1524	42.0569	41.8834	40.6581	44.0115	50.2310
Wo:	42.0437	47.1104	50.1025	51.3789	47.1947	30.8403
Fs:	20.8039	10.8328	8.0140	7.9629	8.7938	18.9286
Ae	3.5100	2.5000	-	-	3.6904	-
Jd	-	-	-	-	-	47.5553
Ka	1.2800	-	-	-	-	-
CaTi	7.6200	4.3800	4.0200	1.6739	2.9203	-
CaCr	-	0.7000	-	-	-	-
CaTs	4.6000	8.6000	12.6900	18.2817	6.9807	22.1376
Ess	7.1100	2.3700	2.7800	-	5.2105	-
F2F3	-	-	-	-	-	-
FeAl	-	-	-	-	-	13.5872
Jo	-	-	-	-	-	-
Di	59.7500	71.5800	73.3500	73.0463	73.5574	-
Hd	-	-	-	0.3630	-	-
En	-	-	-	-	0.0200	16.7199
Fs	11.0900	5.4100	4.9100	6.6351	-	-
Fs-En	5.0400	4.4600	2.2500	-	7.6208	-
inSUM:	1.0000	1.0000	1.0000	0.9917	0.9999	0.8140
resAlT	0.0006	0.0006	0.0008	-0.0157	0.0007	-0.2066

IMA names:
px1 - aluminian [Magnesium-rich] AUGITE
px2 - aluminian Ferroan DIOPSIDE
px3 - aluminian Ferroan DIOPSIDE
px4 - aluminian Ferroan DIOPSIDE
px5 - aluminian Ferroan DIOPSIDE
px6 - OMPHACITE

Appendix B

Ophiolitic rock : dolerite

Chlorite composition data
filename: od204un.dat

	1 chl1	2 chl2	3 chl3	4 chl4
SiO2	29.82	29.52	29.74	30.10
Al2O3	17.65	16.51	16.68	16.62
FeO	15.24	14.34	15.13	15.17
MnO	0.21	0.23	0.00	0.26
Cr2O3	0.00	0.00	0.00	0.18
CaO	0.00	0.30	0.27	0.51
MgO	23.15	22.59	22.60	22.49
K2O	0.00	0.00	0.00	0.11
Na2O	0.42	0.00	0.00	0.00
Sum:	86.49	83.49	84.42	85.44
Si	6.021	6.150	6.141	6.159
Al	4.200	4.054	4.059	4.008
Fe2	2.573	2.498	2.613	2.596
Mn	0.036	0.041	-	0.045
Cr	-	-	-	0.029
Ca	-	0.067	0.060	0.112
Mg	6.967	7.014	6.956	6.859
K	-	-	-	0.029
Na	0.164	-	-	-
inCAT#:	19.961	19.823	19.829	19.837
mg:	73.03	73.74	72.70	72.55

Appendix B

Ophiolitic rock : dolerite

Feldspar composition data
filename: od207pl.dat

	1 pl1	2 pl4	3 pl5	4 pl7	5 pl6	6 pl8	7 pl9	8 pl10c
SiO2	53.70	54.62	53.06	51.38	52.42	51.99	52.72	53.44
Al2O3	28.84	27.87	28.88	30.10	29.29	30.06	29.38	28.68
FeO	0.32	0.00	0.54	0.75	0.57	0.68	0.37	0.61
CaO	11.91	10.79	12.19	13.49	12.82	13.39	12.64	11.74
Na2O	4.62	5.30	4.82	3.94	4.24	4.08	4.33	4.86
Sum:	99.39	98.58	99.49	99.66	99.34	100.20	99.44	99.33

feldspar cation numbers on the basis of 8 oxygens

Si	2.442	2.494	2.421	2.351	2.397	2.363	2.404	2.438
Al	1.546	1.500	1.553	1.623	1.579	1.610	1.579	1.542
Fe2	0.012	-	0.021	0.029	0.022	0.026	0.014	0.023
Ca	0.580	0.528	0.596	0.661	0.628	0.652	0.618	0.574
Na	0.407	0.469	0.426	0.349	0.376	0.359	0.383	0.430
inCAT#:	4.988	4.991	5.016	5.013	5.001	5.011	4.997	5.006
mg:	0.00	0.00	0.00	0.00	0.00	0.00	0.00	0.00
Al4:	0.558	0.506	0.579	0.649	0.603	0.637	0.596	0.562
Al6:	0.988	0.994	0.973	0.973	0.976	0.974	0.983	0.979
Or:	0.000	0.000	0.000	0.000	0.000	0.000	0.000	0.000
Ab:	41.247	47.061	41.708	34.574	37.440	35.538	38.269	42.830
An:	58.753	52.939	58.292	65.426	62.560	64.462	61.731	57.170

	9 pl11
SiO2	54.44
Al2O3	28.29
FeO	0.39
CaO	11.11
Na2O	5.23
Sum:	99.46

feldspar cation numbers on the basis of 8 oxygens

Si	2.472
Al	1.514
Fe2	0.015
Ca	0.540
Na	0.460
inCAT#:	5.001
mg:	0.00
Al4:	0.528
Al6:	0.986
Or:	0.000
Ab:	46.003
An:	53.997

Appendix B

Ophiolitic rock : dolerite

Pyroxene composition data
file-name: od207px.dat
Number of samples: 10

	1 cp3	2 px4	3 px5	4 px6	5 px7	6 px9	7 px8	8 px10
SiO2	52.57	52.73	52.73	52.60	51.90	52.20	51.78	50.37
TiO2	0.24	0.00	0.39	0.50	0.38	0.26	0.35	0.47
Al2O3	4.00	4.08	3.79	4.17	4.53	4.00	4.50	4.98
FeO	15.80	15.46	15.93	15.88	16.47	16.24	16.69	17.44
Cr2O3	0.00	0.00	0.00	0.00	0.35	0.00	0.00	0.00
CaO	12.53	12.85	12.57	12.80	12.79	12.45	12.50	12.20
MgO	13.91	13.63	13.70	13.52	12.79	13.96	13.26	12.38
K2O	0.11	0.00	0.00	0.00	0.00	0.00	0.00	0.00
Na2O	0.56	0.54	0.55	0.42	0.60	0.59	0.57	0.77
Sum	99.72	99.29	99.66	99.89	99.81	99.70	99.65	98.61
T site								
Si4+	1.9645	1.9747	1.9713	1.9617	1.9472	1.9555	1.9452	1.9236
AlIV	0.0355	0.0253	0.0287	0.0383	0.0528	0.0445	0.0548	0.0764
TOTAL:	2.0000	2.0000	2.0000	2.0000	2.0000	2.0000	2.0000	2.0000
M1 site								
AlVI	0.1406	0.1547	0.1382	0.1449	0.1475	0.1321	0.1444	0.1477
Ti4+	0.0067	-	0.0109	0.0140	0.0107	0.0073	0.0098	0.0134
Cr3+	-	-	-	-	0.0103	-	-	-
Mg2+	0.7747	0.7608	0.7634	0.7515	0.7152	0.7794	0.7425	0.7047
Fe2+	0.0780	0.0845	0.0875	0.0896	0.1163	0.0812	0.1033	0.1342
TOTAL:	1.0000	1.0000	1.0000	1.0000	1.0000	1.0000	1.0000	1.0000
M2 site								
Fe2+	0.4157	0.3997	0.4105	0.4056	0.4004	0.4275	0.4210	0.4228
Ca2+	0.5016	0.5156	0.5035	0.5114	0.5141	0.4997	0.5031	0.4992
Na+	0.0457	0.0392	0.0398	0.0303	0.0436	0.0428	0.0415	0.0570
TOTAL:	0.9630	0.9545	0.9538	0.9473	0.9581	0.9700	0.9656	0.9790
iCAT#:	3.9630	3.9545	3.9538	3.9473	3.9581	3.9700	3.9656	3.9790
OXNUM:	5.9994	5.9996	5.9995	5.9995	5.9995	5.9997	5.9994	5.9995
mg#:	0.61	0.61	0.61	0.60	0.58	0.61	0.59	0.56
Q:	1.7700	1.7606	1.7649	1.7581	1.7460	1.7878	1.7699	1.7609
J:	0.0914	0.0784	0.0796	0.0606	0.0872	0.0856	0.0830	0.1140
En:	43.7684	43.2125	43.2546	42.7450	40.9622	43.5955	41.9515	40.0193
Wo:	28.3390	29.2855	28.5285	29.0882	29.4444	27.9506	28.4253	28.3491
Fs:	27.8927	27.5020	28.2169	28.1668	29.5934	28.4540	29.6231	31.6315
ZrAe	-	-	-	-	-	-	-	-
Ae	-	-	-	-	-	-	-	-
Jd	4.7456	4.1069	4.1728	3.1986	4.5507	4.4124	4.2978	5.8223
Nept	-	-	-	-	-	-	-	-
Kosm	-	-	-	-	-	-	-	-
Ka	-	-	-	-	-	-	-	-
CaTi	1.3915	-	2.2856	2.9558	2.2336	1.5052	2.0298	2.7375
CaCr	-	-	-	-	1.0750	-	-	-
CaTs	9.8546	12.1006	10.3166	12.0975	10.8444	9.2062	10.6566	9.2646
Ess	-	-	-	-	-	-	-	-
F2F3	-	-	-	-	-	-	-	-
FeAl	-	-	-	-	-	-	-	-
Jo	-	-	-	-	-	-	-	-
Di	40.8411	41.9172	40.1866	38.9317	39.5053	40.8041	39.4159	38.9888
Hd	-	-	-	-	-	-	-	-
En	-	-	-	-	-	-	-	-
Fs	8.0997	8.8528	9.1738	9.4585	12.1386	8.3711	10.6980	13.7079
Fs-En	35.0675	33.0225	33.8645	33.3580	29.6524	35.7010	32.9018	29.4791
inSUM:	0.9630	0.9545	0.9538	0.9473	0.9581	0.9700	0.9656	0.9790
resAlT	-0.0728	-0.0902	-0.0915	-0.1043	-0.0828	-0.0594	-0.0677	-0.0411

IMA names:
cp3 - [Subcalcic magnesium-rich] AUGITE
px4 - [Subcalcic magnesium-rich] AUGITE
px5 - [Subcalcic magnesium-rich] AUGITE
px6 - [Subcalcic magnesium-rich] AUGITE
px7 - chromian [Subcalcic magnesium-rich] AUGITE
px9 - [Subcalcic magnesium-rich] AUGITE
px8 - [Subcalcic magnesium-rich] AUGITE
px10 - [Subcalcic magnesium-rich] AUGITE

	9	10
	px11	px2
SiO2	52.73	51.97
TiO2	0.32	0.38
Al2O3	3.98	4.17
FeO	16.02	17.14
Cr2O3	0.00	0.00
CaO	12.29	12.48
MgO	13.11	12.96
K2O	0.00	0.10
Na2O	0.53	0.78
Sum	98.98	99.98
T site		
Si4+	1.9823	1.9522
AlIV	0.0177	0.0478
TOTAL:	2.0000	2.0000
M1 site		
AlVI	0.1586	0.1368
Ti4+	0.0090	0.0107
Mg2+	0.7346	0.7256
Fe2+	0.0978	0.1269
TOTAL:	1.0000	1.0000
M2 site		
Fe2+	0.4058	0.4115
Ca2+	0.4950	0.5022
Na+	0.0386	0.0615
TOTAL:	0.9394	0.9752
iCAT#:	3.9394	3.9752
OXNUM:	5.9996	5.9997
mg#:	0.59	0.57
Q:	1.7332	1.7662
J:	0.0772	0.1230
En:	42.3840	41.0826
Wo:	28.5599	28.4339
Fs:	29.0561	30.4835
ZrAe	-	-
Ae	-	-
Jd	4.1090	6.3064
Nept	-	-
Kosm	-	-
Ka	-	-
CaTi	1.9161	2.1944
CaCr	-	-
CaTs	12.7741	7.7215
Ess	-	-
F2F3	-	-
FeAl	-	-
Jo	-	-
Di	38.0030	41.5812
Hd	-	-
En	-	-
Fs	10.4109	13.0127
Fs-En	32.7869	29.1838
inSUM:	0.9394	0.9752
resAlT	-0.1203	-0.0489

IMA names:
px11 - [Subcalcic magnesium-rich] AUGITE
px2 - [Subcalcic magnesium-rich] AUGITE

Appendix B

Ophiolitic rock : dolerite

Amphibole composition data
file-name: od207amp.dat
Number of samples: 8

	1 amp1	2 amp2	3 amp3	4 amp4	5 amp5	6 amp6	7 amp7	8 amp8
SiO2	50.37	51.24	50.52	50.60	51.40	51.39	51.73	51.82
Al2O3	4.98	3.20	3.89	4.47	3.23	3.97	3.98	3.46
TiO2	0.47	0.26	0.32	0.38	0.00	0.49	0.32	0.44
FeO	17.44	16.42	15.23	15.46	15.13	15.07	16.02	15.52
MnO	0.07	0.00	0.00	0.00	0.00	0.00	0.00	0.00
MgO	12.38	12.95	13.39	13.04	13.93	13.28	13.11	13.78
CaO	12.20	12.20	12.03	12.20	12.14	12.53	12.29	12.41
K2O	0.00	0.10	0.10	0.00	0.00	0.00	0.00	0.00
Na2O	0.77	0.00	0.71	0.50	0.44	0.53	0.53	0.55
TOTAL:	98.68	96.37	96.19	96.65	96.27	97.26	97.98	97.98
	Amphibole ion numbers on the basis of 23 (24) oxygens							
Si	7.301	7.549	7.460	7.431	7.540	7.520	7.506	7.506
Al4	0.699	0.451	0.540	0.569	0.460	0.480	0.494	0.494
	8.000	8.000	8.000	8.000	8.000	8.000	8.000	8.000
Al6	0.152	0.105	0.137	0.205	0.098	0.205	0.187	0.097
Ti	0.051	0.029	0.035	0.042	-	0.054	0.035	0.048
Fe3+	0.438	0.418	0.303	0.297	0.420	0.087	0.267	0.294
Mg	2.675	2.844	2.947	2.854	3.046	2.897	2.835	2.975
Fe2+	1.676	1.604	1.578	1.601	1.436	1.757	1.676	1.586
Mn	0.008	-	-	-	-	-	-	-
	5.000	5.000	5.000	4.999	5.000	5.000	5.000	5.000
Fe2+	-	0.001	-	-	-	0.001	-	-
Mn	0.001	-	-	-	-	-	-	-
Ca	1.895	1.926	1.903	1.920	1.908	1.965	1.911	1.926
Na	0.104	-	0.097	0.080	0.092	0.034	0.089	0.074
	2.000	1.927	2.000	2.000	2.000	2.000	2.000	2.000
Na	0.112	-	0.106	0.062	0.033	0.116	0.060	0.080
K	-	0.019	0.019	-	-	-	-	-
	0.112	0.019	0.125	0.062	0.033	0.116	0.060	0.080
mg:	0.559	0.584	0.610	0.600	0.621	0.611	0.593	0.613
mg-Fe2:	0.615	0.639	0.651	0.641	0.680	0.622	0.628	0.652
SUMOX:	23.000	23.001	22.999	22.999	23.000	23.001	23.000	23.000
orCAT#:	15.256	15.082	15.225	15.160	15.172	15.143	15.148	15.177
Ca+Na)B	1.999	1.926	2.000	2.000	2.000	1.999	2.000	2.000
(Na)B	0.104	0.000	0.097	0.080	0.092	0.034	0.089	0.074
(Na+K)A	0.112	0.019	0.125	0.062	0.033	0.116	0.060	0.080

IMA name:
1 amp1 - Calcic Amphibole - Actinolitic-Hornblende
2 amp2 - Calcic Amphibole - Actinolite
3 amp3 - Calcic Amphibole - Actinolitic-Hornblende
4 amp4 - Calcic Amphibole - Actinolitic-Hornblende
5 amp5 - Calcic Amphibole - Actinolite
6 amp6 - Calcic Amphibole - Actinolite
7 amp7 - Calcic Amphibole - Actinolite
8 amp8 - Calcic Amphibole - Actinolite

Appendix B

Woi Formation : basaltic andesite

Feldspar composition data
filename: od4pl.dat

	1 pl1	2 pl2	3 pl6	4 pl7C	5 pl8C	6 pl9
SiO2	51.48	54.82	50.24	47.08	59.31	65.82
TiO2	0.00	0.00	0.00	0.00	0.21	0.27
Al2O3	29.53	27.88	26.91	32.82	25.23	18.56
FeO	0.69	0.98	0.23	0.51	0.71	0.00
CaO	13.50	11.26	9.08	17.25	7.15	0.00
Na2O	3.60	4.67	5.68	1.75	6.77	3.03
Sum:	98.80	99.61	92.14	99.41	99.38	87.68

feldspar cation numbers on the basis of 8 oxygens

Si	2.371	2.487	2.458	2.180	2.660	3.138
Ti	-	-	-	-	0.007	0.010
Al	1.603	1.491	1.552	1.791	1.334	1.043
Fe3	-	-	-	-	-	-
Fe2	0.026	0.037	0.009	0.020	0.027	-
Ca	0.666	0.547	0.476	0.856	0.344	-
Na	0.321	0.411	0.539	0.157	0.589	0.280
inCAT#:	4.988	4.973	5.035	5.003	4.960	4.471
mg:	0.00	0.00	0.00	0.00	0.00	0.00
Al4:	0.629	0.513	0.542	0.820	0.340	-
Al6:	0.974	0.978	1.010	0.971	0.994	1.043
Or:	0.000	0.000	0.000	0.000	0.000	0.000
Ab:	32.547	42.871	53.099	15.503	63.145	%100.000
An:	67.453	57.129	46.901	84.497	36.855	0.000

Appendix B

Woi Formation : andesite

Pyroxene composition data
file-name: od4px.dat
Number of samples: 11

	1 CPX1	2 CPX2	3 CPX3	4 CPX4	5 CPX5	6 CPX6c	7 CPX7c
SiO2	52.31	51.82	52.35	53.19	52.04	52.06	52.84
TiO2	0.36	0.42	0.35	0.40	0.42	0.41	0.58
Al2O3	1.39	2.32	3.04	1.57	1.78	1.87	3.06
Fe2O3	0.00	0.00	0.00	0.00	0.00	0.00	0.00
FeO	9.35	8.09	7.35	9.41	10.96	11.02	8.49
MnO	0.42	0.34	0.27	0.49	0.35	0.36	0.66
MgO	21.31	15.22	16.12	14.58	14.62	14.49	19.58
CaO	13.75	21.13	20.43	20.86	19.46	19.02	13.83
Sum	98.89	99.34	99.91	100.50	99.63	99.23	99.04
T site							
Si4+	1.9217	1.9328	1.9282	1.9685	1.9519	1.9578	1.9376
AlIV	0.0601	0.0672	0.0718	0.0315	0.0481	0.0422	0.0624
Fe3+	0.0182	-	-	-	-	-	-
TOTAL:	2.0000	2.0000	2.0000	2.0000	2.0000	2.0000	2.0000
M1 site							
AlVI	-	0.0348	0.0601	0.0369	0.0305	0.0406	0.0698
Fe3+	0.0575	0.0078	-	-	-	-	-
Ti4+	0.0099	0.0117	0.0096	0.0111	0.0118	0.0115	0.0159
Mg2+	0.9326	0.8462	0.8850	0.8042	0.8173	0.8122	0.9143
Fe2+	-	0.0995	0.0453	0.1478	0.1404	0.1357	-
TOTAL:	1.0000	1.0000	1.0000	1.0000	1.0000	1.0000	1.0000
M2 site							
Mg2+	0.2343	-	-	-	-	-	0.1558
Fe2+	0.2115	0.1450	0.1811	0.1434	0.2033	0.2108	0.2603
Mn2+	0.0130	0.0107	0.0084	0.0153	0.0111	0.0114	0.0204
Ca2+	0.5412	0.8444	0.8062	0.8271	0.7820	0.7663	0.5433
TOTAL:	1.0000	1.0001	0.9957	0.9858	0.9964	0.9885	0.9798
iCAT#:	4.0254	4.0026	3.9957	3.9858	3.9964	3.9885	3.9798
OXNUM:	5.9995	5.9995	5.9995	5.9996	5.9994	5.9992	5.9994
mg#:	0.85	0.78	0.80	0.73	0.70	0.70	0.80
Q:	1.9196	1.9351	1.9176	1.9225	1.9430	1.9250	1.8737
J:	0.0000	0.0000	0.0000	0.0000	0.0000	0.0000	0.0000
En:	58.1039	43.3149	45.9502	41.5007	41.8249	41.9438	56.4965
Wo:	26.9482	43.2228	41.8588	42.6824	40.0184	39.5734	28.6838
Fs:	14.9480	13.4623	12.1911	15.8169	18.1567	18.4828	14.8197
ZrAe	-	-	-	-	-	-	-
Ae	-	-	-	-	-	-	-
Jd	-	-	-	-	-	-	-
Nept	-	-	-	-	-	-	-
Kosm	-	-	-	-	-	-	-
Ka	1.3000	1.0700	0.8436	1.5520	1.1140	1.1533	2.0821
CaTi	1.9800	2.3400	1.9283	2.2520	2.3685	2.3268	3.2456
CaCr	-	-	-	-	-	-	-
CaTs	-	3.4800	6.0360	3.7432	3.0610	4.1072	7.1239
Ess	5.7500	0.7800	-	-	-	-	-
F2F3	-	-	-	-	-	-	-
FeAl	-	-	-	-	-	-	-
Jo	-	-	-	-	-	-	-
Di	46.3900	77.8400	73.0039	77.9063	73.0530	71.0875	45.0806
Hd	-	-	-	-	-	-	-
En	23.4300	-	-	-	-	-	15.9012
Fs	-	9.9500	4.5496	14.5466	14.0907	13.7279	-
Fs-En	21.1500	4.5400	13.6386	-	6.3127	7.5974	26.5666
inSUM:	1.0000	1.0000	0.9957	0.9858	0.9964	0.9885	0.9798
resAlT	0.0010	0.0012	-0.0075	-0.0276	-0.0060	-0.0214	-0.0392

IMA names:
OD4CPX1 - [Subcalcic magnesium-rich] AUGITE
OD4CPX2 - [Magnesium-rich] AUGITE
OD4CPX3 - [Magnesium-rich] AUGITE
OD4CPX4 - [Magnesium-rich] AUGITE
OD4CPX5 - [Magnesium-rich] AUGITE
OD4CPX6c - [Magnesium-rich] AUGITE
OD4CPX7c - [Subcalcic magnesium-rich] AUGITE

Appendix B

Woi Formation : basaltic andesitic clast

Feldspar composition data
filename: or197pl.dat

	1 pl1	2 pl2	3 pl3	4 pl4	5 pl5	6 pl6	7 pl7	8 pl7
SiO2	53.54	52.42	52.72	52.74	52.87	53.29	49.72	47.54
Al2O3	28.48	29.46	28.98	29.05	29.34	29.24	31.80	33.22
FeO	0.74	0.66	0.71	0.78	0.70	0.77	0.56	0.74
CaO	11.94	12.95	12.49	12.65	12.74	12.68	15.23	17.21
MgO	0.27	0.25	0.26	0.00	0.26	0.00	0.26	0.00
K2O	0.55	0.43	0.50	0.50	0.47	0.38	0.16	0.14
Na2O	4.20	3.75	4.07	3.91	3.94	3.74	2.68	1.78
Sum:	99.72	99.92	99.73	99.63	100.32	100.10	100.41	100.63
feldspar cation numbers on the basis of 8 oxygens								
Si	2.435	2.385	2.403	2.406	2.396	2.414	2.264	2.174
Al	1.527	1.580	1.557	1.562	1.567	1.561	1.707	1.791
Fe3	0.025	0.023	0.024	0.027	0.024	0.026	0.019	0.025
Fe2	-	-	-	-	-	-	-	-
Ca	0.582	0.631	0.610	0.618	0.618	0.615	0.743	0.843
Mg	0.018	0.017	0.018	-	0.018	-	0.018	-
K	0.032	0.025	0.029	0.029	0.027	0.022	0.009	0.008
Na	0.370	0.331	0.360	0.346	0.346	0.328	0.236	0.158
inCAT#:	4.990	4.991	5.000	4.987	4.995	4.967	4.996	5.000
mg:	100.00	100.00	100.00	0.00	100.00	0.00	100.00	0.00
Al4:	0.565	0.615	0.597	0.594	0.604	0.586	0.736	0.826
Al6:	0.962	0.965	0.960	0.967	0.962	0.975	0.970	0.965
Or:	3.242	2.523	2.904	2.920	2.733	2.268	0.931	0.803
Ab:	37.632	33.516	36.014	34.824	34.903	34.006	23.920	15.635
An:	59.126	63.961	61.082	62.256	62.364	63.726	75.149	83.563

Appendix B

Woi Formation : basalt

Pyroxene composition data
file-name: or197px.dat
Number of samples: 19

	1 cp1c	2 cp2r	3 cp3	4 cp4	5 cp5	6 cp6	7 cp7	8 cp9c
SiO2	51.36	51.27	51.16	51.77	51.45	51.69	51.55	51.79
TiO2	0.54	0.36	0.51	0.40	0.48	0.45	0.42	0.40
Al2O3	2.49	3.07	2.54	2.20	2.31	2.41	2.29	1.98
FeO	11.19	7.57	10.71	10.45	10.74	10.64	10.27	10.08
MnO	0.41	0.00	0.33	0.40	0.38	0.48	0.37	0.38
CaO	19.25	21.44	19.80	19.60	19.42	19.31	19.69	19.66
MgO	14.51	15.17	14.33	14.66	14.58	14.61	14.91	14.59
Na2O	0.41	0.34	0.55	0.47	0.49	0.55	0.58	0.00
Sum	100.16	99.22	99.93	99.95	99.85	100.14	100.08	98.88
T site								
Si4+	1.9121	1.9037	1.9053	1.9265	1.9176	1.9198	1.9109	1.9513
AlIV	0.0879	0.0963	0.0947	0.0735	0.0824	0.0802	0.0891	0.0487
Fe3+	0.0000	0.0000	-	0.0000	-	-	-	-
TOTAL:	2.0000	2.0000	2.0000	2.0000	2.0000	2.0000	2.0000	2.0000
M1 site								
AlVI	0.0213	0.0381	0.0168	0.0229	0.0190	0.0253	0.0109	0.0392
Fe3+	0.0650	0.0618	0.0881	0.0609	0.0707	0.0683	0.0958	-
Ti4+	0.0151	0.0100	0.0142	0.0111	0.0134	0.0125	0.0117	0.0113
Mg2+	0.8051	0.8396	0.7954	0.8131	0.8100	0.8088	0.8238	0.8193
Fe2+	0.0935	0.0505	0.0855	0.0920	0.0869	0.0851	0.0578	0.1302
TOTAL:	1.0000	1.0000	1.0000	1.0000	1.0000	1.0000	1.0000	1.0000
M2 site								
Fe2+	0.1898	0.1227	0.1599	0.1723	0.1771	0.1770	0.1647	0.1874
Mn2+	0.0128	-	0.0103	0.0125	0.0119	0.0150	0.0116	0.0121
Ca2+	0.7678	0.8529	0.7901	0.7814	0.7755	0.7684	0.7820	0.7936
Na+	0.0295	0.0245	0.0397	0.0338	0.0354	0.0396	0.0417	-
TOTAL:	0.9999	1.0001	1.0000	1.0000	0.9999	1.0000	1.0000	0.9931
iCAT#:	4.0218	4.0207	4.0296	4.0204	4.0237	4.0229	4.0322	3.9931
OXNUM:	5.9994	5.9997	5.9995	5.9993	5.9992	5.9994	5.9997	5.9997
mg#:	0.74	0.83	0.76	0.75	0.75	0.76	0.79	0.72
Q:	1.8562	1.8657	1.8309	1.8588	1.8495	1.8393	1.8283	1.9305
J:	0.0590	0.0490	0.0794	0.0676	0.0708	0.0792	0.0834	0.0000
En:	41.6287	43.5590	41.2274	42.0816	41.9233	42.0680	42.5582	42.1754
Wo:	39.7001	44.2490	40.9527	40.4409	40.1377	39.9667	40.3988	40.8525
Fs:	18.6711	12.1920	17.8199	17.4775	17.9390	17.9653	17.0429	16.9721
Ae	2.9503	2.4500	3.9700	3.3800	3.5404	3.9600	4.1700	-
Jd	-	-	-	-	-	-	-	-
Nept	-	-	-	-	-	-	-	-
Ka	1.2801	-	1.0300	1.2500	1.1901	1.5000	1.1600	1.2184
CaTi	3.0203	2.0000	2.8400	2.2200	2.6803	2.5000	2.3400	2.2757
CaCr	-	-	-	-	-	-	-	-
CaTs	2.1302	3.8100	1.6800	2.2900	1.9002	2.5300	1.0900	3.9472
Ess	3.5504	3.7300	4.8400	2.7100	3.5304	2.8700	5.4100	-
F2F3	-	-	-	-	-	-	-	-
FeAl	-	-	-	-	-	-	-	-
Jo	-	-	-	-	-	-	-	-
Di	68.0868	75.7500	69.6500	70.9200	69.4469	68.9400	69.3600	73.6885
Hd	-	-	-	-	-	-	-	-
En	-	-	-	-	-	-	-	-
Fs	9.3509	5.0500	8.5500	9.2000	8.6909	8.5100	5.7800	13.1105
Fs-En	9.6310	7.2100	7.4400	8.0300	9.0209	9.1900	10.6900	5.7597
inSUM:	0.9999	1.0000	1.0000	1.0000	0.9999	1.0000	1.0000	0.9931
resAlT	0.0009	0.0009	0.0011	0.0013	0.0013	0.0012	0.0007	-0.0131

IMA names:
cp1c - [Magnesium-rich] AUGITE
cp2r - [Magnesium-rich] AUGITE
cp3 - [Magnesium-rich] AUGITE
cp4 - [Magnesium-rich] AUGITE
cp5 - [Magnesium-rich] AUGITE
cp6 - (Magnesium-rich] AUGITE
cp7 - [Magnesium-rich] AUGITE
cp9c - [Magnesium-rich] AUGITE

	9	10	11	12	13	14	15	16
	cp10	op1	op2	op3	op4	op6	op8	op7c
SiO2	51.98	53.25	52.91	53.23	53.00	53.08	52.95	53.44
TiO2	0.43	0.22	0.42	0.28	0.34	0.29	0.22	0.22
Al2O3	2.00	1.36	1.66	1.44	1.45	0.00	1.52	1.50
Fe2O3	0.00	0.00	0.00	19.80	0.00	1.35	0.00	0.00
FeO	10.42	19.20	20.41	19.80	19.50	19.84	19.77	19.51
MnO	0.41	0.73	0.68	0.69	0.68	0.86	0.79	0.80
CaO	19.84	1.83	1.81	1.72	1.76	1.91	1.78	1.75
MgO	14.54	23.48	22.47	23.37	23.35	22.94	23.00	23.58
Na2O	0.37	0.36	0.32	0.00	0.34	0.00	0.00	0.00
Sum	99.99	100.43	100.68	120.33	100.42	100.27	100.03	100.80
T site								
Si4+	1.9367	1.9481	1.9440	1.7192	1.9415	1.9684	1.9558	1.9542
AlIV	0.0633	0.0519	0.0560	0.0547	0.0585	0.0000	0.0442	0.0458
Fe3+	0.0000	0.0000	-	0.2261	0.0000	0.0316	-	-
TOTAL:	2.0000	2.0000	2.0000	2.0000	2.0000	2.0000	2.0000	2.0000
M1 site								
AlVI	0.0245	0.0067	0.0158	-	0.0041	-	0.0220	0.0188
Fe3+	0.0404	0.0579	0.0389	0.2551	0.0588	0.0060	0.0090	0.0141
Ti4+	0.0120	0.0060	0.0116	0.0068	0.0094	0.0080	0.0061	0.0060
Mg2+	0.8075	0.9294	0.9337	0.7381	0.9277	0.9860	0.9629	0.9611
Fe2+	0.1156	-	-	-	-	-	-	-
TOTAL:	1.0000	1.0000	1.0000	1.0000	1.0000	1.0000	1.0000	1.0000
M2 site								
Mg2+	-	0.3509	0.2968	0.3870	0.3472	0.2819	0.3034	0.3242
Fe2+	0.1686	0.5294	0.5882	0.5348	0.5385	0.6153	0.6016	0.5825
Mn2+	0.0129	0.0226	0.0211	0.0188	0.0211	0.0270	0.0247	0.0248
Ca2+	0.7919	0.0717	0.0712	0.0594	0.0691	0.0758	0.0703	0.0685
Na+	0.0267	0.0255	0.0227	-	0.0241	-	-	-
TOTAL:	1.0001	1.0001	1.0000	1.0000	1.0000	1.0000	1.0000	1.0000
iCAT#:	4.0135	4.0194	4.0130	4.0037	4.0197	4.0028	4.0030	4.0047
OXNUM:	5.9995	5.9997	5.9996	5.9939	5.9995	5.9952	5.9995	5.9996
mg#:	0.74	0.71	0.68	0.68	0.70	0.67	0.68	0.69
Q:	1.8836	1.8814	1.8899	1.7193	1.8825	1.9590	1.9382	1.9363
J:	0.0534	0.0510	0.0454	0.0000	0.0482	0.0000	0.0000	0.0000
En:	41.6903	65.2582	63.1058	50.6962	64.9664	62.6557	64.2173	65.0719
Wo:	40.8849	3.6546	3.6515	2.6765	3.5212	3.7458	3.5651	3.4680
Fs:	17.4248	31.0872	33.2427	46.6273	31.5124	33.5985	32.2177	31.4601
ZrAe	-	-	-	-	-	-	-	-
Ae	2.6700	2.5500	2.2700	-	2.4100	-	-	-
Jd	-	-	-	-	-	-	-	-
Nept	-	-	-	-	-	-	-	-
Kosm	-	-	-	-	-	-	-	-
Ka	1.2900	2.2600	2.1100	1.8800	2.1100	2.7000	2.4700	2.4800
CaTi	2.4000	1.2000	2.3200	1.3600	1.8800	1.6000	1.2200	1.2000
CaCr	-	-	-	-	-	-	-	-
CaTs	2.4500	0.6700	1.5800	-	0.4100	-	2.2000	1.8800
Ess	1.3700	3.2400	1.6200	4.5800	3.4700	0.6000	0.9000	1.4100
F2F3	-	-	-	20.9300	-	-	-	-
FeAl	-	-	-	-	-	-	-	-
Jo	-	-	-	-	-	-	-	-
Di	72.9700	2.0600	1.6000	-	1.1500	5.3800	2.7100	2.3600
Hd	-	-	-	-	-	-	-	-
En	-	35.0900	29.6800	38.7000	34.7200	28.1900	30.3400	32.4200
Fs	11.5600	-	-	-	-	-	-	-
Fs-En	5.2900	52.9300	58.8200	32.5500	53.8500	61.5300	60.1600	58.2500
inSUM:	1.0000	1.0000	1.0000	1.0000	1.0000	1.0000	1.0000	1.0000
resAlT	0.0011	0.0008	0.0008	0.0121	0.0009	0.0096	0.0010	0.0009

IMA names:
cp10 - [Magnesium-rich] AUGITE
op1 - Ferroan ENSTATITE
op2 - Ferroan ENSTATITE
op3 - subsilicic Ferroan ENSTATITE
op4 - Ferroan ENSTATITE
op6 - Ferroan ENSTATITE
op8 - Ferroan ENSTATITE
op7c - Ferroan ENSTATITE

	17	18	19
	op9	op10	cp8
SiO2	52.88	52.72	52.06
TiO2	0.25	0.28	0.40
Al2O3	1.32	1.19	2.23
FeO	19.52	19.38	10.16
MnO	0.73	0.54	0.00
CaO	1.69	1.69	19.99
MgO	23.34	23.23	14.65
Na2O	0.00	0.00	1.29
Sum	99.73	99.03	100.78
T site			
Si4+	1.9557	1.9630	1.9064
AlIV	0.0443	0.0370	0.0936
Fe3+	-	-	0.0000
TOTAL:	2.0000	2.0000	2.0000
M1 site			
AlVI	0.0132	0.0152	0.0026
Fe3+	0.0162	0.0054	0.1598
Ti4+	0.0069	0.0078	0.0110
Mg2+	0.9637	0.9716	0.7996
Fe2+	-	-	0.0270
TOTAL:	1.0000	1.0000	1.0000
M2 site			
Mg2+	0.3229	0.3176	-
Fe2+	0.5875	0.5980	0.1243
Mn2+	0.0228	0.0170	-
Ca2+	0.0669	0.0674	0.7842
Na+	-	-	0.0916
TOTAL:	1.0001	1.0000	1.0001
iCAT#:	4.0054	4.0018	4.0540
OXNUM:	5.9995	5.9996	5.9997
mg#:	0.69	0.68	0.84
Q:	1.9410	1.9546	1.7351
J:	0.0000	0.0000	0.1832
En:	64.9798	65.2099	42.1975
Wo:	3.3788	3.4092	41.3848
Fs:	31.6414	31.3809	16.4178
ZrAe	-	-	-
Ae	-	-	9.1600
Jd	-	-	-
Nept	-	-	-
Kosm	-	-	-
Ka	2.2800	1.7000	-
CaTi	1.3800	1.5600	2.2000
CaCr	-	-	-
CaTs	1.3200	1.5200	0.2600
Ess	1.6200	0.5400	6.8200
F2F3	-	-	-
FeAl	-	-	-
Jo	-	-	-
Di	2.3700	3.1200	69.1400
Hd	-	-	-
En	32.2900	31.7600	-
Fs	-	-	2.7000
Fs-En	58.7400	59.8000	9.7200
inSUM:	1.0000	1.0000	1.0000
resAlT	0.0011	0.0008	0.0008

IMA names:
op9 - Ferroan ENSTATITE
op10 - Ferroan ENSTATITE
cp8 - [Magnesium-rich] AUGITE

Appendix B

Guyuti Formation : basaltic andesite

Feldspar composition data of
filename: od154pl.dat

	1 pl1	2 pl2	3 pl3	4 pl4	5 pl5	6 pl6	7 pl7	8 pl9c
SiO2	52.83	51.77	49.23	48.75	46.64	54.74	46.58	53.43
Al2O3	29.03	29.74	31.15	31.75	32.75	27.75	33.21	28.35
FeO	0.61	0.71	0.77	0.80	2.04	1.06	0.54	0.75
CaO	12.69	13.67	15.35	15.91	17.24	11.52	17.63	12.29
K2O	0.41	0.31	0.19	0.20	0.15	0.66	0.19	0.41
Na2O	3.97	3.61	2.76	2.53	2.04	4.51	1.41	4.17
Sum:	99.54	99.81	99.45	99.94	100.86	100.24	99.56	99.40
feldspar cation numbers on the basis of 8 oxygens								
Si	2.412	2.366	2.271	2.242	2.151	2.480	2.158	2.441
Al	1.562	1.602	1.694	1.721	1.780	1.482	1.813	1.527
Fe2	0.023	0.027	0.030	0.031	0.079	0.040	0.021	0.029
Ca	0.621	0.669	0.759	0.784	0.852	0.559	0.875	0.602
K	0.024	0.018	0.011	0.012	0.009	0.038	0.011	0.024
Na	0.351	0.320	0.247	0.226	0.182	0.396	0.127	0.369
inCAT#:	4.994	5.002	5.011	5.015	5.054	4.996	5.004	4.991
mg:	0.00	0.00	0.00	0.00	0.00	0.00	0.00	0.00
Al4:	0.588	0.634	0.729	0.758	0.849	0.520	0.842	0.559
Al6:	0.975	0.968	0.965	0.963	0.932	0.962	0.971	0.968
Or:	2.390	1.787	1.092	1.146	0.844	3.835	1.106	2.392
Ab:	35.281	31.755	24.279	22.089	17.485	39.879	12.500	37.133
An:	62.329	66.458	74.629	76.765	81.672	56.286	86.394	60.474

	9 pl9r
SiO2	48.15
Al2O3	31.72
FeO	0.81
CaO	16.18
K2O	0.00
Na2O	2.21
Sum:	99.07
feldspar cation numbers on the basis of 8 oxygens	
Si	2.233
Al	1.733
Fe2	0.031
Ca	0.804
K	-
Na	0.199
inCAT#:	5.000
mg:	0.00
Al4:	0.767
Al6:	0.966
Or:	0.000
Ab:	19.812
An:	80.188

Appendix B

Guyuti Formation : Basaltic andesite

Pyroxene composition data
file-name: od154px.dat
Number of samples: 16

	1 cp1	2 cp2	3 cp3	4 cp4	5 cp5	6 cp6	7 cp7	8 cp8
SiO2	52.18	50.66	51.71	50.97	52.27	51.91	52.31	51.26
TiO2	0.51	0.79	0.41	0.51	0.40	0.31	0.44	0.69
Al2O3	1.86	2.75	2.24	2.66	1.61	1.60	1.31	2.17
FeO	9.78	9.90	9.24	10.89	10.42	10.14	10.08	10.50
MnO	0.37	0.23	0.45	0.40	0.44	0.33	0.41	0.39
MgO	15.06	13.68	15.64	14.38	15.26	15.81	14.61	14.21
CaO	20.17	21.22	19.70	19.34	19.05	19.13	20.52	19.65
Na2O	0.36	0.51	0.43	0.40	0.54	0.49	0.38	0.42
Sum	100.29	99.74	99.82	99.55	99.99	99.72	100.06	99.29
T site								
Si4+	1.9327	1.8924	1.9150	1.9080	1.9404	1.9263	1.9473	1.9254
AlIV	0.0673	0.1076	0.0850	0.0920	0.0596	0.0699	0.0527	0.0746
Fe3+	-	-	0.0000	0.0000	-	0.0038	0.0000	-
TOTAL:	2.0000	2.0000	2.0000	2.0000	2.0000	2.0000	2.0000	2.0000
M1 site								
AlVI	0.0138	0.0135	0.0128	0.0253	0.0108	-	0.0047	0.0215
Fe3+	0.0502	0.0861	0.0790	0.0659	0.0647	0.0908	0.0499	0.0439
Ti4+	0.0141	0.0221	0.0113	0.0143	0.0111	0.0086	0.0122	0.0194
Mg2+	0.8314	0.7617	0.8633	0.8023	0.8443	0.8744	0.8106	0.7956
Fe2+	0.0905	0.1166	0.0336	0.0922	0.0691	0.0262	0.1226	0.1196
TOTAL:	1.0000	1.0000	1.0000	1.0000	1.0000	1.0000	1.0000	1.0000
M2 site								
Fe2+	0.1622	0.1066	0.1735	0.1828	0.1896	0.1938	0.1413	0.1662
Mn2+	0.0116	0.0072	0.0141	0.0126	0.0138	0.0103	0.0128	0.0124
Ca2+	0.8003	0.8493	0.7816	0.7756	0.7577	0.7606	0.8184	0.7908
Na+	0.0258	0.0369	0.0308	0.0289	0.0388	0.0352	0.0274	0.0306
TOTAL:	0.9999	1.0000	1.0000	0.9999	0.9999	0.9999	0.9999	1.0000
iCAT#:	4.0168	4.0289	4.0265	4.0221	4.0217	4.0318	4.0167	4.0147
OXNUM:	5.9994	5.9997	5.9993	5.9994	5.9995	5.9994	5.9993	5.9995
mg#:	0.77	0.77	0.81	0.74	0.77	0.80	0.75	0.74
Q:	1.8844	1.8342	1.8520	1.8529	1.8607	1.8550	1.8929	1.8722
J:	0.0516	0.0738	0.0616	0.0578	0.0776	0.0704	0.0548	0.0612
En:	42.7191	39.5175	44.3833	41.5398	43.5386	44.6145	41.4502	41.2549
Wo:	41.1212	44.0623	40.1830	40.1574	39.0728	38.8081	41.8490	41.0060
Fs:	16.1597	16.4202	15.4337	18.3028	17.3886	16.5774	16.7008	17.7392
ZrAe	-	-	-	-	-	-	-	-
Ae	2.5803	3.6900	3.0800	2.8903	3.8804	3.5204	2.7403	3.0600
Jd	-	-	-	-	-	-	-	-
Nept	-	-	-	-	-	-	-	-
Kosm	-	-	-	-	-	-	-	-
Ka	1.1601	0.7200	1.4100	1.2601	1.3801	1.0301	1.2801	1.2400
CaTi	2.8203	4.4200	2.2600	2.8603	2.2202	1.7202	2.4402	3.8800
CaTs	1.3801	1.3500	1.2800	2.5303	1.0801	-	0.4700	2.1500
Ess	2.4402	4.9200	4.8200	3.7004	2.5903	5.5606	2.2502	1.3300
F2F3	-	-	-	-	-	-	-	-
FeAl	-	-	-	-	-	-	-	-
Di	73.3973	73.2400	69.8000	68.4769	69.8870	68.7869	76.6877	71.7200
Hd	-	1.0000	-	-	-	-	-	-
Fs	9.0509	10.6600	3.3600	9.2209	6.9107	2.6203	12.2612	11.9600
Fs-En	7.1707	-	13.9900	9.0609	12.0512	16.7617	1.8702	4.6600
inSUM:	0.9999	1.0000	1.0000	0.9999	0.9999	0.9999	0.9999	1.0000
resAlT	0.0009	0.0007	0.0014	0.0011	0.0007	0.0009	0.0011	0.0010

MA names:
cp1 - [Magnesium-rich] AUGITE
cp2 - aluminian [Magnesium-rich] AUGITE
cp3 - [Magnesium-rich] AUGITE
cp4 - [Magnesium-rich] AUGITE
cp5 - [Magnesium-rich] AUGITE
cp6 - [Magnesium-rich] AUGITE
cp7 - [Magnesium-rich] AUGITE
cp8 - [Magnesium-rich] AUGITE

	9 op1	10 op2	11 op3	12 op4	13 op5	14 op6	15 op7	16 op8
SiO2	52.81	53.72	53.17	53.69	53.89	53.15	52.62	53.47
TiO2	0.34	0.00	0.34	0.33	0.26	0.30	0.33	0.47
Al2O3	1.29	0.25	1.17	0.94	1.13	1.10	1.82	1.32
FeO	19.34	20.52	19.71	18.81	18.47	19.93	18.96	19.11
MnO	0.60	0.60	0.61	0.52	0.54	0.71	0.60	0.65
MgO	23.22	23.35	23.14	24.31	24.35	23.16	23.26	23.46
CaO	1.86	0.00	1.92	1.77	1.72	1.87	1.87	0.00
Na2O	0.30	0.00	0.28	0.42	0.16	0.30	0.00	0.00
Sum	99.76	98.44	100.34	100.79	100.52	100.52	99.46	98.48
T site								
Si4+	1.9479	2.0100	1.9532	1.9497	1.9640	1.9497	1.9481	1.9867
AlIV	0.0521	0.0000	0.0468	0.0402	0.0360	0.0475	0.0519	0.0133
Fe3+	-	-	0.0000	0.0101	0.0000	0.0028	0.0000	-
TOTAL:	2.0000	2.0100	2.0000	2.0000	2.0000	2.0000	2.0000	2.0000
M1 site								
AlVI	0.0039	0.0110	0.0038	-	0.0125	-	0.0274	0.0445
Fe3+	0.0499	-	0.0436	0.0609	0.0198	0.0539	0.0051	-
Ti4+	0.0094	-	0.0094	0.0089	0.0071	0.0083	0.0091	0.0131
Mg2+	0.9368	0.9890	0.9432	0.9302	0.9606	0.9378	0.9584	0.9424
TOTAL:	1.0000	1.0000	1.0000	1.0000	1.0000	1.0000	1.0000	1.0000
M2 site								
Mg2+	0.3398	0.3132	0.3238	0.3856	0.3620	0.3286	0.3252	0.3568
Fe2+	0.5466	0.6421	0.5618	0.5002	0.5431	0.5547	0.5819	0.5938
Mn2+	0.0187	0.0190	0.0189	0.0159	0.0166	0.0220	0.0188	0.0204
Ca2+	0.0735	-	0.0755	0.0688	0.0671	0.0735	0.0742	-
Na+	0.0214	-	0.0199	0.0295	0.0113	0.0213	-	-
TOTAL:	1.0000	0.9743	0.9999	1.0000	1.0001	1.0001	1.0001	0.9710
iCAT#:	4.0167	3.9843	4.0146	4.0238	4.0066	4.0190	4.0017	3.9710
OXNUM:	5.9995	5.9998	5.9997	5.9995	5.9997	5.9995	5.9995	5.9997
mg#:	0.70	0.67	0.69	0.72	0.71	0.70	0.69	0.69
Q:	1.8967	1.9443	1.9043	1.8848	1.9328	1.8946	1.9397	1.8930
J:	0.0428	0.0000	0.0398	0.0590	0.0226	0.0426	0.0000	0.0000
En:	64.9570	66.3271	64.4194	66.7343	67.1643	64.1768	65.3697	67.9001
Wo:	3.7399	0.0000	3.8387	3.4894	3.4075	3.7247	3.7788	0.0000
Fs:	31.3031	33.6729	31.7419	29.7763	29.4282	32.0985	30.8515	32.0999
ZrAe	-	-	-	-	-	-	-	-
Ae	2.1400	-	1.9902	2.9500	1.1300	2.1300	-	-
Jd	-	-	-	-	-	-	-	-
Nept	-	-	-	-	-	-	-	-
Kosm	-	-	-	-	-	-	-	-
Ka	1.8700	1.9501	1.8902	1.5900	1.6600	2.2000	1.8800	2.1009
CaTi	1.8800	-	1.8802	1.7800	1.4200	1.6600	1.8200	-
CaCr	-	-	-	-	-	-	-	-
CaTs	0.3900	-	0.3800	-	1.2500	-	2.7400	-
Ess	2.8500	-	2.3702	3.1400	0.8500	3.2600	0.5100	-
F2F3	-	-	-	-	-	-	-	-
FeAl	-	1.1290	-	-	-	-	-	4.5829
Jo	-	-	-	-	-	-	-	-
Di	2.2300	-	2.9203	1.9600	3.1900	2.4300	2.3500	-
Hd	-	-	-	-	-	-	-	-
En	33.9800	32.1462	32.3832	38.5600	36.2000	32.8600	32.5200	36.7456
Fs	-	-	-	-	-	-	-	-
Fs-En	54.6600	64.7747	56.1856	50.0200	54.3000	55.4600	58.1800	56.5705
inSUM:	1.0000	0.9743	0.9999	1.0000	1.0000	1.0000	1.0000	0.9710
resAlT	0.0009	-0.0110	0.0005	0.0011	0.0008	0.0011	0.0012	-0.0312

IMA names:
op1 - Ferroan ENSTATITE
op2 - Ferroan ENSTATITE
op3 - Ferroan ENSTATITE
op4 - Ferroan ENSTATITE
op5 - Ferroan ENSTATITE
op6 - Ferroan ENSTATITE
op7 - Ferroan ENSTATITE
op8 - Ferroan ENSTATITE

Appendix B

Guyuti Formation : basaltic andesite

Feldspar composition data
filename: od160pl.dat

	1 pl1	2 pl2	3 pl3	4 pl4	5 pl5	6 pl6	7 pl6	8 pl8
SiO2	53.80	52.49	52.31	52.28	54.38	51.20	54.49	53.64
Al2O3	28.94	30.41	29.86	30.40	28.77	30.31	28.25	29.20
FeO	0.59	0.54	0.46	0.58	0.48	0.53	0.56	0.48
CaO	12.30	13.51	13.17	13.76	11.92	14.26	11.57	12.45
K2O	0.32	0.18	0.18	0.17	0.41	0.25	0.41	0.32
Na2O	4.14	3.39	3.89	3.64	4.37	3.12	4.41	4.12
Sum:	100.09	100.52	99.87	100.83	100.33	99.67	99.69	100.21

feldspar cation numbers on the basis of 8 oxygens

Si	2.436	2.372	2.381	2.361	2.454	2.342	2.472	2.427
Al	1.545	1.619	1.602	1.618	1.530	1.634	1.511	1.557
Fe2	0.022	0.020	0.018	0.022	0.018	0.020	0.021	0.018
Ca	0.597	0.654	0.642	0.666	0.576	0.699	0.562	0.603
K	0.018	0.010	0.010	0.010	0.023	0.014	0.024	0.018
Na	0.363	0.297	0.343	0.319	0.382	0.277	0.388	0.361
inCAT#:	4.982	4.972	4.995	4.994	4.984	4.986	4.978	4.985
mg:	0.00	0.00	0.00	0.00	0.00	0.00	0.00	0.00
Al4:	0.564	0.628	0.619	0.639	0.546	0.658	0.528	0.573
Al6:	0.981	0.991	0.982	0.978	0.984	0.976	0.983	0.983
Or:	1.880	1.072	1.044	0.976	2.393	1.465	2.433	1.872
Ab:	37.141	30.892	34.468	32.052	38.931	27.949	39.825	36.751
An:	60.979	68.037	64.487	66.972	58.676	70.586	57.741	61.377

	9 pl9
SiO2	52.37
Al2O3	30.32
FeO	0.42
CaO	13.56
K2O	0.23
Na2O	3.64
Sum:	100.54

feldspar cation numbers on the basis of 8 oxygens

Si	2.368
Al	1.616
Fe2	0.016
Ca	0.657
K	0.013
Na	0.319
inCAT#:	4.989
mg:	0.00
Al4:	0.632
Al6:	0.984
Or:	1.334
Ab:	32.255
An:	66.411

Appendix B

Guyuti Formation : basaltic andesite

Pyroxene composition data
file-name: od160px.dat
Number of samples: 4

	1 px1	2 px2	3 px4	4 px3
SiO2	53.00	52.72	52.20	52.87
TiO2	0.28	0.50	0.38	0.46
Al2O3	1.05	1.75	1.83	1.45
FeO	9.76	9.33	10.19	10.51
MnO	0.47	0.30	0.45	0.30
CaO	20.87	21.21	20.38	20.71
MgO	14.50	14.30	14.23	14.09
Na2O	0.00	0.41	0.44	0.34
Sum	99.93	100.52	100.10	100.73
T site				
Si4+	1.9774	1.9519	1.9435	1.9616
AlIV	0.0226	0.0481	0.0565	0.0384
Fe3+	-	-	-	0.0000
TOTAL:	2.0000	2.0000	2.0000	2.0000
M1 site				
AlVI	0.0235	0.0282	0.0238	0.0249
Fe3+	-	0.0204	0.0422	0.0111
Ti4+	0.0078	0.0139	0.0106	0.0128
Mg2+	0.8063	0.7891	0.7896	0.7792
Fe2+	0.1624	0.1484	0.1338	0.1720
TOTAL:	1.0000	1.0000	1.0000	1.0000
M2 site				
Fe2+	0.1421	0.1200	0.1413	0.1430
Mn2+	0.0148	0.0094	0.0142	0.0094
Ca2+	0.8342	0.8414	0.8129	0.8232
Na+	-	0.0294	0.0317	0.0244
TOTAL:	0.9911	1.0002	1.0001	1.0000
iCAT#:	3.9911	4.0068	4.0141	4.0037
OXNUM:	5.9993	5.9997	5.9996	5.9994
mg#:	0.73	0.75	0.74	0.71
Q:	1.9450	1.8989	1.8776	1.9174
J:	0.0000	0.0588	0.0634	0.0488
En:	41.1420	40.9136	40.8273	40.2085
Wo:	42.5656	43.6252	42.0321	42.4790
Fs:	16.2925	15.4612	17.1406	17.3126
ZrAe	-	-	-	-
Ae	-	2.0400	3.1700	1.1100
Jd	-	0.9000	-	1.3300
Nept	-	-	-	-
Kosm	-	-	-	-
Ka	1.4933	0.9400	1.4200	0.9400
CaTi	1.5740	2.7800	2.1200	2.5600
CaCr	-	-	-	-
CaTs	2.3711	1.9200	2.3800	1.1600
Ess	-	-	1.0500	-
F2F3	-	-	-	-
FeAl	-	-	-	-
Jo	-	-	-	-
Di	79.0738	76.5800	75.7400	75.7000
Hd	1.1502	2.8600	-	2.9000
En	-	-	-	-
Fs	14.3376	11.9800	13.3800	14.3000
Fs-En	-	-	0.7400	-
inSUM:	0.9911	1.0000	1.0000	1.0000
resAlT	-0.0165	0.0011	0.0010	0.0012

IMA names:
px1 - [Magnesium-rich] AUGITE
px2 - [Magnesium-rich] AUGITE
px4 - [Magnesium-rich] AUGITE
px3 - [Magnesium-rich] AUGITE

Appendix B

Guyuti Formation : basaltis andesitic clast

Feldspar composition data
filename: od194pl.dat

	1 pl1	2 pl2	3 pl8	4 pl9	5 pl10	6 pl14	7 pl15
SiO2	49.64	49.71	48.72	47.23	52.79	48.06	48.65
Al2O3	31.43	31.00	31.59	32.42	28.62	32.30	32.06
FeO	0.75	0.59	0.82	0.51	0.74	0.61	0.24
CaO	15.27	14.72	15.72	16.84	12.37	16.49	16.30
K2O	2.54	2.82	0.15	0.00	0.31	0.00	0.16
Na2O	0.16	0.20	2.28	2.01	4.31	2.00	2.08
Sum:	99.79	99.04	99.28	99.01	99.14	99.46	99.49

feldspar cation numbers on the basis of 8 oxygens

Si	2.287	2.306	2.251	2.194	2.421	2.218	2.240
Al	1.707	1.695	1.720	1.775	1.547	1.757	1.740
Fe2	0.029	0.023	0.032	0.020	0.028	0.023	0.009
Ca	0.754	0.732	0.778	0.838	0.608	0.815	0.804
K	0.149	0.167	0.009	-	0.018	-	0.009
Na	0.014	0.018	0.204	0.181	0.383	0.179	0.186
inCAT#:	4.941	4.939	4.995	5.008	5.006	4.993	4.988
mg:	0.00	0.00	0.00	0.00	0.00	0.00	0.00
Al4:	0.713	0.694	0.749	0.806	0.579	0.782	0.760
Al6:	0.994	1.000	0.972	0.969	0.968	0.975	0.979
Or:	16.274	18.206	0.888	0.000	1.794	0.000	0.931
Ab:	1.548	1.954	20.599	17.759	37.974	17.993	18.580
An:	82.178	79.841	78.513	82.241	60.232	82.007	80.489

Appendix B

Guyuti Formation : basaltic andesitic clast

Pyroxene composition data
file-name: od194px.dat
Number of samples: 15

	1 cp1	2 cp3	3 cp4	4 cp5	5 cp6	6 cp7	7 cp8	8 cp9
SiO2	52.82	52.30	52.20	52.79	52.43	52.44	52.23	51.18
TiO2	0.35	0.36	0.45	0.39	0.31	0.41	0.46	0.62
Al2O3	1.54	1.59	1.86	1.85	1.87	1.82	1.84	2.58
FeO	9.42	9.25	9.01	9.05	9.14	9.19	9.21	9.52
MnO	0.55	0.43	0.30	0.50	0.42	0.35	0.31	0.35
CaO	20.42	20.37	20.32	20.69	20.10	20.35	20.35	20.22
MgO	14.73	14.87	14.60	14.81	14.78	14.85	14.77	14.28
Na2O	0.54	0.54	0.42	0.45	0.42	0.35	0.39	0.37
Sum	100.37	99.71	99.15	100.55	99.46	99.76	99.56	99.12
T site								
Si4+	1.9544	1.9450	1.9543	1.9485	1.9559	1.9514	1.9475	1.9203
AlIV	0.0456	0.0550	0.0457	0.0515	0.0441	0.0486	0.0525	0.0797
Fe3+	0.0000	-	-	-	0.0000	-	0.0000	-
TOTAL:	2.0000	2.0000	2.0000	2.0000	2.0000	2.0000	2.0000	2.0000
M1 site								
AlVI	0.0214	0.0147	0.0362	0.0291	0.0380	0.0314	0.0282	0.0342
Fe3+	0.0419	0.0573	0.0129	0.0314	0.0183	0.0192	0.0263	0.0365
Ti4+	0.0097	0.0101	0.0127	0.0109	0.0086	0.0114	0.0128	0.0173
Mg2+	0.8126	0.8239	0.8146	0.8150	0.8220	0.8238	0.8207	0.7989
Fe2+	0.1144	0.0940	0.1236	0.1136	0.1131	0.1142	0.1120	0.1131
TOTAL:	1.0000	1.0000	1.0000	1.0000	1.0000	1.0000	1.0000	1.0000
M2 site								
Fe2+	0.1352	0.1363	0.1454	0.1344	0.1537	0.1525	0.1487	0.1492
Mn2+	0.0171	0.0135	0.0093	0.0156	0.0131	0.0110	0.0097	0.0112
Ca2+	0.8094	0.8115	0.8150	0.8182	0.8032	0.8112	0.8131	0.8127
Na+	0.0384	0.0386	0.0303	0.0319	0.0301	0.0255	0.0284	0.0269
TOTAL:	1.0001	0.9999	1.0000	1.0001	1.0001	1.0002	0.9999	1.0000
iCAT#:	4.0140	4.0192	4.0043	4.0105	4.0061	4.0064	4.0088	4.0122
OXNUM:	5.9994	5.9992	5.9992	5.9995	5.9998	5.9999	5.9995	5.9994
mg#:	0.77	0.78	0.75	0.77	0.75	0.76	0.76	0.75
Q:	1.8716	1.8657	1.8986	1.8812	1.8920	1.9017	1.8945	1.8739
J:	0.0768	0.0772	0.0606	0.0638	0.0602	0.0510	0.0568	0.0538
En:	42.0905	42.5458	42.4094	42.2674	42.7368	42.6420	42.5123	41.5747
Wo:	41.9248	41.9055	42.4302	42.4334	41.7594	41.9897	42.1186	42.2929
Fs:	15.9847	15.5487	15.1603	15.2992	15.5038	15.3683	15.3691	16.1324
ZrAe	-	-	-	-	-	-	-	-
Ae	3.8400	3.8604	1.2900	3.1400	1.8300	1.9200	2.6303	2.6900
Jd	-	-	1.7400	0.0500	1.1800	0.6300	0.2100	-
Nept	-	-	-	-	-	-	-	-
Kosm	-	-	-	-	-	-	-	-
Ka	1.7100	1.3501	0.9300	1.5600	1.3100	1.1000	0.9701	1.1200
CaTi	1.9400	2.0202	2.5400	2.1800	1.7200	2.2800	2.5603	3.4600
CaCr	-	-	-	-	-	-	-	-
CaTs	2.1400	1.4701	1.8800	2.8600	2.6200	2.5100	2.6103	3.4200
Ess	0.3500	1.8702	-	-	-	-	-	0.9600
F2F3	-	-	-	-	-	-	-	-
FeAl	-	-	-	-	-	-	-	-
Jo	-	-	-	-	-	-	-	-
Di	76.5100	75.7976	77.0800	76.7800	75.9800	76.3300	76.1476	73.4300
Hd	-	-	-	-	-	-	-	-
En	-	-	-	-	-	-	-	-
Fs	11.4400	9.4009	12.3600	11.3600	11.3100	11.4200	11.2011	11.3100
Fs-En	2.0700	4.2304	2.1800	2.0700	4.0500	3.8100	3.6704	3.6100
inSUM:	1.0000	0.9999	1.0000	1.0000	1.0000	1.0000	0.9999	1.0000
resAlT	0.0013	0.0014	0.0015	0.0011	0.0007	0.0007	0.0008	0.0013

IMA names:
cp1 - [Magnesium-rich] AUGITE
cp3 - [Magnesium-rich] AUGITE
cp4 - [Magnesium-rich] AUGITE
cp5 - [Magnesium-rich] AUGITE
cp6 - [Magnesium-rich] AUGITE
cp7 - [Magnesium-rich] AUGITE
cp8 - [Magnesium-rich] AUGITE
cp9 - [Magnesium-rich] AUGITE

	9	10	11	12	13	14	15
	cp10	cp11	cp12	cp13	cp14	cp15	cp16
SiO2	52.28	52.43	52.44	52.17	52.17	51.91	51.83
TiO2	0.37	0.40	0.43	0.42	0.50	0.49	0.53
Al2O3	2.34	1.66	1.80	1.87	1.94	2.29	2.17
FeO	9.23	9.33	9.37	9.61	9.29	9.57	9.35
MnO	0.24	0.35	0.34	0.00	0.35	0.29	0.35
CaO	20.36	20.62	20.10	20.44	20.27	20.11	19.88
MgO	14.70	14.79	14.75	14.77	14.66	14.57	14.66
Na2O	0.47	0.57	0.28	0.36	0.46	0.32	0.54
Sum	99.98	100.16	99.52	99.64	99.65	99.54	99.30
T site							
Si4+	1.9387	1.9414	1.9588	1.9443	1.9440	1.9388	1.9362
AlIV	0.0613	0.0586	0.0412	0.0557	0.0560	0.0612	0.0638
Fe3+	0.0000	-	-	-	-	0.0000	-
TOTAL:	2.0000	2.0000	2.0000	2.0000	2.0000	2.0000	2.0000
M1 site							
AlVI	0.0408	0.0140	0.0378	0.0262	0.0291	0.0394	0.0317
Fe3+	0.0329	0.0624	-	0.0311	0.0308	0.0168	0.0407
Ti4+	0.0103	0.0110	0.0120	0.0116	0.0141	0.0137	0.0147
Mg2+	0.8124	0.8161	0.8214	0.8205	0.8142	0.8109	0.8159
Fe2+	0.1036	0.0965	0.1288	0.1106	0.1118	0.1192	0.0970
TOTAL:	1.0000	1.0000	1.0000	1.0000	1.0000	1.0000	1.0000
M2 site							
Fe2+	0.1496	0.1299	0.1638	0.1577	0.1468	0.1629	0.1544
Mn2+	0.0074	0.0110	0.0108	-	0.0112	0.0091	0.0111
Ca2+	0.8091	0.8181	0.8043	0.8163	0.8090	0.8047	0.7954
Na+	0.0340	0.0409	0.0206	0.0260	0.0330	0.0234	0.0391
TOTAL:	1.0001	0.9999	0.9995	1.0000	1.0000	1.0001	1.0000
iCAT#:	4.0110	4.0209	3.9995	4.0104	4.0103	4.0056	4.0136
OXNUM:	5.9996	5.9994	5.9995	5.9994	5.9996	5.9996	5.9995
mg#:	0.76	0.78	0.74	0.75	0.76	0.74	0.76
Q:	1.8747	1.8606	1.9183	1.9051	1.8818	1.8977	1.8627
J:	0.0680	0.0818	0.0412	0.0520	0.0660	0.0468	0.0782
En:	42.4230	42.1975	42.5794	42.3768	42.3225	42.1553	42.6169
Wo:	42.2507	42.3009	41.6930	42.1599	42.0522	41.8330	41.5461
Fs:	15.3264	15.5016	15.7275	15.4633	15.6253	16.0116	15.8370
ZrAe	-	-	-	-	-	-	-
Ae	3.2900	4.0904	-	2.6000	3.0800	1.6800	3.9100
Jd	0.1100	-	2.0610	-	0.2200	0.6600	-
Nept	-	-	-	-	-	-	-
Kosm	-	-	-	-	-	-	-
Ka	0.7400	1.1001	1.0805	-	1.1200	0.9100	1.1100
CaTi	2.0600	2.2002	2.4012	2.3200	2.8200	2.7400	2.9400
CaCr	-	-	-	-	-	-	-
CaTs	3.9700	1.4001	1.7209	2.6200	2.6900	3.2800	3.1700
Ess	-	2.1502	-	0.5100	-	-	0.1600
F2F3	-	-	-	-	-	-	-
FeAl	-	-	-	-	-	-	-
Jo	-	-	-	-	-	-	-
Di	74.8800	76.0676	76.3482	76.1800	75.3900	74.4500	73.2700
Hd	-	-	-	-	-	-	-
En	-	-	-	-	-	-	-
Fs	10.3600	9.6510	12.8864	11.0600	11.1800	11.9200	9.7000
Fs-En	4.5900	3.3403	3.5017	4.7100	3.5000	4.3600	5.7400
inSUM:	1.0000	0.9999	0.9995	1.0000	1.0000	1.0000	1.0000
resAlT	0.0010	0.0011	0.0000	0.0012	0.0009	0.0010	0.0011

IMA names:
cp10 - [Magnesium-rich] AUGITE
cp11 - [Magnesium-rich] AUGITE
cp12 - [Magnesium-rich] AUGITE
cp13 - [Magnesium-rich] AUGITE
cp14 - [Magnesium-rich] AUGITE
cp15 - [Magnesium-rich] AUGITE
cp16 - [Magnesium-rich] AUGITE

APPENDIX C

BULK ROCK CHEMICAL ANALYSES

Appendix C

Chemical Analyses of the Tapas Metamorphic rocks

	OD244	OD247	OD240	OR250	OR251	OR252	OR253
SiO_2	56.83	47.72	47.12	42.62	77.03	56.30	56.49
TiO_2	1.00	3.17	2.34	2.98	0.50	1.07	1.29
Al_2O_3	20.39	11.94	14.35	14.12	12.68	14.37	16.48
Fe_2O_3	10.31	17.73	14.39	17.27	4.49	9.21	9.60
MnO	0.20	0.29	0.25	0.29	0.18	0.23	0.20
MgO	4.49	5.83	7.41	9.24	1.56	8.21	7.53
CaO	0.58	7.81	10.23	12.35	0.17	7.19	4.94
Na_2O	1.62	4.28	3.22	0.97	1.13	2.23	2.97
K_2O	3.75	0.26	0.15	0.33	2.92	0.70	0.90
P_2O_5	0.17	0.42	0.23	0.28	0.05	0.18	0.21
Total	99.33	99.44	99.69	100.45	100.71	99.69	100.60
LOI	4.69	1.38	2.42	3.30	3.50	8.48	6.67
Mg#	0.46	0.39	0.51	0.51	0.41	0.64	0.61
Ni	250.3	34.8	55	41.7	26.9	267.5	236.6
Cr	336.5	37.1	172	154	51.9	509.7	425.9
V	242.3	413.4	403.4	492	107	215.6	244.1
Sc	27.1	48.6	50	59.3	13.9	30.4	32.1
Cu	72.7	83.3	127.5	49.7	60	52.2	69.7
Zn	190.1	152.8	256.5	233.1	89.3	120.9	118
Cl	448.4	285	248.5	134.4	<d.l.	207.8	312.4
Ga	23.8	17	19.1	19.1	15.8	17.1	17.6
Pb	9.4	7.3	4.6	11.4	6.6	6.7	11.7
Sr	73.2	117.6	144.2	228.8	18.8	137.3	122.6
Rb	133.4	12.6	5.7	14.9	91.4	24.8	29.4
Ba	856.3	80.5	5.7	6	770.3	138.4	214.4
Zr	183.7	306.4	159.6	190.2	101.4	129	144.8
Nb	10.3	6	2.8	2.9	8.7	7.8	8.1
Th	11.1	0.6	0.1	0.4	9.7	7	6.5
Y	31.2	83.5	51	63.7	24.1	28.8	35.4
La	23.2	4.2	2.3	1.7	11.4	13.1	14.7
Ce	64.5	30.6	18.5	19.4	23.5	37.7	38.2
Nd	26.8	25.1	14.3	15.2	11	17.6	19.8

(<d.l : below detection limit)

Appendix C

Chemical Analyses of the Tapas Metamorphic rocks

	OR260	OR261	OR262	OR264
SiO_2	54.03	52.85	40.80	36.48
TiO_2	1.10	0.98	1.55	2.21
Al_2O_3	15.17	16.34	16.99	11.60
Fe_2O_3	10.15	10.51	16.81	25.23
MnO	0.19	0.16	0.22	0.15
MgO	7.26	5.64	7.08	12.43
CaO	7.31	9.18	10.95	9.12
Na_2O	3.56	3.26	2.32	1.67
K_2O	0.86	0.49	0.87	0.78
P_2O_5	0.08	0.28	2.11	0.03
Total	99.71	99.69	99.70	99.70
LOI	2.21	4.79	2.54	1.91
Mg#	0.59	0.52	0.46	0.49
Ni	65.5	4.1	29.7	39.7
Cr	141.2	3.5	5.8	65.3
V	327.3	258.8	432.8	1018.2
Sc	38.3	33.6	43.7	104.4
Cu	48.8	1.9	11	157.9
Zn	122	117.4	168.8	101.5
Cl	370	198.7	177.7	538
Ga	16.8	17.4	22.8	16.2
Pb	4.8	5	4.8	1.6
Sr	300.2	400.5	368.7	177.4
Rb	24.9	5.9	13.3	6.3
Ba	130.7	102.9	144.3	95.4
Zr	60.7	20.1	39	17.9
Nb	3.3	1.2	1.9	0.7
Th	4.1	1.3	1.1	0.4
Y	37.3	25	36.3	21.8
La	6.8	1.8	5.4	<d.l.
Ce	25.7	9.2	21.8	11.1
Nd	20.4	10.4	20.5	9.4

(<d.l : below detection limit)

Appendix C

Chemical Analyses of the ophiolitic rocks (basaltic rocks)

	OD22	OR50	OR56	OR184	OR186	OR191
SiO_2	51.86	61.28	57.71	54.09	52.87	49.90
TiO_2	0.59	0.53	0.87	1.20	1.16	0.61
Al_2O_3	15.65	17.08	18.10	16.99	16.35	17.01
Fe_2O_3	7.72	5.02	7.02	11.24	10.70	8.43
MnO	0.14	0.18	0.09	0.18	0.19	0.15
MgO	11.03	4.34	3.27	4.54	4.36	8.13
CaO	6.92	4.35	5.60	4.54	7.16	12.02
Na_2O	4.83	5.32	7.55	6.47	6.16	3.42
K_2O	0.51	1.56	0.37	0.59	0.92	0.06
P_2O_5	0.08	0.09	0.24	0.13	0.13	0.09
Total	99.33	99.76	100.82	99.97	100.01	99.82
LOI	5.30	2.22	2.00	2.70	4.98	2.84
Mg#	0.74	0.63	0.48	0.44	0.45	0.66
Ni	188.2	29.1	55.7	20.2	18.2	93.5
Cr	418.1	23.7	64.4	7.8	6.8	194.2
V	243.5	116	202.9	331.6	312.7	217.2
Sc	34	22.5	25	37.7	35.8	35
Cu	59.3	4	56.6	36.9	37.4	56.3
Zn	58.8	51.1	60.5	96.7	89.6	62.4
Cl	< d.l.	636		< d.l.	< d.l.	< d.l.
Ga	13	15.9	16.7	15.3	14.3	13.3
Pb	< d.l.	2	0.8	0.2	1	< d.l.
Sr	130.4	406.6	218.5	148.6	210.9	189.4
Rb	4.2	14.1	3.1	10.7	17.5	0.3
Ba	7.6	31.5	13.5	4.9	4.2	3.8
Zr	43.9	72.9	113.6	98	95	40.8
Nb	0.6	0.8	1.5	1.4	1.2	0.5
Th	< d.l.	< d.l.	0.9	0.5	< d.l.	< d.l.
Y	16.4	12.3	23.3	34.8	32.5	16.9
La	1.5	2.4	7.6	2.9	2.6	1.4
Ce	5.7	7.9	21.3	14.9	12.6	7.5
Nd	5.5	6	15	11.8	9.1	7.2

(<d.l : below detection limit)

Appendix C

Chemical Analyses of the ophiolitic rocks (gabbro)

	OJ91	OR70	OR71	OT49	OJ101	OJ108	OR60
SiO_2	69.81	41.92	42.22	47.37	46.25	46.76	41.50
TiO_2	0.56	0.93	0.94	0.50	0.91	0.07	0.90
Al_2O_3	14.62	16.64	14.12	16.15	20.87	23.32	16.47
Fe_2O_3	5.29	14.39	15.50	8.88	6.72	3.33	14.87
MnO	0.07	0.17	0.21	0.15	0.08	0.06	0.20
MgO	0.78	8.72	10.00	10.79	9.72	9.58	8.74
CaO	1.98	16.11	15.85	14.76	13.83	16.98	16.17
Na_2O	6.92	0.78	0.51	0.96	1.86	0.69	0.48
K_2O	0.41	0.22	0.21	0.02	0.05	0.01	0.10
P_2O_5	0.17	0.04	0.04	0.00	0.01	< d.l.	0.03
Total	100.60	99.93	99.60	99.59	100.29	100.80	99.46
LOI	0.74	1.00	0.95	0.81	1.09	1.24	0.46
Mg#	0.23	0.55	0.56	0.71	0.74	0.85	0.54
Ni	3.6	39.3	34.6	101.7	133.6	216.4	38.9
Cr	11.2	31.1	73.3	358.1	126.1	173.1	34.6
V	21	521.8	575.8	310.1	413.7	35.8	490.7
Sc	14.4	55.2	61.7	49.5	68.6	22.2	52.5
Cu	12.2	14.6	39.1	77.4	431	2.3	28.8
Zn	19.7	72.5	81.6	44	29.6	16.8	76.8
Cl	64.7		204.7	< d.l.	84.8	< d.l.	113.3
Ga	14.4	18.1	15.2	11.2	15.7	12.5	16.4
Pb	< d.l.	2.6	1.6	< d.l.	< d.l.	0.1	2.5
Sr	141.3	336.7	289.8	146.4	326.4	506.4	362.9
Rb	4.5	3.7	3.5	0.5	0.4	0.3	1.7
Ba	20.6	14	18.2	1.4	< d.l.	1.5	7.8
Zr	222.6	6.4	8.7	8.5	16.7	< d.l.	6.6
Nb	3	0.3	0.4	0.3	0.2	0	0.4
Th	0.4	0.6	0.4	0.4	< d.l.	< d.l.	1
Y	59.7	8	9.4	8.6	14.6	2	8.2
La	8.4	< d.l.	< d.l.	0.1	0.3	0	0
Ce	22.6	4.7	2.7	< d.l.	1.3	0.6	1.2
Nd	19.9	2.9	2.5	2.4	3.6	2	2.8

(<d.l : below detection limit)

Appendix C

Chemical Analyses of the ophiolitic rocks (gabbro)

	OR69	OJ76
SiO_2	41.60	59.72
TiO_2	0.99	0.76
Al_2O_3	14.75	17.31
Fe_2O_3	15.74	8.22
MnO	0.21	0.16
MgO	9.31	3.57
CaO	16.16	6.31
Na_2O	0.44	4.30
K_2O	0.11	0.00
P_2O_5	0.02	0.09
Total	99.33	100.44
LOI	0.71	2.93
Mg#	0.54	0.46
Ni	42.6	20.9
Cr	42.6	17.4
V	564.9	234.4
Sc	60.3	24.3
Cu	27.8	4.4
Zn	90	83.5
Cl		< d.l.
Ga	14.9	17.5
Pb	3	1.4
Sr	301.4	271.3
Rb	1.4	0.1
Ba	5.4	1
Zr	6.7	79.1
Nb	0.8	0.7
Th	0.6	0.4
Y	9.3	19.9
La	< d.l.	2.1
Ce	4	10.1
Nd	2.3	6.8

(<d.l : below detection limit)

Appendix C

Chemical Analyses of the Ophiolitic rocks (dolerite)

	OD201	OD202	OD203	OD204	OD207	OD208	OD209
SiO_2	52.48	49.34	53.38	47.42	54.33	48.98	51.21
TiO_2	0.91	0.52	0.97	0.57	1.09	0.21	0.557
Al_2O_3	17.91	18.37	17.49	16.83	16.47	16.03	16.74
Fe_2O_3	11.21	7.46	10.96	8.43	9.75	6.30	7.91
MnO	0.23	0.17	0.25	0.19	0.07	0.11	0.112
MgO	4.95	11.15	4.94	12.30	4.32	12.65	8.75
CaO	7.80	9.57	7.02	11.57	10.46	15.41	12.85
Na_2O	3.38	3.41	3.62	2.41	2.79	0.93	1.88
K_2O	0.91	0.50	1.34	0.26	0.03	0.04	0.03
P_2O_5	0.08	0.05	0.11	0.05	0.12	<d.l.	0.048
Total	99.87	100.55	100.08	100.03	99.43	100.66	100.087
LOI	1.35	4.54	1.47	4.53	0.49	1.49	1.54
Mg#	0.47	0.75	0.47	0.74	0.47	0.80	0.687
Ni	13.1		12.4	215.1	11.6	257.1	86.2
Cr	10.2		9.2	1266.3	3.9	816	143.8
V	377.9		363.1	221.7	361.6	149.4	244.7
Sc	38.3		38.6	34.5	38	45.6	42.5
Cu	330.6		249	90	6.6	5.5	4.3
Zn	40.3		38.8	121.2	12.2	34.6	16.8
Cl	97.8		96.1	<d.l.	85.6	230.3	82.4
Ga	18.9		17.8	13.7	17.4	9.4	13.4
Pb	<d.l.		<d.l.	0.6	<d.l.	<d.l.	<d.l.
Sr	195.1		187.7	208.8	251	103.9	134.1
Rb	5.4		7.7	1.6	0.3	0.1	0
Ba	6.5		15.3	18.6	0.6	<d.l.	0.8
Zr	57.8		64.8	39.9	65.6	6.6	33.8
Nb	0.5		0.3	0.7	1	0.6	0.5
Th	0.1		<d.l.	0.3	<d.l.	0.3	0.4
Y	21.7		23.9	15.4	23.7	6.4	15.6
La	1.1		1.5	2.6	1.6	0.1	0.1
Ce	8.8		7.2	4.5	8.6	0.4	1.2
Nd	6.9		7.7	4.1	5.7	1.7	3.9

(<d.l : below detection limit)

Appendix C

Chemical Analyses of the Ophiolitic rocks (dolerite)

	OD212	OD220	OD233	OD235
SiO_2	52.13	57.63	70.31	56.62
TiO_2	1.09	0.56	0.39	1.19
Al_2O_3	16.61	18.01	14.47	16.70
Fe_2O_3	10.41	5.88	5.26	7.60
MnO	0.21	0.07	0.19	0.09
MgO	5.79	6.72	0.93	2.57
CaO	9.76	5.90	2.01	7.35
Na_2O	3.59	4.28	6.40	6.89
K_2O	0.11	1.01	0.06	0.04
P_2O_5	0.11	0.13	0.10	0.16
Total	99.80	100.19	100.13	99.22
LOI	1.09	3.37	1.09	1.04
Mg#	0.52	0.69	0.26	0.40
Ni	33.6	59.2	8.4	8.3
Cr	48.9	45.9	12.9	5.8
V	320.3	163	35.2	322.9
Sc	39.7	25.7	11.8	32.3
Cu	24.8	6.8	43	7.9
Zn	26.3	57.7	163.2	12.9
Cl	121.6	<d.l.	45.1	<d.l.
Ga	16.4	17.8	17	16.2
Pb	0	1.2	0.8	0.3
Sr	163.3	347.3	141	280.2
Rb	0.3	5.1	0.3	0.3
Ba	5	15.2	9	5.9
Zr	73.8	72.8	166.2	120.6
Nb	1.1	0.6	1.5	1.8
Th	0.3	<d.l.	0.4	0.1
Y	28.3	17	28.8	33.5
La	1.5	3.2	5.5	3.8
Ce	10.9	8.7	14.4	11.8
Nd	8.4	7.8	11.4	11.5

(<d.l : below detection limit)

Appendix C

Chemical Analyses of the Obi Latu Diorite

	OR6	OR7	OR18	OR65
SiO_2	60.51	59.12	53.89	59.26
TiO_2	0.64	0.74	0.77	0.61
Al_2O_3	17.66	17.04	18.66	17.46
Fe_2O_3	3.93	6.23	8.96	6.93
MnO	0.06	0.10	0.18	0.14
MgO	2.83	3.50	3.66	2.92
CaO	7.99	8.15	6.06	7.31
Na_2O	5.17	4.91	4.02	3.04
K_2O	0.17	0.15	3.37	1.80
P_2O_5	0.29	0.27	0.24	0.24
Total	99.26	100.22	99.81	99.70
LOI	0.34	0.16	3.28	1.09
Mg#	0.59	0.53	0.45	0.46
Ni	18.1	22.3	9.7	7.1
Cr	43.3	47.8	16.9	6
V	164.8	187.8	228.4	176.7
Sc	22.5	26	24.5	22.8
Cu	137.4	155.1	28.1	94.1
Zn	27	43.8	73.6	46.9
Cl	596.5	607	198.8	338.6
Ga	15.7	17.1	17.8	15.9
Pb	2.2	4.3	2	2
Sr	362.2	358.5	596.4	339.6
Rb	2.4	1.4	88.7	33.2
Ba	42.5	42.6	351.7	153
Zr	86.4	92.7	76.5	67
Nb	4	4.6	2.9	3.3
Th	1.7	2.4	1.7	1.6
Y	22.5	25	23.8	20.1
La	6.7	6.8	6	6.1
Ce	14.5	15.6	18.9	14.6
Nd	10.4	11.3	11.8	9.5

(<d.l : below detection limit)

Appendix C

Chemical Analyses of the Anggai River Formation (andesites)

	OD34	OD103	OD106
SiO_2	55.85	57.86	57.26
TiO_2	0.76	0.60	0.64
Al_2O_3	16.62	17.33	18.16
Fe_2O_3	8.57	5.47	6.04
MnO	0.16	0.12	0.08
MgO	3.89	6.51	6.14
CaO	6.97	4.90	3.67
Na_2O	2.18	6.76	7.52
K_2O	4.56	0.06	0.06
P_2O_5	0.42	0.09	0.11
Total	99.99	99.70	99.69
LOI	1.76	2.76	2.59
Mg#	0.47	0.70	0.67
Ni	11.6	122.6	62
Cr	34	123.7	62.8
V	235.6	150.2	165.8
Sc	27.5	24.2	26.2
Cu	69.7	1.7	< d.l.
Zn	78.4	64.8	51.2
Cl	< d.l.	< d.l.	< d.l.
Ga	16.5	13.6	14.4
Pb	5.2	0.1	0.6
Sr	525.8	178.5	187.1
Rb	101.5	0.5	0.6
Ba	278	4.5	3.9
Zr	94.7	72.5	82.5
Nb	3.5	0.9	0.8
Th	3.7	0.1	0.9
Y	20.7	16.9	16.2
La	10.9	2	1.7
Ce	27.3	8.2	9.5
Nd	16.7	7.4	7.3

(<d.l : below detection limit)

Appendix C

Chemical Analyses of the Anggai Formation (Sedimentary rocks)

	OD39A	OD39B	OD39C	OD39D	OD39E	0D39F	OD104	OR236
SiO_2	53.01	58.43	53.44	52.34	53.21	52.44	74.82	54.76
TiO_2	0.80	0.73	0.88	0.79	0.80	0.87	0.37	0.74
Al_2O_3	18.09	15.37	17.32	17.41	16.38	16.02	13.47	14.96
Fe_2O_3	11.21	8.14	11.90	12.36	10.59	10.79	2.75	7.95
MnO	0.19	0.24	0.19	0.17	0.36	0.23	0.03	0.17
MgO	6.02	3.00	5.85	6.76	4.66	4.06	0.55	6.84
CaO	2.10	5.24	2.08	2.02	5.52	7.43	1.06	8.44
Na_2O	6.72	6.07	6.37	6.61	5.88	5.45	6.38	5.17
K_2O	1.43	2.34	1.51	1.11	2.17	2.20	0.12	0.58
P_2O_5	0.13	0.14	0.17	0.14	0.14	0.23	0.08	0.09
Total	99.70	99.71	99.71	99.71	99.71	99.71	99.62	99.70
LOI	6.67	5.21	6.10	6.70	5.94	8.25	0.97	2.12
Mg#	0.52	0.42	0.49	0.52	0.47	0.43	0.28	0.67
Ni	14.1	11	11.1	16.1	12.3	14	4.1	70.3
Cr	29.5	22	19.5	26.6	26.6	14	4.1	197.6
V	313.1	337	279.8	388.1	327.1	295.5	11.5	263.4
Sc	46.5	38.2	43.7	43.8	43.9	36.5	8.1	39
Cu	132.7	149.7	120.3	135.1	118.3	129.7	1.5	21.7
Zn	94.8	77.6	106.8	105.2	92.5	103.8	12.4	62.6
Cl	< d.l.	< d.l.	< d.l.	< d.l.	< d.l.	< d.l.	< d.l.	< d.l.
Ga	15.3	15.1	17.7	19.2	17.9	15.9	12.9	12.1
Pb	3.5	5.6	4.8	3.6	3	8.2	0.1	0.3
Sr	115.5	319.6	140.2	100	317.7	263.2	71.4	303.6
Rb	12.8	16.7	34	10.5	16.6	45.1	0.5	4.3
Ba	130.6	244.9	159.4	95.7	182.9	215.4	2.6	30.6
Zr	66.7	62.8	76.3	53.8	59.8	85.6	232.6	53.9
Nb	1.1	1.2	1.4	0.7	1	1.6	1.8	0.5
Th	1.4	0.8	0.9	0.6	0.7	3	0.6	< d.l.
Y	22.6	26.6	25.4	19.7	23.9	22.3	44.6	21.6
La	4.1	6.3	6.5	4.1	4.8	9.4	7.4	1.4
Ce	15.5	16.3	20.4	17.6	15.3	24.3	22.8	6.8
Nd	10.5	12.1	13.4	11.1	10.2	15.2	17.3	7

(<d.l : below detection limit)

Appendix C

Chemical Analyses of the Woi Formation (volcanic rocks)

	OD14	OD15	OD15B	OD16	OD17	OD18	OD19
SiO_2	61.89	62.85	57.74	62.95	63.49	63.17	63.83
TiO_2	0.63	0.63	0.72	0.61	0.56	0.57	0.56
Al_2O_3	16.39	16.82	16.50	17.33	16.31	16.29	16.04
Fe_2O_3	6.45	6.35	7.73	6.34	5.81	5.92	5.91
MnO	0.33	0.11	0.14	0.10	0.11	0.09	0.09
MgO	1.86	1.68	3.81	2.50	2.45	1.85	1.58
CaO	5.45	4.81	7.03	5.64	5.32	5.12	4.93
Na_2O	2.98	3.04	2.95	2.79	3.11	2.93	2.94
K_2O	3.73	3.95	3.03	2.59	3.10	4.03	4.13
P_2O_5	0.28	0.26	0.31	0.22	0.23	0.23	0.23
Total	99.97	100.49	99.96	101.06	100.48	100.19	100.24
LOI	1.31		0.62		2.56		
Mg#	0.32	0.30	0.44	0.39	0.40	0.33	0.30
Ni	12.4	15.3	12.5	7.9	7	8.7	7.7
Cr	22.3	22.1	29.2	9.7	10.6	13.9	10.3
V	174.9	148	207.9	141.8	141	161.3	161.5
Sc	20.8	20.4	22.5	16.5	16.1	18.6	18.3
Cu	131.3	43.7	74.7	45.2	38.3	49.9	33.9
Zn	64.9	57.7	63.7	54.4	53.4	59.6	66.8
Cl	<d.l.	41.3	<d.l.	246.2	318	34.8	34.7
Ga	15.1	14.8	15.6	15.7	15.3	13.8	13.6
Pb	8.9	11.2	8.2	12.2	12.2	11.9	10.9
Sr	387	362.5	457	397.1	362.3	350.6	354
Rb	82.3	85	63.2	100.5	108.7	87.7	90.9
Ba	218.3	185.4	146.7	186.3	200.2	190.8	192.9
Zr	119.1	131.3	100.7	138	147.2	132.2	132.6
Nb	3.7	4	3.2	4.5	4.3	4.3	4.3
Th	4.7	5.2	3.8	5.9	6	5.1	5.3
Y	28.3	19.9	19.8	22.1	24.2	21.1	24.8
La	13.4	11.7	10.3	11.8	13.1	10.8	10.6
Ce	28.2	27.3	24.3	25.8	27.8	24.4	23.9
Nd	17.8	15.4	14.3	14.8	17.1	13.4	13.3

(<d.l : below detection limit)

Appendix C

Chemical Analyses of the Woi Formation (volcanic rocks)

	OD169	OD179	OD180	OD182	OD184	OD185	OD187
SiO_2	59.07	58.20	58.19	58.95	54.40	57.68	53.37
TiO_2	0.69	0.67	0.69	0.67	0.78	0.66	0.77
Al_2O_3	17.11	16.98	16.75	17.31	17.71	17.03	17.08
Fe_2O_3	7.80	7.77	8.14	7.18	8.85	7.93	9.04
MnO	0.16	0.15	0.16	0.14	0.16	0.16	0.14
MgO	3.69	3.77	3.96	3.29	4.79	3.86	5.36
CaO	7.51	7.58	7.57	6.73	8.36	7.34	9.08
Na_2O	3.65	3.53	3.33	2.76	2.75	2.82	2.33
K_2O	0.68	0.70	0.93	2.50	1.57	2.08	1.80
P_2O_5	0.25	0.26	0.27	0.26	0.40	0.27	0.47
Total	100.61	99.61	99.98	99.79	99.78	99.82	99.45
LOI	2.79	2.32	2.41	1.61	0.80	2.09	1.74
Mg#	0.48	0.44	0.44	0.42	0.46	0.44	0.49
Ni	9	8.5	8.9	6.8	18.5	8.3	26.1
Cr	17.4	16.3	17.2	5.4	50.7	15.4	80.7
V	222.7	223.1	220.8	208.6	267.9	218.8	295.9
Sc	24.5	25.3	25.8	23.6	29.8	24.7	32.8
Cu	72.9	75.3	84.7	37.8	142.3	91.2	134.7
Zn	68.3	69.5	68.8	64.3	74.8	68.3	76.3
Cl	<d.l.	<d.l.	<d.l.	85.9	11	66.4	32.9
Ga	16.1	16	16.1	16.1	16.6	15.1	16.1
Pb	6.9	7.4	8	9.1	5.6	7.8	6.1
Sr	709.8	694.2	642.7	428.9	471.6	522	602.1
Rb	72.2	68.7	78.1	75.7	54.1	79.2	37.5
Ba	234.1	332.7	348	126.1	131.1	251.2	105.3
Zr	89.2	85.3	88.6	101.9	59.6	88.5	46.8
Nb	3	2.8	2.9	3.8	2.6	2.9	2
Th	2.1	2.7	2.5	3.1	0.6	2.6	0.6
Y	20.7	20.3	21.8	21	21.9	21.1	19.4
La	10	11.9	10.8	10.6	10.7	11	9.5
Ce	23.4	22.4	23.3	21.5	20.8	23.4	23.5
Nd	13.2	12.6	13.3	13.6	14.5	13.4	15.4

(<d.l : below detection limit)

Appendix C

Chemical Analyses of the Woi Formation (volcanic rocks)

	OD188	OR310	OD 42V
SiO_2	53.55	68.93	66.72
TiO_2	0.79	0.64	0.65
Al_2O_3	17.25	14.63	14.13
Fe_2O_3	9.20	5.38	6.68
MnO	0.16	0.06	0.15
MgO	4.99	0.49	1.37
CaO	8.82	3.81	1.68
Na_2O	2.96	3.06	6.18
K_2O	1.39	2.54	1.80
P_2O_5	0.46	0.13	0.22
Total	99.57	99.66	99.58
LOI	1.00	0.91	1.14
Mg#	0.47	0.13	0.25
Ni	22.4	6.1	4.2
Cr	63.4	7.9	5
V	299.6	85.1	75.7
Sc	33.6	25.3	15.7
Cu	140.4	21.6	56.5
Zn	78.9	33.1	85.2
Cl	144.9	301.7	<d.l.
Ga	17.4	13	14.7
Pb	4.9	8.2	15.1
Sr	540	599.8	54.8
Rb	41	32.1	28
Ba	96.4	357.9	435.6
Zr	46.7	73.9	185.8
Nb	1.8	3	3.9
Th	0.1	1.8	6.1
Y	19	21.3	42.1
La	9	9.8	19.3
Ce	21	22.8	45.4
Nd	13.2	12.6	27.1

(<d.l : below detection limit)

Appendix C

Chemical Analyses of the Guyuti Formation (Volcanic rocks)

	OD154	OD155	OD160	OD194	OD199
SiO_2	55.52	53.30	66.52	56.97	59.19
TiO_2	0.74	0.75	0.58	0.73	0.55
Al_2O_3	17.38	17.77	16.09	17.88	19.76
Fe_2O_3	8.81	9.72	5.37	7.21	5.61
MnO	0.19	0.22	0.06	0.19	0.10
MgO	4.84	5.83	0.79	3.24	1.86
CaO	8.83	9.17	4.96	8.42	7.46
Na_2O	2.66	2.32	4.58	2.65	2.78
K_2O	0.68	0.63	1.04	2.17	2.62
P_2O_5	0.28	0.27	0.21	0.28	0.23
Total	99.92	99.98	100.20	99.74	100.15
LOI	2.13	1.67	1.45	1.49	0.90
Mg#	0.52	0.54	0.23	0.47	0.40
Ni	13.4	12.9	5.7	12.5	9.2
Cr	29.8	28.5	9.1	20.6	12.8
V	271.6	274.4	194.2	281	132.8
Sc	32.8	32.6	22.5	34.7	19.7
Cu	115.6	122.1	50.2	116.3	41.2
Zn	78	81.5	34	72.6	59.1
Cl	<d.l.	<d.l.	<d.l.	<d.l.	<d.l.
Ga	15	16.1	11.9	16.2	16.7
Pb	6.9	5.4	1.2	4.3	5.4
Sr	565.9	458.6	254.9	347	411.2
Rb	19.6	10	16	35.9	43.4
Ba	171.4	80.4	186.7	85.3	134.1
Zr	73	75.9	54.5	64	89.6
Nb	2.7	2.2	2.2	2	2.9
Th	1.4	2	1.2	1.9	1.9
Y	22.1	22.2	15.5	21.4	21.7
La	7.3	7	5.9	6.2	7.2
Ce	17.2	19.7	13.6	17.7	18.1
Nd	11.3	13.2	9	12.5	12

(<d.l : below detection limit)

APPENDIX D

KEY TO DIAGRAMS OF LOGGED SECTIONS

Appendix D

Key to diagrams of logged sections.

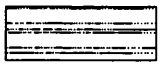 siltstone

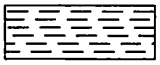 mudstone/muddy sandstone

 sandstone

 calcareous sandstone

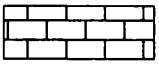 limestone/calcarenite/calcilutite

 conglomerate

 breccia

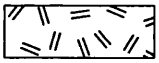 andesitic lava/andesitic breccia

 burrows

 carbonaceous layers

 parallel lamination

 wave lamination

 cross bedding

 gradded bedding

 load cast

OS 19 sample number

OD 39 sample number

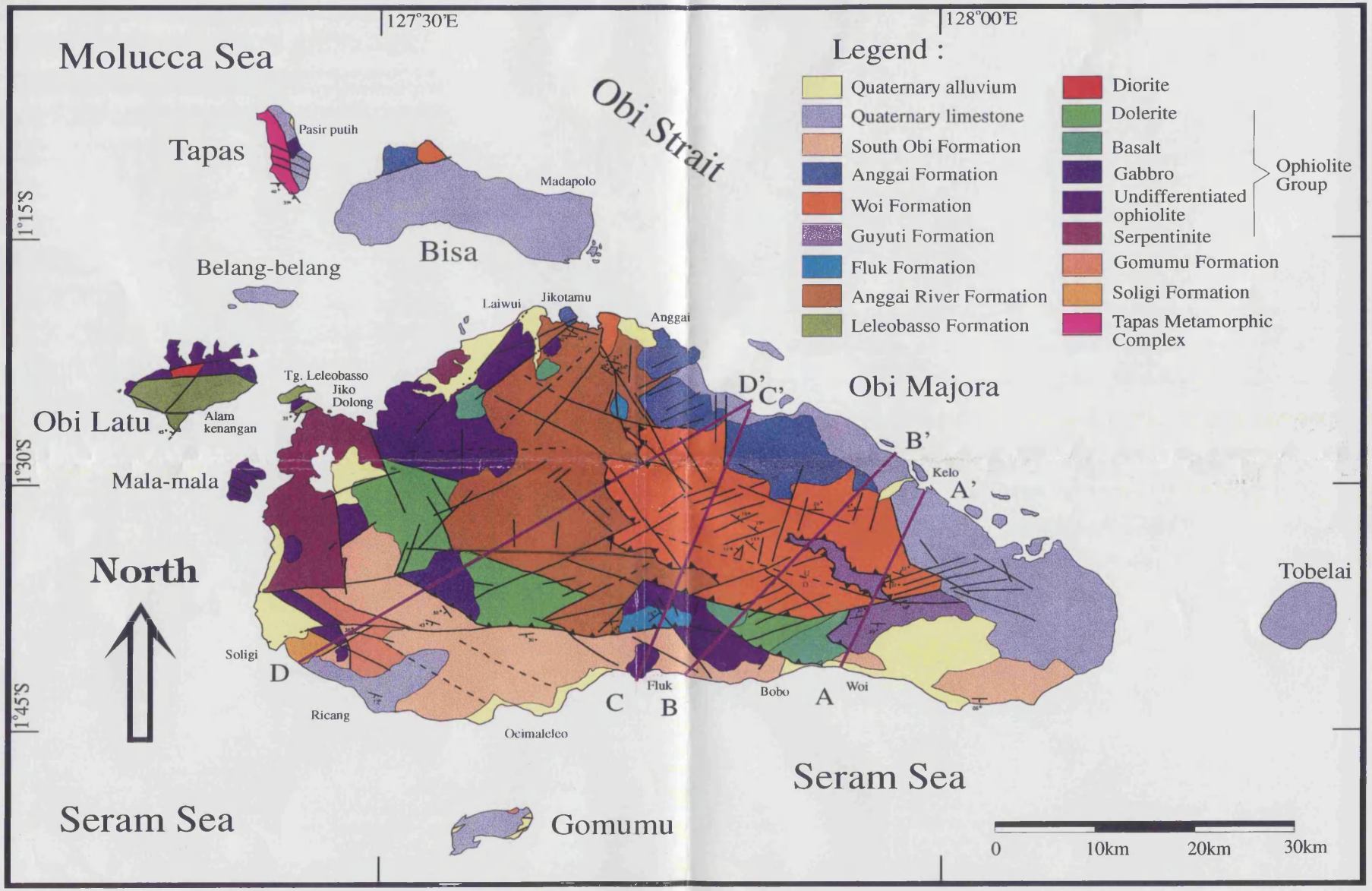

Fig. 2.1 Geological map of the Obi Islands based on this study.